

---

Theses and Dissertations

---

Spring 2012

## Advanced clay nanocomposites based on in situ photopolymerization utilizing novel polymerizable organoclays

Soon Ki Kim  
*University of Iowa*

Follow this and additional works at: <https://ir.uiowa.edu/etd>

 Part of the [Chemical Engineering Commons](#)

Copyright 2012 Soon Ki Kim

This dissertation is available at Iowa Research Online: <https://ir.uiowa.edu/etd/2917>


---

### Recommended Citation

Kim, Soon Ki. "Advanced clay nanocomposites based on in situ photopolymerization utilizing novel polymerizable organoclays." PhD (Doctor of Philosophy) thesis, University of Iowa, 2012.  
<https://doi.org/10.17077/etd.598i69qg>

---

Follow this and additional works at: <https://ir.uiowa.edu/etd>

 Part of the [Chemical Engineering Commons](#)

ADVANCED CLAY NANOCOMPOSITES  
BASED ON *IN SITU* PHOTOPOLYMERIZATION  
UTILIZING NOVEL POLYMERIZABLE ORGANOCCLAYS

by  
Soon Ki Kim

An Abstract

Of a thesis submitted in partial fulfillment  
of the requirements for the Doctor of  
Philosophy degree in Chemical and Biochemical Engineering  
in the Graduate College of  
The University of Iowa

May 2012

Thesis Supervisor: Professor C. Allan Guymon

## ABSTRACT

Polymer nanocomposite technology has had significant impact on material design. With the environmental advantages of photopolymerization, a research has recently focused on producing nanocomposites utilizing inexpensive clay particles based on *in situ* photopolymerization. In this research, novel polymerizable organoclays and thiol-ene photopolymerization have been utilized to develop advanced photopolymer clay nanocomposites and to overcome several limitations in conventional free radical photopolymers. To this end, factors important in nanocomposite processes such as monomer composition, clay dispersion, and photopolymerization behavior in combination with the evolution of ultimate nanocomposite properties have been investigated.

For monomer-organoclay compositions, higher chemical compatibility of components induces enhanced clay exfoliation, resulting in photopolymerization rate increases due to an amplified clay template effect. Additionally, by affecting the stoichiometric ratio between thiol and acrylate double bond in the clay gallery, thiolated organoclays enhance thiol-ene copolymerization with increased final thiol conversion while acrylated organoclays encourage acrylate homopolymerization. In accordance with the reaction behavior, incorporation of thiolated organoclays makes polymer chains more flexible with decreased glass transition temperature due to higher formation of thio-ether linkages while adding acrylated organoclays significantly increases the modulus. Photopolymer nanocomposites also help overcome two major drawbacks in conventional free radical photopolymerization, namely severe polymerization shrinkage and oxygen inhibition during polymerization. With addition of a low level of thiol monomers, the oxygen inhibition in various acrylate systems can be overcome by addition of only 5wt% thiolated organoclay. The same amount of polymerizable organoclay also induces up to 90% decreases in the shrinkage stress for acrylate or thiol-acrylate systems. However,

nonreactive clays do not reduce the stress substantially and even decreases the polymerization rate in air. Additionally, the clay morphology and polymerization behavior are closely related with evolution of ultimate nanocomposite performance. Use of polymerizable organoclay significantly improves overall toughness of nanocomposites by increasing either modulus or elongation at break based on the type of polymerizable organoclay, which demonstrates the promise of this technology as a modulation and/or optimization tool for nanocomposite properties.

Abstract Approved: \_\_\_\_\_  
Thesis Supervisor  
\_\_\_\_\_  
Title and Department  
\_\_\_\_\_  
Date

ADVANCED CLAY NANOCOMPOSITES  
BASED ON *IN SITU* PHOTOPOLYMERIZATION  
UTILIZING NOVEL POLYMERIZABLE ORGANOCCLAYS

by  
Soon Ki Kim

A thesis submitted in partial fulfillment  
of the requirements for the Doctor of  
Philosophy degree in Chemical and Biochemical Engineering  
in the Graduate College of  
The University of Iowa

May 2012

Thesis Supervisor: Professor C. Allan Guymon

Copyright by  
SOON KI KIM  
2012  
All Rights Reserved

Graduate College  
The University of Iowa  
Iowa City, Iowa

CERTIFICATE OF APPROVAL

---

PH.D. THESIS

---

This is to certify that the Ph.D. thesis of

Soon Ki Kim

has been approved by the Examining Committee  
for the thesis requirement for the Doctor of Philosophy  
degree in Chemical and Biochemical Engineering at the May 2012 graduation.

Thesis Committee: \_\_\_\_\_  
C. Allan Guymon, Thesis Supervisor

\_\_\_\_\_  
Alec B. Scranton

\_\_\_\_\_  
Julie L.P. Jessop

\_\_\_\_\_  
Gary Aurand

\_\_\_\_\_  
Tae Hong Lim

To Mother, my beloved wife, Hyeun-jeung, and lovely daughters, Soeun, Goeun,  
who made all things possible for me.



## ACKNOWLEDGMENTS

All of the works in my graduate periods could not have been achieved without help and support from many people. While I have to thank all of them by listing names and contributions, I could not help expressing my heartfelt appreciation to only a few of them due to the limitation in length at this time.

I would like to first thank to my advisor, Dr. Allan Guymon, who has supported me throughout my graduate works with his patience. My all accomplishments in this thesis would not have been possible without his supervision, encouragement, and constructive discussions. Not only for the academic works, but also he has provided the best consultation and guidance for my family life in Iowa. My sincere appreciation also goes out to the other committee members; Drs. Alec B. Scranton, Julie Jessop, Gary Aurand, and Tae-Hong, Lim. I have to value for agreeing to serve my dissertation committee as well as for their precious discussion and indispensable encouragement for my research.

Thanks also to the faculty and the staff in the Department of Chemical and Biochemical Engineering for providing various resources and expertise support to my research. I would like to thank my company, SK Chemicals, to provide me the opportunity for studying abroad. Special thanks would be emphasized to Dr. Tae-woong, Lee, Dr. In-sun, Yoon in SK Chemicals, who continuously inspired me to study for Ph.D. I am also grateful to 'IUCRC center for fundamentals and applications' and 'National Science Foundation' for funding for this research.

I have been also happy to have wonderful and talented colleagues in Guymon research group including past and current members. They became my friends and have

given tremendous help over the past years. I should say special thanks to Kwame Owusu-Adom and Lucas Sievens-Figueroa for helping me to learn everything in the lab and for being together through their residency with valuable daily discussion. I have also enjoyed a great time on working and assisting each other with Bradley Forney and Clinton J. Cook for last four years. All of you will remain to be my good friends.

Lastly, I would like to heartfelt thanks to my family for their unconditional love for my life. I am indebted to my Mother, my parents-in-law, and my brothers for their love, support, and encouragement. I have to express special love and gratitude to my beloved wife, Hyeun-jeung, my lovely daughters, Soeun and Goeun, who have been with me all the times whenever it is happy or hard. My family is surely the best motivation for my life. I love all of you, but could not express enough.

## ABSTRACT

Polymer nanocomposite technology has had significant impact on material design. With the environmental advantages of photopolymerization, a research has recently focused on producing nanocomposites utilizing inexpensive clay particles based on *in situ* photopolymerization. In this research, novel polymerizable organoclays and thiol-ene photopolymerization have been utilized to develop advanced photopolymer clay nanocomposites and to overcome several limitations in conventional free radical photopolymers. To this end, factors important in nanocomposite processes such as monomer composition, clay dispersion, and photopolymerization behavior in combination with the evolution of ultimate nanocomposite properties have been investigated.

For monomer-organoclay compositions, higher chemical compatibility of components induces enhanced clay exfoliation, resulting in photopolymerization rate increases due to an amplified clay template effect. Additionally, by affecting the stoichiometric ratio between thiol and acrylate double bond in the clay gallery, thiolated organoclays enhance thiol-ene copolymerization with increased final thiol conversion while acrylated organoclays encourage acrylate homopolymerization. In accordance with the reaction behavior, incorporation of thiolated organoclays makes polymer chains more flexible with decreased glass transition temperature due to higher formation of thio-ether linkages while adding acrylated organoclays significantly increases the modulus. Photopolymer nanocomposites also help overcome two major drawbacks in conventional free radical photopolymerization, namely severe polymerization shrinkage and oxygen inhibition during polymerization. With addition of a low level of thiol monomers, the oxygen inhibition in various acrylate systems can be overcome by addition of only 5wt% thiolated organoclay. The same amount of polymerizable organoclay also induces up to 90% decreases in the shrinkage stress for acrylate or thiol-acrylate systems. However,

nonreactive clays do not reduce the stress substantially and even decreases the polymerization rate in air. Additionally, the clay morphology and polymerization behavior are closely related with evolution of ultimate nanocomposite performance. Use of polymerizable organoclay significantly improves overall toughness of nanocomposites by increasing either modulus or elongation at break based on the type of polymerizable organoclay, which demonstrates the promise of this technology as a modulation and/or optimization tool for nanocomposite properties.

## TABLE OF CONTENTS

LIST OF TABLES .....	ix
LIST OF FIGURES .....	x
LIST OF SCHEMATICS.....	xiv
<b>CHAPTER</b>	
I. INTRODUCTION AND MOTIVATION.....	1
Background.....	6
Clay nanocomposites .....	7
Surfactants and polymerizable surfactants .....	13
Photopolymerization.....	21
Photopolymerization kinetics .....	23
<i>In situ</i> clay photopolymerization .....	27
Thiol-ene photopolymerization .....	29
Project Summary .....	33
II. OBJECTIVES.....	42
III. MATERIALS AND METHODOLOGY.....	49
Materials .....	49
Surfactant synthesis and clay modification .....	54
Sample Preparation.....	58
Material Characterization .....	60
Notes .....	65
IV. PHOTOPOLYMERIZATION BEHAVIOR IN NANOCOMPOSITES FORMED WITH THIOL-ACRYLATE AND POLYMERIZABLE ORGANOCLAYS .....	66
Introduction.....	67
Experimental.....	70
Materials.....	70
Methods .....	72
Results and Discussion .....	73
Conclusions.....	91
Notes .....	93
V. INFLUENCE OF PHOTOPOLYMERIZATION CHARACTERISTICS ON THERMO-MECHANICAL PROPERTIES OF NANOCOMPOSITES UTILIZING POLYMERIZABLE ORGANOCLAYS IN THIOL-ACRYLATE SYSTEMS .....	96
Introduction.....	95
Experimental.....	100
Materials.....	100
Methods .....	104

	Results and Discussion .....	105
	Conclusions.....	124
	Notes .....	126
VI.	EFFECTS OF POLYMERIZABLE ORGANOCCLAYS ON OXYGEN INHIBITION OF ACRYLATE AND THIOL-ACRYLATE PHOTOPOLYMERIZATION.....	128
	Introduction.....	129
	Experimental.....	134
	Materials.....	134
	Methods .....	135
	Results and Discussion .....	137
	Conclusions.....	159
	Notes .....	161
VII.	DECREASED POLYMERIZATION SHRINKAGE THROUGH INCORPORATING POLYMERIZABLE ORGANOCCLAYS IN ACRYLATE AND THIOL-ACRYLATE PHOTOPOLYMERIZATIONS .....	164
	Introduction.....	165
	Experimental.....	167
	Materials.....	167
	Methods .....	168
	Results and Discussion .....	173
	Conclusions.....	193
	Notes .....	195
VIII.	PHOTOPOLYMER-CLAY NANOCOMPOSITE PERFORMANCE UTILIZING DIFFERENT POLYMERIZABLE ORGANOCCLAYS .....	198
	Introduction.....	199
	Experimental.....	202
	Materials.....	202
	Methods .....	203
	Results and Discussion .....	205
	Conclusions.....	222
	Notes .....	224
VIII.	CONCLUSIONS AND RECOMMENDATIONS .....	226
	BIBLIOGRAPHY.....	240

## LIST OF TABLES

### Table

- 1.1. Chemical formula and characteristic parameter of phyllosilicates .....8
- 7.1. Shrinkage stress of typical acrylate monomers.....178
- 7.2. Shrinkage stress of different formulations with or without 3wt% organoclays .....185
- 7.3. Shrinkage stress of three different formulations with 5wt% organoclays .....185

## LIST OF FIGURES

Figure	
1.1. Typical crystalline structure of layered silicates.....	9
1.2. Types of composites arising from the interaction of clay and polymers.....	12
1.3. Chemical structures of common surfactants and some polymerizable surfactants. Shown are (A) polyoxyethylene (10) cetyl ether (Brij 56), (B) dodecyltrimethylammonium bromide (DTAB), (C) poly(ethylene glycol) – poly(propylene glycol) – poly(ethylene glycol) (Pluronic L92), (D) a Gemini surfactant, (E) long alkyl chain derivative of dimethyl aminomethyl acrylate, (F) trimethyldodecylacrylate ammonium bromide, and (G), diallylmethyldodecyl ammonium bromide.....	17
1.4. Schematic procedures for thiol or epoxy modification from basic acrylated surfactant based on organoclay template methodology.....	19
1.5. Chemical structures of (A) methyl dihydrogenated tallow sulfonate, (Me2HT) (B) tetradecyl trimethylammonium bromide (TTAB), (C) alkyl-2-acryloyloxy(ethyl) dimethylammonium bromide (acrylated) D) tetradecyl 2-(1,6-mercaptohexyl mercaptane) acetoxy(ethyl) dimethylammonium bromide (C14AT; monothiol) (E) tetradecyl 2-(bis(3-mercaptopropionate) mercaptopropionyl trimethylolpropyl) acetocyl(ethyl) dimethylammonium bromide (PSH2; dithiol).....	20
1.6. Chemical structures of commonly used photopolymerizable monomers and oligomer, where $R_1=H$ : acrylic, $R_1=CH_3$ : methacrylic. Shown are (A) (meth)acrylamide, (B) (meth)acrylate, (C) Vinyl monomer, (D) di(meth)acrylate, (E) divinyl monomer, (F) triacrylate monomer, and (G) urethane diacrylate oligomer. ....	22
3.1. Chemical structures of multifunctional acrylate and thiol monomers used in this study. Shown are (A) 1,6-hexanediol diacrylate (HDDA), (B) tripropylene glycol diacrylate (TrPGDA), (C) polymethyleneglycol diacrylate (PEGDA 600, MW=742), (D) trimethylolpropane triacrylate (TMPTA), (E) polyester type polyurethane diacrylate oligomer (CN9009, MW=3,000), (F) 1,6-hexanediol dithiol (HDT), (G) ethyleneglycol di(3-mercaptopropionate) (GDMP), (H) trimethylolpropane tris(3-mercaptopropionate) (TMPTMP), and (I) 2,2 – dimethoxyphenyl acetophenone (DMPA).. ....	52
3.2. Chemical structures of quaternary ammonium surfactants. (A) methyl dihydrogenated tallow sulfonate, (CL93A) (B) tetradecyl trimethylammonium bromide, TTAB (C) tetradecyl-2-acryloyloxy(ethyl) dimethylammonium bromide (C14A) (D) hexadecyl-2-acryloyloxy(ethyl) dimethylammonium bromide (C16A) (E) tetradecyl 2-(1,6-mercaptohexyl mercaptane) acetoxy(ethyl) dimethylammonium bromide (C14AHT; Monothiol) (F) tetradecyl 2-(1,3-mercaptopropionate mercaptopropionyl ethyleneglycol) acetocyl(ethyl) dimethylammonium bromide (C14AGT) (G) tetradecyl 2-(bis(3-mercaptopropionate) mercaptopropionyl trimethylolpropyl) acetocyl(ethyl) dimethylammonium bromide (PSH2; Dithiol) .....	55



4.1. Chemical structures of monomers including (A) 1,6-hexanediol diacrylate (HDDA), (B) tripropylene glycol diacrylate (TrPGDA), (C) 1,6-hexanediol dithiol (HDT), (D) trimethylolpropane triacrylate (TMPTA), (E) trimethylolpropane tris(3-mercaptopropionate) (TMP TMP).....	71
4.2. Chemical structures of surfactants. Shown are (A) methyl dihydrogenated tallow sulfonate, (Me2HT) (B) tetradecyl trimethylammonium bromide (TTAB), (C) tetradecyl-2-acryloyloxy(ethyl) dimethylammonium bromide (C14A) (D) hexadecyl-2-acryloyloxy(ethyl) dimethylammonium bromide (C16A) (E) tetradecyl 2-(1,6-mercaptohexyl mercaptane) acetoxyl(ethyl) dimethylammonium bromide (C14AT; Monothiol), (F) tetradecyl 2-(bis(3-mercaptopropionate) mercaptopropionyl trimethylolpropyl) acetoxyl(ethyl) dimethylammonium bromide (PSH2; Dithiol) .....	72
4.3. Photo-DSC (P-DSC) profiles of 2:1 molar ratio neat HDDA/1,6-HDT (■), 2:1 molar ratio HDDA/1,6-HDT with 3wt% PSH2 thiolated organoclay (▼), and with 3 wt% C16A acrylated organoclay (○). Photopolymerizations were initiated with 0.1 wt% DMPA using 365 nm light at 3.0 mW/cm <sup>2</sup> .....	76
4.4. Acrylate double bond conversion profiles of 2:1 molar ratio HDDA/1,6-HDT. (A) conversion profiles for neat HDDA/HDT (●), HDDA/1,6-HDT with 3 wt% (▽), 5 wt% (□), and 10 wt% (◇) C16A acrylated organoclays, and (B) for neat HDDA/HDT (●), HDDA/1,6-HDT with 3 wt% (▽), 5 wt% (□), and 10 wt% (◇) of PSH2 thiolated organoclay. Photopolymerizations were initiated with 0.1 wt% DMPA using 365 nm light at 3.0 mW/cm <sup>2</sup> .....	77
4.5. Acrylate double bond conversion profiles of 2:1 molar ratio of TrPGDA/1,6-HDT. (A) conversion profiles for neat TrPGDA/1,6-HDT (●), TrPGDA/1,6-HDT with 3 wt% (▽), 5 wt% (□), and 10 wt% (◇) C16A organoclays, and (B) for neat TrPGDA/1,6-HDT (●), TrPGDA/1,6-HDT with 3 wt% (▽), 5 wt% (□), and 10 wt% (◇) PSH2 thiolated organoclay. Photopolymerizations were initiated with 0.1 wt% DMPA using 365 nm light at 3.0 mW/cm <sup>2</sup> .....	79
4.6. Double bond versus thiol conversion at short irradiation times for diacrylate/dithiol mixture with 2:1 molar ratio based on functional groups. Conversion profiles are shown for HDDA/1,6-HDT with 3 wt% C16A acrylated organoclay (●), 3 wt% PSH2 thiolated organoclay (Δ), TrPGDA/1,6-HDT with 3 wt% C16A acrylated organoclay (■) and 3 wt% PSH2 thiolated organoclay (◇). Photopolymerizations were initiated with 0.1 wt% DMPA using 365 nm light at 3.0 mW/cm <sup>2</sup> .....	81
4.7. SAXS profiles of 3wt% TTAB-organoclay (●,○), 3wt% C16A-organoclay (▼,▽), and 3wt% PSH2-organoclay (■,□) in (A) HDDA/HDT and (B) TrPGDA/1,6-HDT mixture with 2:1 acrylate to thiol molar ratio. Filled and empty symbols represent profiles before and after polymerization, respectively. Photopolymerizations were initiated with 0.1 wt% DMPA using 365nm light at 3.0 mW/cm <sup>2</sup> .....	83
4.8. Schematic representation of clay dispersion for (A) 3 wt% C16A acrylated organoclay, and (B) 3 wt% PSH2 thiolated organoclay in HDDA/1,6-HDT mixture and (C) with 3 wt% C16A acrylated organoclay, and (D) with 3 wt% PSH2 thiolated organoclay in TrPGDA/1,6-HDT mixture. Double lines and circles indicate acrylate double bonds and thiol functional groups, respectively. All schemes represent the systems before polymerization.....	84

4.9. Thiol conversion profiles of equimolar TrPGDA/TMPTMP based on functional groups. Shown are conversion profiles for neat TrPGDA/TMPTMP (●) and TrPGDA/TMPTMP with 1 wt% (▽), 3 wt% (□), and 5 wt% (◇), and 10 wt% (▲) PSH2 thiolated organoclay. Photopolymerizations were initiated with 0.1 wt% DMPA using 365 nm light at 3.0 mW/cm <sup>2</sup> .	88
4.10. Double bond versus thiol conversion at short irradiation times for TrPGDA/TMPTMP equimolar mixture based on functional groups. Shown are (A) neat TrPGDA/TMPTMP (●), and TrPGDA/TMPTMP with 1 wt% (Δ), 3wt% (■), 5wt% (◇), and 10 wt% (▲) C16A acrylated organoclay and (B) neat TrPGDA/TMPTMP (●), and TrPGDA/TMPTMP with 1 wt% (Δ), 3wt% (■), 5wt% (◇), and 10 wt% (▲) PSH2 thiolated organoclay. Photopolymerizations were initiated with 0.1 wt% DMPA using 365 nm light at 3.0 mW/cm <sup>2</sup> .	90
5.1. Chemical structures of monomers used in this study including (1) tripropylene glycol diacrylate (TrPGDA), (2) ethyleneglycol di(3-mercaptopropionate) (GDMP), (3) 1,6-hexanediol diacrylate (HDDA), (4) 1,6-hexanediol dithiol (HDT), (5) trimethylolpropane triacrylate (TMPTA), and (6) trimethylolpropane tris(3-mercaptopropionate) (TMPTMP)	101
5.2. Chemical structures of quaternary ammonium surfactants used for clay structure modification. Shown are (7) methyl dihydrogenated tallow sulfonate, (CL93A), (8) hexadecyl-2-acryloyloxy(ethyl) dimethylammonium bromide (C16A), (9) tetradecyl 2-(1,6-mercaptohexyl mercaptane) acetoxyl(ethyl) dimethylammonium bromide (C14AHT; Monothiol), (10) tetradecyl 2-(1,3-mercaptopropionate mercaptopropionyl ethyleneglycol)acetoxyl(ethyl) dimethylammonium bromide (C14AGT), and (11) tetradecyl 2-(bis(3-mercaptopropionate) mercaptopropionyl trimethylolpropyl) acetoxyl(ethyl) dimethylammonium bromide (PSH2; Dithiol)	103
5.3. SAXS profiles of 3wt% Cloisite 93A-organoclay (○), 3wt% C16A-organoclay (●), 3wt% C14AHT-organoclay (▽), 3wt% C14AGT-organoclay (▼), and 3wt% PSH2-organoclay (■) in TrPGDA/GDMP mixture with 2:1 acrylate to thiol molar ratio.	107
5.4. Functional group conversion profiles of organoclays in 2:1 molar ratio TrPGDA/GDMP mixtures. Shown are (A) acrylate conversion profiles for neat TrPGDA/GDMP (●), TrPGDA/GDMP with 3 wt% C16A (▽), 3 wt% C14AHT (▲), 3wt% C14AGT(◇), and 3 wt% PSH2 (■) organoclays, and (B) for thiol conversion profiles for neat TrPGDA/GDMP (●), TrPGDA/GDMP with 3 wt% C16A (▽), 3 wt% C14AHT (▲), 3wt% C14AGT(◇), and 3 wt% PSH2 (■) organoclays. Photopolymerizations were initiated with 0.1 wt% DMPA using 365 nm light at 3.0 mW/cm <sup>2</sup> .	109
5.5. Double bond versus thiol conversion at short irradiation times for 2:1 molar ratio TrPGDA/GDMP mixtures. Conversion profiles are shown for neat TrPGDA/GDMP (●), TrPGDA/GDMP with 3 wt% C16A-acrylated organoclay (▽), 3 wt% C14AHT-thiolated organoclay (▲), 3 wt% of C14AGT-acrylated organoclay (◇) and 3 wt% of PSH2 thiolated organoclay (■). Photopolymerizations were initiated with 0.1 wt% DMPA using 365 nm light at 3.0 mW/cm <sup>2</sup> .	111

- 5.6. Dark acrylate conversion profiles of acrylate/thiol 2:1 molar mixtures based on functional group with or without organoclays. (A) conversion profiles for neat TrPGDA/GDMP (●), TrPGDA/GDMP with 3 wt% C16A organoclay (○), and 3 wt% PSH2 organoclay (▼), and (B) for neat TrPGDA/TMPTMP (●), TrPGDA/TMPTMP with 3 wt% C16A organoclay (○), and 3 wt% PSH2 organoclay (▼). UV light was shuttered after 6, 12, 18, and 24 seconds of irradiation at 3 mW/cm<sup>2</sup>. 0.1 wt% DMPA was used for initiation ..... 113
- 5.7. Dark thiol conversion profiles of acrylate/thiol 2:1 molar mixtures based on functional group with or without organoclays. (A) conversion profiles for neat TrPGDA/GDMP (●), TrPGDA/GDMP with 3 wt% C16A organoclay (○), and 3 wt% PSH2 organoclay (▼), and (B) for neat TrPGDA/TMPTMP (●), TrPGDA/TMPTMP with 3 wt% C16A organoclay (○), and 3 wt% PSH2 organoclay (▼). UV light was shuttered after 6, 12, 18, and 24 seconds of irradiation at 3 mW/cm<sup>2</sup>. 0.1 wt% DMPA was used for initiation ..... 115
- 5.8. Schematic representation of residual radical compositions in clay galleries after shutting off the UV with short period of initial irradiation (A) for the system with acrylated organoclay, and (B) for the system with thiolated organoclay. Used symbols are for unreacted acrylate double bonds (=), for unreacted thiol groups (■), for various propagating radicals (●) including primary thiyl radicals, acrylic radicals, and secondary radicals from reaction between thiyl radical and acrylate double bond, respectively ..... 117
- 5.9. RTIR thiol conversion profiles of HDDA/TMPTMP (●), TMPTA/1,6-HDT (▽), and TMPTA/TMPTMP (■) mixtures having 2:1 molar ratio based on functional groups. Shown are (A) conversion profiles for systems with 3 wt% C16A acrylated organoclays and (B) for systems with 3 wt% PSH2 thiolated organoclays. Photopolymerizations were initiated with 0.1 wt% DMPA using 365 nm light at 3.0 mW/cm<sup>2</sup> ..... 119
- 5.10. (A) Storage modulus profiles of 2:1 molar ratio TrPGDA/GDMP mixtures for neat TrPGDA/GDMP (●), TrPGDA/GDMP with 3 wt% C16A-acrylated organoclay (○), and 3 wt% PSH2 thiolated organoclay (▼). (B) Young's modulus of neat TrPGDA/GDMP system and TrPGDA/GDMP systems with addition of 3 wt% different type of organoclays. Samples were photopolymerized with 0.1 wt% DMPA using 365 nm light at 3.6 mW/cm<sup>2</sup> ..... 121
- 5.11. Tan δ profiles as a function of temperature of 2:1 acrylate/thiol molar ratio mixtures. A) profiles for neat TrPGDA/GDMP, TrPGDA/GDMP with 3 wt% CL93A nonreactive organoclay, 3 wt% C16A acrylated organoclay, 3 wt% C14AGT thiolated organoclay, and 3 wt% PSH2 thiolated organoclay, and (B) for neat TrPGDA/GDMP, TrPGDA/TMPTMP with 3 wt% C16A acrylated organoclay, 3 wt% PSH2 thiolated organoclay. Samples were photopolymerized with 0.1 wt% DMPA using 365 nm light at 3.6 mW/cm<sup>2</sup> ..... 123
- 6.1. Chemical structures of (A) 1,6-hexanediol diacrylate (HDDA), (B) tripropylene glycol diacrylate (TrPGDA), (C) polyethyleneglycol diacrylate (PEGDA, MW=742), (D) trimethylolpropane tris(3-mercaptopropionate) (TMPTMP), (E) polyurethane diacrylate oligomer (CN9009), (F) methyl dihydrogenated tallow sulfonate, (CL93A) (G) hexadecyl-2-acryloyloxy (ethyl) dimethylammonium bromide (C16A) (H) tetradecyl 2-(bis(3-mercaptopropionate) mercaptopropionyl trimethylolpropyl) acetoc(ethyl) dimethylammonium bromide (PSH2; Dithiol) ..... 136

- 6.2. Photo-DSC polymerization profiles of HDDA (●), PEGDA/TrPGDA (50wt%/50wt%) (○), and CN9009/PEGDA/TrPGDA (30wt%/30wt%/40wt%) (▼) systems based on weight. Samples were polymerized with approximately 3.0mW/cm<sup>2</sup> full UV light using 0.2wt% DMPA in air, respectively. The profile for PEGDA/TrPGDA in nitrogen (Δ) is included for comparison.....140
- 6.3. Photo-DSC polymerization profiles of two acrylate systems with increased concentration of TMPTMP thiol monomer. Photopolymerization was initiated with approximately 3.0mW/cm<sup>2</sup> full spectra UV light and each monomer system contained 0.2wt% DMPA. Shown are profiles in air for (A) neat HDDA (●), and HDDA with 5 mol% (○), 10 mol% (▼), 20 mol% (Δ), and 30 mol% (■) thiol groups and (B) neat PEGDA/TrPGDA (50wt%/50wt%) (●), and PEGDA/TrPGDA (50wt%/50wt%) with 5 mol% (○), 10 mol% (▼), 20 mol% (Δ), and 30 mol% (■) thiol based on functional group ratio. For comparison, heat release profile of the system with 30 mol% thiol polymerized in nitrogen is included in each figure (□) .....142
- 6.4. Photo-DSC polymerization profiles of PEGDA/TrPGDA (50wt%/50wt%) mixtures with different types of organoclays. Shown are profiles of neat PEGDA/TrPGDA (●), and PEGDA/TrPGDA with 5wt% Cloisite 93A non-reactive organoclay (○), 5wt% of C16A acrylated polymerizable organoclay (Δ), 5wt% of PSH2 thiolated polymerizable organoclay (▼). Samples were polymerized with 3.2mW/cm<sup>2</sup> full UV light using 0.2wt% DMPA in air.....145
- 6.5. Photo-DSC polymerization profiles of HDDA systems with up to 30 mol% based on functional group TMPTMP trithiol with addition of (A) 5wt% C16A acrylated and (B) 5wt% PSH2 thiolated polymerizable organoclay. Samples were polymerized with 3.0mW/cm<sup>2</sup> full spectra UV light using 0.2wt% DMPA in air. Shown are profiles of neat HDDA (●), and HDDA with 5 mol% (○), 10 mol% (▼), 20 mol% (Δ), and 30 mol% (■) thiol. For comparison, the system with 30 mol% thiol including 5wt% PSH2 organoclay is also polymerized in nitrogen and included in each figure (□) .....148
- 6.6. Photo-DSC polymerization profiles of PEGDA/TrPGDA (50wt%/50wt%) systems containing 20 mol% thiol from TMPTMP based on functional group ratio plotted by (A) heat flow rates and (B) overall theoretical conversions as a function of polymerization time. Samples were polymerized with 3.2mW/cm<sup>2</sup> UV light using 0.2wt% DMPA in air. Shown are profiles of neat PEGDA/TrPGDA (●), and PEGDA/TrPGDA with 5 wt% Cloisite 93A organoclay (○), 5wt% PSH2 thiolated organoclay (▼), and 5wt% C16A acrylated organoclay (Δ). For comparison, the system containing 20mol% thiol with 5wt% PSH2 organoclay is also polymerized in nitrogen and included in each figure (□).....150
- 6.7. Photo-DSC polymerization profiles of CN9009/PEGDA/TrPGDA (30wt%/30wt%/40wt%) systems containing 20 mol% TMPTMP monomer based on functional group ratio, plotted by overall theoretical conversions as a function of polymerization time. Samples were polymerized at 2.9mW/cm<sup>2</sup> UV light using 0.2wt% DMPA in air. Shown are profiles of neat CN9009/PEGDA/TrPGDA (●), and CN9009/PEGDA/TrPGDA with 5 wt% Cloisite 93A organoclay (○), 5wt% PSH2 thiolated organoclay (▼), and 5wt% C16A acrylated organoclay (Δ). For comparison, the polymerization profile in nitrogen for the neat system containing 20mol% thiol is included (□).....152

6.8. Photo-DSC polymerization profiles of the neat HDDA system (●), HDDA system with 5wt% C16A acrylated organoclay (▼), and with 5wt% of PSH2 thiolated organoclay (○). Samples were polymerized with 3.0mW/cm <sup>2</sup> UV light using 0.2wt% DMPA in air .....	155
6.9. RTIR conversion profiles of PEGDA/TrPGDA (50wt%/50wt%) systems containing different amount of TMPTMP monomer with addition of 5wt% C16A acrylated organoclay. Photopolymerization was initiated with 3.2mW/cm <sup>2</sup> UV light and 0.2wt% DMPA in air. (A) acrylate double bond conversion of PEGDA/TrPGDA (●), and PEGDA/TrPGDA with 10 mol% (○), 15 mol% (▼), 20 mol% (Δ), and 30 mol% (■) thiol, and (B) thiol conversion of PEGDA/TrPGDA with 10 mol% (○), 15 mol% (▼), 20 mol% (Δ), and 30 mol% (■) of thiol based on functional group ratio. ....	157
6.10. RTIR final thiol conversion profiles as a function of thiol mol% of PEGDA/TrPGDA (50wt%/50wt%) systems with addition of 5wt% polymerizable organoclays. Thiol mol% is controlled by increasing TMPTMP monomers up to 30mol% based on functional group ratio. Photopolymerization was initiated with 3.2mW/cm <sup>2</sup> UV light using 0.2wt% DMPA in air. Shown are final thiol conversions of the systems with 5wt% C16A acrylate organoclay (○) and with 5wt% PSH2 thiolated organoclay (●).....	158
7.1. Chemical structures of (A) 1,6-hexanediol diacrylate (HDDA), (B) tripropylene glycol diacrylate (TrPGDA), (C) polyethyleneglycol diacrylate (PEGDA, MW=742), (D) trimethylolpropane triacrylate (TMPTA), (E) trimethylol propane tris(3-mercaptopropionate) (TMPTMP), (F) polyurethane diacrylate oligomer (CN9009). Additionally, the chemical structure of organoclay modifiers (G) methyl dihydrogenated tallow sulfonate (CL93A), (H) hexadecyl-2-acryloyloxy(ethyl) dimethylammonium bromide (C16A), (I) tetradecyl 2-(bis(3-mercaptopropionate) mercaptopropionyl trimethylol propyl) acetoc(ethyl) dimethylammonium bromide (PSH2; Dithiol) .....	169
7.2. An illustration of the procedure (modified from ASTM D6991) for evaluating shrinkage stress during photopolymerization .....	171
7.3. Polymerization induced volume shrinkage for PEGDA/TrPGDA/TMPTMP systems as a function of thiol mole ratio controlled by the amount of TMPTMP trithiol monomer into PEGDA/TrPGDA (50/50) mixture based on weight. Samples were photopolymerized with 0.5 wt% DMPA for 20 minutes at 3.3 mW/cm <sup>2</sup> using a medium pressure mercury UV lamp .....	175
7.4. Polymerization induced volume shrinkage for PEGDA/TrPGDA (50/50) acrylate mixtures and PEGDA/TrPGDA /TMPTMP (50/50/15.6) thiol-acrylate mixtures including 20 mol% thiol without and with addition of 3wt% polymerizable organoclays. Ratios are based on mass. Samples were photopolymerized with 0.5 wt% DMPA for 20 minutes at 3.3 mW/cm <sup>2</sup> using a medium pressure mercury UV lamp. ....	177
7.5. (A) Polymerization induced shrinkage stress and (B) deflection of the steel plates induced by shrinkage stress for neat TMPTMA, CN9009/PEGDA/TrPGDA (30/30/40) acrylate mixture, and TMPTA/TMPTMP (60/40) thiol-acrylate mixture. Ratios are based on mass. Samples were photopolymerized with 0.5 wt% DMPA for 20 minutes at 15.0 mW/cm <sup>2</sup> using 365 nm UV light .....	180

- 7.6. Near-IR spectra for neat TMPTA systems before (solid line) and after irradiation for specified time. Spectra were obtained using separate samples after irradiation for 2, 4, 6, 10, and 300 seconds, respectively. Samples were photopolymerized with 0.5 wt% DMPA at 5.5 mW/cm<sup>2</sup> using 365 nm UV.....181
- 7.7. Shrinkage stress as a function of conversion for neat TMPTA (●) and TMPTA/TMPTMP (60/40) mixture (○) based on weight. Samples were photopolymerized with 0.5 wt% DMPA using 365 nm UV at 5.5 mW/cm<sup>2</sup>.....183
- 7.8. Polymerization induced shrinkage stress (A) for TMPTA (○) and CN9009/TrPGDA/TMPTMP (30/30/40) acrylate mixture (●), and (B) for TMPTMA/TMPTMP (60/40) thiol-acrylate formulations (◆) with 5wt% organoclays. Ratios are based on mass. Samples were photopolymerized with 0.5 wt% DMPA for 20 minutes at 15.0 mW/cm<sup>2</sup> using 365 nm UV light .....187
- 7.9. Final acrylate conversions obtained by simultaneous near-IR measurements during shrinkage tests for TMPTA systems without or with 5wt% organoclays. Samples were photopolymerized with 0.5 wt% DMPA for 20 minutes at 15.0 mW/cm<sup>2</sup> using 365 nm UV light.....188
- 7.10. RTIR conversion profiles of thiol groups for TMPTA/TMPTMP (60/40) mixtures based on weight. Shown are thiol conversions for neat TMPTA/TMPTMP (●), with addition of 5wt% Cloisite Na natural clay (○), 5wt% Cloisite 93A organoclay (▼), 5 wt% C16Aorganoclay (Δ), and 5 wt% PSH2 organoclay (■). Samples were photopolymerized with 0.5 wt% DMPA for 20 minutes at 15.0 mW/cm<sup>2</sup> using 365 nm UV .....190
- 7.11. Shrinkage stress profiles as a function of clay wt% for (A) CN9009/TrPGDA/TMPTMA (30/30/40) acrylate mixture and (B) TMPTA/TMPTMP (60/40) thiol-acrylate mixture based on weight ratio with different types of clays. Shown are shrinkage stress profiles for the systems with Cloisite Na natural clay (◆), Cloisite 93A organoclay (○), C16A-acrylated organoclay (▼), and PSH2 thiolated organoclay Samples were photopolymerized with 0.5 wt% DMPA for 20 minutes at 15.0 mW/cm<sup>2</sup> using 365 nm UV light .....192
- 8.1. Chemical structures of monomers used in this study including (A) tripropylene glycol diacrylate (TrPGDA) (B) polyethyleneglycol diacrylate (PEGDA600, MW=742), (C) trimethylolpropane tris(3-mercaptopropionate) (TMPTMP), and (D) polyurethane diacrylate oligomer (CN9009). Additionally, structures of clay modifiers including (E) methyl dihydrogenated tallow sulfonate, (CL93A) (F) hexadecyl-2-acryloyloxy(ethyl) dimethylammonium bromide (C16A), and (G) tetradecyl 2-(bis(3-mercaptopropionate) mercaptopropionyl trimethylolpropyl) acetocyl(ethyl) dimethylammonium bromide (PSH2; Dithiol) are shown .....204
- 8.2. RTIR conversion profiles of CN9009/PEGDA/TRPGDA (3:3:4 by mass) mixtures including 20mol% thiol from TMPTMP with and without addition of 3wt% organoclays. Shown are profiles of (A) acrylate conversion for neat CN9009/PEGDA/TRPGDA (●), CN9009/PEGDA/TRPGDA/ TMPTMP with 3 wt% CL93A (▽), 3 wt% C16A (■), and 3 wt% PSH2 (◇) organoclay and (B) thiol conversion for neat CN9009/PEGDA/TRPGDA/ TMPTMP (●), CN9009/PEGDA/TRPGDA/TMPTMP with 3 wt% CL93A (▽), 3 wt% C16A (■), and 3 wt% PSH2 (◇) organoclay. Polymerizations were initiated with 0.2 wt% DMPA using 365nm light at 3.0 mW/cm<sup>2</sup> .....208

- 8.3. Storage modulus profiles of CN9009/PEGDA/TRPGDA (3:3:4 by mass) mixtures including 20mol% thiol from TMPTMP with and without addition of 5wt% organoclays. Shown are profiles for neat CN9009/PEGDA/TRPGDA/TMPTMP (●), CN9009/PEGDA/TRPGDA/ TMPTMP with 5 wt% CL93A (○), with 5 wt% C16A-acrylated organoclay (▼), and 5 wt% PSH2 thiolated organoclay (Δ). Samples were photopolymerized with 0.5 wt% DMPA using 365 nm light at 3.6 mW/cm<sup>2</sup> .....210
- 8.4. Tan δ profiles as a function of temperature of CN9009/PEGDA/ TRPGDA (3:3:4 by mass) mixtures including 20mol% thiol from TMPTMP with increase of organoclay amount. (A) the systems with 1wt%, 3wt%, and 5wt% C16A acrylated organoclays and (B) with 1wt%, 3wt%, and 5wt% PSH2 thiolated organoclays. The profile for the neat CN9009/PEGDA/TRPGDA /TMPTMP system is included in each figure for comparison. Samples were photopolymerized with 0.5 wt% DMPA using 365 nm light at 3.6 mW/cm<sup>2</sup> .....211
- 8.5. DMA tensile profiles of CN9009/PEGDA/TRPGDA (3:3:4 by mass) mixtures including 20mol% thiol from TMPTMP with increase of organoclay amount. Shown are profiles of the systems (A) with 1wt%, 3wt%, and 5wt% PSH2 thiolated organoclays and (B) with 1wt%, 3wt%, and 5wt% C16A acrylated organoclays. The profile for the neat CN9009/PEGDA/TRPGDA/ TMPTMP system is included in each Figure for comparison. Samples were photopolymerized with 0.5 wt% DMPA using 365 nm light at 3.6 mW/cm<sup>2</sup> .....213
- 8.6. Comparison of DMA tensile profiles by adding 3wt% different type of organoclays into CN9009/PEGDA/TRPGDA (3:3:4 by mass) mixtures including 20mol% thiol from TMPTMP. The profile for the neat system is included for comparison. Samples were photopolymerized with 0.5 wt% DMPA using 365 nm light at 3.6 mW/cm<sup>2</sup> .....215
- 8.7. Comparison of relative toughness of the systems without or with addition of 3wt% different organoclays into (A) CN9009/PEGDA/TRPGDA (3:3:4 by mass) acrylate mixtures and (B) CN9009/PEGDA/TRPGDA (3:3:4 by mass) thiol-acrylate mixtures including 20mol% thiol from TMPTMP. Toughness is calculated from the area of stress-strain curves in Figure 8.5 and 8.6.....217
- 8.8. Water weight loss profiles as a function of time from water vapor permeation tests based on the ASTM E96 standard with and without addition of 3wt% organoclay into CN9009/PEGDA/TRPGDA (3:3:4 by mass) mixtures including 8mol% thiol from TMPTMP. Shown are profiles normalized of with 100μm thick films for neat CN9009/PEGDA/TRPGDA/ TMPTMP (●), CN9009/PEGDA/TRPGDA/TMPTMP with 3 wt% CL Na natural clay (○), with 3 wt% CL93A organoclay (▼), with 3 wt% C16A-acrylated organoclay (Δ, ■), and with 3wt% PSH2 thiolated organoclays (□, ◆). Samples were photopolymerized with 0.5 wt% DMPA using 250~450 nm light at 18 mW/cm<sup>2</sup>. The result using Mylar PET (100μm) film (◇) is included for evaluation of experimental accuracy. ....219
- 8.9. Water Vapor Transmission Rate (WVTR) as a function of (organo)clay type in the thiol-acrylate systems based on CN9009/PEGDA/TRPGDA (3:3:4 by mass) mixtures including 8mol% thiol from TMPTMP without or with addition of 3wt% different type of organoclay. WVTR is calculated utilizing the results from Figure 8.8.....220

- 8.10. TGA thermal degradation profiles in air of (A) PEGDA/TrPGDA (50:50 by mass) systems with gradual increase of TMPTMP thiol monomers up to 30 mol% and (B) PEGDA/TrPGDA (50:50 by mass) systems including 20mol% thiol from TMPTMP without or with addition of 5wt% organoclays. Samples were polymerized at  $3.0\text{mW/cm}^2$  using 0.2wt% DMPA. ....221



## LIST OF SCHEMATICS

### Scheme

1.1. Radical chain transfer mechanisms in thiol-ene reaction. ....	30
1.2. Schematic expression of the reaction mechanisms of thiol-ene systems in the presence of oxygen. ....	32
6.1. Radical chain transfer mechanisms in thiol-ene reaction. Reactions represent (6.1) initiation of primary thiyl radicals, (6.2) formation of secondary radicals, and (6.3) secondary radical chain transfer to thiol groups.....	131
6.2. Schematic expression of the reaction mechanism of thiol-ene systems in the presence of oxygen. ....	132

## CHAPTER 1

### INTRODUCTION AND MOTIVATION

Composition materials, commonly referred to as composites, are materials traditionally comprised of two or more constituents having inherently different physical or chemical properties or both. In most cases, composite materials show macroscopically or microscopically phase-separated morphology according to the original dimension of each component as well as the extent of interaction between the components during mixing process. Composite have been widely utilized to obtain desired performance in materials for several thousand years. From ancient examples such as wattle and daub, bricks made of straw and mud, and composite bows combining two different wood types, various composites exist in a wide variety of modern daily-life products such as bathtubs, fishing poles, and concrete that is used more than any other artificial composite materials today.[1,2]

In terms of material science engineering, composites have been more specifically defined as any combination of different materials, typically two, in which one of the components acts as a reinforcing element and is incorporated into another matrix material. Reinforcing materials are typically much stronger with low densities than the matrix material.[3] More specifically, most reinforcing materials are inorganic materials such as metals or ceramics in the form of fibers, sheets, or particles whereas the common continuous matrix phase is composed of natural or synthetic organic materials. Composites are therefore often known as inorganic-organic hybrid technology. When the composite materials are designed and processed appropriately, they combine the advantages of the inorganic material with the basic properties of the organic matrix materials to achieve desirable qualities not available by using each material individually. The primary aim of processing composites is thus to improve material properties such as

stiffness, toughness, small molecule barrier characteristics, and dimensional stability by incorporating inorganic fillers that can bind, strengthen, or fill the organic phases. Additionally, composites often reduce material cost by adding inexpensive and readily available inorganic fillers or enhance processibility by incorporation of lubricant particles.

Polymers are the most commonly and widely used synthetic materials for various applications of composites. Since the early use of natural polymers, this polymer composite technology has been commonly applied for enhancing the performances of final products. A well-known example is the manufacture of black automobile tires by combining natural rubber with carbon black from the early twentieth century. In this combination, carbon black not only enhances the strength of rubber as a reinforcing filler but also increases tire life by improving barrier and heat dissipating properties.[4] Likewise, combination of a number of synthetic polymers with other materials has often allowed unique properties. Typical examples of synthetic polymer composites include glass, carbon, silica, mica, or polymer-fiber-reinforced thermoplastic or thermosetting plastics.[5,6] Glass fibers have been commonly used for preparing fiber-reinforced polymer composites when embedding into thermosetting resins such as an epoxy or unsaturated polyester resin. Carbon fiber is another fiber-like filler that has been widely used and usually provides extremely high levels of strength and stiffness. Many carbon-fiber composites can exhibit several times the stiffness of steel.

In preparation of polymer composites, numerous types of polymers have been utilized for the matrices when considering both the compatibility with reinforcing fillers and end performance. Based on the diversity of combinations between matrix materials and fillers and the resulting unique and excellent performance characteristics, polymer composites combining thermoplastic or thermosetting resins with a suitable choice of fillers have been utilized in many engineering applications such as aircraft components, automobile parts, boat bodies, and chemical reactors.

Recent research has shown the distinctive properties of smaller size fillers; typically nanometer sized particles, and opened diverse possibilities for utilization. Many studies have focused on investigation of the size effects of fillers on the ultimate composite including physical,[6-8] electro-optical,[9,10] and barrier properties.[11,12] Over the past two decades, this interest has led to significant progress in not only developing new type of fillers but also in controlling the structure and the dimension of fillers on the nanometer scale. A wide range of nanoparticles are currently available and used for preparing polymer composites. Typical examples of such nanoparticles are rod shape carbon nanotubes,[13,14] plate like carbon sheets such as graphene,[15,16] and simple spherical dimension particles based on various metal complexes such as silver, gold, silica, zinc or titanium based oxides, and carbon black.[17-19] Depending upon the performances and processing factors of polymer incorporating nanocomposites or nanocomposites, numerous polymer-nanoparticle combinations have been developed and are being applied for various applications including high performance engineering materials and biomaterials.

While many nanoparticles have been investigated to produce polymer nanocomposites, unfortunately most are relatively difficult to produce and thus quite expensive compared to conventional fillers. This cost factor has been one of the significant limitations for real application of the nanocomposite technology. Recently, quite inexpensive clay nanoparticles which are easily obtained have attracted much research interest industrially and academically for inclusion in various polymer matrices with nanometer scale dispersion. The physical plate-like structure and chemical nature of clay particles allow a nano-scale dispersed morphology in polymer matrices by simple delaminating chemistry, leading to significant property enhancement.[20-22] In the preparation of nanocomposites utilizing natural clay minerals, however, there still remain several critical challenges such as sufficient and/or complete delaminating of each clay plate, preventing the dispersed plates from re-aggregating, and reducing or eliminating

solvents that are commonly used during delaminating process. *In situ* preparation of polymer-clay nanocomposites has been proposed as a promising tool for overcoming such difficulties in conventional composite processes and promises many other advantages.[21-24] Based on previous work studying *in situ* polymerization utilizing clay minerals, Toyota research first applied the technology in industrial production in the early 1990s.[25,26] Various polymer systems were then investigated to form clay polymer nanocomposites utilizing one-pot *in situ* polymerization. More recently free radical polymerization clay systems have been examined and it has been proposed to apply this *in situ* polymerization technique to the field of photopolymer materials.[27-30]

Photopolymerization utilizes light energy to form polymers and, therefore, may provide a simple method for *in situ* preparation of polymer-clay nanocomposites from well dispersed clay-monomer formulations.[28,30] Conventional composite manufacturing processes involve either melt-mixing of polymer with inorganic fillers or solvent based processes and thus usually cause thermal degradation of the polymer or release large amounts of volatile organic compounds (VOC) during the process.[31,32] *In situ* photopolymerization may overcome these drawbacks of conventional processes by producing polymer through irradiation at ambient temperature with 100% solid content. Forming nanocomposites by *in situ* photopolymerization thus allows ultra-fast productivity, easy spatial and temporal control, and an environmentally friendly process. [27-28, 36-37]

Incorporation of clay particles into photopolymerization systems, however, may significantly influence the reaction behavior of the systems due to additional interaction between organic reactants and inorganic clay particles, subsequently resulting in different evolution of ultimate composite properties. Furthermore, previous work studying clay nanocomposites have demonstrated that the modification of clays with organic surfactants is necessary for achieving nanometer scale dispersion of clay particles. This modification makes the interplay among factors during *in situ* polymerization more

complicated. Not only the structure of surfactant used for clay modification but also its compatibility with reactants may significantly influence the degree of interactions between each component in the system, resulting in differences in aspects such as morphology of clay particles in the system before and after polymerization, reaction mechanism and kinetics, and resultant properties of cured composites. In order to achieve an advanced composite material based on *in situ* photopolymerization, therefore, a fundamental understanding of all the processing factors is essential.

In the fast few years, research groups have investigated clay photopolymer nanocomposite systems based on conventional acrylate or methacrylate free radical polymerization systems initiated by UV irradiation.[27-30, 39-41] Remarkable progress has been achieved in understanding the important factors in processing nanocomposites, which include clay modification, dispersion of clay particles into the reaction mixtures, its formation of ultimate clay morphology, and the concomitant effects on both reaction behavior and final composite properties. Whereas substantial improvements have been achieved compared to conventional micrometer scale dispersed composites, several challenges still exist. For instance, although acrylate-based photopolymerization is widely used in numerous applications, improvements in several properties such as shrinkage during polymerization, gas barrier properties, and abrasion and impact resistance are needed for enhancing performance of these materials. [42,43] The addition of dispersed clay particles, however, has still not eliminated these disadvantages to any significant degree. In addition, previous work has mainly depended on the use of non-reactive organic surfactants in surface modification of clay particles, which is likely reason that only achieved partially delaminated or intercalated clay morphology at best was achieved in most cases. Because complete delamination of clay particles is critical for maximization of filler effects to produce a true nanocomposite,[33, 44-46] it may be expected that further improvement in nanocomposite performances could be realized if

with increased interactions between the particles and monomers by incorporating polymerizable functional groups into the surfactant structure.

Additionally, thiol-ene step-growth copolymerization has been extensively studied recently. This new category of photopolymerization process provides many advantages including absence of oxygen inhibition, low shrinkage, and increased toughness.[47-52] In conjunction with suitable polymerizable organoclays, photopolymer-clay nanocomposites formed using these advanced photopolymerization techniques could be a primary candidate for overcoming drawbacks of conventional photopolymer systems. However, little is known regarding the effects of organoclays on photopolymerization kinetics and final properties for these promising photopolymerization systems. Due to the inherently different reaction mechanism of step-growth copolymerization, photopolymerization behavior of thiol-ene photopolymer clay nanocomposites could be quite different from that of conventional acrylate systems. This research therefore particularly focuses on examining the overall processing factors in clay modification utilizing novel polymerizable organoclays, dispersion of clay particles in the reaction mixture, and polymerization of the mixture utilizing various thiol-ene photopolymerization systems.

### Background

In this chapter, the background for investigating the use of polymerizable organoclays to develop advanced photopolymer clay nanocomposites based on *in situ* photopolymerization utilizing various acrylate and thiol-acrylate photopolymerization techniques is provided. To present a basic understanding for this research, four fundamental technical issues will be discussed. The first section describes the principles in fabricating clay nanocomposites dealing with the structure of clay particles,

delaminating chemistry via surface modification, and dispersion processes in reaction mixtures. The second section is devoted to details in fundamental surfactant chemistry and the preparation of polymerizable surfactants which are utilized in this research for achieving the overall goal. Next, the third section introduces the concept of free radical photopolymerization processes and details related with *in situ* clay nanocomposite photopolymerization. The fourth section will explain advanced thiol-ene photopolymerization including kinetics and reaction mechanisms involved, particularly focusing on the advantages overcoming the limitations in contemporary (meth)acrylic photopolymerization systems. Finally, an overview of the research investigating the overall impact of polymerizable organoclays on nanocomposite processes and ultimate performance will be provided with potential uses in photopolymer applications.

### Clay nanocomposites

Clay minerals are commonly referred to as a hydrous aluminium phyllosilicate which includes different cations such as iron, magnesium, and various alkali metals. The structures of clay minerals are similar to those of micas based on flat hexagonal sheets. From the chemical composition and the crystalline structure of the phyllosilicates, materials in this category are also often referred as 'layered silicates' in many industrial uses. These clay minerals are very common and found in numerous areas including a variety of sedimentary rocks. Clays basically consist of tetrahedral sheets and octahedral sheets, usually categorized by the ratio of these two sheets in the structure. For instance, a 2:1 clay structure indicates that one octahedral sheet is sandwiched between two tetrahedral sheets in the stacked morphology of clay particles.[32, 53-54] While 1:1 and 2:1 structures of clay minerals are naturally found, the 2:1 structure, often referred as a smectite structure, is more common in clay materials. In the formation of a 2:1 structure,



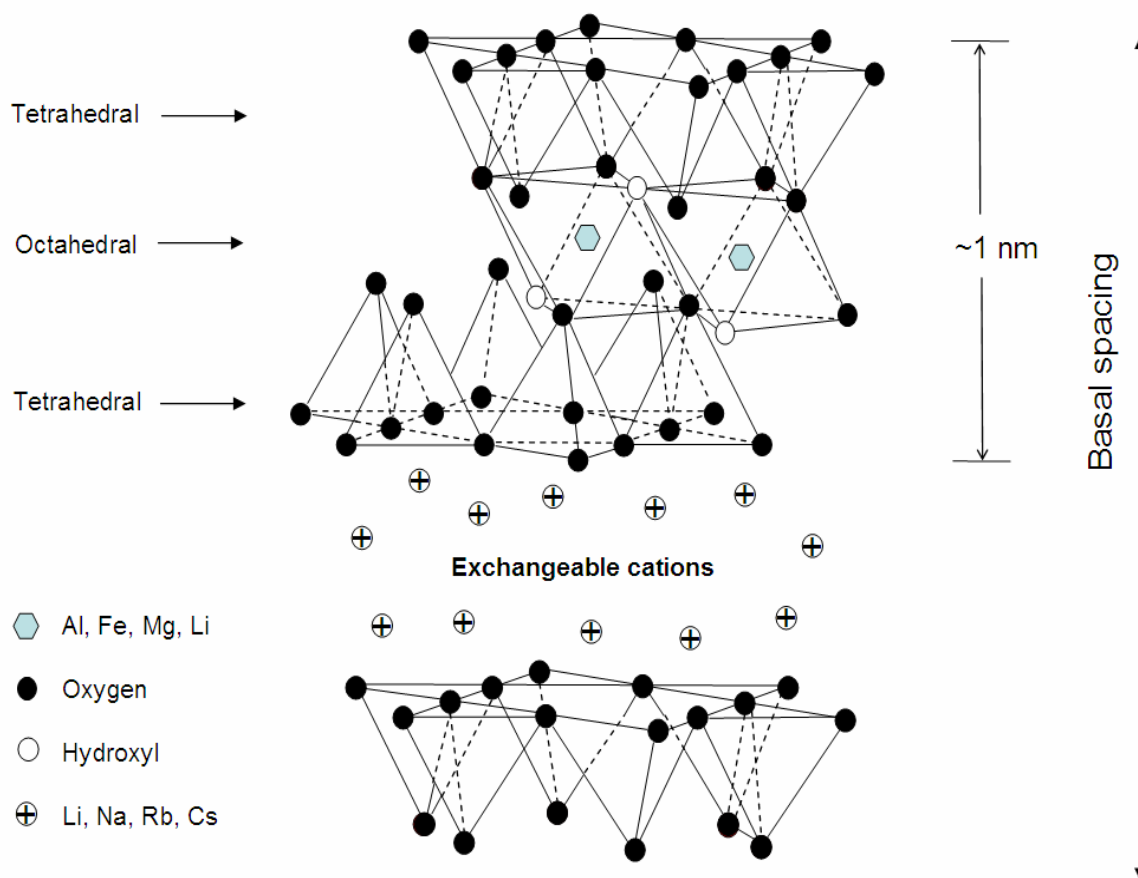
bonding between the tetrahedral and octahedral sheets requires that the tetrahedral sheet be corrugated or twisted, resulting in a ditrigonal distortion to the hexagonal array, followed by flattening of the octahedral sheet. This minimizes the overall distortion forces of the crystallite and thereby induces a layered flat structure. Because each of these layers is weakly stacked together with a regular van der Waals gap, small molecules can easily intercalate between the layers. [55] For this reason, the phyllosilicates that are most commonly used in the preparation of nanocomposite materials belong to the structural family of 2:1 layered silicates such as montmorillonite (MMT), hectorite, and saponite. Details regarding the chemical formula for these representative 2:1 layered silicates are provided in Table 1.

Figure 1.1 shows a schematic of the crystal structure of a 2:1 smectite layered silicate. Each layer thickness is approximately 1nm and the lateral dimensions of the layers vary from 50nm to several hundreds nm. Stacking of the layers based on ionic interaction between counter ions in each layer generates a regular van der Waals distance called the interlayer or gallery.[56,57] Isomorphic substitution within the layers generates negative charges that are counterbalanced by alkali cations existing in the galleries. These negative charges are, however, not critical point charges but are often hydrated charges spreading over the layer surface and its edges evenly.[33,58]

**Table 1.1.** Chemical formula and characteristic parameter of phyllosilicates

<b>2:1 Phyllosilicate</b>	<b>Chemical formula</b>	<b>CEC (mequiv/100 g)</b>	<b>Particle length (nm)</b>
<b>Montmorillonite</b>	$M_x(Al_{4-x}Mg_x)Si_8O_{20}(OH)_4$	110	100 - 150
<b>Hectorite</b>	$M_x(Mg_{6-x}Li_x)Si_8O_{20}(OH)_4$	120	200 - 300
<b>Saponite</b>	$M_xMg_6(Si_{8-x}Al_x)Si_8O_{20}(OH)_4$	87	50 -60

M, monovalent cation; x, degree of isomorphous substitution (between 0.5 and 1.3).



**Figure 1.1.** Typical crystalline structure of layered silicates.

Montmorillonite, hectorite, and saponite layered silicates, the commonly used clay minerals, may have two types of structures, i.e. tetrahedral-substituted and octahedral substituted. In the tetrahedrally substituted structure, the negative charges are placed mainly on the surface of silicate layers while the charges in octahedrally substituted structure are located at the edges. Due to a structure variation in a crystal lattice, this charge is not locally constant but rather varies from layer to layer. Therefore, the charges should be considered as an average value of the whole crystal. This

difference in negative surface charges caused by the structure variation in the layered silicates can be characterized by the cation exchange capacity (CEC) expressed in meq/100g that demonstrates the polarity of a clay mineral.

In order to prepare polymer-layered silicate nanocomposites (PLS) or commonly called polymer-clay nanocomposites with designed performance, clay particles should be dispersed into polymer matrices as independent and individual layers as much as possible. Aforementioned hydrated interlayer galleries of clay particles provide many strategies for achieving nanometer scale dispersion of each silicate layer in polymer matrices. Much research has been devoted to exfoliating the clay layers utilizing solvating characteristics of layered silicates via three typical methodologies including exfoliation-adsorption,[59-61] melt intercalation,[32, 62-63] and *in situ* intercalated polymerization.[21-24]

In the exfoliation-adsorption process, the clay particle is first exfoliated into single layers in a favorable solvent. Due to the inherently weak forces involving in the stacking of the silicate layers in clay particles, this exfoliation of clay is easily achieved by using appropriate solvents that are also capable of dissolving the designated polymer. Afterward, polymers are dissolved in the filler solution and polymer chains diffuse into exfoliated interlayer to adsorb on the surface of the delaminated layers. By evaporating the solvent, intercalated nanocomposite morphologies are obtained. The second method based on melt blending is usually used for thermoplastic polymers. Clay is mixed with molten polymers that are sufficiently compatible with the clay surface. The polymer chains move slowly into the interlayer and eventually form either an intercalated or an exfoliated (when highly compatible to the clay surface) nanocomposite structure. In the third technique, clay is first swollen in a liquid monomer mixture for several hours to allow sufficient monomer diffusion into the gallery. The nanocomposite material is then directly obtained by polymerizing the filler-monomer mixture utilizing heat or light energy. This method has many advantages compared to the other two techniques by avoiding the use of solvent or heat during the process. While the melt-blending

technology is still widely preferred in many industrial nanocomposite preparations based on the easy adaptation of existing polymer processing equipment, thermal degradation of polymer matrices often causes undesirable properties and thus many research studies have contributed to developing nanocomposites based on the *in situ* procedure.[64,65]

Since *in situ* inter-lamellar polymerizations were first introduced in the early 1960s,[66] polymer-clay nanocomposites based on *in situ* polymerization techniques have been widely studied to improve various properties of polymeric materials.[67-69] For *in situ* clay nanocomposite system, the degree of delamination of each silicate layer in the clay particles with intercalated or exfoliated morphology relies primarily on both the surface modification chemistry and the conditions of the composite process. Upon proper dispersion in polymer matrices, the nanometer dimensions of clays with very high surface area allow much higher polymer-filler interaction, resulting in potential significant property enhancement of the ultimate nanocomposites.[56] The morphology of clay dispersion plays a critical role in enhancing the final properties of nanocomposites. Depending on the degree of interfacial interaction between polymer and clay, three kinds of clay dispersion can be achieved as shown in Figure 1.2.[33]

When polymer chains are unable to diffuse into the clay interlayer, a phase separated morphology is formed, having similar characteristics of traditional microcomposites. For intercalated clay dispersions, some polymer chains insert into the clay galleries, and well-ordered multilayer morphology is obtained. In this state, enhancement in composite properties is relatively insignificant and similar to that of ceramic materials. In exfoliated clay nanocomposites, clay particles are completely delaminated and individual clay layers are separated in continuous polymer matrices with uniformly dispersed morphology. This clay morphology allows large interactions between clay and polymer, which allows significant increase in performance with relatively small amounts of clay loading. For this reason, exfoliation of clays has allowed significant enhancement of the mechanical, thermal, and gas barrier properties of

polymer materials.[29,44,70,71] For instance, exfoliated clay nanocomposites produce over 60% improvement in modulus and tensile properties in comparison to macro-scale composites in organoclay-acrylic systems. Simultaneously, in accordance with our research goal, particular emphasis will be placed on understanding exfoliation behavior.

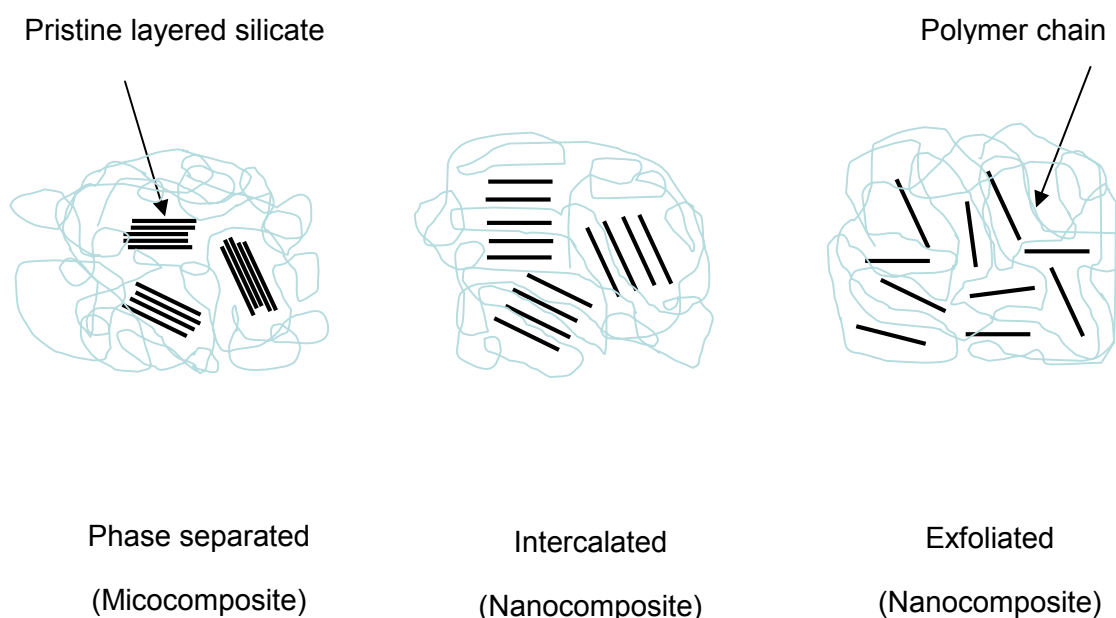


**Figure 1.2.** Types of composites arising from interaction of clay and polymers.

Achieving exfoliated clay dispersions is thus most desirable, but relatively difficult in clay nanocomposite processing. Exfoliation essentially requires surface modification of clays due to the inherent high polarity of clay, which involves fine tuning the surface chemistry of clay using ion exchange with organic and inorganic cations. The dispersion degree of the layered silicate in a certain polymer matrix depends on the chemical compatibility between the polymer and the interlayer cations. Pristine layered silicates usually contain hydrated  $\text{Na}^+$  or  $\text{K}^+$  ions [72]. Therefore, unmodified layered

silicates are very polar and only miscible with hydrophilic polymers such as poly(ethylene oxide) and poly(vinyl alcohol).[73,74]

In order to provide an enhanced compatibility to various polymer matrices, the polar clay surface is typically modified to be more organophilic. This change is generally achieved by ion-exchange utilizing suitable organic surfactants such as primary, secondary, tertiary, and quaternary alkylammonium or alkylphosphonium cations. While numerous organic surfactants have been studied for clay processing, the most important category of surfactants that are widely used in polymer clay nanocomposite process is quaternary ammonium salts due to their high ion exchange efficacy. These organic surfactants in organoclay structure significantly lower the surface energy of the clay layers and thereby polymer chains can be more easily wetted on the layer surface generating a larger interlayer distance.[46,66,75-82] Because the degree of surfactant-monomer/polymer interaction is crucial for achieving nanometer scale dispersion of clay layers and thus also critically affects the nanocomposite properties, consideration of surfactant chemistry is necessary for control in the nanocomposite formation process.

### Surfactants and polymerizable surfactants

Surfactants are organic compounds with an amphiphilic molecule structure which contains both hydrophobic (non-polar) groups and hydrophilic (polar) groups. When surfactants are mixed in water, the hydrophilic water soluble group is likely to remain in the water phase, whereas hydrophobic water insoluble groups prefer to self-associate or segregate at the air-water interface. If the water includes organic components such as oil and monomer, hydrophobic groups (usually with a long aliphatic tail structure) extends to the oil phase while the polar head groups remain in the water phase, resulting in the formation of a water-organic phase interface. This mechanism is used in emulsion and

suspension polymerization process. As discussed, this behavior of the amphiphilic surfactant molecules may allow the covering of the polar clay surface with hydrophobic non-polar alkyl tails due to the high affinity between the hydrophilic head group in surfactants and the polar silicate surface, resulting in significant increase in the organophilic characteristics of clays.

A wide variety of surfactants are used in applications including detergent, cosmetics, paints, and more advanced lyotropic liquid crystals (LLC). Based on the specific purpose of utilizing surfactants, the structure of surfactant varies. Surfactants can be non-ionic and cationic according to the structure of the polar head group. Both types of surfactants typically have long aliphatic chains producing the hydrophobicity of the surfactant molecules. Non-ionic surfactants consist of longer and larger polar head groups than in ionic surfactant structures due to their comparatively low polarity. While diblock structures of non-ionic surfactant consisting of one polar chain with one non-polar chain is common, some triblock surfactants have been also developed for pharmaceutical applications, in which two different polar chains are incorporated.[83] With higher polarity compared to common non-ionic surfactants, ionic surfactants based mostly on cationic head groups are used for various engineering applications but are not limited with the development of diverse structures in building up the surfactant molecules.

Quaternary ammonium surfactants widely used in clay surface modification are a cationic in nature. When the quaternary ammonium surfactants are mixed with clay particles in aqueous solution, the cationic ammonium head groups anchor onto the clay surface that are negatively charged. The attached long hydrophobic alkyl chains remain in the interlayer gallery of the clay particle. Diverse ordered structures can thus be formed based on both the surfactant concentration and the structure of attached alkyl chains such as length and branching degree. By increasing the surfactant concentration, more ordered alignment of surfactant molecules in the gallery is obtained. The surfactants are further aligned with formation of bi- and even tri-layers by further increasing the

concentration. Differences in the surfactant chain structure attached to head group also affects the extent of surfactant molecule alignment with similar concept. Because the degree of alignment and the thickness of surfactant layer are directly related to the exfoliated interlayer distance, control of surfactant structure and use of effective concentration are important for achieving clay exfoliation.[84]

In the clay surface modification utilizing quaternary ammonium surfactants, the hydrophobic long alkyl chains in the surfactant significantly lower the polarity of clay surface, resulting in increase of clay-polymer compatibility that can hopefully induce enhanced clay delaminating during *in situ* polymerization processes.[32,33,70,85,86] Exfoliated clay morphologies highly desired for maximization of property improvement are only formed when each clay layer is sufficiently delaminated and randomly dispersed in the polymer matrix. Successful clay exfoliation, however, is quite challenging due to the inherent aggregation characteristics of clays. As discussed, exfoliated clay morphology is crucial for nanocomposite property. Many research efforts have contributed to achieving enhanced clay exfoliation based on clay modification utilizing quaternary ammonium surfactants in *in situ* polymerization. Pinnavaia *et al.* has developed thermoset polymer nanocomposites utilizing epoxy precursors with significantly improved thermo-mechanical properties compared to microscale composite materials.[87-89] For photopolymers, Decker *et al.* first showed development of photopolymer clay nanocomposites based on *in situ* photopolymerization utilizing commercially available organoclays modified by quaternary ammonium surfactants.[27,28,90] Subsequent studies have demonstrated that quaternary ammonium surfactants can facilitate highly delaminated clay dispersion for *in situ* photopolymerization systems utilizing multifunctional acrylate based monomers.[39-41,85,86]

Most of the surfactants utilized in these studies were non-reactive surfactants and are not capable of being incorporated into the polymer network covalently. Without



chemical reaction, polymer-clay interactions mainly depend on the affinity between surfactant molecules and polymer chains. These non-reactive surfactants thus have inherent limitation in effectiveness. The degree of clay exfoliation is still not sufficient and reaches intermediate intercalated morphology at best. Additionally, the non-reactive surfactants remain as impurities in the composites system, which might cause long-term leaching problems that affect the final performance.[91] Because closer interaction between fillers and polymer matrices usually induces significant improvement in many performances in composite systems, the increase of interaction based on strong covalent bonds between the organic layer on organoclay particles and polymer chains may present a new avenue in development of advanced photopolymer clay nanocomposites with fully exfoliated clay morphology.

In other areas such as LLC photopolymerization, tools for overcoming this limitation of non-reactive surfactants can be found. In these research fields, incorporation of reactive groups that are capable of polymerizing into stable vesicles and assemblies has been investigated to enhance mechanical stability of LLCs by stabilizing the ordered structure of the materials. To this end, various types of reactive quaternary ammonium surfactants that incorporate (meth)acrylate functional groups in the structure were developed by many research groups such as Regen *et al.*, and Nagai *et al.* [92-94] Figure 1.3 shows examples of chemical structures for these reactive surfactants. For comparison, the structures of conventional diblock, triblock, and cationic surfactants are also included.

If these (meth)acrylate based reactive surfactants could be used in organic modification of clay surfaces, increased polymer-particle interactions through strong covalent bond connections would be achieved and subsequently significant enhancement in nanocomposite properties may be possible. On the basis of this expectation, this research will utilize polymerizable novel surfactants bearing relevant functional groups to photopolymerization systems to modify the clay surface. Polymerizable surfactants can react with monomers and incorporate into polymer matrices during the polymerization.

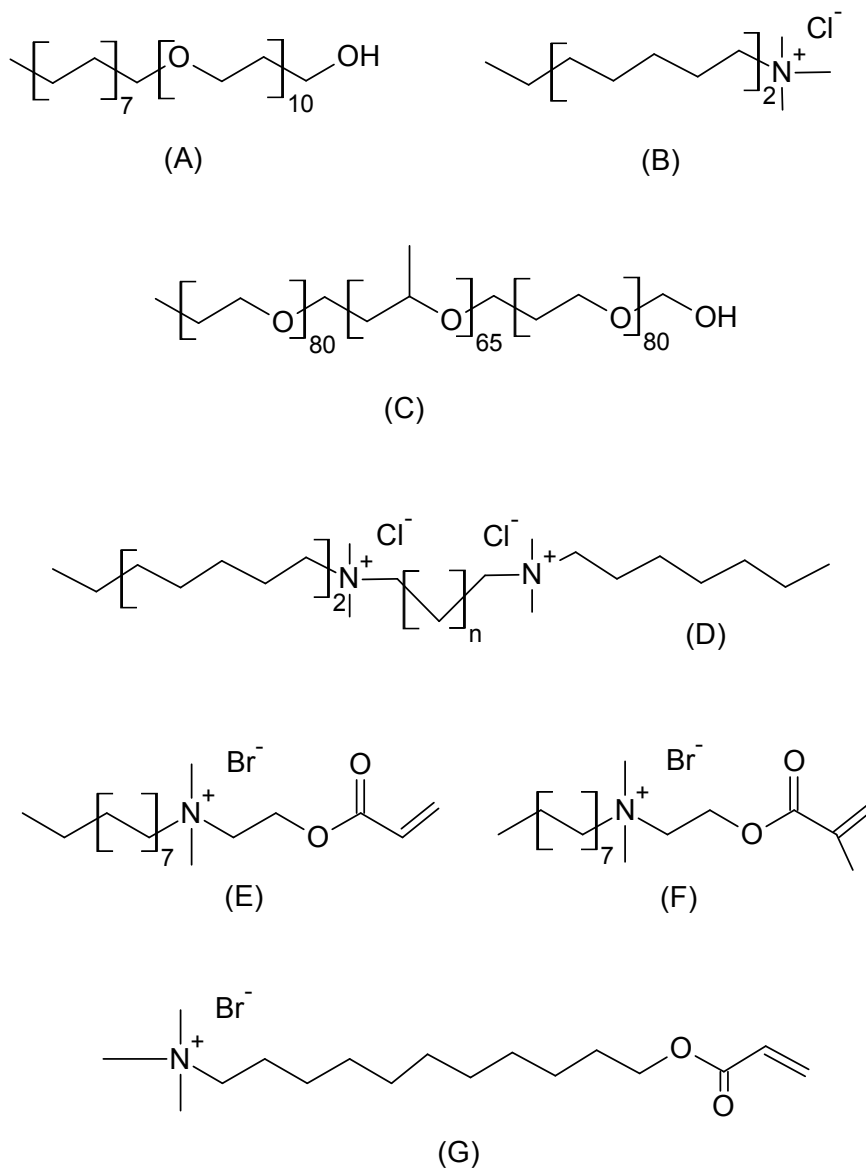


**Figure 1.3.** Chemical structures of common surfactants and some polymerizable surfactants. Shown are (A) polyoxyethylene (10) cetyl ether (Brij 56), (B) dodecyltrimethylammonium bromide (DTAB), (C) poly(ethylene glycol) – poly(propylene glycol) – poly(ethylene glycol) (Pluronic L92), (D) a Gemini surfactant, (E) long alkyl chain derivative of dimethyl aminomethyl acrylate, (F) trimethyldodecylacrylate ammonium bromide, and (G), diallylmethyldodecyl ammonium bromide.

Increased interaction between clay surfaces and polymer networks can also facilitate the further exfoliation of clay platelets during the polymerization process, resulting in

additional property enhancement, as well as increase of polymerization rate. For this reason, the research will utilize polymerizable organoclays modified by reactive surfactants. Specific efforts will focus on how the morphology of the nanocomposites relates to their final properties and what other important factors are correlated for *in situ* photopolymer clay nanocomposite process. Understanding these relationships will facilitate direct application of this technique based on novel polymerizable organoclays.

To this end, research will study the overall effects of polymerizable surfactants through common radical and thiol-ene systems. Controlling formulation variables in selection of monomers and organoclays will be important to compare the results between systems. Most importantly, polymerizable surfactants must be prepared with consideration to several factors such as the type of substituted reactive moiety, its position, attached alkyl chain length, and number of reactive groups in their structure. For instance, in previous work, surfactants having thiol groups showed different results in both exfoliation behavior and polymerization kinetics of clay nanocomposite systems from that of acrylic functionalized materials.[95] Some polymerizable surfactants are commercially available and others with thiol functional group will be prepared through appropriate procedures as shown in Figure 1.4. Introduction of epoxy functionality in polymerizable surfactant structure is also included to present an example of the diversity for further functional group substitution based on this technique.

In Figure 1.4, to obtain thiol functional surfactant structure at the clay surface, an appropriate acrylate functional surfactant is prepared following the synthetic methodologies developed by Nagai et al.[93,96,97] Acrylate functionalized surfactant is then anchored onto each clay layer surface to produce an acrylated organoclay via typical organic modification processes of clay particles. Substitution of thiol groups into the surfactant structure can be performed utilizing this acrylate functionalized organoclay through clay template reaction. Replacement of the acrylate functional group to thiol is easily achieved via Michael addition reaction between the acrylic double bond and thiol

from suitable multifunctional thiol monomers.[98] Further clay template functional group modification is possible by utilizing an appropriate multifunctional monomeric modifier. For instance, as shown in Figure 1.4, epoxy functionality on polymerizable organoclay surface can be introduced by reaction between a difunctional monomer including double bond and epoxy group with thiol functionalized organoclay via the same Michael addition reaction mechanism. Examples of the chemical structures of some nonreactive and representative photopolymerizable surfactants that will be utilized in this work are provided in Fig. 1.5.

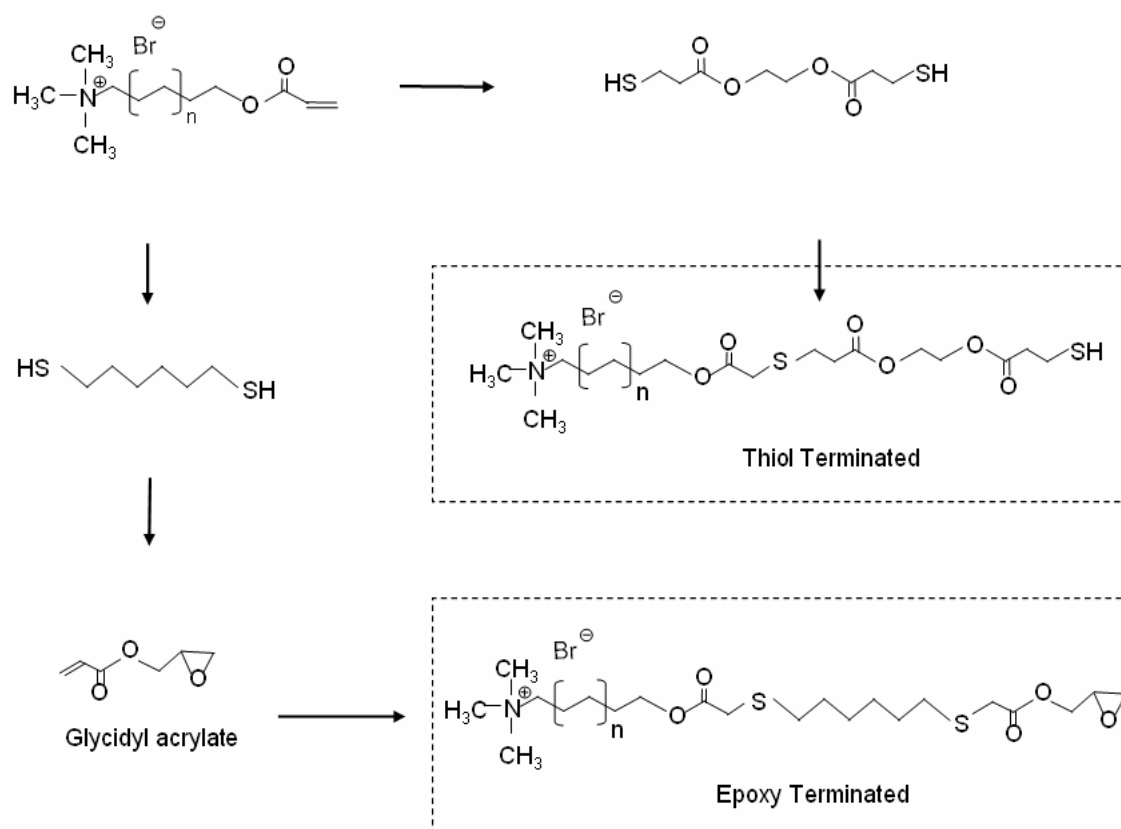


**Figure 1.4.** Schematic procedures for thiol or epoxy modification from basic acrylated surfactant based on organoclay template methodology.

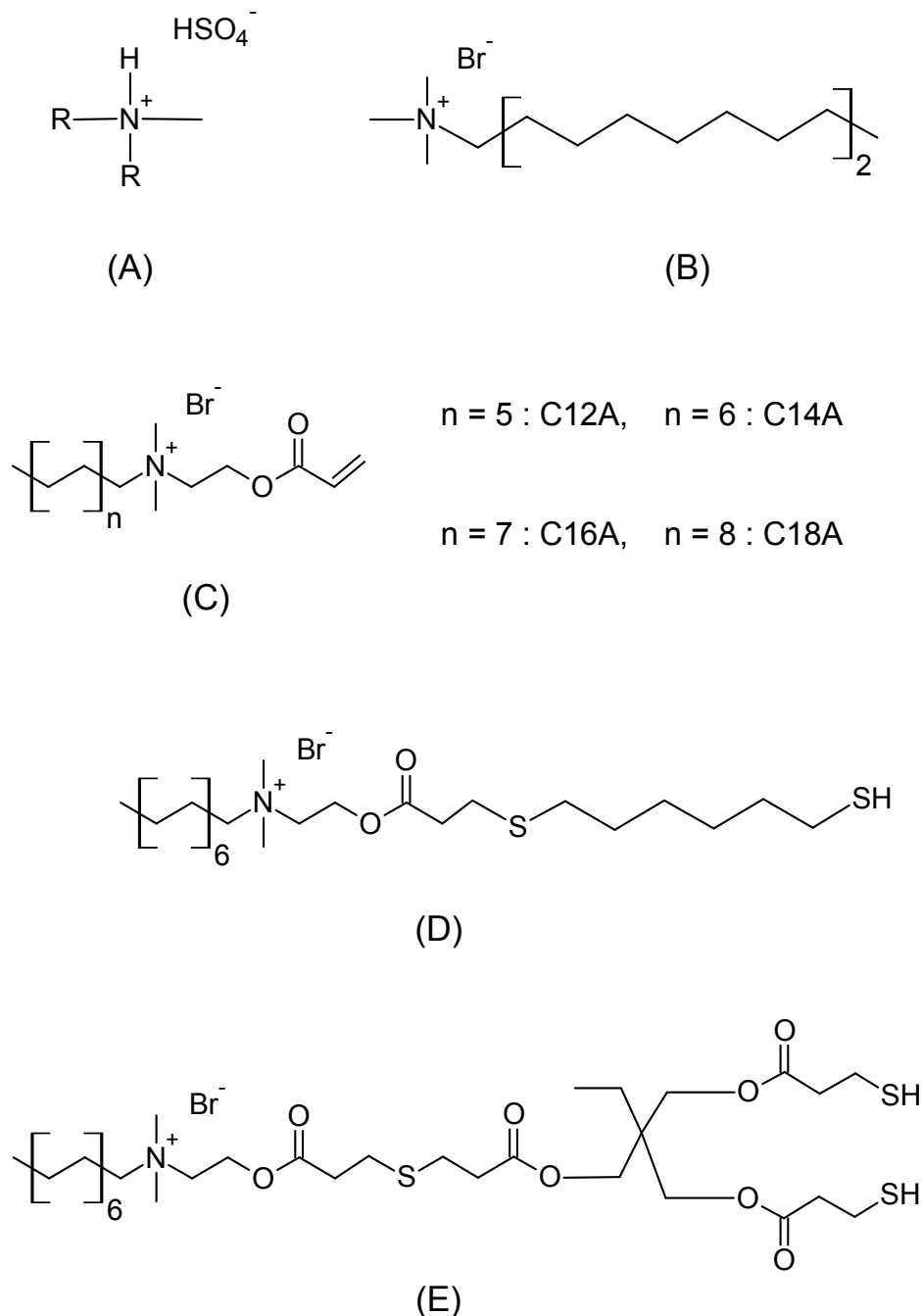


**Figure 1.5.** Chemical structures of (A) methyl dihydrogenated tallow sulfonate, (Me2HT) (B) tetradecyl trimethylammonium bromide (TTAB), (C) alkyl-2-acryloyloxy(ethyl) dimethylammonium bromide (acrylated) (D) tetradecyl 2-(1,6-mercaptohexyl mercaptane) acetoxy(ethyl) dimethylammonium bromide (C14AT; monothiol) (E) tetradecyl 2-(bis(3-mercaptopropionate) mercaptopropionyl trimethylolpropyl) acetoxy(ethyl) dimethylammonium bromide (PSH2; dithiol).

## Photopolymerization

Due to their vast commercial applicability and a wide variety of properties, photopolymers have been applied extensively and attracted continued research interest. Based on a wide range of commercially available building blocks such as monomers and multifunctional oligomers, various photopolymers have been developed satisfying the requirements of numerous applications such as coatings, adhesives, paint and inks, and other films. While many types of photopolymerization techniques have been developed and utilized to produce the photopolymers, this section mainly focuses on free radical photopolymerization in which the generation of radicals from photosensitive compounds relies on light energy.[99] The use of light energy for inducing polymerization presents many advantages compared to conventional thermal or solvent polymerization processes. The photopolymerization process forming cured networks very rapidly progresses mostly at ambient temperature with higher energy efficiency than other thermal polymerization processes. In addition, solventless formulations with 100% solid content can avoid release of volatile organic compounds.[32-36]

Photoinitiated polymerizations occur via production of radicals through ultraviolet or visible light irradiation of a suitable photoinitiator in the presence of appropriate monomers.[100] Diverse monomers and oligomers can be combined to control both the process characteristics and final properties of cured polymers. While (meth)acrylates and (meth)acrylamides are most commonly used monomers for current industrial photopolymer productions due to their high polymerization rates, diallyl, styrenics, and other various types of vinyl monomers are also used in photopolymerization applications. Examples of some photopolymerizable monomers including acrylate, methacrylate, and acrylamide monomers are shown in Figure 1.6.

Polymerization of monovinyl monomers usually generates linear and/or branched

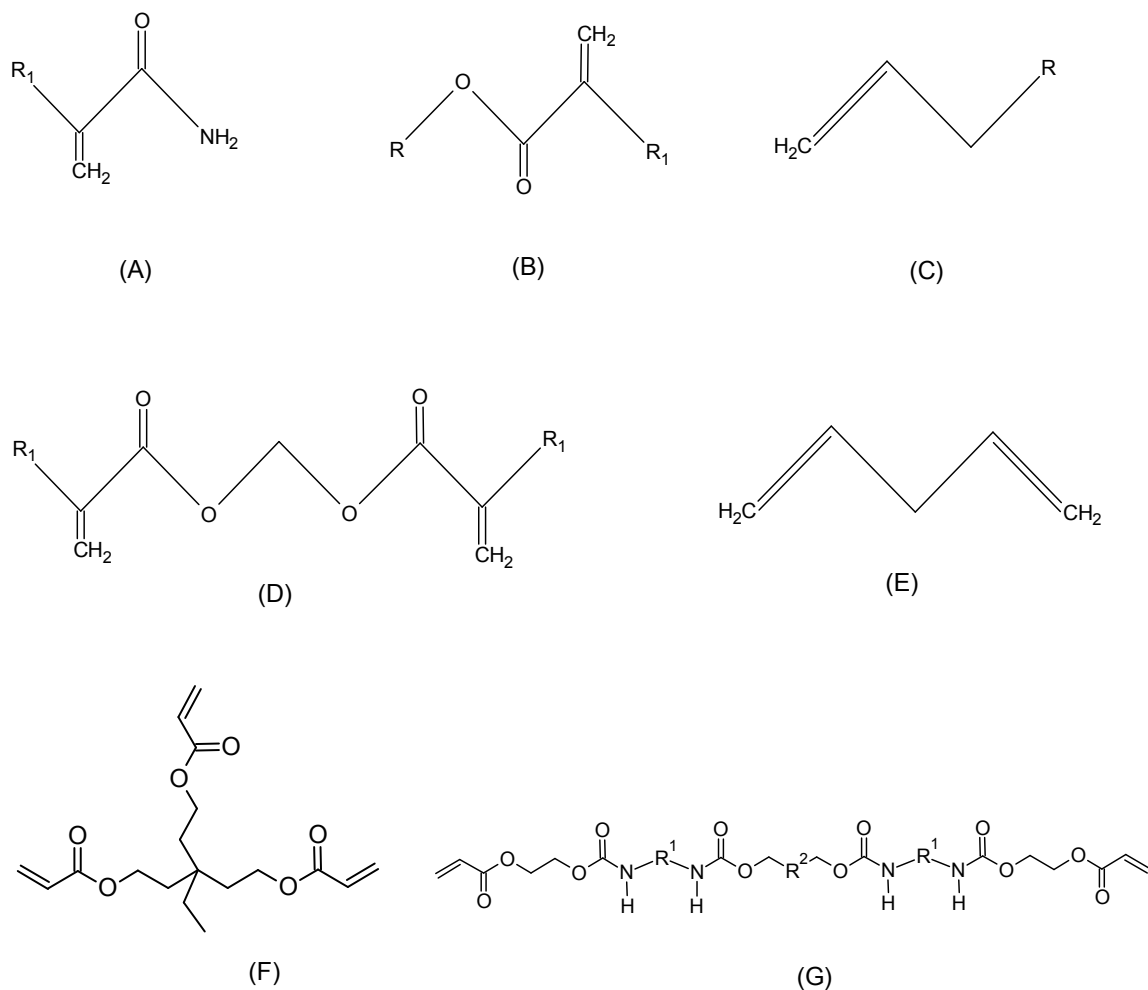


**Figure 1.6.** Chemical structures of commonly used photopolymerizable monomers and oligomer, where  $R_1=H$ : acrylic,  $R_1=CH_3$ : methacrylic. Shown are (A) (meth)acrylamide, (B) (meth)acrylate, (C) Vinyl monomer, (D) di(meth)acrylate, (E) divinyl monomer, (F) triacrylate monomer, and (G) urethane diacrylate oligomer.

polymers. Multifunctional monomers such as di- or tri-, even tetra-vinyl monomers induce highly cross-linked three dimensional networks. A particular challenge in photopolymerization is overcoming light attenuation in either thick polymerization systems or systems including fillers. Reduction of light energy through the thickness of

the film results in significant decrease in the rate and final conversion of photopolymerization and subsequent deterioration of ultimate performance.[101,102] Commonly utilized methods to circumvent these drawbacks in photopolymerization are use of either high light intensities or high concentration of photoinitiator or both. Another major disadvantage in free radical photopolymerization is severe oxygen inhibition when polymerization occurs in air. To overcome this inhibition, various strategies have been developed, including inert gas purging, blocking oxygen using an impermeable film, or incorporating specific monomers such as vinyl ether or thiol. Unfortunately, all of these methods create other problems such as increased processing cost and changes in properties.

### Photopolymerization kinetics

The photopolymerization process consists of three main steps, i.e. initiation, propagation, and termination. In the initiation step, photosensitive compounds, often called photoinitiators, decompose into free radicals based on homolytic dissociation that commonly yields a pair of primary radicals. To aid light energy absorption and thus enhance initiating reaction efficacy, photosensitizers that can absorb light energy and transfer the energy to initiator molecules are often also used in many industrial systems. The radicals produced promptly add to double bond in a monomer molecule, resulting in formation of chain initiating radicals ( $M_1\bullet$ ). These two initiation reactions are described in Equations 1.1 and 1.2 where  $h\nu$  represents a photon absorbed by the photoinitiator,  $k_i$  representing the rate constant for the initiation reaction.







In the propagation reaction, chain initiating radicals propagate by adding to other monomer double bonds to form a polymer chain as shown in Equation 1.3 and 1.4 where  $k_p$  represents the rate constant of propagation. This rate constant of propagation ( $k_p$ ) is assumed to be independent of the polymer chain length  $n$ . The propagation reaction is very fast, forming high molecular weight polymer typically in less than one second.



At a point during the propagation reaction, the radicals in the growing polymer chains are eliminated by termination. Two types of termination reactions are possible. The more common bimolecular termination occurs when any two free-radicals in the system react or combine as shown in Equation 1.5. Termination is also possible by hydrogen abstraction in a disproportionation reaction depicted in Equation 1.6 below.  $M_m \bullet$  and  $M_n \bullet$  represent two different radical chains that combine to form a non-reacting polymer and  $k_{tc}$  and  $k_{td}$  represent the rate constants for termination by bimolecular termination and disproportionation reaction, respectively.



The rate of polymerization ( $R_p$ ) is defined as the rate of disappearance of monomer. In addition, considering that the overall number of propagating species is far greater than the initiating radicals, the overall rate of polymerization can be simplified as in Equation 1.7. In a free radical polymerization system, the concentration of growing polymer radicals is typically very low ( $\sim 10^{-8}$  M) and difficult to measure accurately.[99] The steady state assumption, i.e. that the rate of free radical production in the initiation step is equivalent to the rate of consumption in the termination step, leads to Equation 1.8. Substituting Equation 1.8 into 1.7 yields Equation 1.9, which assumes that the rate of change in  $[M\bullet]$  is approximately constant during the reaction. This allows evaluation of photopolymerization rate without direct information regarding free radical concentration. For these equations,  $[M]$  is the concentration of double bonds and  $[M\bullet]$  is the concentration of propagating free-radicals, with the assumption that the monomer concentration is unaffected by the monomer consumed in the initiation step.

$$-\frac{d[M]}{dt} = R_p = k_p [M\bullet][M] \quad (1.7)$$

$$R_i = R_t = k_t [M\bullet]^2 \quad (1.8)$$

$$R_p = k_p [M] \left( \frac{R_i}{2k_t} \right)^{1/2} \quad (1.9)$$

In the case of photopolymerization, the rate of initiation ( $R_i$ ) is a function of photoinitiator efficiency ( $\phi$ ) and absorbed light intensity ( $I_a$ ). Equation 1.10 includes multiple of 2 because photo-cleavage of photoinitiator molecules usually yields two free radical species. Equations 1.10 and 1.11 show the basic rate for free radical polymerization processes.

$$R_i = 2\phi I_a \quad (1.10)$$

$$R_p = k_p [M] \left( \frac{\phi I_a}{k_t} \right)^{1/2} \quad (1.11)$$

$$I'_a = I_0 (1 - e^{-2.3\epsilon[A]D}) \quad (1.12)$$

Substitution of Equation 1.10 into Equation 1.9 yields the rate of polymerization (Equation 1.11) for a photopolymerization process. While Equation 1.11 reasonably describes the photopolymerization of an idealized system, it is inadequate for describing typical UV-curable formulations which may contain fillers and other additives. Additives or even monomers that absorb incident light at similar wavelengths as like the photoinitiator would influence the polymerization behavior. The intensity of absorbed light varies with the depth of the substrate being photopolymerized as shown in Equation 1.12. In Equation 1.12, the absorbed light intensity is calculated according to the Beer-Lambert law, which is a function of the incident light intensity ( $I_0$ ), the molar absorptivity of the photoinitiator ( $\epsilon$ ), the concentration of absorbing species  $[A]$  and the intensity of absorbed light ( $I'_a$ ) at distance ( $D$ ) measured from the surface at which the incident light first contacts the reaction mixture. The rate of photopolymerization can then be calculated from Equation 1.13, which is obtained by substituting Equation 1.12 into 1.11.

$$R_p = k_p [M] \left( \frac{\phi I_0 (1 - e^{-2.3\epsilon[A]D})}{k_t} \right)^{1/2} \quad (1.13)$$

The rate of photopolymerization at any depth across a specimen could be calculated utilizing Equation 1.13 if the molar absorptivity, light intensity at that point

and the distance from the surface to the depth are known. Upon careful examination of this equation, the size of inorganic filler particles that absorb and scatter the incident light in most cases should be reduced to minimize the reduction in light energy when fillers are incorporated to produce polymer composites. Various instrumental methodologies such as photo-differential scanning calorimetry (photo-DSC) and real time Fourier transform infrared spectroscopy (RTIR) can be utilized to examine the rate of bulk photopolymerization with details to be described later in the methods section.

Many factors can affect photopolymerization and subsequently influences the resulting polymer properties. Important factors include autoacceleration (or often referred as Trommsdorff effect), oxygen inhibition, and polymerization shrinkage. The acceleration of the polymerization rate, which is found in many photopolymerization systems, is due to an increase in system viscosity by the formation of high molecular polymer chains which critically restricts the diffusion mobility of the propagating radicals, thereby decreasing the termination rate.[99,103] Oxygen inhibition can limit or completely prevent polymerization in many free radical systems by quenching of the excited states of the initiator and/or by reacting with the radicals in the system. The generated peroxide radical usually does not induce propagation due to its low reactivity.[99] High shrinkage during photopolymerization and subsequent stress are also important drawbacks of multifunctional (meth)acrylate systems.[104] In this study, therefore, efforts are devoted to mitigating these two concerns regarding oxygen inhibition and polymerization shrinkage by incorporating reactive clay and the thiol-ene step growth mechanism into acrylate photopolymerization systems.

#### *In situ* clay photopolymerization

As discussed previously section, several methods have been developed to prepare polymer layered-silicates nanocomposites (PLS). Clay can be also delaminated into

individual platelets by solvent after incorporation of polymer into the solvent when the solvent based exfoliation-adsorption processing method is utilized. The clay nanocomposites are formed after evaporating the solvent. In melt intercalation, molten polymer is mixed with clays by high shear forces at high temperatures. The first successful discovery of polymer-clay nanocomposites based on this melt intercalation method was reported by the Toyota Research group.[86] Significant enhancement in mechanical, physical and thermal properties of Nylon 6 was achieved by the addition of very low amounts of clay (~5 wt %). Since this time, tremendous effort has been devoted to developing polymer-clay nanocomposites based on many polymer systems.[105-112] The majority of research, however, has focused on conventional polymer-processing techniques such as melt extrusion and solvent blending. With *in situ* intercalative polymerization, liquid monomers first diffuse into the clay interlayer and then are polymerized to produce cross-linked polymer networks between the intercalated layers. Among the several technologies for preparing the clay nanocomposites, much attention has been placed on *in situ* intercalative polymerization because this process involves no solvent treatment and no potentially detrimental polymer thermal degradation as compared to other conventional processes.

Recently, increased environmental concerns have led many industrial and academic research groups to focus on developing new polymer nanocomposite processing technology without use of thermal energy or solvent intermediates during the process. For this reason, during the last decade, nanocomposites materials formed via light-induced polymerization have been studied based on the many desirable aspects of this unique technology with respect to both ease of processing and final performance of the composites. Photopolymerization uses only light energy for the polymerization, and polymers can be rapidly produced at ambient temperature with 100% solid content. Producing nanocomposites by *in situ* photopolymerization thus offers a number of advantages in the preparation of clay nanocomposites. First, a solvent free formulation

affords no emission of volatile organic compounds (VOC) during the process. Second, control of the swelling time allows optimal interpenetration of the resin into the clay platelets, which is helpful for exfoliation of clays. Third, an ultrafast polymerization proceeds at the desired rate by adjusting the light intensity and/or the concentration of photoinitiators at the ambient temperature, resulting in less energy requirement and avoiding thermal degradation during the photopolymer clay nanocomposite process.[28,36,40,71]

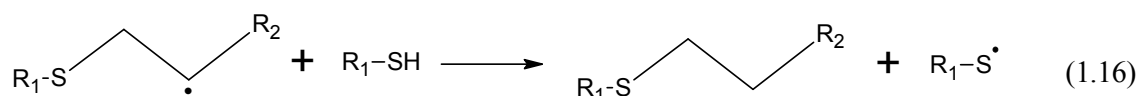
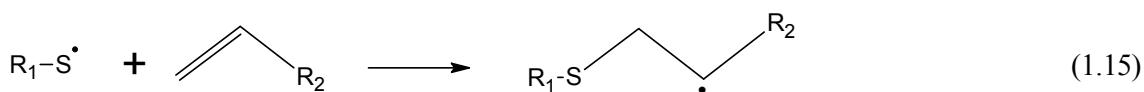
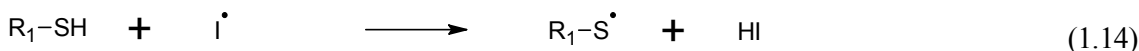
Since Decker *et al* first studied *in situ* photopolymerization techniques in processing clay-polymer nanocomposite,[27] research groups have investigated factors affecting photopolymerization behavior and final properties of clay nanocomposites. For instance, Uhl *et al* demonstrated that the incorporation of clays significantly increased mechanical and thermal properties of composites while it decreased the rate of photopolymerization to some degree. Better delaminating of clays was achieved by organic modification of the clay surface inducing significant increase in thermo-mechanical properties.[29]

### Thiol-ene photopolymerization

Thiol-ene photopolymerization is a promising and emerging technique for overcoming the drawbacks of acrylate-based photopolymerization. Thiol-ene photopolymerization occurs via a step-growth reaction mechanism that produces a more homogeneous network structure than acrylate homopolymerization, which could reduce the shrinkage during photopolymerization.[47-50] Properties of the network system can also be quite diverse based on the wide variety of commercially available monomers with ene functionality.[48] Thiol-ene photopolymers can be produced from the reaction between multifunctional thiol monomers and any component including terminal carbon-

carbon double bonds (enes).[113] These chemical species include alkenes, acrylates, vinyl/allyl ethers, norbonenes and allylisocyanurates.

Recently, Hoyle and Bowman have extensively studied this copolymerization between double bonds and thiol groups to develop unique photopolymer systems overcoming many drawbacks of free-radical photopolymerization including oxygen inhibition.[95, 114-117] The addition of thiol monomers into ene systems, including various vinyl and (meth)acrylate systems, significantly changes the reaction mechanism from a free-radical chain growth to a step-growth reaction. In a standard thiol-ene copolymerization, thiol monomers act as a chain transfer agent and polymerization progresses via alternating reaction between the propagation of a thiyl radical with a double bond and the chain transfer reaction of a radical to a thiol to regenerate the thiyl radical as illustrated in scheme 1.14 by equations 1.14 to 1.16.[42]



**Scheme 1.1.** Radical chain transfer mechanisms in thiol-ene reaction.

Equations 1.14 to 1.16 describe the initiation, propagation and termination steps in thiol-ene reactions. The reaction is initiated by a sulfur-hydrogen bond cleavage or

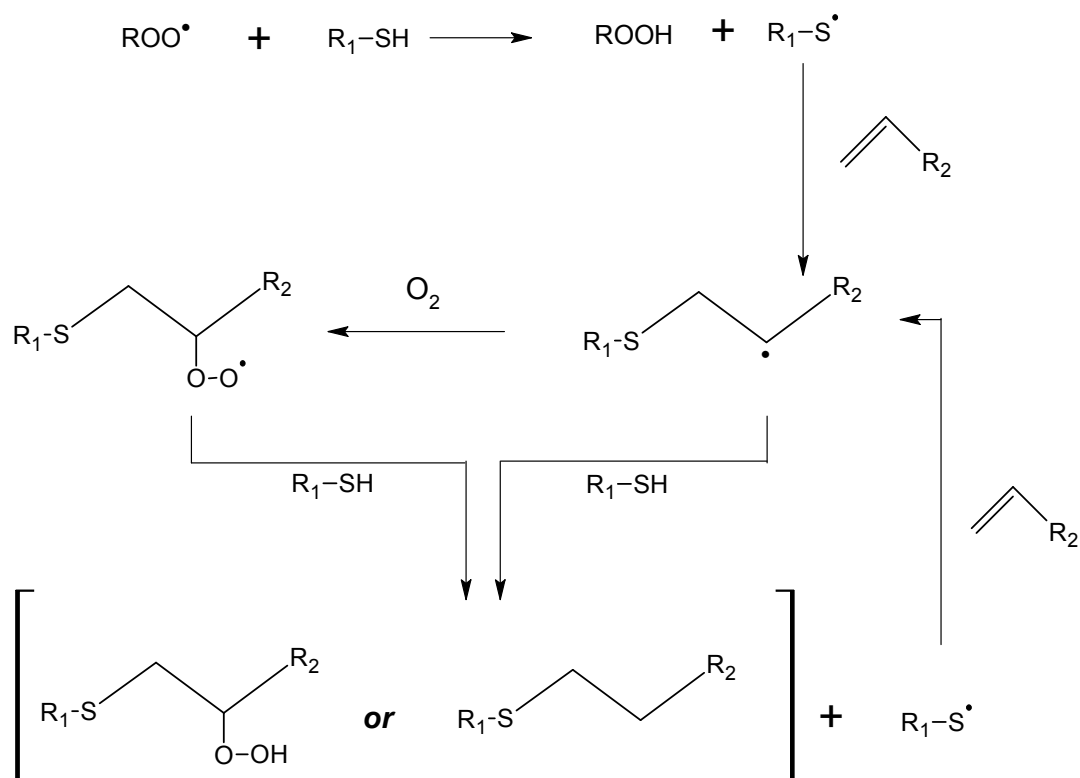
hydrogen abstraction by the photoinitiator molecule to produce a thiyl radical (Equation 1.14). Propagation subsequently proceeds through two reactions as described in Equation 1.15 and 1.16. The produced thiyl radical is added to double bond in the ene monomer to form a secondary carbon radical (Equation 1.15). The secondary carbon radical then abstracts hydrogen from other thiol monomer to regenerate thiyl radical as shown in Equation 1.16. Overall, propagation in thiol-ene photochemistry proceeds via a step growth chain reaction mechanism. The two step propagation mechanisms lead to slow development of high molecular weight polymer. Termination occurs by coupling of any two radicals in the system.

These step-growth mechanisms based on this radical chain transfer to thiol monomers can reduce oxygen inhibition of the polymerization occurring in air. Scheme 1.2 outlines thiol-ene reactions when oxygen molecules are present.[102,118] Because the radical scavenging rate by oxygen is much higher than the propagation rate, most of the initiated radicals react with oxygen. While the resulting low reactivity peroxide radicals do not react with double bonds, the radicals may transfer to thiols thereby acting as chain transfer agents to generate thiyl radicals by hydrogen abstraction. These regenerated thiyl radicals then can either initiate the propagation reaction or consume oxygen molecules in the system rapidly via repeated reaction, resulting in successful propagation with rapid consumption of oxygen molecules in the system.[118,119]

This step-growth mechanism of thiol-ene systems delays gelation because high molecular polymer is formed only at higher conversions. This process is beneficial for reducing polymerization shrinkage due to facile rearrangement of polymer chains in the liquid reactant mixture until the system reaches high conversion.[120,121] On the other hand, hard and tough cured materials are not easily obtained due to flexible thioether linkages.[47-52] Incorporation of inorganic fillers into such a polymer system often increases mechanical properties such as modulus and toughness and thus would be helpful for overcoming this shortcoming of thiol-ene polymerization. Inorganic fillers



such as organoclays are also advantageous for decreasing polymerization shrinkage by reducing effective organic volume in the systems.[122-124] In addition, the incorporation of organoclays into thiol-ene systems may present enhanced gas barrier property by generating longer length for gaseous materials.[36,44]



**Scheme 1.2.** Schematic expression of the reaction mechanisms of thiol-ene systems in the presence of oxygen.

In thiol-ene photopolymerization, the stoichiometric balance between thiol and ene functional groups critically affects not only the photopolymerization kinetics but also the final properties because thiol can only react with ene groups. For this reason, the type of functional group on clay surfaces should be more important in thiol-ene systems than

for systems based on acrylate compositions. Both the type of functional group on clay surfaces and the difference in monomer incorporation into clay galleries could affect the stoichiometric balance at the clay surface, resulting in different behavior during the photopolymerization process.[95] However, little is known regarding the effects of inorganic particle and their surface functionality on thiol-ene polymerization behavior, especially in clay-photopolymer systems. Lee *et al.* studied the effect of functional group on polymerization kinetics of thiol-acrylated system with thiol functionalized silica nanoparticles.[125] Due to a stoichiometric imbalance at the spherical silica surface and immobilization of propagating thiyl-radicals, the polymerization rate decreased to some degree while there was no change with non-reactive particles. Because the result was for spherical nanoparticles, not for layered particles, further understanding in photopolymerization based on thiol-ene composition with polymerizable organoclays could promise significant insight into reactivity effects. Additionally, the reaction takes place via a step mechanism which is accompanied by lower shrinkage thereby allowing greater application for thiol-ene nanocomposites.

### Project Summary

Producing clay nanocomposites based on *in situ* photopolymerization combines the unique advantages of UV curing technology with potential enhanced performance upon addition of nano-structured materials. The goal of this research is the development of photopolymer clay nanocomposites having enhanced physical, thermal and barrier properties utilizing novel polymerizable organoclays and unique thiol-ene photopolymerization technique. In clay nanocomposite processing, obtaining well-exfoliated clay dispersions plays a critical role in final properties and requires the modification of clay surfaces by surfactants to improve compatibility in polymer matrices.

Polymerizable surfactants can incorporate into polymer matrices during the UV curing process. The accompanying increased interaction between clay surfaces and polymer networks can not only facilitate clay exfoliation but also allow further property improvement. In addition, the improvement of several characteristics such as shrinkage during polymerization, gas barrier properties, and impact resistance is desirable to enhance contemporary photopolymer applications. In conjunction with unique thiol-ene copolymerization techniques, well-exfoliated photopolymer clay nanocomposites based on suitable polymerizable organoclays could be the prime candidates for the goal.

To this end, this work entails extensive studies to understand overall effects caused by the incorporation of polymerizable organoclays in *in situ* acrylate and thiol-ene photopolymerization system. The body of this research is divided into three main sections. The first section contributes to understanding the fundamental factors in nanocomposite processes and the relation with composite properties. The factors governing nanocomposite formation such as monomer composition and clay dispersion is outlined in chapter 4 with emphasis on the critical impacts on polymerization kinetics and mechanism. With further examination of the impacts of the type of reactive group in the polymerizable organoclays on polymerization mechanism, chapter 5 focuses on discussing how differences in photopolymerization behavior affects the basic thermo-mechanical properties of nanocomposites.

The second section of this research mainly deals with the important challenge of overcoming two major drawbacks in conventional free radical photopolymerization, i.e. severe polymerization shrinkage and oxygen inhibition. Chapter 6 discusses the synergetic effects of incorporating polymerizable organoclays with thiol on oxygen inhibition by examining the polymerization rates of various acrylate and thiol-acrylate systems in the presence and absence of oxygen. To investigate the specific effects of polymerizable organoclays on the polymerization shrinkage during photopolymerization, volume shrinkage and shrinkage stress of controlled acrylate and thiol-acrylate

formulations with varied clay type will be examined in chapter 7 utilizing an appropriate ASTM method. The final section of this work (chapter 8) further investigates the overall effects of polymerizable organoclays on various ultimate performance aspects of photopolymer clay nanocomposites including mechanical and tensile properties, toughness, and gas barrier characterization to provide practical information for design of advanced photopolymer clay nanocomposites.

By overcoming the drawbacks of conventional surfactants and thus achieving better clay exfoliation with higher interaction between polymer and polymerizable organoclays, advanced methods for photopolymer clay nanocomposites with unique properties have been developed. Understanding of the role of polymerizable organoclays in processing clay nanocomposites will also increase the fundamental knowledge in photopolymerization systems with inorganic fillers.

Notes

1. Shaffer, G. D. *J. Field Archaeology* **1993**, 20(1), 59.
2. Lomborg, B. *The Skeptical Environmentalist: Measuring the Real State of the World.*; Cambridge University Press: Ney York, **2001**, p.138.
3. Schaffer, A.; Saxena, S. D.; Antolovich, T. H.; Sanders, Jr.; and Warner. S.B. *The Science and Design of Engineering Materials*; IRWIN [now McGraw-Hill]: Chicago, **1999**.
4. Anderson, H. A. *CARBON BLACK INDUSTRY*; Handbook of Texas Online (<http://www.tshaonline.org/handbook/online/articles/doc01>): Texas State Historical Association, accessed December 27, **2011**.
5. Kim, H. S.; Yang, S. H.; Kim, J.; Park, H. J. *J. Thermal Analysis and Calorimetry* **2004**, 76, 395.
6. Karian, H. G *Handbook of Polypropylene and Polypropylene Composites*; Marcel Dekker: Ney York, **1999**, p.1.
7. Thwe, M. M.; Liao, K. *Composite. Part A*, **2002**, 33, 43.
8. Jana, S. C.; Prieto, A. J. *Appl. Polym. Sci.* **2002**, 86, 2159.
9. Baughman, R. H.; Zahkidov, A. A.; De Heer, W. A. *Science* **2002**, 297, 787.
10. Moniruzzaman, M.; Winey, K. I. *Macromolecules* **2006**, 39, 5194.
11. Brule, B.; Flat, J. J. *Macromol. Symp.* **2006**, 233, 210.
12. Matteucci, S.; Kusuma, V. A.; Sanders, D.; Swinnea, S.; Freeman, B. D. *J. Membr. Sci.* **2008**, 307, 196.
13. Moniruzzaman, M.; Winey, K. I. *Macromolecules* **2006**, 39, 5194.
14. Hatton, R. A.; Miller, A. J.; Silva, R. R. P. *J. Mater. Chem.* **2008**, 18, 1183.
15. Shen, T.; Gu, J. J.; Xu, M.; Wu, Y. Q.; Bolen, M.L.; Capano, M. A.; Engel, L.W.; Ye, P. D. *Appl. Phys. Lett.* **2009**, 95, 172105.
16. Chakrabarti, A; Lu, J.; Skrabutenas, J. C.; Xu, T.; Xiao, Z.; Maguire, J. A.; Hosmane, N. S. *Journal of Materials Chemistry* **2011**, 21, 9491.
17. Medalia A. I. *Rubber Chem. Technol.* **1986**, 59, 432.
18. Karásek, L.; Sumita. M. *J. Mat Sci* **1996**, 31(2), 281.
19. Seymour, R. B. *Polymer Composites VSP*, **1990**, p. 48.
20. Rigbi, Z. *Adv. Polym. Sci.* **1980**, 36, 21.

21. Mark, J. E.; Pan, S. J. *Makromol. Chem., Rapid Commun.* **1982**, 3, 681.
22. Jiang, C.Y.; Mark, J. E. *Makromol. Chem.* **1984**, 185, 2609.
23. Wang, W. N.; Lenggoro, I. W.; Okuyama, K. *J. Coll. Int. Sci.* **2005**, 288, 423.
24. Grubbs, R. R. *Polymer Rev.* **2007**, 47, 197.
25. Okada, A.; Kawasumi, M.; Kurauchi, T.; Kamigaito, O. *Polym. Prepr.* **1987**, 28, 447.
26. Usuku, A.; Kojima, Y.; Kawasumi, M.; Okada, A.; Fukushima, Y.; Kurauchi, T.; Kamigaito, O. *J. Mater. Res.* **1993**, 8, 1185.
27. Decker, C.; Zahouily, K.; Keller, L.; Benfarhi, S.; Bendaikha, T.; Baron, J. *J. Mater. Sci.*, **2002**, 37, 4831.
28. Decker, C.; Keller, L.; Zahouily, K.; Benfarhi, S. *Polymer* **2005**, 46, 6640.
29. Uhl, F. M.; Davuluri, S. P.; Wong, S. C.; Webster, D. C. *Chem. Mater.* **2004**, 16, 1135.
30. Uhl, F. M.; Webster, D. C.; Davuluri, S. P.; Wong, S. C. *Euro. Polymer J.* **2006**, 42, 2596.
31. Roffey, C.G. *Photopolymerisation of Surface Coatings*; Wiley: New York **1982**.
32. Vaia, R. A.; Giannelis, E. P. *Macromolecules* **1997**, 30, 7990.
33. Alexandre, M. ; Dubois, P. *Mater. Sci. Eng.* **2000**, 28, 1.
34. Beck, E.; Lokai, M.; Keil, E.; Nissler, H. *RadTech North America*, **1996**, 160.
35. Gilman, J.W. *Appl. Clay Sci.* **1999**, 15, 31.
36. Zahouily, K.; Benfarhi, S.; Bendaikha, T.; Baron. J. *Rad Tech Europe Conf.* **2001**, 583.
37. Zahouily; K., Decker, C.; Benfarhi, S.; Baron. **2002**, *RadTech North America*
38. Decker, C. *Macromol. Rapid Commun.* **2002**, **23**, 1067.
39. Bongiovanni, R.; Ronchetti, M. S.; Turcato, E.A. *J. Colloid & Interf. Sci.* **2006**, 296, 515.
40. Uhl, F. M.; Hinderliter, B. R.; Davuluri, S. P.; Croll, S. G. *Mater. Res. Soc.* **2004**, 16, 203.
41. Uhl, F. M.; Davuluri, S. P.; Wong, S. C.; Webster, D. C. *ANTEC Conf.* **2004**, 1892.
42. Decker, C. *Polym. Int.* **1998**, 45, 133.

43. Decker, C. *Prog. Polym. Sci.* **1996**, 21, 593.
44. Ray, S. S.; Okamoto, M. *Prog. Polym. Sci.* **2003**, 28, 1539.
45. Uhl, F. M.; Davuluri, S. P.; Wong, S. C.; Webster, D.C. *Polymer* **2004**, 45, 6175.
46. Fu, X.; Qutubuddin, S. *Polymer* **2001**, 42, 807.
47. Hoyle, C. E.; Lee, T. Y.; Roper, T. *J. Polym. Sci. A: Poly. Chem.*, **2004**, 42, 5301.
48. Cramer, N. B.; Scott, J. P.; Bowman, C. N. *Macromolecules* **2002**, 35, 5361.
49. Morgan, C. R.; Magnota, F.; Ketley, A. D. *J. Polym. Sci.* **1977**, 15, 627.
50. Carioscia, J. A.; Lu, H.; Stanbury, J. W.; Bowman, C. N. *Dent. Mater.* **2005**, 21, 1137.
51. Senyurt, A. F.; Wei, H.; Hoyle, C. E.; Piland, S. G.; Gould, T. E. *Macromolecules* **2007**, 40, 4901.
52. Li, Q.; Zhou, H.; Wicks, D. A.; Hoyle, C. E. *J. Polym. Sci.*, **2007**, 45, 5103.
53. Aguzzi, C.; Cerezo, P.; Viseras, C.; Caramella, C. *Appl. Clay Sci.* **2007**, 36, 22.
54. Vaccari, A. *Appl. Clay Sci.* **1999**, 14, 161.
55. Theng, B. K. G. *The Chemistry of Clay-Organic Reactions*; Wiley: New York, **1974**.
56. Kawasumi, M. *J. of Polym. Sci. Part A* **2004**, **42**, 819.
57. Morlat, S.; Mailhot, B.; Gonzalez, D.; Gardette, J. *Chem. of Mater.* **2004**, **16**, 377.
58. Sposito, N.; Skipper, N. T.; Sutton, R.; Park, S. H.; Soper, A. K.; Greathouse, J. A. *Proc. Natl. Acad. Sci.* **1999**, 96, 3358.
59. Li, Y.; Ishida, H. *Polymer* **2003**, 44, 6571.
60. Filippi, S.; Mameli, E.; Marazzato, C.; Magagnini, P. *Euro. Polym. J.* **2007**, 43, 1645.
61. Lee, C. H.; Kim, H. B.; Lim, S. T.; Choi, H. J.; Jhon, M. S. *J. Mater. Sci.* **2005**, 40, 3981.
62. Balazs, A.C.; Singh, C.; Zhulina, E. *Macromolecules* **1998**, 31, 8370.
63. Lyatskaya, Y.; Balazs, A. C. *Macromolecules* **1998**, 31, 6676.
64. Shah, R. K.; Paul, D. R. *Polymer*, **2006**, 47, 4075.

65. Gelfer, M. Y.; Burger, C.; Nawani, P.; Hsiao, B. S.; Chu, B.; Si, M.; Rafailovich, M.; Panek, G.; Jeschke, G.; Gunnar, F. A. Y.; Gilman, J. W. *Clays Clay Miner.* **2007**, *55*, 140.
66. Blumstein, A. J. *Polym. Sci. Part A.* **1965**, *3*, 2665.
67. Giannelis, E. P.; Krishnamoorti, R.; Manias, E. *Adv. Polym. Sci.* **1999**, *118*, 108.
68. Carrado, K. A. *J. Appl. Clay Sci.* **2000**, *17*, 1.
69. Zhang, Q.; Fu, Q.; Jiang, L.; Lei, Y. *Polym. Int.* **2000**, *48*, 1561.
70. LeBaron, P. C.; Wang, Z.; Pinnavaia, T. J. *J. Appl. Clay Sci.* **1999**, *15*, 11. v2.
71. Keller, S. L.; Decker, C.; Zahouily, K.; Benfarhi, S.; Le Meins, J. M.; Mische-Brendle, J. *Polymer* **2004**, *45*, 7437.
72. Brindly, S. W.; Brown, G. *Crystal structure of clay minerals and their X-ray diffraction*; Mineralogical Society: London, **1980**.
73. Aranda, P.; Ruiz-Hitzky, E. *Chem Mater* **1992**, *4*, 1395.
74. Greenland, D. J. *J. Colloid Sci* **1963**, *18*, 647.
75. Krishnamoorti, r.; Vaia, R. A.; Giannelis, E. P. *Chem Mater* **1996**, *8*, 1728.
76. Porter, T. L.; Hagerman, M.E.; Reynolds, B. P.; Eastman, M. E. *J Polym Sci, Part B: Polym Phys* **1998**, *36*, 673.
77. Hasegawa, N.; Okamoto, H.; Kawasumi, M.; Usuki, A. *J Appl Polym Sci* **1999**, *74*, 3359.
78. Noh, M. W.; Lee, D. C. *Polym Bull* **1999**, *42*, 619.
79. Weimer, M. W.; Chen, H.; Giannelis, E.P.; Sogah, D.Y. *J Am Chem Soc* **1999**, *121*, 1615.
80. Gilman, J. W.; Awad, W. H.; Davis, R. D.; Shields, J.; Harris, Jr. R. H.; Davis, C.; Morgan, A. B.; Sutto, T. E.; Callahan, J.; Trulove, P. C.; DeLong, H. C. *Chem Mater* **2002**, *14*, 3776.
81. Gao, D.; Heimann, R. B.; Williams, M. C.; Wardhaugh, L. T.; Muhammad, M. *J Mater Sci* **1999**, *34*, 1543.
82. Xia, X.; Yih, J.; D'Souza, N. A.; Hu, Z. *Polymer* **2003**, *44*, 3389.
83. Small, D. M. *J. Coll. Int. Sci.* **1977**, *58*, 581.
84. Li, Y.; Ishida, H. *Langmuir* **2003**, *19*, 2479.
85. Gottler, L. A.; Lee, K.; Thakkar, Y. H. *Poymer Reviews* **2007**, *47*, 291.
86. Ogawa, M.; Kuroda, K. *Bull. Chem. Soc. Jap.* **1997**, *70*, 2593.



87. Wang, J. H.; Young, T. H.; Lin, D. J.; Sun, M. K.; Huag, H. S.; Cheng, L. P. *Macromol. Mater. Eng.* **2006**, 291, 661.
88. LeBaron, P. C.; Pinnavaia, T. J. *Chem. Mater.* **2001**, 13, 3760.
89. Wang, Z.; Pinnavaia, T. J. *Chem. Mater.* **1998**, 10, 3769.
90. Decker, C.; Zahouily, K.; Keller, L.; Benfarhi, S.; Bendaikha, T.; Baron, J. *Proc. RadTech North America*, **2002**, 309.
91. Tan, H. ; Nie. *J. Appl. Polym. Sci.* **2007**, 106, 2656.
92. Jayasuriya, N.; Bosak, S.; Regen, S. L. *J. Amer. Chem. Soc.* **1990**, 112, 5851.
93. Takahashi, K.; Kido, J.; Kuramoto, N.; Nagai, K. *J. Coll. Int. Sci.* **1995**, 172, 63.
94. Michas, J.; Paleos, C. M.; Dais, P. *Liquid Crystals* **1989**, 5, 1737.
95. Owusu-Adom, K.; Guymon, C. A. *Macromolecules*, **2009**, 42, 3275.
96. Hamid S. M.; Sherrington D. C. *Polymer* **1987**, 28, 325.
97. McGrath, K. M.; Sherrington, D.C. *Polymer* **2006**, 37, 1453.
98. Owusu-Adom, K.; Guymon, C. A. *Macromolecules* **2009**, 42, 180.
99. Odian, G. *Principles of Polymerization*, 4<sup>th</sup> ed; John Wiley & Sons: Hoboken, NJ, **2004**.
100. Pappas, S. P. *Encyclopedia of Polymer Science and Engineering*; Pappas, S.P., Ed.; Wiley-Interscience: Ney York, **1988**, Vol. 11, p.186.
101. Davidenko N.; Garcí'a O.; Sastre, R. *J. Appl. Polym. Sci.* **1995**, 97, 1016.
102. Decker, C.; Jenkins, A. D. *Macromolecules*, **1985**, 18, 1241.
103. North, A.M. *Reactivity, Mechanism, and Structure in Polymer Chemistry*; Wiley-Interscience, **1974**.
104. Chung, C. M.; Kim, M. S.; Roh, Y. S. *J. Mater. Sci. Lett.* **2002**, 21, 1093.
105. Owusu-Adom, K.; Guymon, C. A. *Polymer* **2008**, 49, 2636.
106. Morlat, S.; Mailhot, B.; Gonzalez, D.; Gardette, J. *Chem. of Mater.* **2004**, 16, 377.
107. Bottino, F. A.; Fabbri, E.; Fragala, I. L.; Malandrino, G.; Orestano, A.; Pilatti, F.; Pollicino, A. *Macromolecular Rapid Communications* **2003**, 24, 1079.
108. Zhang, G. ; Jiang, C. ; Su, C. ; Zhang, H. *J. Polym. Sci.: Polym.* **2003**, 89, 3155.

109. Okamoto, M.; Morita, S.; Taguchi, H.; Kim, Y. H.; Kotaka, T.; Tateyama, H. *Polymer* **2000**, *41*, 3887.
110. Fan, X.; Xia, C.; Advincula, R. C. *Langmuir*, **2003**, *19*, 4381.
111. Zeng, C.; Lee, L. J. *Macromolecules*, **2001**, *34*, 3098.
112. Jeon, H. S.; Rameshwaram, J. K.; Kim, G.; Weinkauf, D. H. *Polymer*, **2003**, *44*, 5749.
113. Rust, F. F.; Vaughan, W. E. *U.S. Pat. 2,392,294*, **1946**.
114. Wei, H.; Li, Q.; Ojelade, M.; Madbouly, S.; Otaigbe, J. U.; Hoyle, C. E. *Macromolecules* **2007**, *40*, 8788.
115. Cramer, N. B.; Reddy, S. K.; Lu, H.; Cross, T.; Raj, R.; Bowman, C. N. *J. Polym. Sci. A: Polym. Chem.*, **2004**, *42*, 1752.
116. Lee, T. Y.; Smith, Z.; Reddy, S. K.; Cramer, N. B.; Bowman, C. N. *Macromolecules* **2007**, *40*, 1466.
117. Kim, S. K.; Guymon, C. A. *J. Polym. Sci. A: Polym. Chem.* **2010**, *49*, 465.
118. O'Brien, A. K.; Cramer, N. B.; Bowman, C. N. *J. Polym. Sci. Part A: Polym. Chem.* **2006**, *44*, 2007.
119. Cramer, N. B.; Bowman, C. N. *J. Polym. Sci. Part A: Polym. Chem* **2001**, *39*, 3311.
120. Lu, H.; Carioscia, J. A.; Stansbury, J. W.; Bowman, C. N. *Dent. Mater.* **2005**, *21*, 1129.
121. Reddy, S. K., Cramer, N. B.; Kalvaitas, M., Lee, T. Y.; Bowman, C. N. *Aust. J. Chem.* **2006**, *59*, 586-593.
122. Goldman, M. *Australian Dental J.* **1983**, *28*(3), 156.
123. Kleverlaan, C.J. ; ornelis, Feilzer A.J. *Dent. Mater.* **2005**, *21*, 1150.
124. Lu, H. ; Stansbury, J.W. ; Bowman, C. N. *Dent. Mater.* **2004**, *20*, 979.
125. Lee, T. Y.; Bowman, C. N. *Polymer* **2006**, *47*, 6057.

## CHAPTER 2

### OBJECTIVES

Considerable academic and industrial research has focused on developing advanced polymer nanocomposites using nanometer-scale fillers to achieve desirable polymer properties such as high mechanical, thermal, and flame resistant properties. The extremely large surface area of nano-fillers affords increases in these properties and other performance characteristics of the polymer composites with relatively small amounts of loading compared to that of micrometer-scale fillers. Among many potential types of fillers, clays have attracted much interest due to their commercial availability and simple delaminating chemistry. By achieving well-dispersed clay morphology in polymer matrices with nanometer scale dimension of particles, it has been demonstrated that these clay nanocomposites can exhibit unique properties compared to conventional polymer composites. With rapid expansion of photopolymer applications due to many advantages in processing and performance aspects, some recent research has studied clay nanocomposites based on photopolymerization systems in pursuing a new category of advanced materials. While significant improvement in various performances of photopolymers by incorporating nanometer-scale dispersion of clay particles has been demonstrated, few studies have been performed for understanding the fundamental factors in the clay dispersion process and its impacts on photopolymerization behavior as well as final nanocomposite properties. In addition, the majority of prior work for photopolymer clay nanocomposites were based primarily on (meth)acrylate systems for which improvement in disadvantages such as oxygen inhibition and toughness for potential applications is necessary.

Meanwhile, the development of advanced photopolymer clay nanocomposites with enhanced physical, thermal and barrier properties, the goal of this research,

essentially involves not only the selection of suitable photopolymerization systems but also the careful control of clay nanocomposite formulation and processes. Successful results will thus incorporate material design, complete exfoliation of clay particles, and systematical understanding of the effects of engineering parameters on both overall polymerization behavior and ultimate composite properties. To accomplish this goal, the most important aspect of this research is the bridge between two unique technologies, i.e. the use of polymerizable organoclays and *in situ* photopolymerization. In addition to study of acrylate photopolymer systems, this research also utilizes advanced thiol-ene photopolymerizations that can overcome the drawbacks of conventional acrylic based photopolymer systems. The successful accomplishment of this research thus promises to produce enhanced photopolymer nanocomposites with low levels of oxygen inhibition, reduced polymerization shrinkage, enhanced gas barrier capability, and increased impact and abrasion resistance. Amongst diverse ene monomers for thiol-ene formulations, acrylate monomers are preferably used based on their variety and commercial availability that promises better applicability of the results from this research. While the use of polymerizable organoclays instead of nonreactive analogues could more significantly contribute to final composite properties by directly incorporation into the polymer network via chemical reaction, they may also affect the processing factors such as the polymerization behavior and the clay exfoliation during the preparation of composite materials. For achieving the goal of this research, therefore, it is necessary to understand overall effects caused by the incorporation of polymerizable organoclays in an *in situ* thiol-ene photopolymerization system and the corresponding relationship with composite properties. This goal will therefore be achieved by;

1. Preparing polymerizable organoclays bearing appropriate functional groups in accordance with photopolymerization systems and characterizing the effects of

both the structure and the type of functional group in polymerizable organoclays on clay exfoliation, photopolymerization kinetics, and its mechanism.

2. Correlating the degree of clay exfoliation and polymerization behavior with fundamental mechanical and thermal properties of ultimate photopolymer clay nanocomposites.
3. Examining the organoclay influence on processing factors such as oxygen inhibition and polymerization shrinkage that have been two of the most important drawbacks of photopolymer materials.
4. Optimizing and evaluating ultimate nanocomposite performance via composition and dispersion morphology in processing nanocomposites.

By accomplishing the first objective (Chapter 4), the relationship between clay exfoliation and photopolymerization behavior such as reaction kinetics and mechanisms for acrylate and thiol-acrylate compositions will be elucidated. In order to study the important factors affecting the dispersion morphology of organoclay particles and polymerization behavior, various types of multifunctional acrylate and thiol-acrylate monomer systems will be examined by varying the types of organoclays incorporated. To this end, the structures of organoclay, including polymerizable and nonreactive, will be controlled by changing the type of substituted reactive moiety, its position, attached alkyl chain length, and number of reactive groups in the surfactant structures used for clay modification. For the purpose of examining the effect of compatibility between monomers and organoclays on clay exfoliation and polymerization behavior, monomer compositions will be also carefully designed considering polarity, functionality, and viscosity of acrylate and thiol monomers. The photopolymerization behavior of these

acrylate and thiol-acrylate systems will be then investigated with and without addition of nonreactive or polymerizable organoclays bearing acrylate or thiol reactive moieties on the clay surface. The degree of clay exfoliation in these nanocomposite systems will be also examined and correlated to the polymerization behavior of the systems.

In the preparation of clay photopolymer nanocomposites, it is also crucial to understand the effects of organoclays on final properties of the cured photopolymer systems. Fulfillment of objective 2 (Chapter 5) is thus essential to provide comprehensive and practical information for designing clay nanocomposite materials that exhibit enhanced properties. To understand fundamental factors in clay exfoliation and photopolymerization behavior, the second objective will further study how the difference in photopolymerization behavior affects the ultimate thermal and mechanical properties of nanocomposites. In addition to this basic kinetic study, dark curing experiments will also be performed for deeper understanding the impact of organoclays on reaction mechanisms. Thermo-mechanical properties such as glass transition temperature and modulus of ultimate nanocomposites will be examined and then correlated with the reaction behavior of the systems. With the knowledge in controlling clay exfoliation and photopolymerization behavior in *in situ* acrylate and thiol-acrylate photopolymerization with polymerizable organoclays, further understanding of the relation between the reaction behavior and final nanocomposite properties will contribute to expanding the use of polymerizable organoclays.

Photopolymers based on multifunctional (meth)acrylate monomers forming highly cross-linked networks allow outstanding performance of materials with high thermal and mechanical properties. Despite these advantages, several disadvantages often limit photopolymer applications. Severe oxygen inhibition and high polymerization shrinkage in acrylate-based photopolymerization have been of particular concern. Based on accomplishing the first two objectives which study reaction behavior and thermo-mechanical property with clays, the third objective (Chapter 6 and 7) examines the

possibility of additional positive effects of polymerizable organoclays on oxygen inhibition and polymerization shrinkage of acrylate and thiol-acrylate systems. The addition of clay particles in photopolymer systems may inevitably affect the extent of oxygen inhibition and polymerization shrinkage by decreasing the diffusion rate of oxygen molecules and/or by reducing effective organic volume in the systems to some degree. The fundamental hypothesis supporting the third objective is that increased interaction between clays and polymers as well as any change in reaction mechanism by the functional groups of polymerizable organoclays may induce additional improvements in oxygen inhibition and polymerization shrinkage. To verify and generalize this assumption, various acrylate and thiol-acrylate systems that have different degrees of oxygen inhibition and shrinkage will be studied and compared.

In chapter 6, the effect of polymerizable organoclays on oxygen inhibition of acrylate and thiol-acrylate systems in which oxygen inhibits the polymerization to various extents will be examined. In order to clearly identify the net clay effects on oxygen inhibition, various acrylate monomer systems will be examined with different levels of inherent oxygen inhibition. Controlled amounts of thiol will also be added to the acrylate mixtures to examine the thiol effect on oxygen inhibition. The synergetic effects of incorporating polymerizable organoclays on oxygen inhibition will be then examined at various thiol concentrations by comparing the results with the neat systems. The photopolymerization behavior will be investigated utilizing photo-DSC and real-time FTIR in the presence of oxygen and the rates in nitrogen atmosphere will be used as the comparison criteria for the degree of oxygen inhibition. The most interesting question in examining the clay effects is whether oxygen inhibition is different based on the type of organoclays, or more specifically by the type of functional groups on the clay surface. If existed and significant improvement is possible by incorporating appropriate types of polymerizable organoclays, the results from the study may show promise for many applications that must be processed in air.

Using a similar concept for the work in chapter 6, chapter 7 will investigate the effects of polymerizable organoclays on the polymerization shrinkage of both acrylate and thiol-acrylate systems. The effects of incorporating thiol monomers into acrylate mixture will be examined prior to incorporating organoclays to demonstrate the net clay effect on polymerization shrinkage. To investigate the effects of adding organoclays on polymerization shrinkage, both the volume shrinkage and shrinkage stress, typical comparison criteria for polymerization shrinkage, of acrylate and thiol-acrylate formulations will be examined during photopolymerization with and without addition of (organo)clays based on appropriate ASTM standards. In addition to examining these basic shrinkage characteristics of the systems, simultaneous conversion analysis utilizing near-IR and RTIR instrumentals will be performed for further understanding of the evolution behavior of polymerization shrinkage. Knowledge obtained from accomplishing the third objective will be highly useful for overcoming such major disadvantages of conventional (meth)acrylate photopolymerization.

According to organic-inorganic composite theory, use of well dispersed inorganic fillers often improves many performance characteristics of polymer systems. With a greater degree of increased interaction between clay surface and polymer matrix via chemical reaction with organic phase by incorporating the functional groups in the clay structure, it may be expected that much improvement on the ultimate composite performances could be achieved with polymerizable organoclays than that by conventional non-reactive organoclays. To verify this hypothesis, the fifth objective (Chapter 8) further investigates the overall effects of polymerizable organoclays on various performance characteristics of photopolymer clay nanocomposites based on both acrylate and thiol-acrylate photopolymerization systems. Mechanical properties based on tensile experiments and thermal stability will be examined utilizing dynamic mechanical analysis (DMA) and thermo gravimetric analysis (TGA), respectively. Gas barrier properties which are important characteristics for major photopolymer applications such



as coating and film packaging will be studied as the addition of plate-shape clay particles may enhance the barrier properties by generating longer path-length for gas molecules to diffuse. To study the organoclay effect on improving the gas barrier properties of various photopolymer clay systems, the water vapor transmission rate will be compared utilizing an industrial ASTM standard by changing the monomers as well as organoclay type. The results obtained by completing this final objective should provide further information beneficial for design of advanced photopolymer clay nanocomposites exhibiting superior performance to that in conventional acrylate photopolymer materials.

In accomplishing all objectives, the relationships between polymerization behavior and ultimate performances of nanocomposite materials will be elucidated. Fundamental understanding regarding the influence of clay morphology, organoclay-monomer interactions on photopolymerization behavior as well as thermo-mechanical and physical properties will present useful knowledge in control of the nanocomposite process and performance while ultimately contributing to developing advanced photopolymer materials and new applications. In addition, the knowledge from this research may be also used for current photopolymer fabrication by utilizing polymerizable organoclays as a polymer modifier to modulate polymerization behavior, thermo-mechanical properties, and other processing characteristics such as polymerization shrinkage and oxygen inhibition.

## CHAPTER 3

### MATERIALS AND METHODOLOGY

This chapter describes the materials and methods used to fabricate various organoclays and examine the degree of organoclay exfoliation, photopolymerization behavior, and thermal and mechanical properties of photopolymer clay nanocomposites in fulfillment of the objectives for this research. The materials section of this chapter describes monomers for acrylate and thiol-acrylate formulations, photoinitiators, and organic surfactants that are used for surface modification of clays. The method sections discuss the synthesis of polymerizable surfactants, fabrication of organically modified clay, sample preparation, and characterization procedures for thermo-mechanical analysis as well as other performance evaluations. The polymerization kinetics and mechanisms were examined with the complementary techniques of photo-differential scanning calorimetry (PDSC) and real-time infrared spectroscopy (RTIR). Additionally, RTIR is used to characterize synthesized surfactants and organically modified clays. Small angle X-ray scattering (SAX) analyses were used to monitor organoclay dispersion in various monomer mixtures before and after photopolymerization. The characterization of various thermo-mechanical properties including glass transition temperature, modulus of the cured photopolymers, and tensile properties by DMA analysis is described. Finally, the last section of this chapter discusses the modification and use of methodologies for diverse performance evaluations based on ASTM standards.

#### Materials

This research will mainly deal with the effects of incorporating organoclays on photopolymerization behavior and overall performance of nanocomposites focused

especially on advanced thiol-acrylate photopolymerization systems. It essentially involves organic modification of the clay surface utilizing various types of organic surfactants with potential difference in hydrophilic characteristics based on chemical structures. Natural clays are inherently very polar materials but can be changed to organophilic ones by surface modification utilizing surfactants. In addition, clay modification to produce diverse polymerizable organoclays often requires repeated organic modifications to change the reactive groups on the clay surface to different types of functional groups which may induces further differences in hydrophilicity. If there is a considerable difference in hydrophilicity of organoclays, monomer polarity might be a potentially important factor in designing monomer systems because the interaction between organoclays and monomers significantly depends upon chemical compatibility of components in the system as well as the viscosity of ultimate formulation in general. The selection of materials is thus critical for accomplishing the objectives of this research. In addition, final composite properties and polymerization kinetics will be controlled through the selection of appropriate reactive monomers and oligomers, photoinitiators, and polymerizable surfactants. For these reasons, the important variables for the selection of monomers and oligomers are polarity, viscosity, structure, and functionality, all of which may have a significant impact on final properties and exfoliation behavior in clay dispersion. Based on this premise, various monomers were used to investigate the effect of organoclays on both the processing factors and ultimate properties of photopolymer clay nanocomposites.

Therefore, to examine the effect of monomer structure on clay exfoliation and polymerization behavior, two di-acrylate monomers with variable polarities were used in this research. 1,6-hexanediol diacrylate (HDDA) was compared with less hydrophobic tripropylene glycol diacrylate (TrPGDA). Poly(ethylene glycol) diacrylate with number average molecular weight 740 (PEGDA 600) were utilized when required to increase the hydrophilic nature of the monomer composition and/or to induce enhanced flexibility of

the cured materials for an easy preparation of film or plate like samples. Trimethylolpropane triacrylate (TMPTA) was selected as a higher functionality acrylate monomer and used as a model system with the highest polymerization shrinkage. To increase system viscosity for studying the viscosity effects in the nanocomposite process, polyester based urethane acrylate oligomer (CN9009, MW= approximately 3,000) was used as a higher molecular weight oligomer. CN9009 was also used for significantly increasing the toughness of cured films. All monomers were obtained from Sartomer (Exton, PA) and used without further purification.

In choosing the thiol monomers, 1,6-Hexanedithiol (HDT, from Aldrich), which has a similar structure to HDDA, was used as the basic difunctional thiol with a relatively hydrophobic nature. When it is needed to increase polarity of thiol monomer, HDT was replaced by more polar glycol di-3-mercaptopropionate (GDMP, from Bruno Bock Chemische Fabric GMBH & Co., Hamburg, Germany). Trimethylolpropane trimercaptopropionate (TMPTMP, from Aldrich) that has a similar structure as trifunctional TMPTA was used as a trifunctional thiol monomer to produce higher cross linking density. 2,2-dimethoxyphenyl acetophenone (DMPA, Ciba Specialty Chemicals) was used as a free radical photoinitiator in all experiments. The structures for these multifunctional acrylate/thiol monomers and the photoinitiator are illustrated in Figure3.1. In addition to these monomers, tetrahydrofuran (THF – Aldrich), diethyl amine (DEA – Aldrich), ethanol and methanol (Aaper Alcohol and Chemical, Shelbyville, KY) were used as solvents in synthetic procedures of various surfactants.

Controlling formulation variables with consistency in selection of monomers and organoclays will be important for comparing the results between the characterizations of certain properties. Most importantly, polymerizable surfactants must be prepared considering several factors such as the type of substituted reactive moiety, its

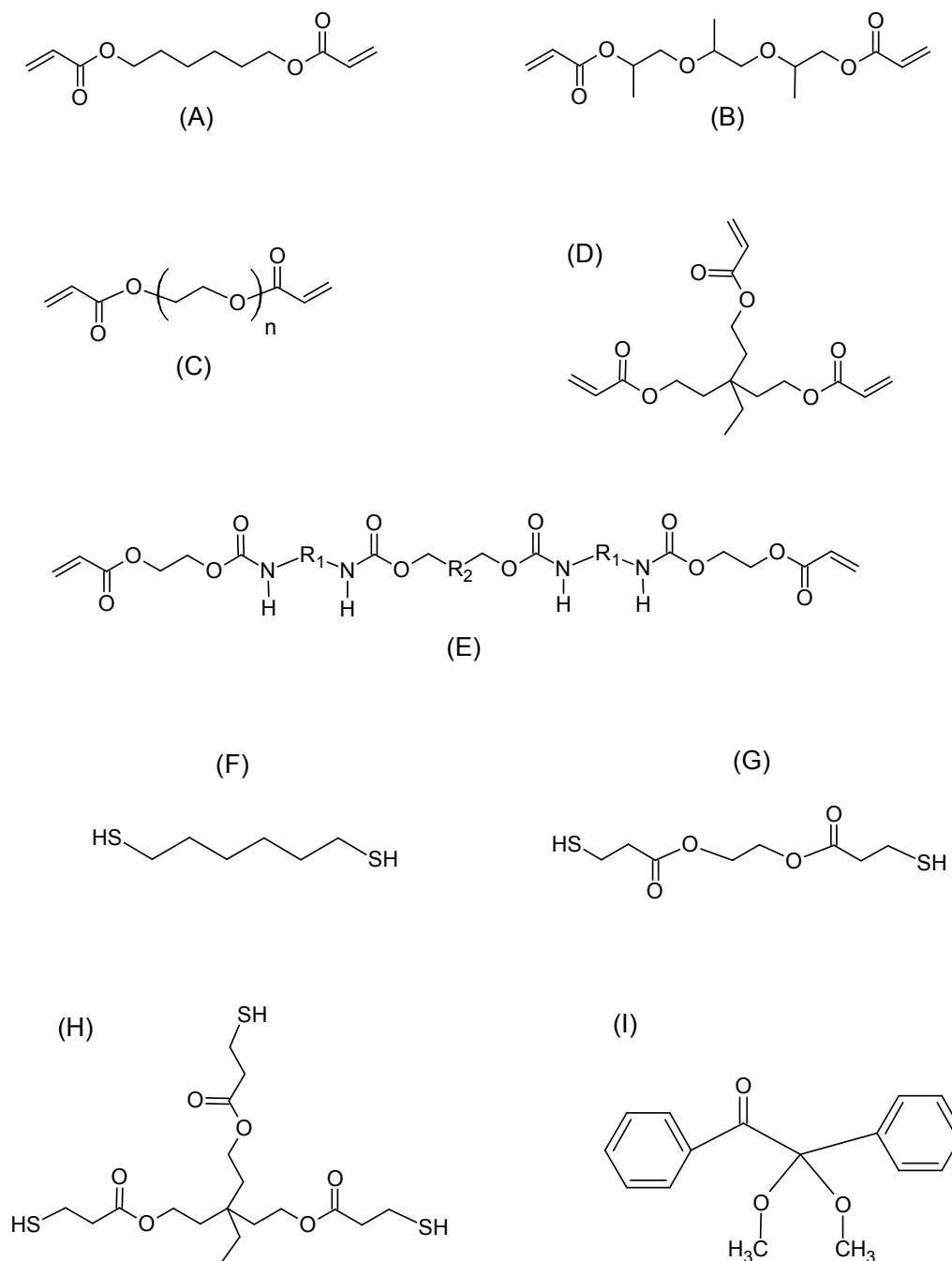


**Figure 3.1.** Chemical structures of multifunctional acrylate and thiol monomers used in this study. Shown are (A) 1,6-hexanediol diacrylate (HDDA), (B) tripropylene glycol diacrylate (TrPGDA), (C) polymethyleneglycol diacrylate (PEGDA 600, MW=742), (D) trimethylolpropane triacrylate (TMPTA), (E) polyester type polyurethane diacrylate oligomer (CN9009, MW=3,000), (F) 1,6-hexanediol dithiol (HDT), (G) ethyleneglycol di(3-mercaptopropionate) (GDMP), (H) trimethylolpropane tris(3-mercaptopropionate) (TMPTMP), and (I) 2,2-dimethoxyphenyl acetophenone (DMPA).

position, attached alkyl chain length, and number of reactive groups in their structure corresponding to polymerization systems.

The organoclays used in this study were either developed in the lab or obtained from Southern Clay Products (Gonzales, Texas). Cloisite 93A is commercially available nonreactive organoclay (CL 93A) that has a cation exchange capacity (CEC) of 90meq/100g clay. CL 93A is modified by the quaternary ammonium surfactant including methyl dihydrogenated tallow (Me2HT, HT = ~65% C18, ~30% C16, ~5% C14) in the structure. CL93A is inherently hydrophobic due to long alkyl chain HT moieties on the surface. This clay was used as a model commercial nonreactive organoclay from industry for comparative studies. Another nonreactive organoclay was prepared in the lab utilizing tetradecyltrimethyl ammonium bromide (TTAB, Aldrich) and also used in the purpose of comparison. For easy identification, all organoclays will be referred to as a surfactant name followed by organoclay. For instance, TTAB organoclays indicates the organoclay modified with TTAB surfactant. A natural montmorillonite Cloisite Na clay from Southern Clay Products (CL Na, CEC = 92.6meq/100g clay) was used as the pristine clay for generating organoclays via surfactant modification. Organoclays bearing these surfactants were produced following typical cation exchange procedures.[1]

In addition, various types of polymerizable organoclays were prepared utilizing relevant polymerizable surfactants that are TTAB analogues but include acrylate and thiol functionalities in the structures. Hexadecyl 2-acryloyloxy(ethyl) dimethylammonium bromide (C16A) was utilized to generate the polymerizable organoclay with acrylate functional groups on the clay surface. Thiolated quaternary ammonium surfactants were developed from tetradecyl 2-acryloyloxy(ethyl) dimethylammonium bromide (C14A) surfactant. After producing the C14A acrylated organoclays by modifying Cloisite Na pristine clay using C14A surfactant, further modification to incorporate thiol functional groups in the surfactant structures was then conducted utilizing appropriate thiol monomers as discussed later. All surfactants were

synthesized based on previously described methods. [2-4] Chemical structures of surfactants used in producing organoclays including both nonreactive and polymerizable versions are shown in Figure 3.2.

### Surfactant synthesis and clay modification

Acrylated quaternary ammonium bromide including C14A and C16A were synthesized following procedures previously described by McGrath et al. and Nagai et al.[1,5] Equimolar amounts of 2-(dimethylamino)-ethyl acrylate and an alkyl bromide were charged into a round bottom flask. 50mL acetone was added to the mixture and brought to a temperature of 40°C. The reaction mixture was stirred continuously at this temperature for three days and followed by removing acetone through vacuum evaporation utilizing a rotary evaporator. Anhydrous diethyl ether was added to the crude product and stored at 4°C for 48 hours. The anhydrous ether was removed by vacuum filtration and the product was recrystallized several times to purify in dry ethyl acetate. Obtained white crystalline powder was then dried overnight in a vacuum oven. FTIR was used to characterize the product afterwards.

As an example, the synthesis of C16A is accomplished by charging 10.0g (0.068 mol) of 2-(dimethylamino)ethyl acrylate into a 500mL round bottom flask with a stir bar. The flask is placed in an oil bath at 40°C. 21.5g of 1-bromotetradecane (0.067mol) is added to the mixture with 50mL of acetone. The round bottom flask was sealed and a needle inserted into the stopper to vent the reaction. Reaction was allowed to continue for three days. The mixture was removed and the acetone evaporated by rotary evaporation. Anhydrous diethyl ether was added to the oily crude product and stored in a refrigerator for two days. The anhydrous diethyl ether was filtered afterwards to leave white powder precipitates. The precipitates was dissolved in approximately 100mL of ethyl acetate and

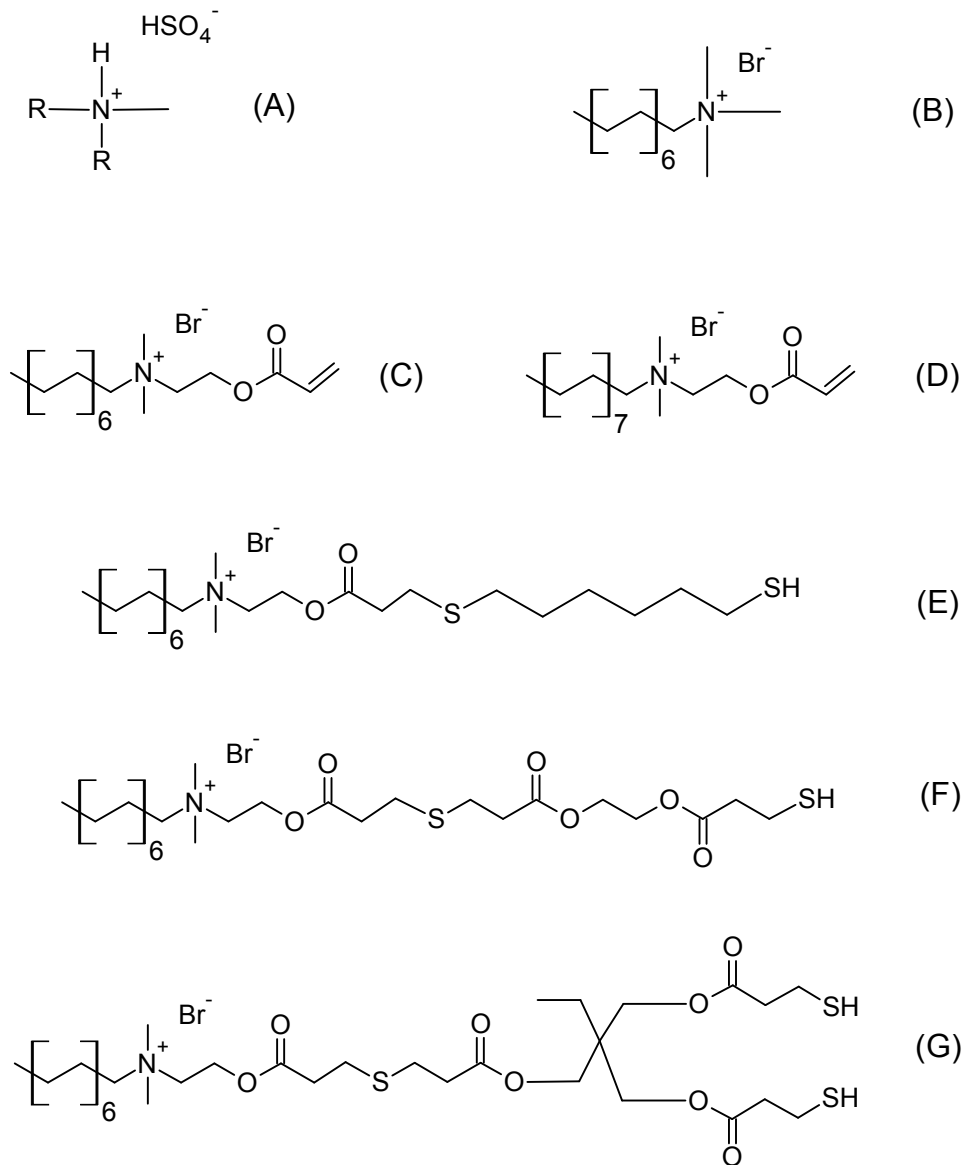


**Figure 3.2.** Chemical structures of quaternary ammonium surfactants used for clay structure modification. Shown are (A) methyl dihydrogenated tallow sulfonate, (CL93A) (B) tetradecyl trimethylammonium bromide, TTAB (C) tetradecyl-2-acryloyloxy(ethyl) dimethylammonium bromide (C14A) (D) hexadecyl-2-acryloyloxy(ethyl) dimethylammonium bromide (C16A) (E) tetradecyl 2-(1,6-mercaptohexyl mercaptane) acetoxy(ethyl) dimethylammonium bromide (C14AHT; Monothiol) (F) tetradecyl 2-(1,3-mercaptopropionate mercaptopropionyl ethyleneglycol)acetoxy(ethyl) dimethylammonium bromide (C14AGT) (G) tetradecyl 2-(bis(3-mercaptopropionate) mercaptopropionyl trimethylolpropyl) acetoxy(ethyl) dimethylammonium bromide (PSH2; Dithiol).



the mixture was heated for facile dissolution. Three milliliters (3mL) of hexane was added to crystallize the product. The crystallization process was repeated three times in ethyl acetate to obtain pure product in high yield. The final product was dried overnight in a vacuum. FTIR was used to confirm presence of carbon-carbon double bond (C=C out of plane stretch at  $810\text{ cm}^{-1}$ ), carbonyl (C=O peak at  $1735\text{ cm}^{-1}$ ) and methylene ( $\text{CH}_2$  stretch at  $2860\text{ cm}^{-1}$  and  $2940\text{ cm}^{-1}$ ) peaks. FTIR characterization of the surfactants was accomplished using a Thermo Nicolet Nexus 670 Fourier transform infrared spectrometer (FTIR). The FTIR was fitted with a liquid nitrogen cooled MTG detector and four scans per second were recorded with 64 scans per spectrum collected. Other polymerizable surfactants with acrylate functional groups and variable aliphatic chain length in the surfactant structure were synthesized according to the same procedure utilizing acrylate and different chain length precursors.

In order to modify clay surfaces with polymerizable surfactants, Cloisite Na (Southern Clay Products, Gonzalez, TX), a natural montmorillonite containing sodium cations between silicate platelets, was ion exchanged using acrylate or thiol functionalized quaternary ammonium surfactants as described in the literature. [1] As an example, the synthesis of C14A acrylated organoclay including one acrylate double bond in each surfactant structure is described in detail. 10g of Cloisite Na natural clay was added to 2,000mL of ethanol/water (50/50 weight ratio) mixture and stirred vigorously at least for 30 minutes. The clay mixture was then sonicated for 1 hour and cooled to room temperature. Meanwhile, 4.2g of C14A (sufficient to achieve 100% cation exchange capacity with 10% excess from the theoretical amount) was dissolved in 200mL methanol. The surfactant solution was added to the clay mixture and stirred continuously for 24 hours. The resulting mixture is washed several times with aqueous ethanol solution (50/50 volume ratio) and centrifuged after every wash. The wet product was freeze-dried at  $-100^\circ\text{C}$  under high vacuum. The cation exchange process was evaluated utilizing FTIR spectroscopy. Absorbance peaks in the FTIR spectra characteristic of C=C double bonds

( $810\text{cm}^{-1}$  out of plane bend), carbonyl ( $1735\text{ cm}^{-1}$ ) and methylene groups ( $2850\text{cm}^{-1}$  and  $2920\text{cm}^{-1}$ ) in the surfactants confirmed the presence of surfactants in the organoclay. C16A acrylated organoclay was produced the same process except for utilizing hexadecyl-2-acryloyloxy(ethyl) dimethylammonium bromide (C16A surfactant).

Thiol functionalized organoclays were synthesized by incorporating a multifunctional thiol monomer into C14A acrylated organoclay modified by tetradecyl-2-acryloyloxy(ethyl) dimethylammonium bromide (C14A surfactant) via Michael addition reaction based on procedures reported elsewhere. [6] C14A surfactant has the same structure as C16A surfactant except for that the carbon number in the alkyl tail group is fourteen instead of sixteen. Based on ease of purification in the synthesis processes, C14A organoclay is used as the basic acrylate organoclay to generate thiolated organoclays. Three types of different thiolated organoclays were prepared to control both the structure and functionality of thiol groups on the clay surfaces. To provide monothiol functional group in each surfactant structure, 1,6-hexanedithiol (HDT) or GDMP was reacted with C14A acrylated organoclays. In the same manner, trithiol functional TMPTMP was utilized to produce dithiol functionality in each surfactant structure (PSH2). Again, for easy comparison of polymerizable organoclay types, acrylated organoclays or thiolated organoclays will be identified with the name of surfactant used in the clay modification. For instance, C14AHT organoclay indicates the thiolated organoclay produced from the reaction between C14A acrylated organoclay and 1,6-hexanedithiol (HDT) while C14AGT indicates the thiolated organoclay produced from C14A acrylated organoclay and GDMP dithiol monomer. In order to provide an example in thiol modification of acrylated organoclays, the preparation processes thiolated organoclay including two thiols in each surfactant structure (PSH2) are described.

5g of dry C14A organoclay was weighed into a round bottom flask followed by adding 50mL THF. The mixture was stirred continuously for 30 minutes followed by sonication for one hour to aid clay dispersion. After cooling the mixture to room

temperature, excess thiol (5g, relevant to approximately 10 times dosage compared to theoretical amount) was added and stirred for another 30 minutes. Diethyl amine (1 mol %) was added drop-wise to catalyze the thiol-acrylate reaction under continuous stirring for 24 hours. Afterwards, the mixture was separated by centrifugation and washed several times with THF to remove all unreacted reagents. The resulting organoclay was freeze-dried and characterized for the presence of thiol functional groups utilizing FTIR. Successful thiol modification of C14A acrylated organoclay was verified by disappearing of acrylate peak ( $C=C$  at  $810\text{ cm}^{-1}$ ) with new generation of thiol peak ( $SH$  at  $2570\text{ cm}^{-1}$ ), indicating the existence of thiols on the clay structure.

#### Sample Preparation

In order to investigate the exfoliation behavior and morphology of the clay dispersion before and after polymerization, designated amount of organoclays were weighed into a 15mL vial and 10g of monomer mixture were added followed by mixing via a vortex mixer. The clay-monomer mixture was then sonicated for two hours in a water bath with temperature not exceeding  $35^{\circ}\text{C}$  to minimize any potential reaction. Photoinitiator was added after sonication to prevent initiator decomposition during the process. Especially for thiol-acrylate mixtures, organoclay were mixed with acrylate monomer first and then thiol monomers were added after the sonication process to prevent the mixture from self-initiation. Once the photoinitiators were incorporated, the reaction mixtures were kept at about  $-6^{\circ}\text{C}$  by covering the sample vial with aluminum foil for better preservation of samples without significant premature photopolymerization. Small angle X-ray diffraction (SAXS) that can provide quantitative extent of clay exfoliation was utilized to compare the exfoliation behavior of clays in the monomer mixture and the polymer. A Nonius FR590 X-ray apparatus with a standard copper target

Rontgen tube radiation source ( $\lambda = 1.54 \text{ \AA}$ ) at 40kV and 30mA intensity, a camera, a collimation system of the Kratky type, and a PSD 50M position sensitive linear detector (Hercus M. Braun, Graz) was used to characterize the dispersion behavior. [7] The extent of dispersion was evaluated based on the position of the primary X-ray peak as well as the breadth of the peak. Interlayer distances between two adjacent clay platelets are represented by the peak of the primary beam for intercalated organoclay morphologies. Upon exfoliation, the periodic 2 theta scattering peaks disappear from the SAXS spectra. To determine morphological changes and extent of clay exfoliation, Bragg's law (Equation 3.1) was used to correlate the peak position with spacing of clay platelets. Where  $n$  is an integer,  $\lambda$  is the wavelength of incident wave,  $d$  is the spacing between the clay plates, and  $\theta$  is the angle between the incident ray and the scattering planes.

$$n\lambda = 2d \sin \theta \quad (3.1)$$

Rectangular sample bars were used for examining dynamic mechanical analysis (DMA), thermo-gravimetric analysis (TGA), and other performance evaluations such as volume shrinkage and tensile experiments. To fabricate the samples with appropriate dimensions (1~2mm x 13mm x 25mm, / thickness x width x length), liquid monomer mixtures were injected between two microscope slides end-capped with 2 mm spacers. The glass mold was then placed into a nitrogen-purged box fitted with a 200W medium pressure mercury-xenon lamp. Photopolymerization was initiated at approximate 3.0 mW/cm<sup>2</sup> light intensity for 10 minutes on each side. To fabricate the 110 $\mu$ m thin composite films for examining gas barrier properties based on ASTM standard, controlled amounts of liquid monomer mixtures were placed between thick glass plates (20mm x 150mm x 150 mm / thickness x width x length). Glass plates were covered with 100 $\mu$ m thick polyvinylidene difluoride film for easy releasing the cured polymer films. On

one of the glass plates, thin tape spacers were attached to control the cured film thickness. After placing the monomer mixtures on the bottom glass plate, bubbles were removed by applying a vacuum to prevent pin-hole formation. Afterward, the upper plate was covered, followed by tightly clamping. The mold was then exposed to 250~450 nm UV light at 18 mW/cm<sup>2</sup> for 5 minutes on each side.

### Material Characterization

Photo-differential calorimetry (PDSC) and real time infrared spectroscopy (RTIR) were used for studying the photopolymerization behavior. Photopolymerization rates were monitored using a Perkin Elmer Diamond differential scanning calorimeter modified with a medium pressure mercury arc lamp (PDSC). Rates of photopolymerization were measured using the full spectrum of UV light emitted by the lamp or 365 nm light by penetrating the UV filter. Neutral density filters were also used to control light intensity if needed. Photopolymerization rates were compared using the evolved heat during the polymerization as recorded. [8] From the exothermic heat in the sample cell due to polymerization reaction, both polymerization rates and the conversion of functional group were calculated according to the equations (3.2) and (3.3) as follows:

$$\frac{R_p}{[M]} = \frac{\Delta Q \cdot M_w}{n \cdot \Delta H_{p1} \cdot m} \quad (3.2)$$

$$\frac{R_p}{[M]} = \Delta Q \left[ \left( \frac{M_w}{n \cdot \Delta H_{p1} \cdot m} \right)_{\text{acrylate}} + \left( \frac{M_w}{n \cdot \Delta H_{p2} \cdot m} \right)_{\text{thiol}} \right] \quad (3.3)$$

where  $R_p$  represents the rate of polymerization,  $H_p$  is the theoretical heat of polymerization and  $Q$  is the evolved heat as measured by PDSC,  $n$  is functionality of monomers,  $M_w$  represents the molecular weight of monomer, and  $m$  is the sample mass. Equation (1) is for pure acrylic polymerization and (2) is for thiol-ene (thiol-acrylate) copolymerization. Equation (2) is normalized to the total concentration of reactive species in the formulation to eliminate concentration dependence effects when comparing photopolymerization rates for different formulations. Polymerization heat for acrylate double bonds ( $\Delta H_{p1}$ ) is equal to 86,194 J/mol from literature [9] and that for thiol groups ( $\Delta H_{p2}$ ) is determined to be approximately 63,000 J/mol through the basic kinetic studies.

Real time infrared spectroscopy (RTIR, Thermo Nicolet Nexus 670) will be used as a complementary method to PDSC. Even though double bond conversion can be calculated from PDSC data, RTIR provides more accurate conversion profiles. Furthermore, RTIR gives separate conversion profiles for different functional groups such as thiol and acrylate based on the absorbance frequencies that are specific to individual functional groups. RTIR kinetic studies were conducted by sandwiching approximately 25 $\mu$ L samples between two sodium chloride slides. Polymerization was carried out in a nitrogen purge box fitted with a horizontal sample stage. Measurements were performed at ambient temperature after purging the RTIR chamber for 6 minutes with dry nitrogen gas. An UV beam was provided by an optical fiber cable from a medium pressure mercury lamp (EXPO Acticure). Changes in the intensity of the IR absorbance peak characteristic of specific functional groups were monitored at the wavelength of interest. Both area and height of the absorbance peaks of functional groups change continuously as they react during polymerization. These absorbance changes are then used to calculate the conversion of functional groups according to the equation (3.4)

$$\alpha = 1 - (A_t/A_0) \quad (3.4)$$

where  $\alpha$  represents functional group conversion,  $A_0$  represents absorbance at time zero and  $A_t$  is the absorbance at a certain time  $t$  during photopolymerization. For thiol-acrylate systems, functional group conversion was evaluated by monitoring the decrease in the height of the absorbance peak at  $810\text{ cm}^{-1}$  for acrylate and at  $2575\text{ cm}^{-1}$  for thiol. Photopolymerization reactions were initiated with a  $365\text{ nm}$  light at  $3.0\text{ mW/cm}^2$ .

Dynamic mechanic analysis (DMA- Q800 DMA TA Instruments) was conducted to investigate the effect of organoclays on ultimate mechanical properties. To measure the modulus and glass transition temperature, rectangular sample bars ( $2\text{ mm} \times 13\text{ mm} \times 25\text{ mm}$ ) were heated from  $-100^\circ\text{C}$  to  $100^\circ\text{C}$  at  $3^\circ\text{C}/\text{min}$ . Measurements were made in tensile mode with a single cantilever oscillating at  $1\text{ Hz}$ . Storage modulus and  $\tan \delta$  using a deformation strain of  $0.05\%$  were recorded and plotted against temperature to determine the glass transition temperature ( $T_g$ ) of the material, often recognized as the temperature corresponding to the peak in the  $\tan \delta$  temperature profile. Tensile experiments were conducted based on DMA controlled force tensile mode with  $0.5\text{ N/min}$  ramp rate at  $30^\circ\text{C}$  using rectangular specimen ( $1\text{ mm} \times 5\text{ mm} \times 20\text{ mm}$ ). Young's modulus calculation was performed utilizing the slope of the stress-strain curve in the early linear regime (less than  $10\%$  strain). Thermal stability of photopolymer clay nanocomposites was examined utilizing thermo-gravimetric analysis (TGA, Perkin Elmer Pyris 1). Approximately  $8\text{ mg}$  of sample prepared using the same photopolymerization conditions as for the DMA experiment was heated from  $30^\circ\text{C}$  to  $700^\circ\text{C}$  at a heating rate of  $10^\circ\text{C}/\text{min}$  in air.

Volume shrinkage during photopolymerization was evaluated based on the density difference between liquid monomer mixture and its photopolymerized solid sample. The density of liquid monomer mixtures ( $D_L$ ) were evaluated at  $25^\circ\text{C}$  by measuring the mass of a  $100\text{ ml}$  sample. The liquid monomer mixture was then inserted into a sandwiched glass plate mold and polymerized using  $3.3\text{ mW/cm}^2$  light from a medium pressure mercury UV lamp for  $20$  minutes. To measure the volume of

polymerized samples, cured sample bars were immersed into water and sonicated for 2 minutes to remove any bubbles on the sample surface. Solid density ( $D_s$ ) was calculated from the weight of cured polymer and increased water volume. Volume shrinkage was then determined from the density difference between liquid monomers and polymerized solid samples using equation (3.5).

$$\text{Volume Shrinkage (\%)} = \left( \frac{\left( \frac{1}{D_L} \right) - \left( \frac{1}{D_s} \right)}{\left( \frac{1}{D_L} \right)} \right) \times 100(\%) \quad (3.5)$$

In order to evaluate the shrinkage stress of monomer mixtures during photopolymerization, a cantilever beam method modified from an ASTM standard was utilized. Liquid monomer mixture with controlled coating thickness and length is placed on a stainless steel plate (SUS-304) with 0.1 mm thickness. Once the coated plate, which is tightly clamped on one side, is exposed to UV light, the metal plate deforms due to shrinkage stress through polymerization, and the height of the unclamped side changes from its initial value. The shrinkage stress is then calculated from the height difference of unclamped side between before and after polymerization based on Corcoran's relation as shown in (3.6).

$$S = \left( \frac{hE_s t^3}{3L^2 c(t+c)(1-\gamma_s)} \right) + \left( \frac{hE_c(t+c)}{L_2(1-\gamma_c)} \right) \quad (3.6)$$

where, S is shrinkage stress (MPa), h is the deflection of the cantilever (mm),  $E_s$  is the elastic modulus of the stainless steel substrate (193,000 MPa for SUS 304 steel), [10]  $\gamma_s$  is the Poisson's ratio of the substrate (0.25 for SUS304 steel), [10]  $E_c$  is the elastic modulus



of the coating materials (e.g. 14.5 MPa for thiol-acrylate compositions including 20mol% thiol functional groups as measured by DMA at 23° C),  $\gamma_c$  is the Poisson's ratio of the coating, L is the length of the coating, t is the thickness of the substrate, and c is the thickness of the coating.

To investigate the impact of adding organoclay into photopolymer system on gas barrier properties, the water vapor transmission rate (WVTR) through photopolymer clay nanocomposite films including 3wt% various (organo)clays was examined using an apparatus based on an ASTM standard [11] utilizing 100 $\mu$ m thin nanocomposite films in comparison with neat systems. A glass vessel with a 12cm diameter opening was used as a test dish and covered by the nanocomposite films followed by an effective seal using adhesive films. Before covering the WVTR vessel with the prepared thin films, 100g of distilled water was charged into the vessel. All parts were assembled with an effective seal using adhesive films. After recording initial weights, the sealed vessels were placed in a convection hood controlled at 23°C and mass loss was measured. WVTR per unit area was, then, compared considering the thickness of composite films. In studying the gas transfer rate, homogeneity in the thickness of the thin film and the absence of defects is critical to achieve good experimental results. The ultimate cured film thickness was thus controlled to 100 microns at most 5% error. To compare the experimental reproducibility with the ASTM standard, 100  $\mu$ m PET film (Mylar) was used as the control system. The measured WVTR value of the PET film was compared with the literature value obtained based on a similar methodology. [12]

Notes

1. Lagaly, G.; Beneke, K. *Colloid Polym. Sci.* **1991**, 269, 1198.
2. McGrath, K. M.; Drummond, C. J. *Colloid Polym. Sci.* **1996**, 274, 612.
3. Joynes, D.; Sherrington, D. C. *Polymer* **2006**, 37, 1453.
4. Eastoe, J.; Summers, M.; Heenan, R. K. *Chem. Mater.* **2000**, 12, 3533.
5. Nagai K.; Ohishi, Y. *J. Polym. Sci., Part A*, **1987**, 25, 1.
6. Owusu-Adom, K.; Guymon, C. A. *Macromolecules* **2009**, 42, 3275.
7. Katti, K. S.; Sikdar, D.; Katti, D. R.; Ghosh, P.; Verma, D. *Polymer* **2006**, 47, 403.
8. Anseth, K. S.; Wang, C. M.; Bowman, C. N. *Macromolecules* **1994**, 27, 650.
9. Odian, G. *Principles of Polymerization*, 4<sup>th</sup> ed.; John Wiley & Sons: Hoboken, NJ, **2004**.
10. ASTM D 6991– 05, "Standard Test Method for Measurements of Internal Stresses in Organic Coatings by Cantilever (Beam) Method".
11. ASTM E96M-05, "Standard Test Methods for Water Vapor Transmission of Materials".
12. Auras, A. R.; Singh S. P.; Singh J. J. *Packaging Technology and Science* **2005**, 18(4), 207.

## CHAPTER 4

### PHOTOPOLYMERIZATION BEHAVIOR IN NANOCOMPOSITES FORMED WITH THIOL-ACRYLATE AND POLYMERIZABLE ORGANOCCLAYS

Due to the inherent characteristics of the thiol-ene step growth mechanism in preparation of thiol-ene photopolymer clay nanocomposites, the ratio between thiol and ene functional groups at and near the organoclay surfaces may have a significant effect on the polymerization behavior. This study investigates the influence of monomer composition and the type of polymerizable organoclay on thiol-acrylate photopolymerization behavior in preparation of photocurable clay nanocomposite systems. To this end, two types of polymerizable organoclays with acrylate or thiol functional group on the clay surfaces were compared in monomer compositions with different polarity and functionality. Real time infrared spectroscopy (RTIR) was used to characterize polymerization behavior in conjunction with photo-DSC. The degree of clay exfoliation was evaluated utilizing small angle x-ray scattering (SAXS) and correlated with photopolymerization behavior. Higher chemical compatibility of components induced enhanced clay exfoliation resulting in increase in photopolymerization rate. By affecting the stoichiometric ratio of functional groups in the clay gallery, thiolated organoclays enhance thiol-ene reaction while acrylated organoclays encourage acrylate homopolymerization. In addition, inducing more propagating thiyl radicals on the organoclay surfaces by increasing functionality of thiol monomer also facilitates thiol-ene copolymerization while the increase of acrylate functionality reduces final thiol conversion.

## Introduction

In recent decades considerable research interest has been devoted to hybrid polymer-clay nanocomposites because incorporation of clays dispersed at nanoscale dimensions into a polymer matrix can significantly improve performance such as mechanical and barrier properties, thermal stability, and chemical resistance with a very low clay concentration, typically below 5 wt%.[1-8] Photopolymerization could provide a simple method for *in situ* preparation of polymer-clay nanocomposites from well dispersed clay-monomer formulations.[7-9] Conventional composite manufacturing processes involve either melt-mixing of polymer with inorganic fillers or solvent based processes that may cause thermal degradation of the polymer, while releasing large amounts of volatile organic compounds (VOC) during the process.[2,3,10,11] *In situ* photopolymerization may overcome such drawbacks of conventional processes by using light energy for the polymerization, and producing polymer at ambient temperature with 100% solid content. Forming nanocomposites by *in situ* photopolymerization thus may allow fast production, spatial and temporal control of polymerization, and an environmentally friendly process.[7, 11-14]

In the preparation of polymer clay nanocomposites, the degree of clay exfoliation is critical for the ultimate nanocomposites performance.[3-5] Achieving clay exfoliation, however, is difficult due to the strong ionic attractions between the clay platelets.[14,15] Surface modification of clay to enhance compatibility with polymer is thus required to achieve clay exfoliation by overcoming electrostatic forces.[2-4,16,17] Quaternary ammonium surfactants have been studied to this end for highly delaminated clay dispersions in *in situ* polymerization.[16-21]

More recently, polymerizable surfactants with reactive functional groups have been investigated to modify the clay surface. Clays with reactive groups via modification using polymerizable surfactants can react with monomers and be incorporated into

polymer matrices during the photopolymerization process.[22,23] Generally, the addition of fillers decreases the photopolymerization rate by both scattering and absorbing the incident light that initiates photopolymerization.[24] In the preparation of photopolymer-clay nanocomposites, incorporation of only 1 wt% natural clay into a diacrylate monomer significantly lowers photopolymerization rate and further decreases were observed by increasing clay concentration up to 10 wt%.[22] However, when clays are modified by appropriate polymerizable surfactants, the rate either decreases to a much lower degree or even increases over neat systems. Previous research based on (meth)acrylate monomers demonstrates that the degree of clay exfoliation and the incorporation of appropriate functional groups on clay surfaces governs the photopolymerization behavior as well as final composite properties.[22,23,25] Well exfoliated clay particles induce higher rate of photopolymerization with the addition of polymerizable organoclays. It is believed that clay surfaces with large aspect ratios can interact with reactive monomers.[22,26] In addition, the decrease in termination rate by immobilization of the propagating chain during the photopolymerization can compensate for the light interference induced by clays.[27] Similarly, surface modification of inorganic fillers with reactive organic molecules produces many advantages because of increased interaction between fillers and organic phases based on strong covalent bonds. Such organically modified inorganic materials have been of significant interest in many fields such as nano-reactors from organo-layered silicates [28], polymer-graphene nanocomposites [29], clay nanocomposites via cationic photopolymerization [30], and grafted clay nanocomposites based on atom transfer radical polymerization.[31]

While acrylate-based photopolymerization is currently used in numerous applications, improvements of several aspects of photopolymers including shrinkage during polymerization, gas barrier properties, and abrasion and impact resistance are necessary for potential applications.[32,33] Thiol-ene photopolymerization is a promising and emerging technology to overcome some drawbacks of (meth)acrylate-based

photopolymerization. Thiol-ene photopolymerization occurs via a step-growth reaction mechanism that produces a more homogeneous network structure than acrylate homopolymerization, which decreases shrinkage during photopolymerization.[34-37] Properties of the network system can also be quite diverse based on the wide variety of commercially available monomers with ene functionality.[34] On the other hand, hard and tough materials are not easily obtained due to flexible thioether linkages.[34,37-39] The addition of suitable amounts of organoclay may facilitate higher mechanical properties in thiol-ene system. In addition, the incorporation of organoclays into thiol-ene systems may allow enhanced gas barrier property by generating longer diffusion pathlength for gaseous materials.[3,5] In addition, due to the inherent characteristics of step-growth reaction mechanism with thiol-ene photopolymerization, the photopolymerization behavior of thiol-ene photopolymer clay nanocomposites could be quite different from that of acrylate systems. Both the type of functional group on the clay surface and monomer composition in the clay galleries could affect the stoichiometric balance at the clay surface, resulting in different behavior during the photopolymerization process.[40] Because the properties of thiol-ene photopolymer clay nanocomposites depend largely on the degree of exfoliation as well as the network structure of the ultimate nanocomposite, understanding the relationship between photopolymerization behavior and clay exfoliation is important to achieve desirable properties of the thiol-ene composition with organoclays.[25, 41]

This research, therefore, studies the relationship between clay exfoliation and photopolymerization kinetics for thiol-ene compositions utilizing polymerizable surfactants with different functional groups. The photopolymerization behavior of selected thiol-acrylate systems was investigated with the addition of polymerizable organoclays bearing acrylate or thiol reactive moieties on their surface. The degree of clay exfoliation was examined and correlated to the polymerization kinetics of the system. To examine the effect of monomer structure on clay exfoliation, considering polarity and

cross-link density, diacrylates or triacrylates were copolymerized with dithiol or trithiol. With potential improvement of different characteristics, well-designed thiol-acrylate photopolymer-clay nanocomposites with use of suitable polymerizable surfactants could be a primary candidate for enhancing photopolymer applications.

## Experimental

### Materials

For thiol-acrylate polymerization, two difunctional acrylate monomers, 1,6-hexanediol diacrylate (HDDA) and tripropyleneglycol diacrylate (TrPGDA) were supplied by Sartomer Inc. (Exton, PA). 1,6-hexanedithiol (HDT) and trimethylolpropane trimercaptpropionate (TMPTMP) were obtained from Aldrich.

In order to develop polymerizable organoclays, Cloisite Na (Southern Clay Products – Gonzalez, TX), a natural montmorillonite with sodium cations between silicate platelets, was ion exchanged with acrylate or thiol modified quaternary ammonium surfactants as described elsewhere.[23] Hexadecyl-2-acryloyloxy(ethyl) dimethylammonium bromide (C16A) is an acrylated quaternary ammonium surfactant synthesized following methodologies described previously.[42] Organoclays with thiol functional groups were synthesized by incorporating a multifunctional thiol monomer into acrylate modified organoclays via a Michael addition reaction.[25] For example, dithiol functional clay (PSH2) was prepared through reaction of an acrylated organoclay with tetradecyl-2-acryloyloxy(ethyl) dimethylammonium bromide (C14A) on the surface and the tri-thiol functional TMPTMP. Hereafter, polymerizable clays will be indicated as acrylated or thiolated organoclays with the abbreviation of the surfactant identifying the dispersant. Two types of non reactive organoclays were used for comparison. Cloisite 93A (CL93A, Southern Clay Products), a montmorillonite clay modified with

dihydrogenated tallow, was used to represent a typical commercial nonreactive organoclay. TTAB organoclay modified by trimethyl tetradecylammoniumbromide (TTAB, Aldrich) was produced by ion exchange procedure using Cloisite Na.[23] The chemical structures of monomers and surfactants used in this research are illustrated in Figure 4.1 and Figure 4.2. 2,2-dimethoxyphenyl acetophenone (DMPA, Ciba Specialty Chemicals) was used as the free radical photoinitiator in all experiments. All chemicals including monomers and clays were used as received.

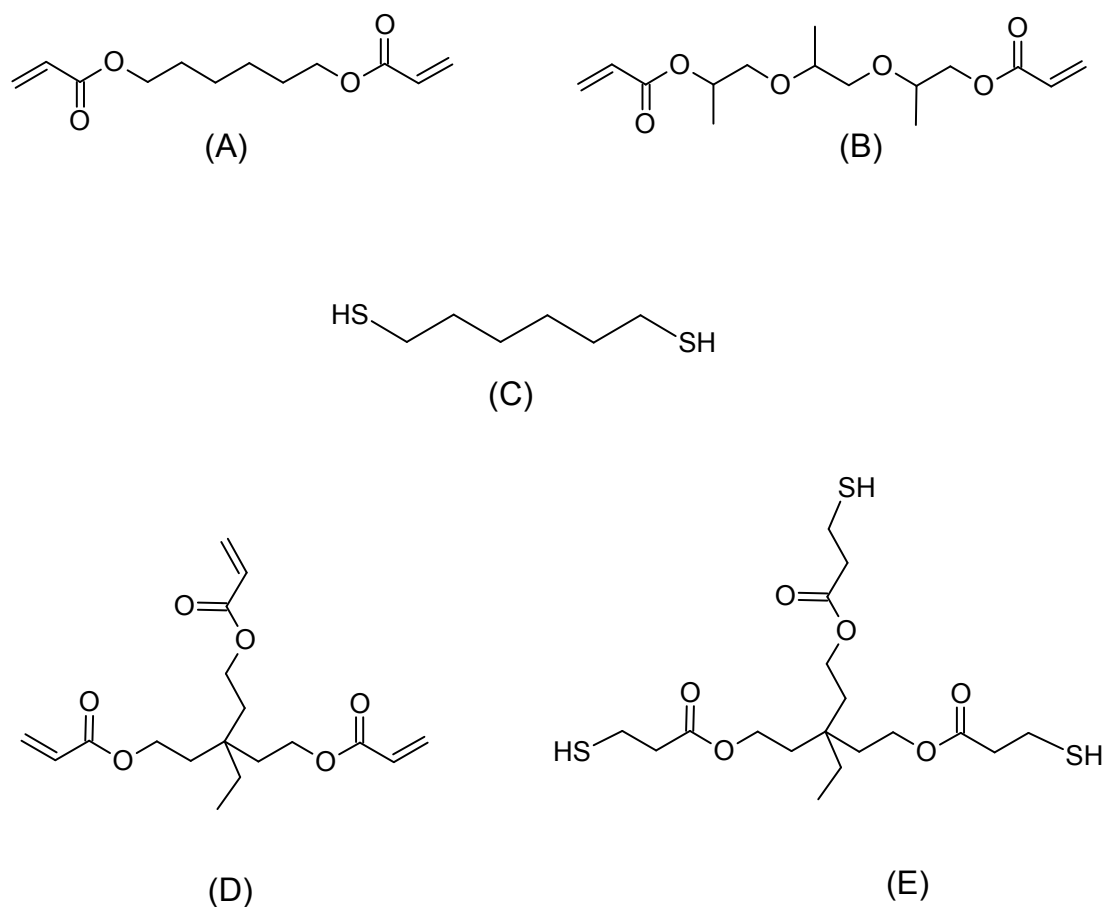


**Figure 4.1.** Chemical structures of monomers including (A) 1,6-hexanediol diacrylate (HDDA), (B) tripropylene glycol diacrylate (TrPGDA), (C) 1,6-hexanediol dithiol (HDT), (D) trimethylolpropane triacrylate (TMPTA), (E) trimethylolpropane tris(3-mercaptopropionate) (TMPTMP).



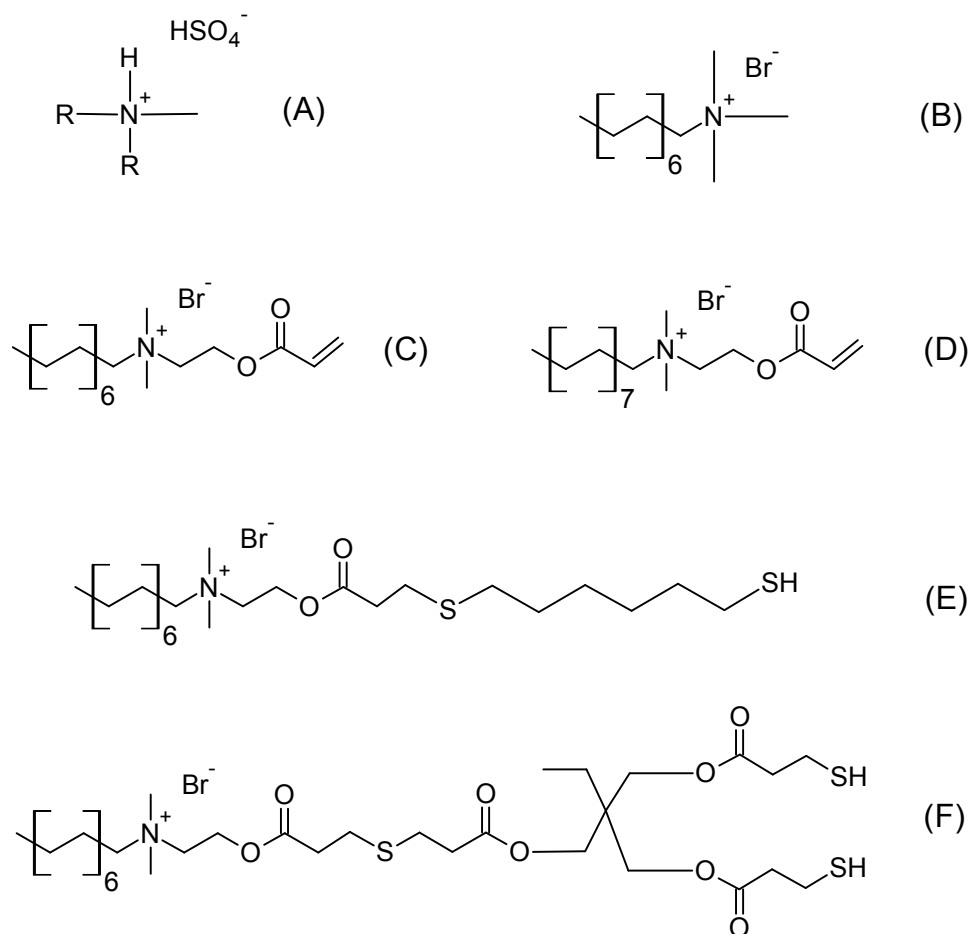


**Figure 4.2.** Chemical structures of surfactants used to modify clay surfaces. Shown are (A) methyl dihydrogenated tallow sulfonate, (Me2HT) (B) tetradecyl trimethylammonium bromide (TTAB), (C) tetradecyl-2-acryloyloxy(ethyl) dimethylammonium bromide (C14A) (D) hexadecyl-2-acryloyloxy(ethyl) dimethylammonium bromide (C16A) (E) tetradecyl 2-(1,6-mercaptohexyl mercaptane) acetoxy(ethyl) dimethylammonium bromide (C14AT; Monothiol), (F) tetradecyl 2-(bis(3-mercaptopropionate) mercaptopropionyl trimethylolpropyl) acetoxy(ethyl) dimethylammonium bromide (PSH2; Dithiol).

## Methods

Polymerization kinetics for thiol-ene photopolymerization was examined using real time infrared spectroscopy (RTIR, Thermo Nicolet Nexus 670). Monomer samples

were placed between two sodium chloride plates. Analysis was performed under ambient temperature while purging with nitrogen. The UV initiating source was provided from a medium pressure mercury lamp (EXPO Acticure) equipped with an optical fiber. During the polymerization, RTIR absorption spectra were continuously collected with 6 scans per second. Acrylate conversion was evaluated using the absorption band at  $810\text{ cm}^{-1}$  while thiol conversion was monitored at  $2575\text{ cm}^{-1}$ . [43] Conversion profiles as a function of time were obtained by monitoring the decrease in the height of the absorbance peak during polymerization. All polymerization reactions were performed with a 365 nm light at the irradiation intensity of  $3.0\text{mW/cm}^2$  at measured on sample surface.

Photopolymerization rates were also monitored using a Perkin Elmer Diamond differential scanning calorimeter modified with a medium pressure mercury arc lamp (photo-DSC). Rates of photopolymerization were measured using a 365 nm light at the irradiation intensity of  $3.0\text{mW/cm}^2$ . Photopolymerization rates were compared using the evolved heat during the polymerization as recorded by photo-DSC. [44]

Small angle x-ray scattering (SAXS) studies were used to evaluate the exfoliation of organoclays in liquid monomers and in the final polymer. A Nonius FR590 X-ray apparatus equipped with a Cu  $K\alpha$  radiation source ( $\lambda = 1.54\text{ \AA}$ ) at 40kV and 30mA intensity was utilized for SAXS experiments. [45]

### Results and Discussion

In thiol-ene photopolymerization, the stoichiometric balance between thiol and ene functional groups significantly affect not only the photopolymerization kinetics but also the final properties as the thiol can only react with ene groups. For this reason, the type of functional group on clay surfaces should be more important in thiol-ene systems than systems based only on acrylates. Lee et al. studied the effect of functional group on

polymerization kinetics of thiol-acrylated system with thiol functionalized silica nanoparticles.[40] Due to a stoichiometric imbalance at the spherical silica surface and immobilization of propagating thiyl-radicals, the polymerization rate decreased to some degree while there was no change with nonreactive particles.

In a recent study in our research group based on the thiol-acrylate systems (TrPGDA/TMPTMP), it was found that significant differences in polymerization kinetics existed between systems with thiolated organoclays versus acrylated organoclays.[25] While acrylated organoclays increase conversions of acrylate and thiol functional groups simultaneously, thiolated organoclays increase thiol conversion only. These results strongly indicate that different interfacial interactions exist between particle surfaces and monomers based on the type of functional group in the organoclay. Systematic investigation of these phenomena will facilitate understanding regarding the effect of organoclay type on photopolymerization behavior and clay exfoliation in thiol-ene photopolymerization, which are critical factors determining the ultimate composites properties.

Additionally, the difference in monomer diffusivity into clay galleries between thiol and ene monomers could potentially affect the stoichiometric balance especially near the functionalized clay surfaces. Previous research based on acrylate systems revealed that monomer diffusivity, which is closely related with the degree of clay exfoliation, is mainly affected by monomer characteristics such as polarity, functionality, and mobility.[23] Natural clays are inherently very polar materials and must be changed to be more compatible with organic species by surface modification utilizing organic surfactants.[3-5] Organoclays will exhibit different polarity depending upon how they have been modified. For instance, the viscosity and pH of organoclay solutions in solvent change with each modification step. In relatively polar EtOH/Water mixtures, thiolated organoclay exhibits lower solution viscosity than acrylated organoclays, which means thiolated organoclay is less hydrophilic than the parent acrylated organoclay. To enhance

the compatibility between monomers and organoclays, it is important that the polarity of organoclays be close to that of the monomers.

Acrylate and thiol monomers were selected considering several factors such as polarity, functionality, and structure to examine the effect of monomer structure on both clay exfoliation and thiol-ene reaction behavior. Two difunctional acrylate monomers were used in this study. More hydrophobic 1,6-hexanediol diacrylate (HDDA) was compared with less hydrophobic tripropyleneglycol diacrylate (TrPGDA). In choosing the thiol monomers, 1,6-hexanedithiol (HDT), which has a similar structure to HDDA, was selected as the difunctional thiol and trimethylolpropane trimercaptopropionate (TMPTMP) was used as a trifunctional thiol monomer to increase cross link density. For the thiol-acrylate mixture, the mole ratio of acrylate monomer to thiol monomer was evaluated from an equimolar ratio to a ratio 2:1 with excess acrylate. Equimolar mixtures of diacrylate and dithiol monomers, however, produce materials too soft and weak due to low thiol conversion to allow further experimentation for evaluating thermo-mechanical properties. To allow sufficient mechanical properties and thiol conversion, a 2 to 1 diacrylate to dithiol molar ratio was used for the thiol-acrylate mixtures unless otherwise noted.

In order to investigate the difference in reaction behavior based on the type of organoclays, 3 wt% C16A acrylated organoclay or PSH2 thiolated organoclay was mixed into an HDDA/HDT mixture (2:1 molar ratio of reactive groups). Photo-DSC was used to compare the polymerization profiles between the systems incorporating different organoclays. Figure 4.3 shows the heat evolved during photopolymerization as a function of time for these mixtures. The photopolymerization rate is much faster when thiolated organoclay is incorporated than the rate with incorporated acrylated organoclay. In addition, the polymerization rate with 3 wt% thiolated organoclays does not decrease much from that of an unfilled thiol-acrylate mixture while acrylated organoclays decrease the polymerization rate of the thiol-acrylate system significantly.

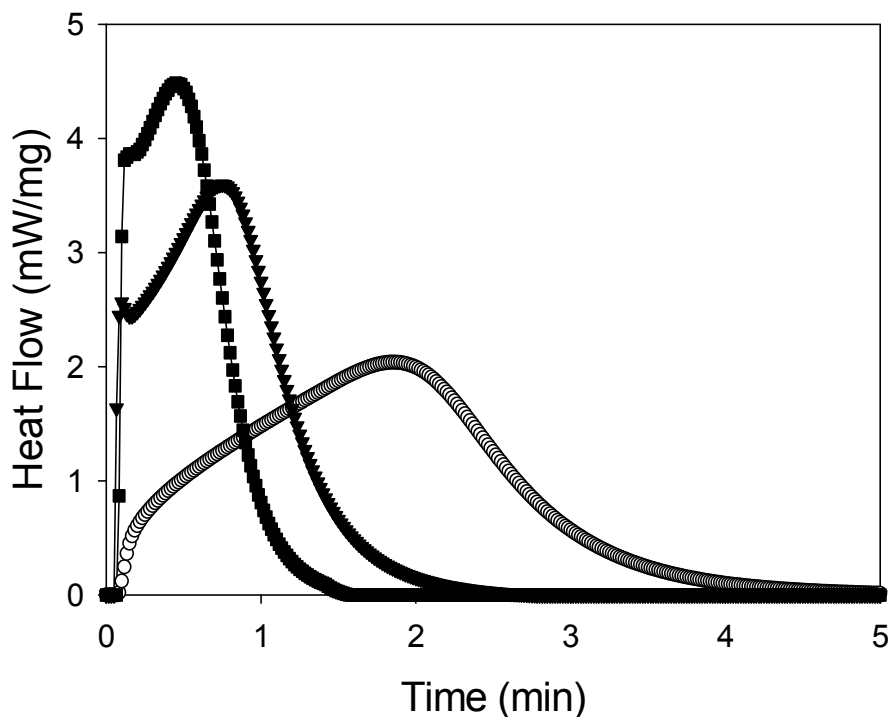


**Figure 4.3.** Photo-DSC (P-DSC) profiles of 2:1 molar ratio neat HDDA/1,6-HDT (■), 2:1 molar ratio HDDA/1,6-HDT with 3wt% PSH2 thiolated organoclay (▼), and with 3 wt% C16A acrylated organoclay (○). Photopolymerizations were initiated with 0.1 wt% DMPA using 365 nm light at  $3.0 \text{ mW/cm}^2$

To clarify the different effect of two polymerizable organoclays, RTIR was utilized to examine functional group conversion as the organoclay concentration is increased to 10wt%. The acrylate conversion as a function of time for the 2:1 HDDA/HDT mixture is shown in Figure 4.4. When C16A acrylated organoclay is used, the rate of photopolymerization decreases significantly by adding 3 wt% clay and then increases slightly by increasing the amount of clay up to 10 wt% as shown in Figure 4.4 (A). These decreases in the rate indicate that the effect of light interference from the clay particles is more dominant than any rate-enhancing effect induced by the reactive clay surface. As the clay concentration increases, the influence of the clay surface starts to

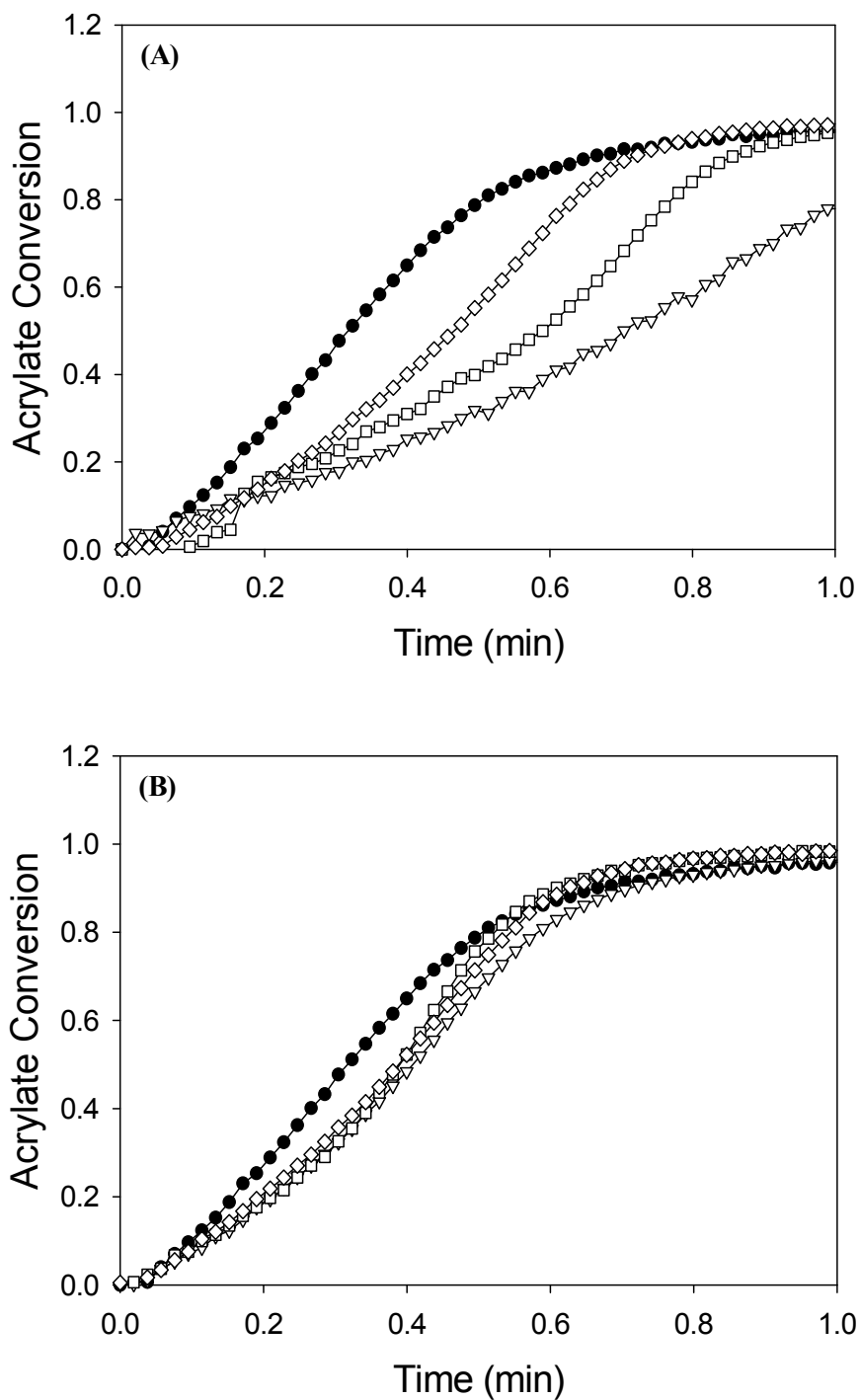


**Figure 4.4.** Acrylate double bond conversion profiles of 2:1 molar ratio HDDA/1,6-HDT. Shown are (A) conversion profiles for neat HDDA/HDT (●), HDDA/1,6-HDT with 3 wt% (▽), 5 wt% (□), and 10 wt% (◇) C16A acrylated organoclays, and (B) for neat HDDA/HDT (●), HDDA/1,6-HDT with 3 wt% (▽), 5 wt% (□), and 10 wt% (◇) of PSH2 thiolated organoclay. Photopolymerizations were initiated with 0.1 wt% DMPA using 365 nm light at  $3.0 \text{ mW/cm}^2$ .

increase the rate compensating for the negative effect to some degree. On the other hand, incorporation of a thiolated organoclay induces no significant decrease in photopolymerization rate as shown in Figure 4.4 (B). In addition, the polymerization rate does not change significantly upon increasing the clay concentration. This behavior indicates that any reduction in light intensity by adding organoclays is balanced by increases in rate based on surface interactions of clay with monomers. One potentially important mechanism of such surface interactions is the immobilization of propagating radicals on the clay surface. The immobilization of radicals would significantly reduce the bimolecular termination rate resulting in overall increase of polymerization rate.

Different thiol-ene compositions were also examined to understand the effect of organoclays if the polarity of monomer is changed. In order to control the polarity of the monomer system and determine the effect on photopolymerization kinetics, the more polar TrPGDA was used in a 2:1 mole ratio TrPGDA/HDT mixture with different amounts of polymerizable organoclays modified with different functional groups. Figure 4.5 (A) and (B) show the RTIR acrylate conversion profiles of the TrPGDA/HDT compositions as a function of time with acrylated and thiolated organoclays. Clay concentrations up to 10 wt% were examined. In contrast to the trend of the HDDA/HDT system, the addition of organoclays into TrPGDA/HDT systems increases polymerization rate regardless of the organoclay type. In Figure 4.5 (A), adding 3 wt% acrylated organoclays increases polymerization rate significantly. No further increase in polymerization rate was observed upon further increase in the clay concentration to 10 wt%. As shown in Figure 4.5 (B), the addition of thiolated organoclays into TrPGDA/HDT systems also enhances polymerization rate with a similar trend to that of acrylated organoclays. Accordingly, the conversion profiles of the thiol functional group for the same systems in Figure 4.5 (A) and (B) exhibits a similar trend to that of acrylate functional group in terms of polymerization rate (not shown). An important difference is that thiolated organoclays increase final thiol conversion and reaction rate with increasing

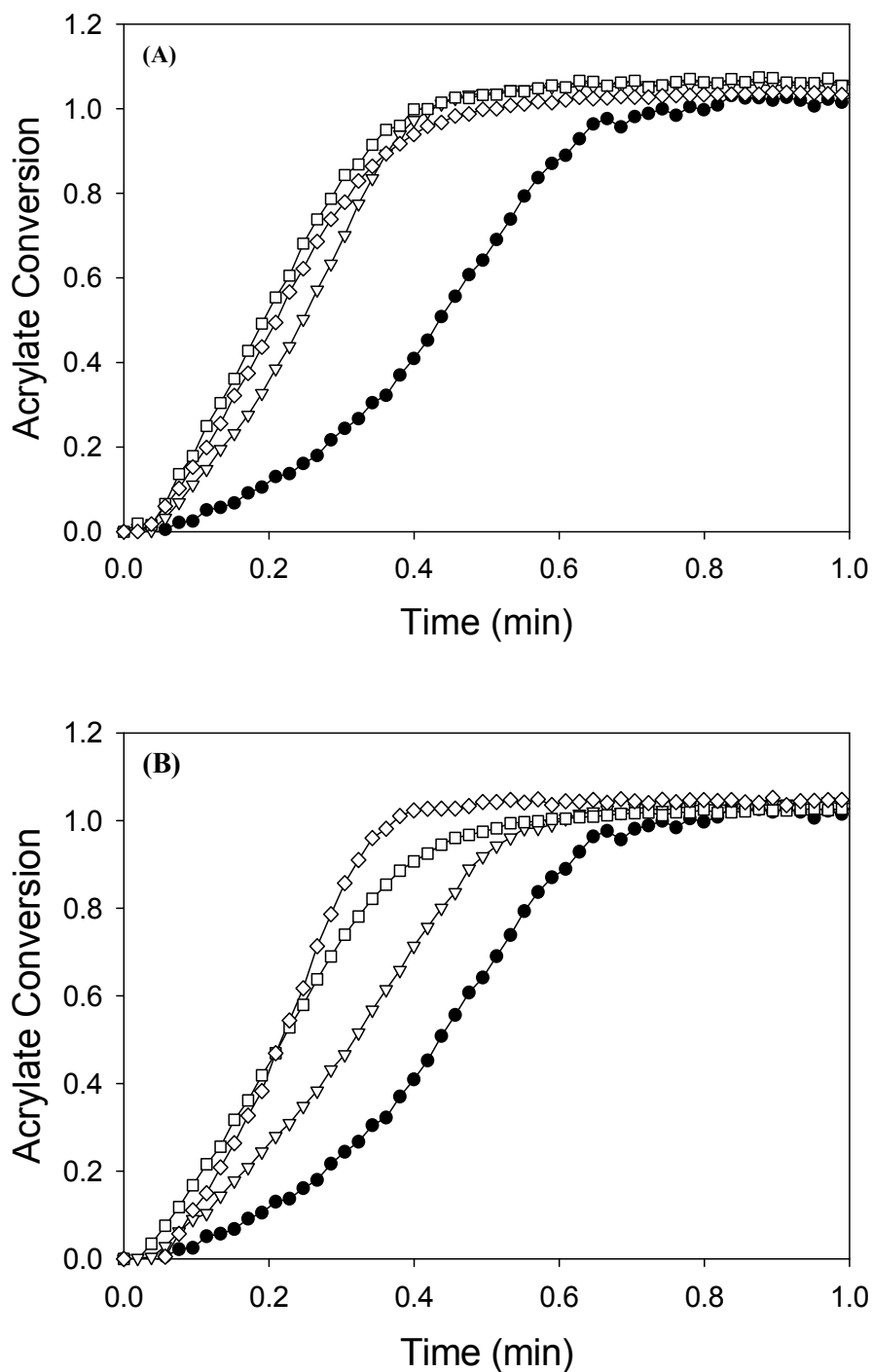


**Figure 4.5.** Acrylate double bond conversion profiles of 2:1 molar ratio of TrPGDA/1,6-HDT. Shown are (A) conversion profiles for neat TrPGDA/1,6-HDT (●), TrPGDA/1,6-HDT with 3 wt% (▽), 5 wt% (□), and 10 wt% (◇) C16A acrylated organoclays, and (B) for neat TrPGDA/1,6-HDT (●), TrPGDA/1,6-HDT with 3 wt% (▽), 5 wt% (□), and 10 wt% (◇) PSH2 thiolated organoclay. Photopolymerizations were initiated with 0.1 wt% DMPA using 365 nm light at 3.0 mW/cm<sup>2</sup>.



clay concentration while acrylated organoclays enhance only the reaction rate. Adding 10 wt% thiolated organoclays increases final thiol conversion from 0.57 for the unfilled neat TrPGDA/HDT system to 0.76. Overall, comparing the polymerization profiles in Figure 4.4 and 4.5, quite different polymerization behavior is observed for HDDA/HDT and TrPGDA/HDT systems with the addition of organoclays. Because thiol can react with only the acrylate double bond while acrylate can react with both thiol and acrylate, it is reasonable to assume that the affinity of the different reacting species might be a critical factor to determine the degree of thiol-ene reaction during the photopolymerization process.

Further studies were devoted to understanding the effect of interaction between components on polymerization behavior of the systems with different compositions. Four thiol-ene systems, HDDA/HDT and TrPGDA/HDT mixtures with either 3 wt% C16A acrylated or PSH2 thiolated organoclays were used as model compositions. Figure 4.6 shows acrylate conversion as a function of thiol conversion as determined by RTIR for each system up to 80% acrylate conversion. A higher slope indicates that polymerization involves more acrylate homopolymerization and a lower slope shows enhancement of the thiol-ene step growth copolymerization. The profiles for the HDDA/HDT system show lower slopes indicating enhanced step-growth thiol-ene reaction than for the TrPGDA/HDT system that shows more acrylate homopolymerization. Interestingly, for the HDDA/HDT with thiolated organoclays, the slope is approximately unity, indicating equivalent rates of acrylate and thiol conversion. The enhanced step growth reaction in HDDA/HDT systems is the primary reason that the reaction rates of the HDDA/HDT system are significantly slower than those of the TrPGDA/HDT system as shown in Figure 4.4 and Figure 4.5 previously because the thiol-ene step growth reaction is slower than acrylate homopolymerization. This difference is primarily due to higher compatibility between HDDA and HDT than that of the TrPGDA/HDT system based on the similarity in monomer structure. Enhanced thiol-ene copolymerization in

HDDA/HDT mixtures increases the final thiol conversion up to 50% higher than TrPGDA/HDT mixture. Interestingly, when comparing profiles for acrylate and thiolated organoclays, the incorporation of thiolated clays encourages thiol-ene step-growth reaction regardless of monomer composition. These results strongly suggest that chemical compatibility between acrylate monomer and thiol monomer as well as monomer-organoclay compatibility are important for determining polymerization kinetics and mechanism.

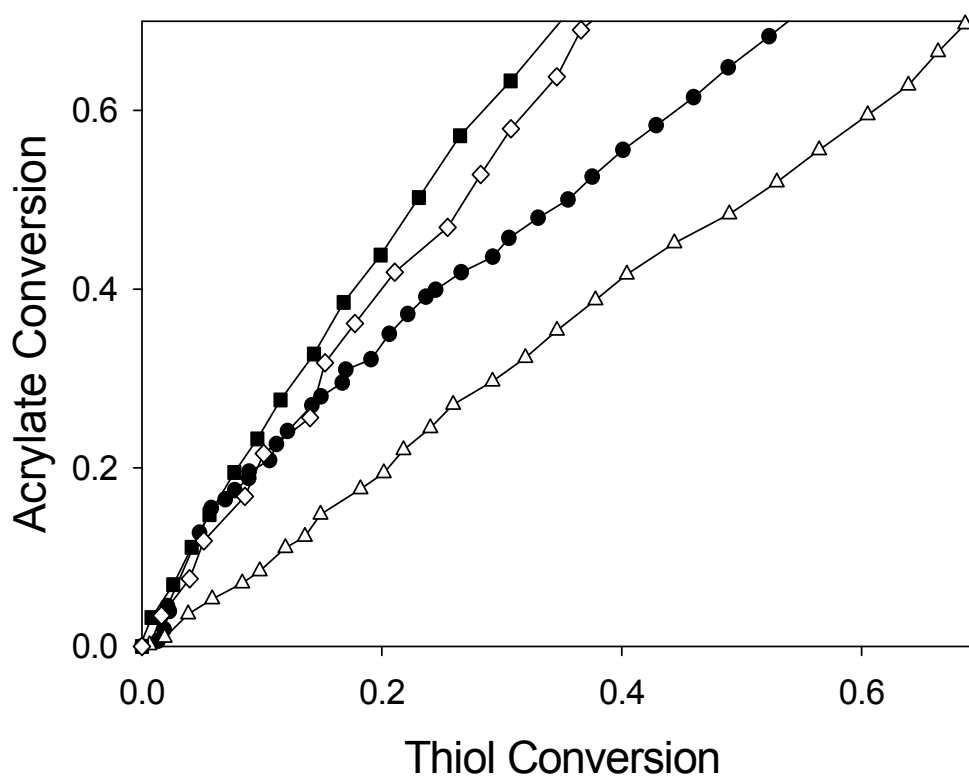


**Figure 4.6.** Double bond versus thiol conversion at short irradiation times for diacrylate/dithiol mixture with 2:1 molar ratio based on functional groups. Conversion profiles are shown for HDDA/1,6-HDT with 3 wt% C16A acrylated organoclay (●), 3 wt% PSH2 thiolated organoclay (Δ), TrPGDA/1,6-HDT with 3 wt% C16A acrylated organoclay (■) and 3 wt% PSH2 thiolated organoclay (◇). Photopolymerizations were initiated with 0.1 wt% DMPA using 365 nm light at 3.0 mW/cm<sup>2</sup>.

Because the degree of clay exfoliation is an indicator for overall monomer-clay compatibility of the system and also important for understanding the effect of the clay surface functionality during the photopolymerization, exfoliation behavior of HDDA/HDT and TrPGDA/HDT compositions with 3 wt% organoclay was studied utilizing small angle X-ray scattering (SAXS). In SAXS profiles for the systems in Figure 4.7, intensity as a function of X-ray scattering angle is plotted after normalizing and offsetting to allow facile comparison. Figure 4.7 (A) shows the SAXS results of different organoclays in an HDDA/HDT mixture. When incorporated into the thiol-acrylate system, both TTAB non-reactive organoclay and C16A acrylated organoclay show a noticeable primary peak at  $2.4^\circ$  and small secondary peak around  $5^\circ$   $2\theta$  corresponding to d-spacing of 3.7 nm and 1.8 nm respectively. After polymerization, a significant decrease in intensity for the primary peak as well as complete elimination of the secondary peak is observed for both systems, indicating further exfoliation through polymerization. Thiolated organoclay, however, shows no meaningful peaks before and after polymerization indicating complete exfoliation with at least 8.8 nm d-spacing which is the detection limit of the instrument.

On the other hand, the exfoliation behavior with two polymerizable organoclays in the TrPGDA/HDT mixture is quite different from the HDDA/HDT system as shown in Figure 4.7 (B). The TTAB non-reactive organoclay system shows a similar profile to the HDDA/HDT mixture. A more significant primary peak at  $2.4^\circ$  with small secondary peak around  $5^\circ$  is observed but no changes are observed upon polymerization, indicating only an intercalated morphology is achieved for this non-reactive organoclay. C16A acrylated organoclay, however, is almost completely exfoliated in this monomer mixture. Only one weak peak around  $2^\circ$  could be seen denoting existence of very small amounts of particles having d-spacing of approximately 4 nm. Thiolated organoclay showed intermediate exfoliation before polymerization and complete exfoliation after polymerization. The exfoliation behavior in Figure 4.7 implies acrylated organoclay has greater compatibility

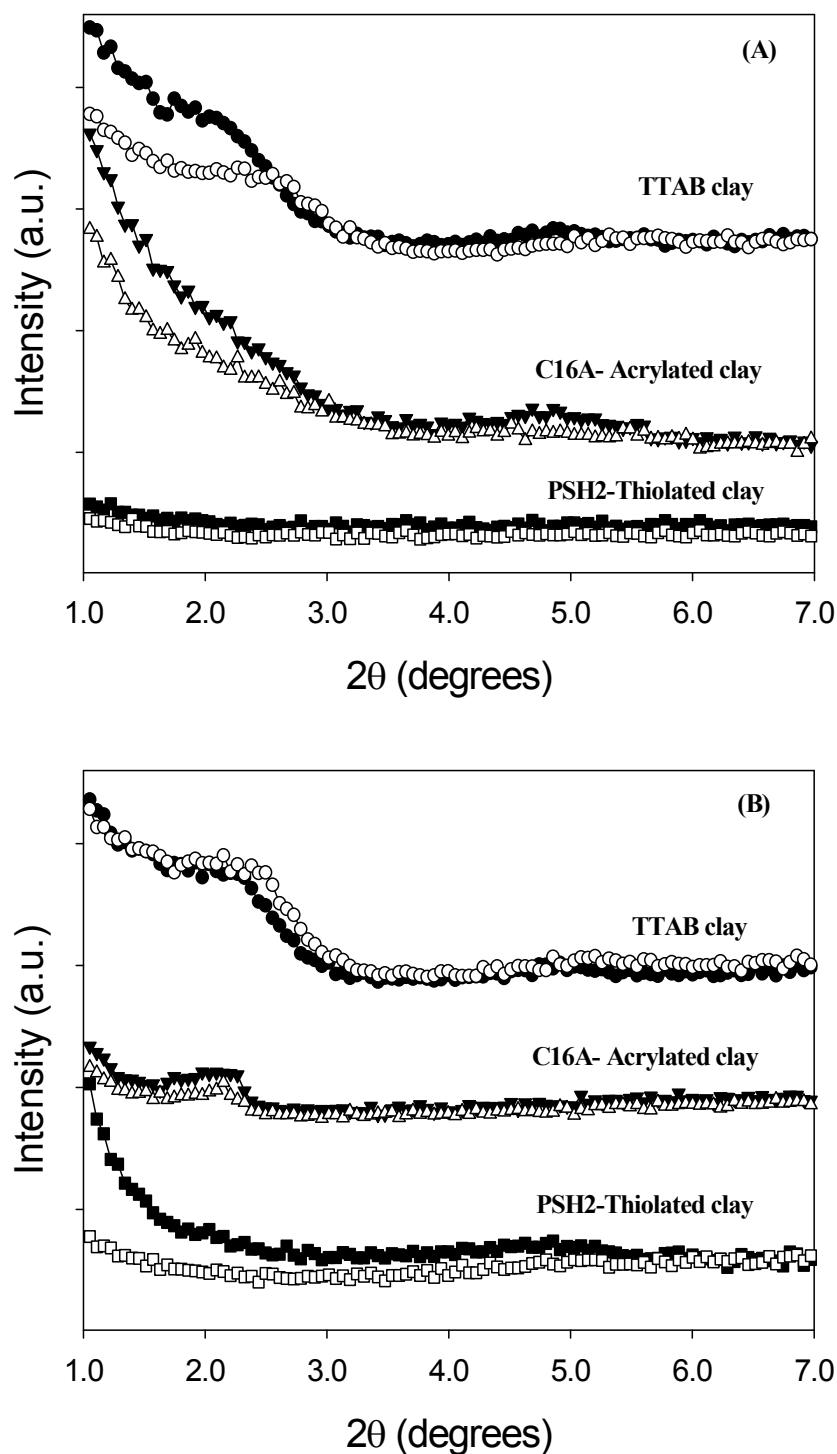


**Figure 4.7.** SAXS profiles of 3wt% TTAB-organoclay ( $\bullet, \circ$ ), 3wt% C16A-organoclay ( $\blacktriangledown, \triangledown$ ), and 3wt% PSH2-organoclay ( $\blacksquare, \square$ ) in (A) HDDA/HDT and (B) TrPGDA/1,6-HDT mixture with 2:1 acrylate to thiol molar ratio. Filled and empty symbols represent profiles before and after polymerization, respectively. Photopolymerizations were initiated with 0.1 wt% DMPA using 365nm light at 3.0 mW/cm<sup>2</sup>.

with more polar monomer systems while the compatibility of thiolated organoclay decreases with increasing polarity of the monomer system. This behavior is mainly observed because the thiolated organoclays are less polar due to organic modification of the acrylated organoclays, thereby exhibiting greater affinity to and greater exfoliation in a less polar monomer system.

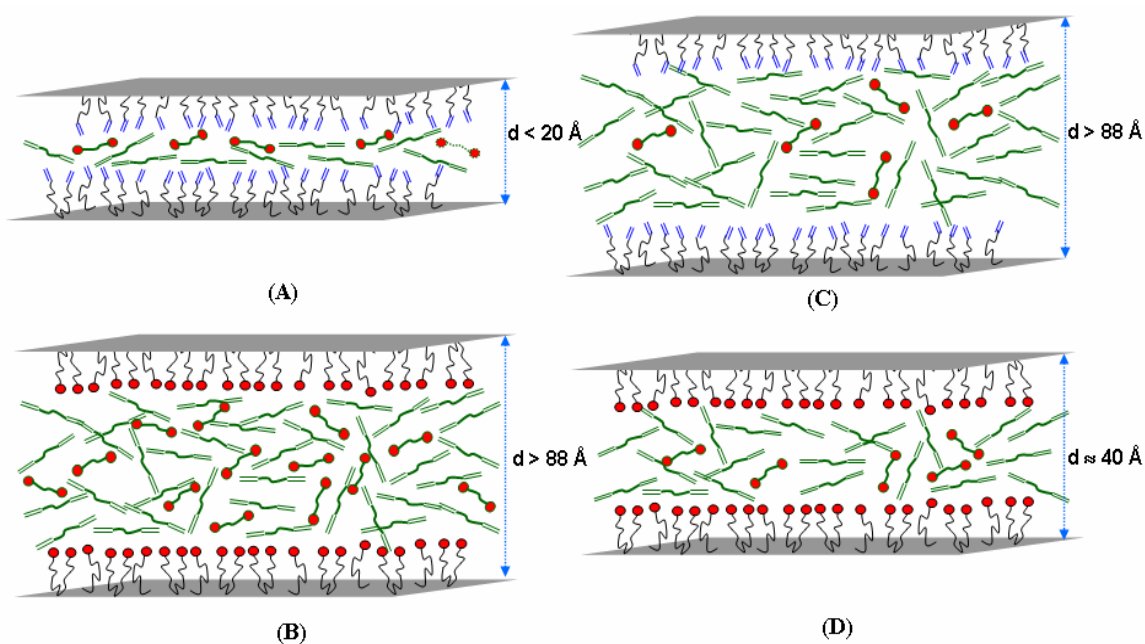


**Figure 4.8.** Schematic representation of clay dispersion for (A) 3 wt% C16A acrylated organoclay, and (B) 3 wt% PSH2 thiolated organoclay in HDDA/1,6-HDT mixture and (C) with 3 wt% C16A acrylated organoclay, and (D) with 3 wt% PSH2 thiolated organoclay in TrPGDA/1,6-HDT mixture. Double lines and circles indicate acrylate double bonds and thiol functional groups, respectively. All schemes represent the systems before polymerization.

To illustrate how the chemical compatibility as indicated from exfoliation results could affect polymerization behavior, the thiol-acrylate organoclay systems from Figure

4.7 are schematically represented in Figure 4.8. Only one clay gallery between two clay layers is used to demonstrate the interfacial interaction between organoclay and monomer mixture of each system. Scheme A and B show simplified representations of acrylated and thiolated organoclays respectively in the HDDA/HDT monomer mixture consistent with the results from Figure 4.7 (A). Scheme C and D show representations of acrylated and thiolated organoclays in the TrPGDA/HDT mixture from Figure 4.7 (B). In accordance with SAXS results, scheme B (thiolated clays in HDDA/HDT) and scheme C (acrylated clays in TrPGDA/HDT) show a larger d-spacing to represent complete clay exfoliation. On the other hand, scheme A (acrylated clays in HDDA/HDT) and D (thiolated clays in TrPGDA/HDT) show intercalated clay structure and intermediate exfoliation. All schemes represent the systems before polymerization. Compared to the other formulations, relatively small amounts of monomer are present in the clay gallery of acrylated clays in HDDA/HDT (A) that shows intercalated clay dispersion. The portion of monomer that can interact with the reactive clay surfaces, thus, would be smaller than in highly exfoliated systems. At certain clay concentrations, therefore, any clay surface effects would be small during polymerization, resulting in a decrease in overall polymerization rate based on decreases in initiation through light scattering (See Figure 4.4 (A) for relevant polymerization profiles.).

In comparing schemes A and C, the major difference between the two systems is the type of acrylate monomer. Because HDT does not allow high degrees of exfoliation of acrylated organoclays with HDDA as represented in scheme A, it is evident that the enhancement in clay exfoliation in TrPGDA/HDT with acrylated clays is mainly due to a higher concentration of TrPGDA in the clay gallery. With the additional acrylate functional groups on the acrylated organoclays, this system essentially develops an acrylate rich environment in the clay gallery resulting in the most dominant acrylate homopolymerization. On the other hand, HDDA/HDT with thiolated clays shows a large increase in d-spacing from Figure 4.8 (A) as the organoclay is changed to one that is thiol

functionalized. This change results in more of the less polar HDDA and HDT into the clay gallery due to the inherently less polar nature of the thiolated organoclays. In contrast, the d-spacing in TrPGDA/HDT is reduced when the acrylated clay is replaced by thiolated organoclay. The concentration of the more polar TrPGDA in the clay gallery is restricted by the decrease in polarity of the organoclay. With thiol functional groups on the surface of thiolated organoclays, the functional group ratio between acrylate and thiol is more favorable for thiol-ene copolymerization than when acrylate groups are on the clay surface.

Based on this compatibility difference between clays and monomer mixtures, addition of polymerizable organoclays can either increase or decrease the reaction rate of thiol-acrylate systems simply based on the type of organoclays. For instance, because thiolated clay exhibits greater compatibility with HDDA than acrylated clay, the polymerization rate in the HDDA/HDT system with thiolated clay is enhanced in comparison to the neat thiol-acrylate system while the rate in the system with acrylated clay decreases. In addition, more favorable functional group ratios in clay galleries for thiol-ene reaction by using thiolated organoclay induces higher thiol conversions for both HDDA/HDT and TrPGDA/HDT systems than those of systems with acrylated organoclay in Figure 4.4 and 4.5. Considering that overall polymerization behavior reflects reaction in the bulk as well as in the clay galleries, the schematic in Figure 4.8 is consistent with the polymerization behavior of monomer mixtures with different organoclays in Figure 4.4, 4.5 and 4.6. Chemical compatibility and the type of functional group on the clay surface significantly impact the degree of clay exfoliation and monomer composition near the organoclay surfaces. In addition, these factors have a significant impact on the overall polymerization behavior.

As the type of functional group on the clay surface plays such an important role in exfoliation and polymerization behavior, the monomer functionality may also be a critical factor before and during polymerization because an increase in functionality will produce

more immobilized propagating radicals by reacting with radicals on the clay surfaces. To examine the impact of functionality on thiol-ene photopolymerization behavior, diacrylate or dithiol monomers were replaced by triacrylates and trithiol monomers. Thiol functionality was increased by incorporating the trithiol TMPTMP. In order to achieve higher degree of clay exfoliation for both acrylated and thiolated organoclays, TrPGDA was used as the acrylate monomer based on enhanced compatibility as described previously. When diacrylate/dithiol systems were evaluated, a 2 to 1 functional ratio was used because equimolar diacrylate/dithiol mixtures are too weak to allow further thermomechanical evaluation of cured samples for subsequent studies. An increase in functionality of monomers allows production of materials with sufficient mechanical stability when prepared using an equimolar functional group ratio. To allow more facile examination of the polymerization behavior of acrylate and thiol groups, equimolar TrPGDA/TMPTMP mixture based on functional group ratio was used to study the clay effects in a high functionality system. According to the SAXS experiments to evaluate clay exfoliation with addition of 3 wt% of acrylated or thiolated organoclays for this mixture, both polymerizable organoclays were almost completely exfoliated (not shown). No meaningful peaks could be found in SAXS profiles when using either polymerizable organoclay. With this degree of clay exfoliation, it is reasonable to believe that the functional groups on the clay surface may exhibit a significant effect on polymerization behavior.

To understand the importance of the organoclay on polymerization behavior in this higher functionality system, RTIR experiments were performed. Thiol conversions as a function of time are shown in Figure 4.9 with increased concentration of thiolated organoclays. When acrylated organoclays are added, the final conversion as well as polymerization rate for both acrylate and thiol functional groups are not changed significantly indicating that the polymerization mechanism is not affected significantly (not shown). On the other hand, addition of thiolated organoclays markedly changes



polymerization behavior from that of unfilled TrPGDA/TMPTMP system as shown in Figure 4.9. The unfilled TrPGDA/TMPTMP system exhibits a final thiol conversion of 0.5. Interestingly, final thiol conversion increases significantly with increased clay concentration. When 5 wt% thiolated organoclay is added, the final thiol conversion increases to 0.75, a 50% enhancement from the ultimate conversion of the unfilled system. Further addition of organoclays continues to enhance final thiol conversion and also increases the rate of photopolymerization.

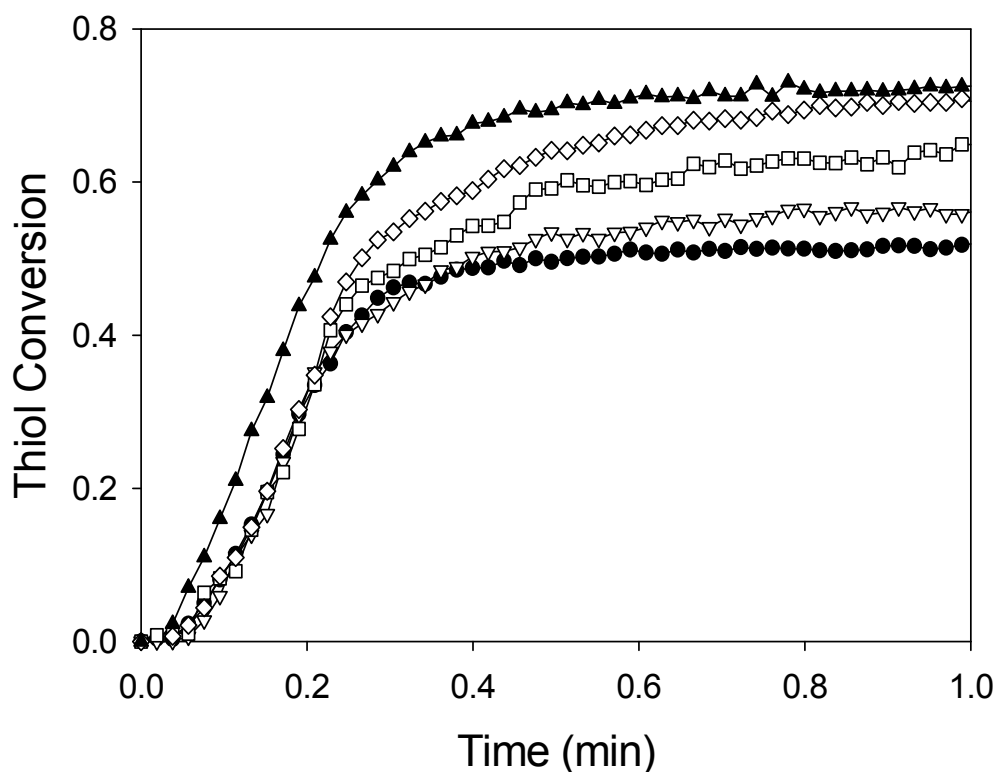


**Figure 4.9.** Thiol conversion profiles of equimolar TrPGDA/TMPTMP based on functional groups. Shown are conversion profiles for neat TrPGDA/TMPTMP (●) and TrPGDA/TMPTMP with 1 wt% (▽), 3 wt% (□), and 5 wt% (◇), and 10 wt% (▲) PSH2 thiolated organoclay. Photopolymerizations were initiated with 0.1 wt% DMPA using 365 nm light at 3.0 mW/cm<sup>2</sup>.

In order to compare the effect of polymerizable organoclays on polymerization mechanism, acrylate conversion was plotted as a function of thiol conversion for filled and unfilled TrPGDA/TMPTMP systems in Figure 4.10 where polymerization behavior approaches an alternating thiol-acrylate copolymerization as the slope approaches the  $y = x$  line. As shown in Figure 4.10 (A), acrylate homopolymerization dominates the unfilled TrPGDA/TMPTMP polymerization based on the large slope. The addition of acrylated organoclays does not change this polymerization behavior as indicated by the similar slope. The addition of thiolated organoclays, however, substantially alters the polymerization behavior as shown in Figure 4.10 (B). Only 1 wt% thiolated organoclays significantly lowers the slope. Continued decreases in slope are observed with increased clay concentration. At the onset of polymerization for lower clay concentrations, the polymerization appears to primarily proceed as a thiol-ene copolymerization and then shifts to acrylate homopolymerization as the overall acrylate conversion approaches 0.6 at which point the slope rapidly increases. While not as prevalent at higher concentration, this shift in behavior is observed at all clay percentages. It is apparent that thiolated organoclays significantly enhance thiol-ene copolymerization up to this point and then the effect is decreased by increasing system viscosity that restricts further diffusion of monomers into the clay galleries. Interestingly, the enhancement of thiol-ene reaction by adding the same amount of thiolated organoclay in trithiol systems is much larger than that of diacrylate/dithiol systems. For instance, while 10 wt% thiolated organoclays in the TrPGDA/HDT mixture increases final thiol conversion about 20% over that of the unfilled system, the thiol conversions for the moderately cross-linked TrPGDA/TMPTMP mixture using the same amount of thiolated organoclays is enhanced more than 25%. This difference between dithiol and trithiol systems suggests that increased functionality of thiol monomers induces synergetic effects in enhancing step-growth thiol-ene copolymerization and thiol conversion. This behavior could be produced as higher functionality thiol monomers generate more immobilized propagating thiyl

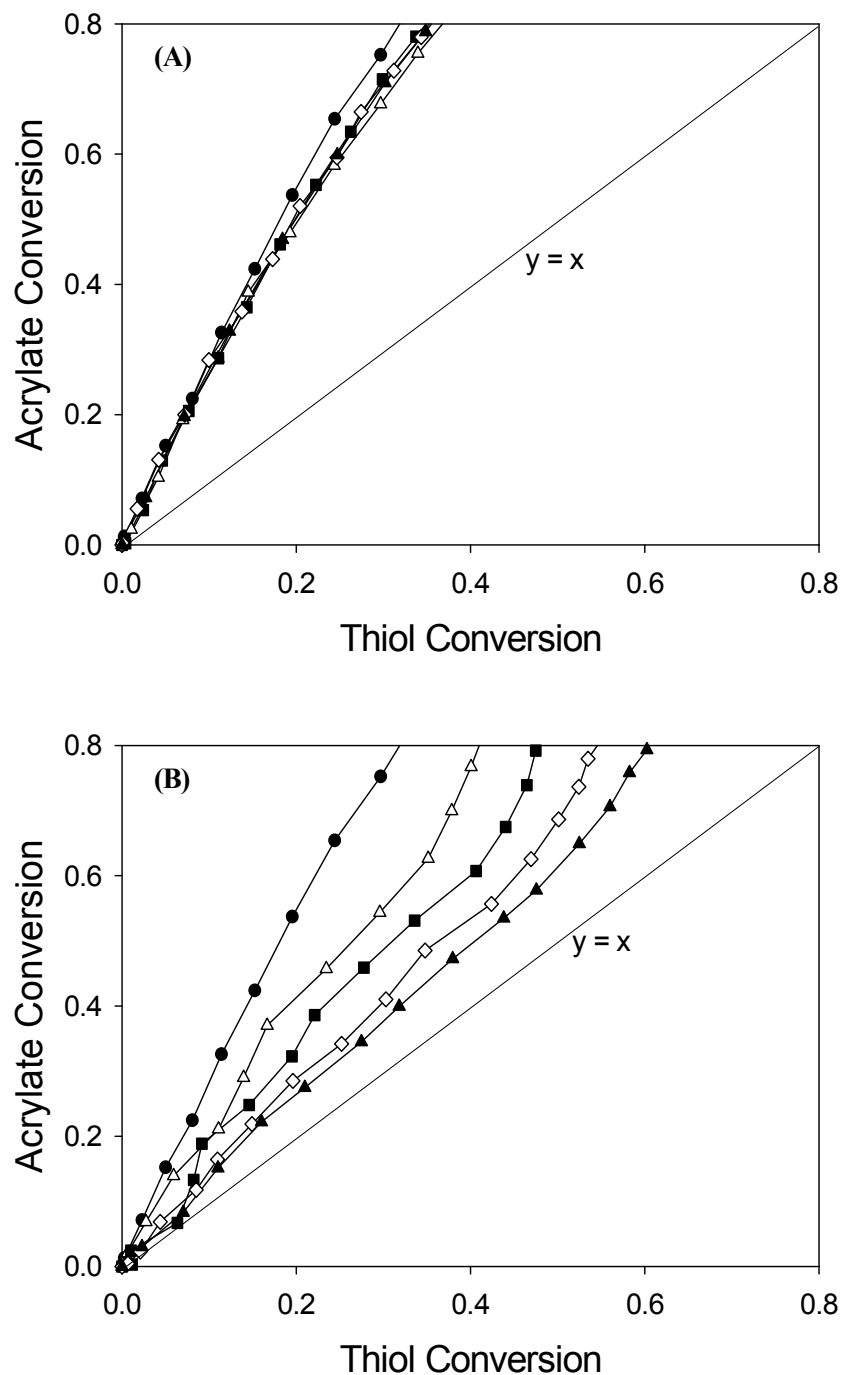


**Figure 4.10.** Double bond versus thiol conversion at short irradiation times for TrPGDA/TMPTMP equimolar mixture based on functional groups. Shown are (A) neat TrPGDA/TMPTMP (●), and TrPGDA/TMPTMP with 1 wt% (Δ), 3wt% (■), 5wt% (◇), and 10 wt% (▲) C16A acrylated organoclay and (B) neat TrPGDA/TMPTMP (●), and TrPGDA/TMPTMP with 1 wt% (Δ), 3wt% (■), 5wt% (◇), and 10 wt% (▲) PSH2 thiolated organoclay. Photopolymerizations were initiated with 0.1 wt% DMPA using 365 nm light at 3.0 mW/cm<sup>2</sup>.

radicals on the organoclay surfaces during the photopolymerization, which results in decreases of the bimolecular termination reaction.

In summary, to overcome the drawbacks of conventional organoclays and to achieve better clay exfoliation based on higher interaction between monomers and organoclays, photopolymerizable groups have been introduced on clay surfaces and both clay exfoliation and photopolymerization behavior have been studied using thiol-acrylate monomer systems. SAXS results show that different degrees of clay exfoliation between acrylate and thiolated organoclays are achieved according to the chemical similarity and compatibility of organoclay and monomer system. Both the degree of clay exfoliation and the type of polymerizable group on the clay surface change the polymerization behavior and mechanism, In turn, the difference in final conversion of monomers and in the ultimate network structure could be used to control the ultimate properties of the nanocomposite. . Understanding the role of polymerizable organoclays in photopolymer systems is thus important to facilitate control of nanocomposites characteristics and potentially enhance photopolymerization applications.

### Conclusions

The effects of both monomer structure and the type of polymerizable organoclay on the thiol-ene photopolymerization behavior have been investigated. Monomer polarity, monomer functionality, and the functional groups on the organoclay surfaces significantly impact both the degree of clay exfoliation and photopolymerization kinetics. The addition of polymerizable organoclays increases photopolymerization rate in sufficiently exfoliated clay systems while the rate decreases with lower degrees of clay exfoliation. With clay exfoliation, the effective surface area is increased resulting in immobilization of a greater number of the propagating radicals and decreased termination.

Chemical compatibility between monomers and organoclays is the primary factor influencing clay exfoliation. In addition, the type of functional group on the organoclay surfaces directs polymerization behavior not only by affecting the stoichiometric balance between thiol and ene functional groups in the clay galleries but also by determining the type of initial radicals on the clay surfaces. Thiolated organoclays enhance thiol-ene reaction and thiol conversion while acrylated organoclays encourage acrylate homopolymerization. Similarly, increase of thiol functionality facilitates thiol-ene copolymerization with much higher thiol conversion. On the other hand, the increase of acrylate functionality reduces the thiol-ene copolymerization and produces lower thiol conversion.

Notes

1. Rodriguez, F.; Cohen, C., Ober, C. K.; Archer, L. A., *Principles of Polymer Systems*, Taylor & Francis, New York, **2003**, Ch.9, 405.
2. Vaia, R. A.; Giannelis, E. P. *Macromolecules* **1997**, 30, 7990.
3. Alexandre, M.; Dubois, P. *Mater. Sci. Eng.* **2000**, 28, 1.
4. LeBaron, P. C.; Wang, Z.; Pinnavaia, T. J. *Appl. Clay Sci.* **1999**, 15, 11.
5. Ray, S. S.; Okamoto, M. *Prog. Polym. Sci.* **2003**, 28, 1539.
6. Zanetti, M.; Lomakin, S.; Camino, G. *Macromol. Mater. Eng.* **2000**, 279, 1.
7. Okada, A.; Fukumori, K.; Usuki, A.; Kojima, Y.; Sato, N.; Kurauchi, T.; Kamigaito, O. *Polym. Prepr.* **1991**, 32, 540.
8. Decker, C.; Keller, L.; Zahouily, K.; Benfarhi, S. *Polymer* **2005**, 46, 6640.
9. Uhl, F. M.; Davuluri S. P.; Wong S. C.; Webster D. C. *Chem. Mater.* **2004**, 16, 1135.
10. Beck, E.; Lokai, E.; Nissler, H. *RadTech Int. North America, Nashville* **1996**, 160.
11. Gilman, J.W. *Appl. Clay Sci.* **1999**, 15, 31.
12. Zahouily, K.; Benfarhi, S.; Bendaikha, T.; Baron, J. *Rad Tech Europe Conf.* **2001**, 583.
13. Zahouily, K.; Decker, C.; Benfarhi, S. *J. Proc. RadTech North America* **2002**
14. Decker, C. *Macromol. Rapid Commun.* **2002**, 23, 1067.
15. Kawasumi, M. *J. Polym. Sci. A: Poly. Chem.* **2004**, 42, 819.
16. Ogawa, M.; Kuroda, K.; *Bull. Chem. Soc. Jpn.* **1997**, 70, 2593.
17. Gottler, L. A.; Lee, K.; Thakkar, Y. H. *Polymer Reviews* **2007**, 47, 291.
18. Bongiovanni, R.; Ronchetti, M. S.; Turcato, E.A. *J. of Colloid & Interface Sci.* **2006**, 296, 515.
19. Decker, C.; Zahouily, K.; Keller, L.; Benfarhi, S.; Bendaikha, T.; Baron, J. *J. of Mater. Sci.* **2002**, 37, 4831.
20. Uhl, F. M.; Hinderliter, B. R.; Davuluri, S. P.; Croll, S. G. *Mater. Res. Soc.* **2004**, 16, 203.
21. Tan, H.; Nie, J. *J. Polym. Sci. A: Poly. Chem.* **2007**, 106, 2656.

22. Owusu-Adom, K.; Guymon, C. A. *Polymer* **2008**, 49, 2636.
23. Owusu-Adom, K.; Guymon, C. A. *Macromolecules* **2009**, 42, 180
24. Davidenko, N.; Garcí'a, O.; Sastre, R. *J. Appl. Polym. Sci.* **1995**, 97, 1016.
25. Owusu-Adom, K.; Guymon, C. A. *Macromolecules* **2009**, 42, 3275.
26. Clapper, J. D.; Guymon, C. A. *Macromolecules* **2007**, 40, 1101.
27. Polowinski, S. *Prog. Polym. Sci.* **2002**, 27, 537.
28. Leone, G.; Boglia, A.; Bertini, F.; Canetti, M.; Giovanni, R. *J. Polym. Sci. A: Poly. Chem.* **2010**, 48, 4473.
29. Pramoda, K. P.; Hussain, H.; Koh, H.M.; Tan, H.R.; He, C. B. *J. Polym. Sci. A: Poly. Chem.* **2010**, 48, 4262.
30. Oral, A.; Tasdelen, M.A.; Demirel, A.L.; Yagci, Y. *J. Polym. Sci. A: Poly. Chem.* **2009**, 47, 5328.
31. Karesoja, M.; Jokinen, H.; Karjalainen, E.; Pulkkinen, P.; Torkkeli, M.; Soininen, A.; Ruokolainen, J.; Tenhu, H. *J. Polym. Sci. A: Poly. Chem.* **2009**, 47, 3086.
32. Decker, C. *Polym. Int.* **1998**, 45, 133.
33. Decker, C. *Prog. Polym. Sci.* **1996**, 21, 593.
34. Hoyle, C. E.; Lee, T. Y.; Roper, T. *J. Polym. Sci. A: Poly. Chem.*, **2004**, 42, 5301.
35. Cramer, N. B.; Scott, J. P.; Bowman, C. N. *Macromolecules* **2002**, 35, 5361.
36. Morgan, C. R.; Magnota, F.; Ketley, A. D. *J. Polym. Sci.: Polym. Chem. Ed.* **1977**, 15, 627.
37. Carioscia, J. A.; Lu, H.; Stanbury, J. W.; Bowman, C. N. *Dent. Mater.* **2005**, 21, 1137.
38. Senyurt, A. F.; Wei, H.; Hoyle, C. E.; Piland, S. G.; Gould, T. E. *Macromolecules* **2007**, 40, 4901.
39. Li, Q.; Zhou, H.; Wicks, D. A.; Hoyle, C. E. *J. Polym. Sci. A: Polym. Chem.*, **2007**, 45, 5103.
40. Lee, T. Y.; Bowman, C. N. *Polymer*, **2006**, 47, 6057.
41. Fu, X.; Qutubuddin, S.; *Polymer* **2001**, 42, 807.
42. Hamid, S. M.; Sherrington D. C. *Polymer* **1987**, 28, 325.
43. Lee, T. Y.; Carioscia, J.; Smith, Z.; Bowman, C. N. *Macromolecules* **2007**, 40, 1473.

44. Anseth, K. S.; Wang, C. M.; Bowman, C. N. *Macromolecules* **1994**, 27, 650.
45. Hill, L. W. *Prog. Org. Coat.* **1997**, 31, 235.



## CHAPTER 5

### INFLUENCE OF PHOTOPOLYMERIZATION CHARACTERISTICS ON THERMO-MECHANICAL PROPERTIES OF NANOCOMPOSITES UTILIZING POLYMERIZABLE ORGANOCCLAYS IN THIOL-ACRYLATE SYSTEMS

To produce clay nanocomposites, photopolymerizable organoclays can react with monomers and incorporate into polymer matrices during the UV curing process. This research investigates the effects of polymerizable organoclays on the reaction behavior as well as the ultimate composite properties based on *in situ* thiol-ene photopolymerization. To this end, different types of polymerizable organoclays, prepared by changing the functional group structure, were examined in various thiol-acrylate systems. Small angle X-ray diffraction was used to examine the degree of clay exfoliation. Photopolymerization behavior was characterized using real time infrared spectroscopy. Dynamic mechanical analysis was used for analyzing both mechanical and thermal properties. With sufficient clay exfoliation, the incorporation of thiol groups on the clay surfaces significantly increases the photopolymerization rate and final thiol conversion, whereas acrylate group conversion does not change significantly. While increasing monomer functionality does decrease final thiol conversion, the increase of thiol functionality of organoclays enhances thiol-ene step growth reaction. Dark curing results suggest that the structure of propagating radicals on the clay surface varies by the type of polymerizable organoclays, changing the reaction behavior of the system. In accordance with the reaction behavior, the incorporation of acrylated organoclays significantly increases the storage modulus by inducing dominant acrylate homopolymerization. Addition of thiolated organoclays, on the other hand, makes more flexible polymer chains due to increased thio-ether linkages.

## Introduction

In order to achieve desirable polymer properties such as high mechanical, thermal, and flame resistant properties, considerable research attention has been given to polymer nanocomposites using nanometer-scale fillers.[1-3] The large surface area of nano-fillers affords increases in mechanical, thermal properties and other performance characteristics of the polymer composites with relatively small amounts of loading compared to that of micro-scale fillers.[4,5] Among many potential fillers, much academic and industrial interest has focused on clays due to their commercial availability and simple delaminating chemistry. These clay nanocomposites, if the clay is well-dispersed in polymer matrices, exhibit unique properties compared to conventional macro-scaled polymer composites [6]. Obtaining well-exfoliated clay dispersion during the preparation of polymer clay nanocomposites is thus critical for maximizing the improvement of ultimate composite performance.[7,8]

Exfoliated clay morphologies are formed when each clay layer is sufficiently delaminated and randomly dispersed in the polymer matrix. In this clay morphology, the interaction between clay and polymer is substantial, which allows significant increases in performance with relatively small amounts of clay. Montmorillonite, a commonly used 2:1 phyllosilicate clay, is composed of negatively charged platelets counterbalanced by exchangeable cations in the gallery. These strong ionic attractions hold stacked sheets closely together.[9,10] In order to overcome electrostatic forces and achieve clay exfoliation, surface modification of clay is needed to enhance compatibility to polymer.[2-4,11,12] It has been shown that quaternary ammonium surfactants can facilitate highly delaminated clay dispersion in *in situ* photopolymerization.[13-16] However, even with this modification of the clay surface using quaternary ammonium surfactants, complete clay exfoliation is not typically achieved. Because most surfactants used are non-reactive and do not participate in the polymerization reaction, the lack of

interaction between monomers and organoclay surface may limit clay exfoliation. From this premise, our research group has recently investigated novel polymerizable surfactants with reactive functional groups for clay surface modification.

One specific area which polymerizable organoclays could provide substantial advantages is photo-cured materials. Photocuring, or photopolymerization, uses only light energy to initiate the polymerization, and polymers can be rapidly produced at ambient temperature with 100% solid content. Producing clay nanocomposites by *in situ* photopolymerization could thus allow ultra-fast production, spatial and temporal control, and an environmentally friendly process.[17-19] In the preparation of clay polymer nanocomposites utilizing *in situ* photopolymerization, reactive organoclays modified with photopolymerizable surfactants can incorporate into polymer matrices by reacting with monomers during the photopolymerization process. Increased interaction between clay surfaces and polymer networks may also facilitate the further exfoliation of clay platelets during the polymerization process, resulting in additional property enhancement, as well as increase of overall polymerization rate.[20,21]

In addition, improvements regarding several aspects of acrylic photopolymers, including low impact resistance, poor gas barrier properties, high shrinkage, and oxygen inhibition during polymerization, could allow further growth in acrylic photopolymer applications.[22,23] In conjunction with suitable polymerizable organoclays, photopolymer-clay nanocomposites based on advanced thiol-ene photopolymerization technique could specifically provide such improvements. With the homogeneous network structure and step-growth reaction mechanism of thiol-ene photopolymerization, shrinkage and oxygen inhibition could be minimized during photopolymerization.[24-27] The incorporation of organoclays into thiol-ene system may not only increase the hardness and toughness that are usually lacking in neat thiol-ene photopolymers due to the inherent flexible thioether linkages, but also present enhanced gas barrier properties by generating longer path-length for gaseous materials.[3,4,23,26-28] Well-designed

thiol-ene photopolymer-clay nanocomposites utilizing suitable polymerizable organoclays, thus, could overcome several drawbacks in acrylic photopolymer materials.

In order to develop advanced thiol-ene photopolymer-clay nanocomposites, it is important to understand the effects of organoclay on photopolymerization kinetics and final properties of the thiol-ene photopolymer. Polymerization behavior of thiol-ene systems using acrylates as the ene containing monomer with polymerizable organoclays are quite different from that of neat acrylate systems due to the inherent characteristics of the step-growth mechanism. Thiol-acrylate copolymerization involves competition between acrylate homopolymerization. Ultimate conversion of both functional groups and polymerization rate depend upon the functional group ratio between thiol and double bond.[29-31] In previous studies, factors important in clay exfoliation and photopolymerization kinetics of thiol-acrylate systems with polymerizable organoclay were investigated.[32,33] Overall chemical compatibility of components in the system between monomers and organoclays as well as between monomers was the primary driving force for achieving clay exfoliation and determined monomer composition in the clay galleries. When organoclays are sufficiently exfoliated, the addition of polymerizable organoclays increases photopolymerization rate while lower degree of clay exfoliation decreases the rate. The type of functional group on the organoclay surface is also critical for determining polymerization behavior as the stoichiometric ratio between thiol and double bond in the clay gallery is significantly affected. Thiolated organoclays enhance thiol-ene reaction while acrylated organoclays encourage acrylate homopolymerization.

All these differences in polymerization behavior by incorporating organoclays may affect final performance of the nanocomposites. This study focuses on demonstrating how the difference in photopolymerization behavior affects the ultimate thermal and mechanical properties of photopolymerized nanocomposites. Fundamental kinetic studies demonstrate how the structure of polymerizable organoclays affects

overall polymerization behavior. Dark curing experiments facilitate understanding of the reaction mechanism that induces the differences in the polymerization behavior. Thermo-mechanical properties such as glass transition temperature and modulus of ultimate nanocomposites are examined and correlated to the reaction behavior of the systems. The combined information from knowledge in clay morphology and photopolymerization behavior from *in situ* thiol-acrylate photopolymerization with polymerizable organoclays is essential for design of advanced photopolymer-clay nanocomposites that allows improvements in acrylate photopolymer systems.

## Experimental

### Materials

1,6-hexanediol diacrylate (HDDA) and tripropyleneglycol diacrylate (TrPGDA) were supplied from Sartomer Inc. (Exton, PA). 1,6-hexanedithiol (HDT, from Aldrich) and Glycol di-3-mercaptopropionate (GDMP, from Bruno Bock Chemische Fabric GMBH & Co., Hamburg, Germany) were used as difunctional thiol monomers. Trifunctional trimethylolpropane triacrylate (TMPTA) and trimethylolpropane trimercaptpropionate (TMPTMP) were purchased from Aldrich. The chemical structures of monomers used in this research are illustrated in Figure 5.1.

In order to modify clay surfaces with polymerizable surfactants, Cloisite Na (Southern Clay Products – Gonzalez, TX), a natural montmorillonite containing sodium cations between silicate platelets, was ion exchanged using acrylate or thiol functionalized quaternary ammonium surfactants as described elsewhere.[21,34] Acrylated organoclay bearing acrylate functional groups on the clay surfaces was produced utilizing hexadecyl-2-acryloyloxy(ethyl) dimethylammonium bromide (C16A surfactant) synthesized following the methodologies described previously.[35,36] Thiol

functionalized organoclays were synthesized by incorporating a multifunctional thiol monomer into C14A acrylated organoclay modified by tetradecyl-2-acryloyloxy(ethyl) dimethylammonium bromide (C14A surfactant) via Michael addition reaction based on procedures reported elsewhere.[21]

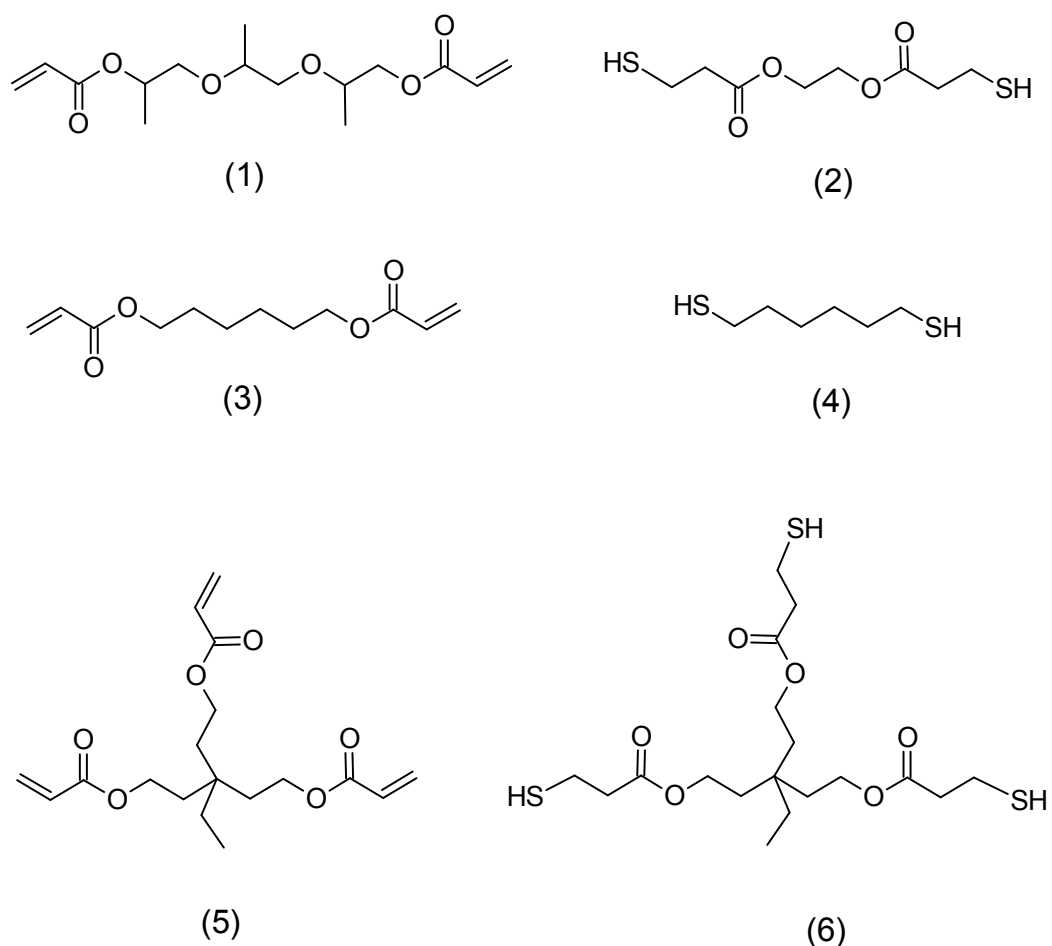


**Figure 5.1.** Chemical structures of monomers used in this study including (1) tripropylene glycol diacrylate (TrPGDA), (2) ethyleneglycol di(3-mercaptopropionate) (GDMP), (3) 1,6-hexanediol diacrylate (HDDA), (4) 1,6-hexanediol dithiol (HDT), (5) trimethylolpropane triacrylate (TMPTA), and (6) trimethylolpropane tris(3-mercaptopropionate) (TMPTMP).

C14A surfactant has the same structure as C16A surfactant except for that the carbon number in the alkyl tail group is fourteen instead of sixteen. Based on ease of purification in the synthesis processes, C14A organoclay is used as the acrylate organoclay to generate thiolated organoclays. Three types of different thiolated organoclays were prepared to control both the structure and functionality of thiol groups on the clay surfaces.

To provide monothiol functional groups on the organoclay structure, 1,6-hexanedithiol (HDT) or GDMP was reacted with C14A acrylated organoclays. In the same manner, tri-thiol functional TMPTMP was utilized to produce dithiol functional groups in the clay structure (PSH2). For comparison, Cloisite 93A (CL93A, Southern Clay Products), a montmorillonite clay modified with dihydrogenated tallow, was used to represent commercial nonreactive organoclays. The chemical structures of surfactants used in this research are illustrated in Figure 5.2. Hereafter, acrylated organoclays or thiolated organoclays will be identified with the name of surfactant used in the clay modification. For example, C14AHT organoclays indicates the thiolated organoclay produced from the reaction between C14A acrylated clay and 1,6-hexanedithiol while C14AGT indicates the thiolated organoclay produced from C14A acrylated organoclay and GDMP. Except where noted, 0.1 wt% 2,2-dimethoxyphenyl acetophenone (DMPA, Ciba Specialty Chemicals) was used as a free radical photoinitiator in all experiments. All chemicals including monomers and clays were used as received.

To investigate the impact of prepared organoclays, organoclay was combined with the monomer using a vortex mixer. The clay-monomer system was then sonicated for two hours in a controlled temperature water bath not exceeding 35°C to minimize any potential reaction. Photoinitiator was added after sonication not to allow initiator decomposition during the process. For thiol-acrylate mixtures, organoclay was mixed with acrylate monomer, and thiol monomers were added after the sonication process to prevent from self-initiation.[24] Once the photoinitiators were incorporated, the reaction

mixtures were kept at  $-6^{\circ}\text{C}$  and covered with aluminum foil to prevent for premature photoinitiation.

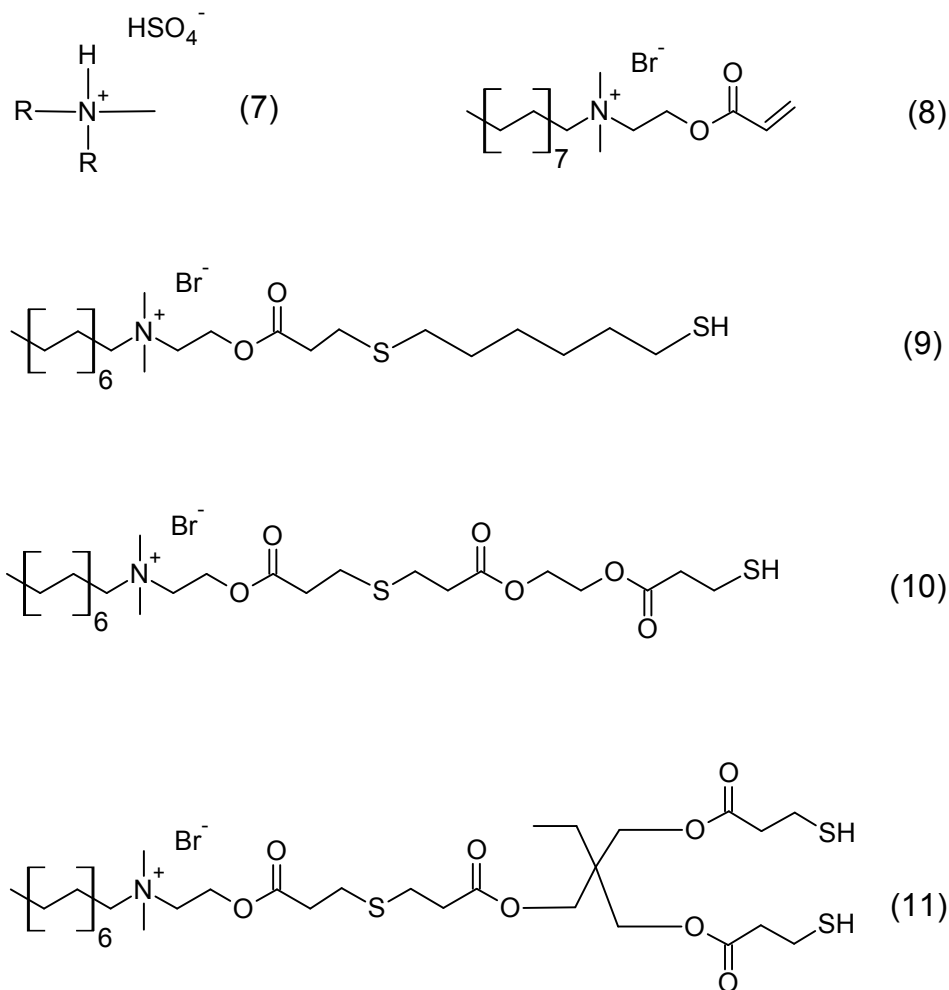


**Figure 5.2.** Chemical structures of quaternary ammonium surfactants used for clay structure modification. Shown are (7) methyl dihydrogenated tallow sulfonate, (CL93A), (8) hexadecyl-2-acryloyloxy(ethyl) dimethylammonium bromide (C16A), (9) tetradecyl 2-(1,6-mercaptohexyl mercaptane) acetoxy(ethyl) dimethylammonium bromide (C14AHT; Monothiol), (10) tetradecyl 2-(1,3-mercaptopropionate mercaptopropionyl ethyleneglycol)acetoxy(ethyl) dimethylammonium bromide (C14AGT), and (11) tetradecyl 2-(bis(3-mercaptopropionate) mercaptopropionyl trimethylolpropyl) acetoxy(ethyl) dimethylammonium bromide (PSH2; Dithiol).



## Methods

Thiol-ene photopolymerization kinetics was studied using real time infrared spectroscopy (RTIR, Thermo Nicolet Nexus 670). RTIR samples were prepared by sandwiching monomer mixtures between two sodium chloride plates. Measurements were performed at ambient temperature after purging the RTIR chamber for 6 minutes with dry nitrogen gas. UV light was provided by an optical fiber from a medium pressure mercury lamp (EXPO Acticure). Functional group conversion was evaluated by monitoring the decrease in the height of the absorbance peak at  $810\text{ cm}^{-1}$  for acrylate and at  $2575\text{ cm}^{-1}$  for thiol.[25] Photopolymerization reactions were initiated with a 365 nm light at  $3.0\text{mW/cm}^2$  irradiation intensity.

Dark curing experiments were performed by shuttering the light at designated times to control the initial conversion under illumination. Spectra were thereafter monitored to determine in functional group conversion without irradiation. Any conversion changes after shuttering the light was recorded for 5 minutes allowing sufficient time for post cure. These after-effects experiments [37,38] were utilized to understand termination behavior in the presence of organoclays.

Small angle x-ray scattering (SAXS) studies were used to evaluate the exfoliation degree of organoclays in liquid monomers. A Nonius FR590 X-ray apparatus equipped with a Cu K $\alpha$  radiation source ( $\lambda = 1.54\text{ \AA}$ ) at 40kV and 30mA intensity was utilized for SAXS experiments.[39]

Dynamic mechanical analysis (DMA- Q800 DMA TA Instruments) was conducted to investigate the effect of organoclays on ultimate mechanical properties. To fabricate the samples having dimensions of 2 x 13 x 25mm, liquid monomer mixtures were injected between two microscope slides end-capped with 2 mm spacers. The sample was then irradiated for ten minutes on each side under nitrogen atmosphere. To measure the modulus and glass transition temperature, samples were heated from -100C to 100C

at 3°C/min. Measurements were made using two point bending mode at 1Hz frequency. Young's modulus was evaluated at 30°C using tensile mode with a designated force rate (0.5 N/m). The modulus calculation was performed utilizing the slope of the stress-strain curve in the early linear regime (less than 10% strain).

### Results and Discussion

Previous research [20,21] has demonstrated that the incorporation of polymerizable organoclays into photopolymerization systems can enhance the polymerization rate, whereas the rate usually decreases due to reduction in incident light energy when other inorganic fillers are added.[40] It is believed that immobilization of the propagating radicals on the polymerizable organoclay surfaces decreases termination rate thereby compensating for the light interference of clays. On the other hand, if a system is composed of two or more types of functional groups with different reactivity as well as different reaction mechanisms, both the functional groups on the organoclay surfaces and the compatibility to certain monomers could also significantly affect the reaction behavior. Recently, we have reported the effect of monomer structure on both clay exfoliation and thiol-ene photopolymerization behavior using various thiol-acrylate monomer mixtures.[33] By changing the monomer composition as well as the type of polymerizable organoclays, different degrees of clay exfoliation were achieved. Interestingly, chemical compatibility between monomers and organoclay is the primary factor influencing clay exfoliation. Greater clay exfoliation enhances overall photopolymerization rate in the same manner as shown elsewhere in acrylate systems.[33] More interestingly, the type of functional group on clay surfaces significantly affects the polymerization mechanisms of the given thiol-acrylate systems. Thiolated organoclays enhance thiol-ene reaction and thiol conversion while acrylated

organoclays facilitate acrylate homopolymerization. The type of functional group on the organoclay surfaces directs polymerization behavior by affecting the stoichiometric balance between thiol and ene functional groups in the clay galleries as well as by determining the primary type of radicals on the clay surfaces.

To understand the effects of polymerizable organoclays on the reaction behavior of thiol-acrylate systems more clearly, kinetic studies have been performed when changing the inherent nature of the organoclay structure such as polarity, functionality, and the types of functional groups. Figure 5.2 (8) to (11) show surfactant structures for four different polymerizable organoclays. Using acrylated organoclay (modified by C14A, Figure 5.2 (8)), three types of thiolated organoclays have been prepared by reacting different thiol monomers with basic C14A acrylated organoclay to control the structure of reactive moieties. C14AHT organoclay (Figure 5.2 (9)) was generated by using 1,6-hexanedithiol (HDT), a relatively hydrophobic thiol monomer. In the preparation of C14AGT organoclay (Figure 5.2 (10)), HDT was replaced by more the polar GDMP dithiol to increase hydrophilicity of end reactive groups. In the same manner, TMPTMP trithiol was used to increase the functionality of organoclay, generating difunctional reactive moieties on the clay surfaces as shown in Figure 5.2 (11).

On the other hand, the degree of clay exfoliation can also significantly affect the photopolymerization kinetics of thiol-ene clay systems. In order to examine the net effect of organoclay structure on polymerization behavior without confounding clay exfoliation effects, it is desirable for the systems to have a similar and sufficient degree of clay exfoliation. To this end, the degree of clay exfoliation using the designed polymerizable organoclays was examined prior to kinetic study. The TrPGDA/GDMP mixture with moderate cross-linking density was selected for the monomer systems. A 2:1 molar ratio between acrylate and thiol monomers was used to produce a tough material suitable for further experiments.

Clay exfoliation behavior of TrPGDA/GDMP compositions with 3 wt% organoclays was studied utilizing small angle X-ray scattering (SAXS) with results illustrated in Figure 5.3. In SAXS profiles for the systems in Figure 5.3, intensity as a function of X-ray scattering angle before polymerization is plotted and offset for facile comparison. The mixture with nonreactive Cloisite 93A (CL93A) organoclay is included as a model system. As shown in Figure 5.3, the profile for the CL93A organoclay system exhibits a noticeable primary peak at  $2.4^\circ$  and a small secondary peak around  $5^\circ$   $2\theta$  corresponding to d-spacing of 3.7 nm and 1.8 nm respectively.

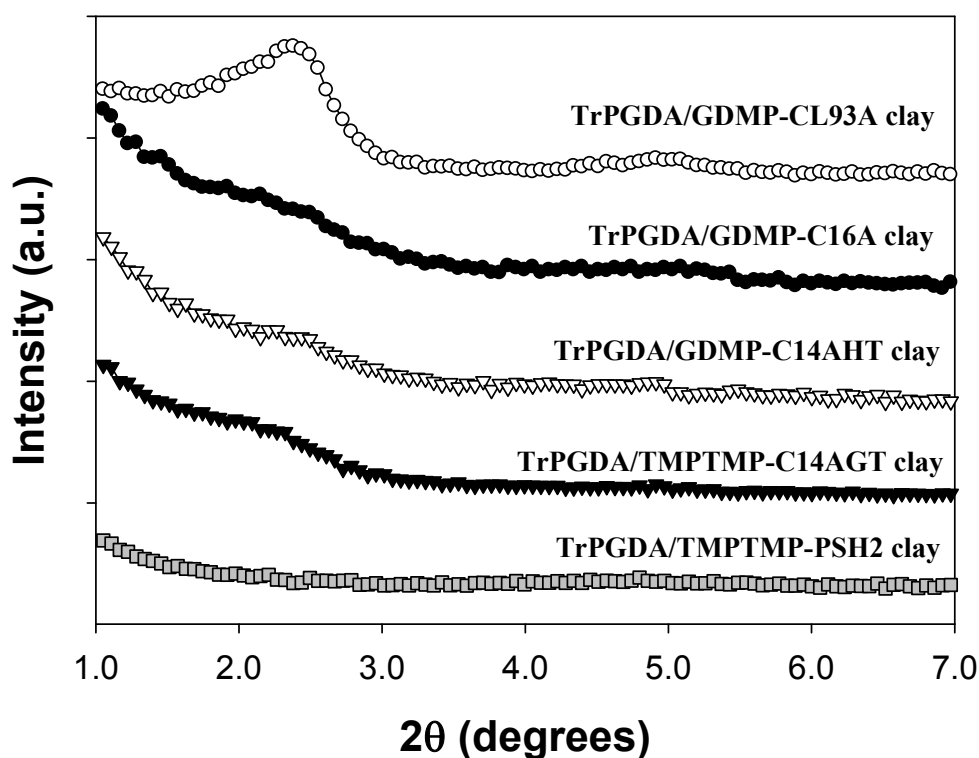


**Figure 5.3.** SAXS profiles of 3wt% Cloisite 93A-organoclay ( $\circ$ ), 3wt% C16A-organoclay ( $\bullet$ ), 3wt% C14AHT-organoclay ( $\nabla$ ), 3wt% C14AGT-organoclay ( $\blacktriangledown$ ), and 3wt% PSH2-organoclay ( $\blacksquare$ ) in TrPGDA/GDMP mixture with 2:1 acrylate to thiol molar ratio.

The exfoliation behavior of the system with polymerizable organoclays is quite different. For each polymerizable organoclay systems, the primary peak is significantly decreased if not completely absent with no meaningful secondary peak indicating significant enhancement in clay exfoliation. C16A, C14AHT, and C14AGT clay systems show almost the same degree of clay exfoliation. The greater exfoliation of PSH2 organoclay is likely due to its bulky structure. The exfoliation behavior from Figure 5.3 demonstrates that all polymerizable organoclays have sufficient compatibility with the TrPGDA/GDMP system and thus any difference in polymerization behavior between organoclay systems should primarily result from changes in chemical structure.

To investigate the effects of functional group structure on photopolymerization kinetics, RTIR was used to compare the polymerization profiles of systems incorporating different organoclays. The acrylate conversion and thiol conversion as a function of time for 2:1 TrPGDA/GDMP mixtures based on functional group ratio are shown in Figure 5.4. As shown in the profiles (Figure 5.4(A)), the incorporation of polymerizable organoclays slightly increases polymerization rate regardless of the organoclay type. Ultimate acrylate conversion reaches unity in all systems including the neat system with no clay addition. Thiol conversion profiles in Figure 5.4(B), however, show different behavior based on the type of organoclays. When C16A acrylated organoclay is used, the conversion profile is not significantly changed from that of the neat system. On the other hand, incorporation of a thiolated organoclays induces significant increase in photopolymerization rate and final thiol conversion. Ultimate thiol conversion after 6 minutes irradiation increases from around 0.6 (for the neat system) to approximately 0.8 for the three thiolated clay systems. It also appears that the structure of thiolated organoclay induces slight changes in the thiol reaction rate. Compared to two thiolated organoclays modified by monofunctional surfactants such as C14AHT or C14AGT (hereafter designated as the monofunctional thiolated organoclays), PSH2 thiolated organoclays with two functional groups in the surfactant structure (hereafter designated

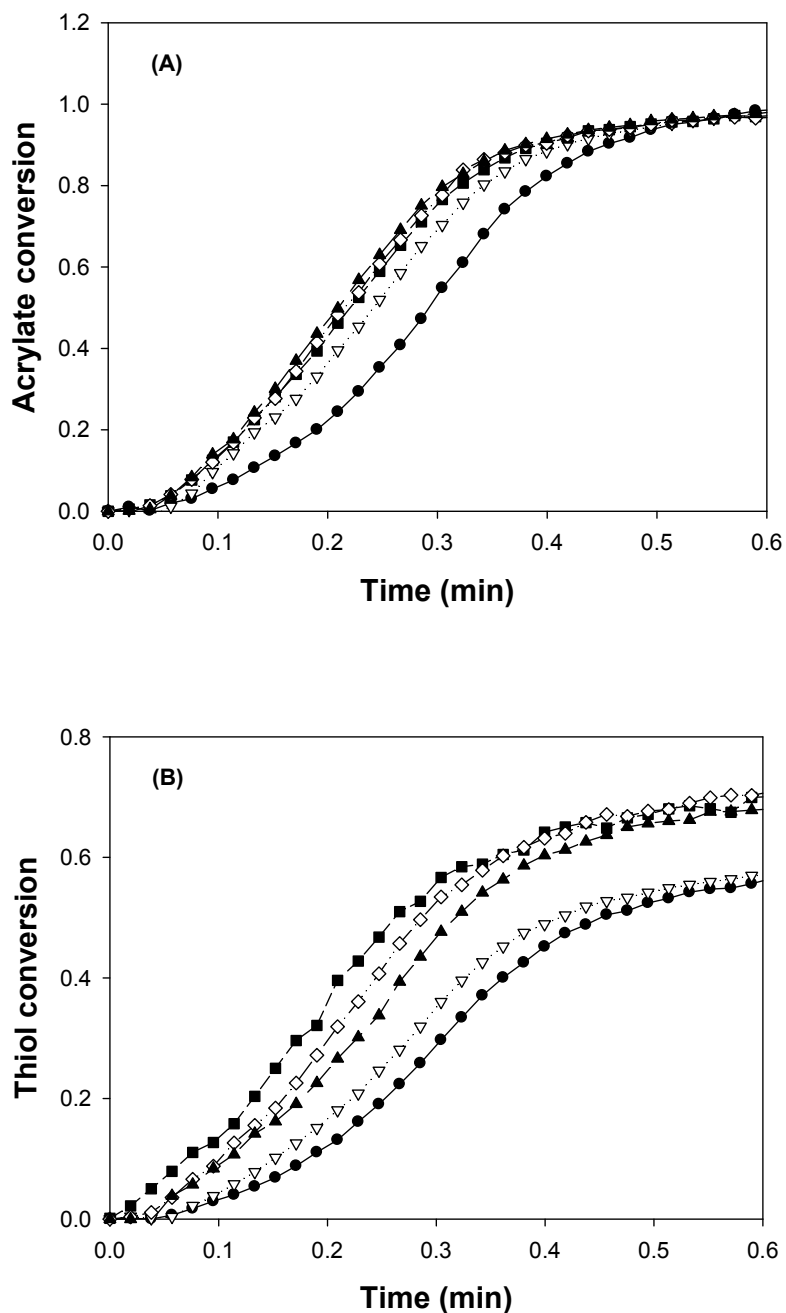


**Figure 5.4.** Functional group conversion profiles of organoclays in 2:1 molar ratio TrPGDA/GDMP mixtures. Shown are (A) acrylate conversion profiles for neat TrPGDA/GDMP (●), TrPGDA/GDMP with 3 wt% C16A (▽), 3 wt% C14AHT (▲), 3wt% C14AGT(◇), and 3 wt% PSH2 (■) organoclays, and (B) for thiol conversion profiles for neat TrPGDA/GDMP (●), TrPGDA/GDMP with 3 wt% C16A (▽), 3 wt% C14AHT (▲), 3wt% C14AGT(◇), and 3 wt% PSH2 (■) organoclays. Photopolymerizations were initiated with 0.1 wt% DMPA using 365 nm light at 3.0 mW/cm<sup>2</sup>.

as the difunctional thiolated organoclay) induces slightly faster thiol reaction. The increase in thiol functionality on the organoclay surface may induce greater generation of propagating thiyl radicals during the polymerization thereby increasing the polymerization rate.

Although the structure difference in the thiolated organoclays does not induce significant changes in the basic kinetic profiles of the systems as shown in Figure 5.4(B), further analysis reveals that the organoclay structure can alter the polymerization mechanism of the thiol-acrylate systems considerably. The acrylate conversion as a function of thiol conversion up to 80% acrylate conversion for each system in Figure 5.4 is plotted in Figure 5.5 utilizing the same RTIR experimental results. In these correlation curves, a lower slope shows greater thiol conversion indicating enhancement of the thiol-ene step growth copolymerization.

Similar to other thiol-acrylate systems discussed previously [33], acrylated organoclay encourages acrylate homopolymerization and thiolated organoclays facilitates thiol-ene step growth reaction. The addition of 3wt% acrylated C16A organoclay produces a slope slightly higher than that of neat system indicating that polymerization involves more acrylate homopolymerization. Adding the same amount of monofunctional thiolated organoclays such as C14AHT, C14AGT, or PSH2 organoclays, on the other hand, enhances step-growth thiol-ene reaction. Interestingly, compared to monofunctional C14AHT and C14AGT organoclays, difunctional PSH2 organoclay induces much higher thiol-ene reaction. This different behavior in difunctional PSH2 organoclay system is possibly due to the increase of total number of functional groups on the clay surface which induces more propagating thiyl radicals in the clay galleries than the systems with the same amount of monofunctional organoclays. In comparing the monofunctional thiolated organoclays, the incorporation C14AGT organoclays, produced by using GDMP, induces slightly higher thiol-ene step growth reaction than the use of C14AHT organoclay modified by 1,6-hexanedithol. It is reasonable to assume the

structural similarity of end functional group on the clay surfaces and GDMP in the monomer system increases the interaction between components inducing greater thiol-ene polymerization.

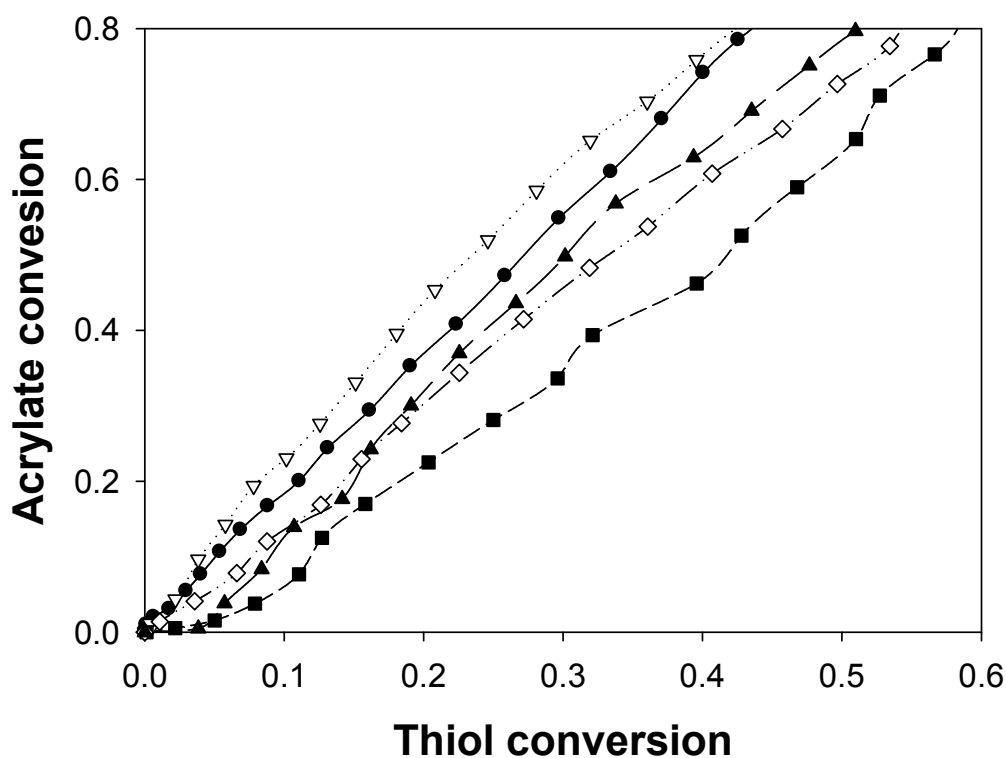


**Figure 5.5.** Double bond versus thiol conversion at short irradiation times for 2:1 molar ratio TrPGDA/GDMP mixtures. Conversion profiles are shown for neat TrPGDA/GDMP (●), TrPGDA/GDMP with 3 wt% C16A-acrylated organoclay (▽), 3 wt% C14AHT-thiolated organoclay (▲), 3 wt% of C14AGT-acrylated organoclay (◇) and 3 wt% of PSH2 thiolated organoclay (■). Photopolymerizations were initiated with 0.1 wt% DMPA using 365 nm light at 3.0 mW/cm<sup>2</sup>.

The RTIR kinetic studies from the TrPGDA/GDMP system strongly suggest that the type of functional group as well as the structure of the organic modifier for the clay significantly influence the photopolymerization behavior of thiol-ene systems. To gain



further understanding of the mechanism causing the difference in photopolymerization behavior, dark cure experiments were performed to monitor the reaction after shuttering the light and eliminating initiation.[37,38] Once no more light reacted the sample, no new radicals can be generated. Any apparent reaction thereafter is induced reaction from residual radicals in the system. By comparing the dark curing behavior of the neat system without organoclay with that of systems including polymerizable organoclays, effects of the functionality and chemistry of organoclay surfaces on the photopolymerization mechanism can be further elucidated.

Dark curing behavior for thiol-acrylate systems containing 3wt% C16A acrylated organoclays or PSH2 thiolated organoclays are shown in Figure 5.6 from systems with various initial conversions achieved during illumination. Moderately cross-linked TrPGDA/GDMP (diacrylate/dithiol) systems with a 2:1 molar ratio based on functional groups was compared with more highly cross-linked TrPGDA/TMPTMP (diacrylate/trithiol) mixtures with the same functional group ratio. Each monomer mixture without any clay was also evaluated for comparison. In Figure 5.6 (A) and (B), dark acrylate conversion as a function of illuminated conversion from RTIR experiments is plotted for TrPGDA/GDMP and TrPGDA/TMPTMP systems, respectively. To control the initial illuminated conversion, the light was shuttered after illumination for 6, 12, 18 and 24 seconds.

Regardless of organoclay type and monomer composition, dark conversion increases as the illuminated conversion reaches about 0.4. This behavior is observed because the increased system viscosity at higher illuminated conversions decreases the rate of bimolecular termination due to diffusion limitations on the propagating radicals. The only difference between the neat two monomer systems is that the illuminated conversions at relatively early polymerization stages of the TrPGDA/TMPTMP system (after 6 sec and 12 sec of illumination) are higher than those of TrPGDA/GDMP systems, dark conversion at those points of time are thus slightly higher due to the aforementioned

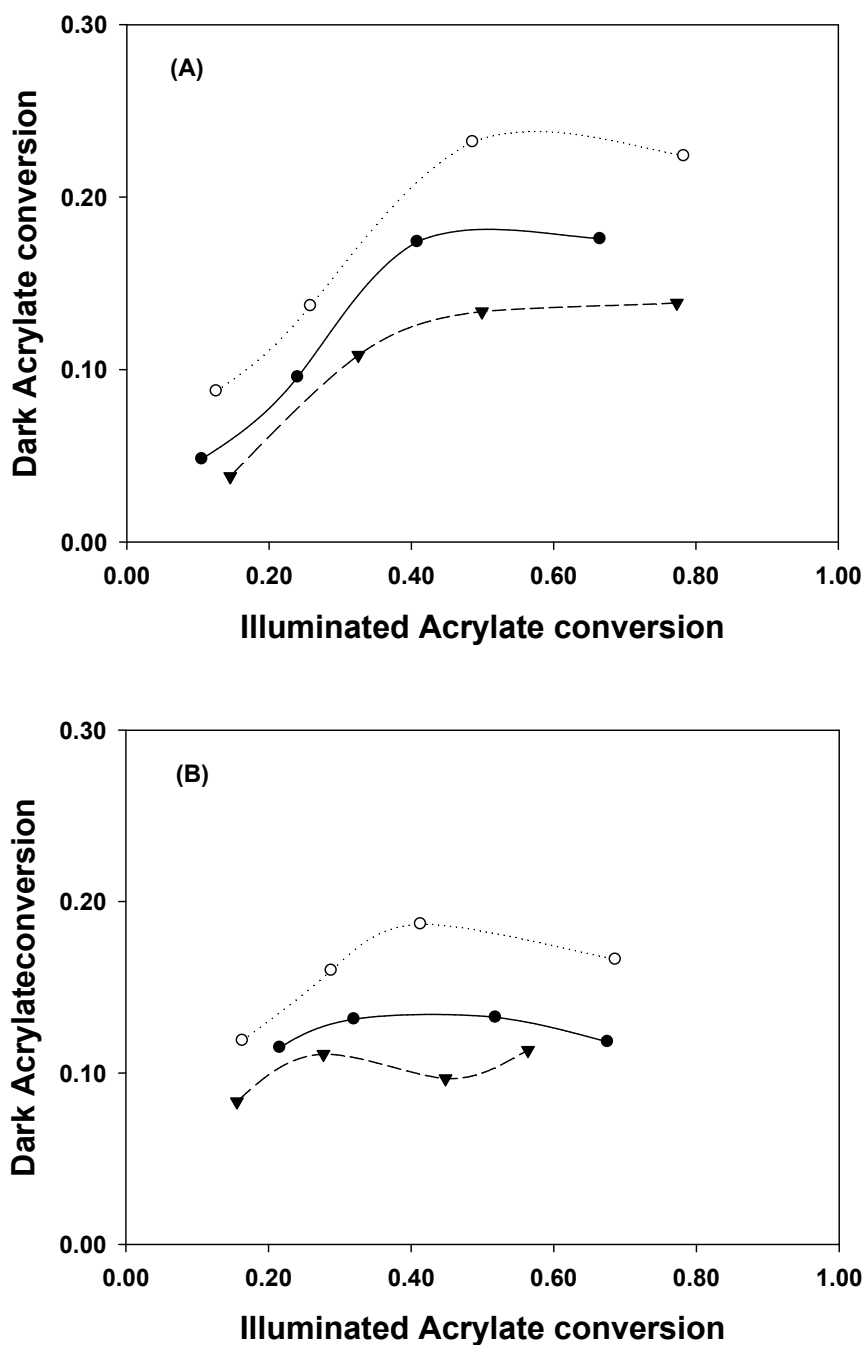


**Figure 5.6.** Dark acrylate conversion profiles of acrylate/thiol 2:1 molar mixtures based on functional group with or without organoclays. Shown are (A) conversion profiles for neat TrPGDA/GDMP (●), TrPGDA/GDMP with 3 wt% C16A-acrylated organoclay (○), and 3 wt% PSH2 thiolated organoclay (▼), and (B) for neat TrPGDA/TMPTMP (●), TrPGDA/TMPTMP with 3 wt% C16A-acrylated organoclay (○), and 3 wt% PSH2 thiolated organoclay (▼). UV light was shuttered after 6, 12, 18, and 24 seconds of irradiation at 3 mW/cm<sup>2</sup>. 0.1wt% DMPA was used for initiation.

viscosity effect. In addition, although all experimental systems have different initial illuminated conversions, acrylated organoclay systems always show a higher dark acrylate conversion than the neat systems while thiolated organoclay systems exhibit a lower dark conversion in both monomer compositions. These differences may arise from the different characteristics of the radicals on each organoclay surface. With added acrylated organoclays, the dark acrylate conversion is much higher than for neat systems perhaps due to the immobilization of propagating acrylate chain radicals on the organoclay surface, which results in reduction of bimolecular termination based on the significantly lower mobility of the radicals. Residual acrylate radicals on the acrylated organoclay surface are likely to have much longer radical lifetimes than those in bulk regions of the system. This immobilization of radicals makes the effective concentration of residual radicals in the system with acrylated organoclay always higher than the neat system for all initial illuminated conversions. On the other hand, the lower dark acrylate conversions of the systems with thiolated organoclays suggest a somewhat different reaction mechanism that restricts the acrylate homopolymerization during the dark curing. Because most of the immobilized residual radicals on the surface of thiolated organoclays are inherently thiyl radicals or secondary radicals originating from the thiol groups on the organoclay, greater thiol-ene reaction could occur than that observed in the neat system, resulting in lower dark acrylate conversion in thiolated organoclay systems.

Dark thiol conversions for both monomer systems exhibit slightly different behavior from those of dark acrylate-conversions. As shown in Figure 5.7 (A) for TrPGDA/GDMP system and (B) for TrPGDA/TMPTMP system, the extent of dark thiol-conversion for all illuminated conversions is about one-half the dark acrylate-conversions in Figure 5.6. This behavior is at least in part due to the lower illuminated conversion of thiol functional groups. Based on the 2:1 molar ratio of the monomer systems, collision probability is lower between residual radicals and thiol monomers.

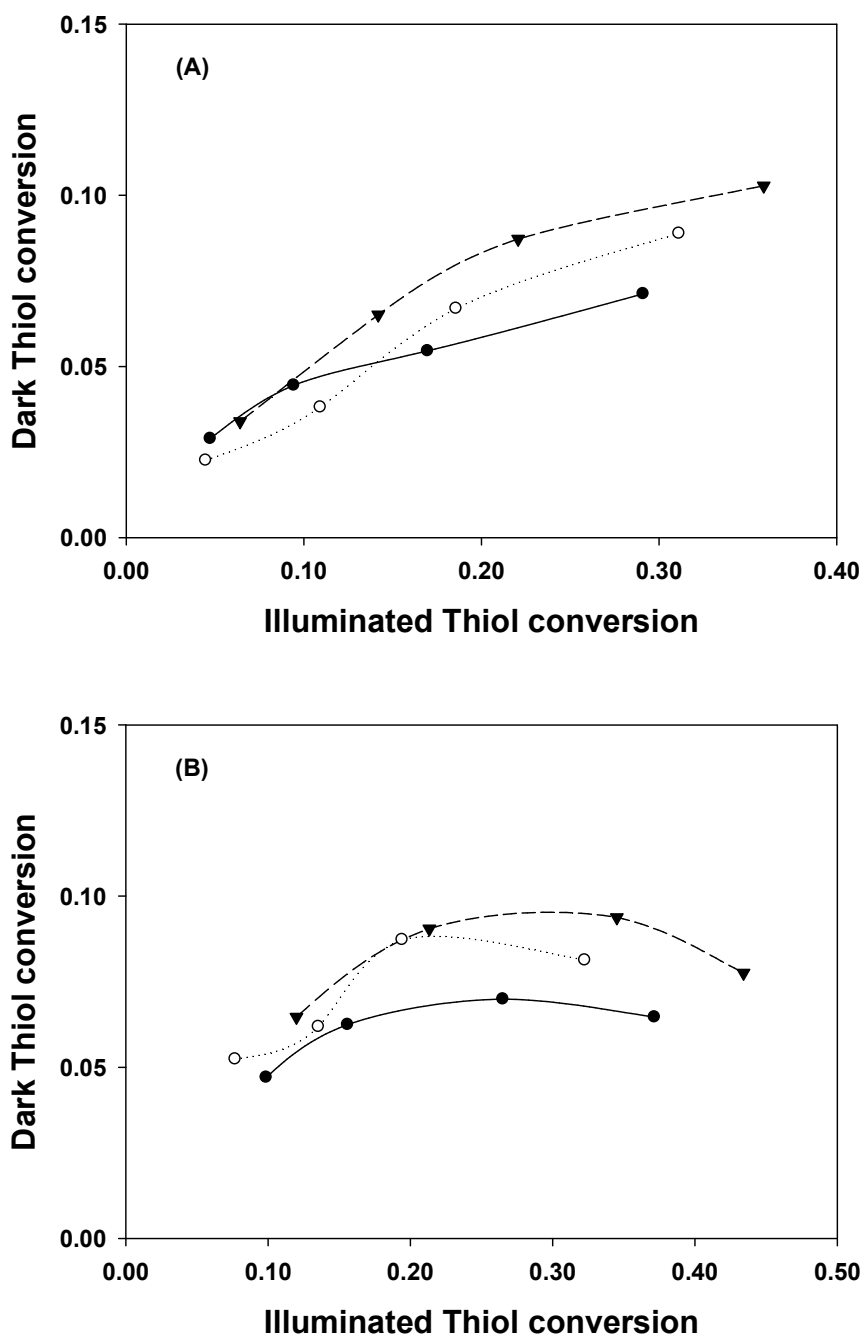


**Figure 5.7.** Dark thiol conversion profiles of acrylate/thiol 2:1 molar mixtures based on functional group with or without organoclays. Shown are (A) conversion profiles for neat TrPGDA/GDMP (●), TrPGDA/GDMP with 3 wt% C16A-acrylated organoclay (○), and 3 wt% PSH2 thiolated organoclay (▼), and (B) for neat TrPGDA/TMPTMP (●), TrPGDA/TMPTMP with 3 wt% C16A-acrylated organoclay (○), and 3 wt% PSH2 thiolated organoclay (▼). UV light was shuttered after 6, 12, 18, and 24 seconds of irradiation at 3 mW/cm<sup>2</sup>. 0.1wt% DMPA was used for initiation.

Interestingly, thiolated organoclay systems exhibit higher dark thiol-conversions compared to neat and acrylated organoclay systems regardless of monomer composition. This behavior is observed as large number of secondary residual radicals, formed by reaction between thiyl radicals on thiolated clay surfaces and acrylate double bonds, are present in the clay gallery after short period of illumination. Because these secondary radicals are preferably transferred to other thiol groups to produce thiyl radicals [24], thiol-ene copolymerization will be facilitated when compared to the acrylated organoclay systems. This difference in dark curing behavior also confirms that thiolated organoclay accelerates the thiol-ene copolymerization through significant formation of thiyl radicals on the clay surfaces.

Figure 5.8 shows a representation of the clay surfaces to provide a basis for understanding the different effects of polymerizable organoclays on dark curing behavior. As shown in Figure 5.8 (A), the residual radicals on the surfaces of acrylated organoclays essentially originate from the acrylic double bond and therefore can rapidly react with other acrylate and/or thiol monomers, resulting in much higher dark acrylate conversions. While the residual radicals on the surfaces of thiolated organoclays are also immobilized as in the systems with acrylated organoclays, the radicals originate from thiol groups attached to the anchored surfactants. In addition, as represented in Figure 5.8 (B), it is expected that a relatively large number of secondary radicals can be formed after short periods of illumination by reaction between the thiyl radicals on the clay surfaces and acrylate double bonds in monomers. The thiyl radicals will react with double bonds of acrylated monomers while the propagating secondary radicals can either react with another thiol monomer to regenerate thiyl radicals or react with another acrylate double bond for chain propagation. In this step-growth mechanism for thiol-ene reaction involving either hydrogen abstraction or chain transfer in each step, the reaction rate of thiol-ene copolymerization is usually slower than acrylate homopolymerization.[41,42] Because the rate of radical termination is much faster than that of radical transfer in

general, the effective radical concentration on the surfaces of thiolated organoclay rapidly decreases if there is no further radical initiation.

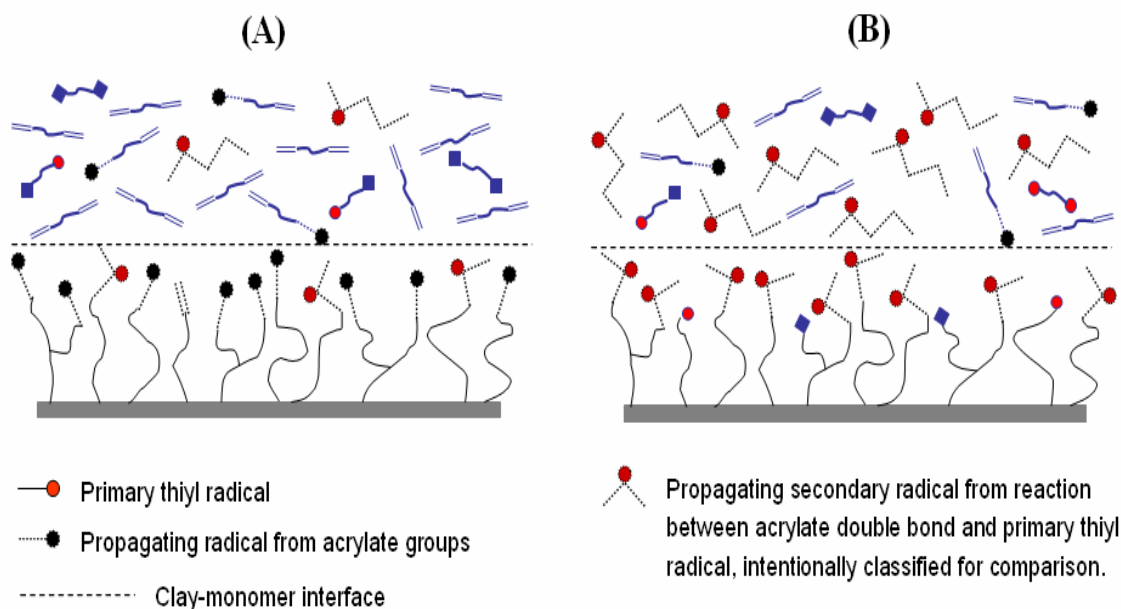


**Figure 5.8.** Schematic representation of residual radical compositions in clay galleries after shutting off the UV with short period of initial irradiation (A) for the system with acrylated organoclay, and (B) for the system with thiolated organoclay. Used symbols are for unreacted acrylate double bonds (=), for unreacted thiol groups (■), for various propagating radicals (●) including primary thiyl radicals, acrylic radicals, and secondary radicals from reaction between thiyl radical and acrylate double bond, respectively.

To this point, RTIR kinetic studies and dark curing experimental results reveal that increase of functionality on clay surfaces enhances the thiol-ene reaction of the systems. Increasing monomer functionality may also impact polymerization behavior as the functionality on organoclay surfaces will increase once the formation of radicals begins. The reaction between functional groups on the organoclay surfaces and higher functionality monomers will consequently increase the number of functional groups

immobilized on the clay surface. Monomer functionality is thus another important factor to control and to maximize ultimate conversion. To examine monomer functionality effects on the reaction behavior of polymerizable organoclay systems, monomer systems including trifunctional thiols and triacrylates were prepared to control the functionality of the systems. A 2:1 mole ratio based on functional groups between acrylate and thiol monomer was used. 1,6-hexanediol diacrylate (HDDA) was used as the diacrylate monomer and mixed with the trithiol TMPTMP. The average functionality of this system is 2.33 theoretically, assuming no acrylate homopolymerization occurs. The monomer functionality increases slightly to 2.67. 1,6-hexanedithiol (HDT) is combined with trimethylolpropane triacrylate (TMPTA) that have similar monomer structures to the HDDA-TMPTMP system. Finally, monomer functionality increases to 3.00 by using triacrylate TMPTA and trithiols TMPTMP as the acrylate and thiol monomers.

The polymerization profiles of thiol conversion as a function of time based on RTIR experiments of these three compositions are illustrated in Figure 5.9 (A) with 3 wt% C16A acrylated organoclays and (B) with 3 wt% PSH2 thiolated organoclays. The use of thiolated organoclays generally enhances the final thiol conversion of HDDA/TMPTMP and TMPTA/HDT systems in Figure 5.9 (B) almost 10% compared to those with acrylated organoclays in Figure 5.9 (A). Ultimate thiol conversions of TMPTA/TMPTMP systems with higher functionality, however, do not change with different organoclays. In addition, the final thiol conversion significantly decreases with increase of monomer functionality. Because no decrease in final thiol conversion with enhanced thiol-ene reaction was observed by increasing the organoclay functionality as discussed previously in Figure 5.4 and 5.5, it is reasonable to believe that the increase of organoclay functionality induced by increasing monomer functionality might enhance the thiol-ene reaction resulting in no significant decrease in thiol conversion. These decreases in final thiol conversion by increasing functionality of the monomer imply that the viscosity build-up by fast gelation resulting from high monomer functionality prevents

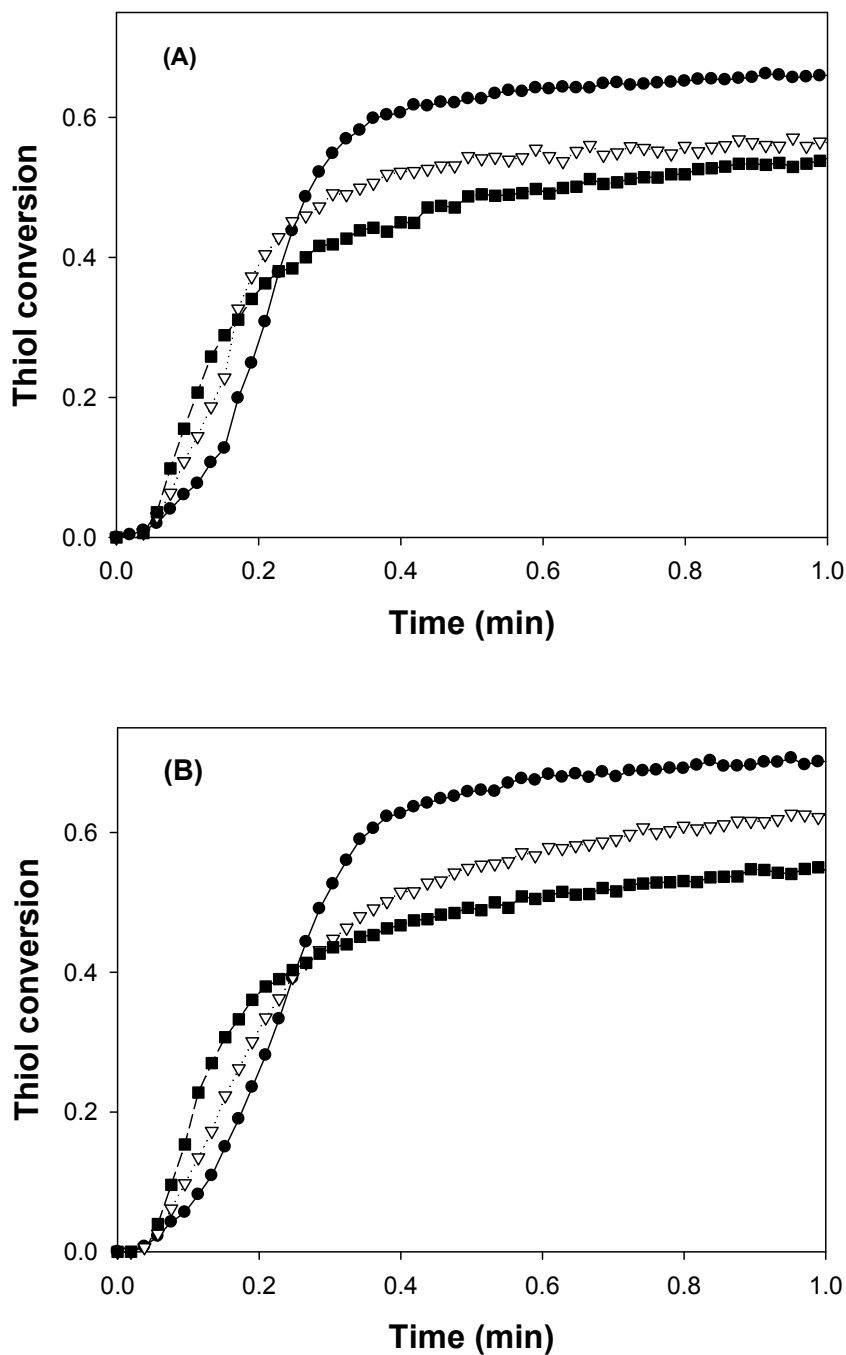


**Figure 5.9.** RTIR thiol conversion profiles of HDDA/TMPTMP (●), TMPTA/1,6-HDT (▽), and TMPTA/TMPTMP (■) mixtures having 2:1 molar ratio based on functional groups. Shown are (A) conversion profiles for systems with 3 wt% C16A acrylated organoclays and (B) for systems with 3wt% PSH2 thiolated organoclays. Photopolymerizations were initiated with 0.1 wt% DMPA using 365 nm light at 3.0 mW/cm<sup>2</sup>.



the possible conversion increase that would result based on the high organoclay functionality. To achieve high thiol conversion for thiol-acrylate systems, therefore, providing more functional groups (preferably more initial thiol groups) on organoclay surfaces appears to be more effective than the use of higher functionality monomers.

Because the ultimate goal of this research is the development of advanced photopolymer-clay nanocomposites having improved performance utilizing polymerizable organoclays, understanding the relation between polymerization kinetics and their final properties is important. To examine the effect of photopolymerization behavior on thermo-mechanical properties of thiol-ene photopolymer-clay systems, dynamic mechanical analysis (DMA) experiments were conducted for the same TrPGDA/GDMP systems utilized in kinetic studies. The storage modulus profiles as a function of temperature for the systems with addition of 3 wt% organoclays are shown in Figure 5.10 (A). For this moderately cross-linked system, the incorporation of 3wt% acrylated organoclays enhances the rubbery storage modulus, whereas the modulus of thiolated organoclay system increases just slightly over that of the neat system. It is apparent that dominant acrylate homopolymerization in acrylated organoclay system generates higher modulus than in thiolated organoclay systems where the polymerization occurs via enhanced thiol-ene step growth mechanism as discussed in Figure 5.5, resulting in softening of polymer chains by the formation of flexible thio-ether linkages. Interestingly, the incorporation of thiolated organoclays induces an increase in rubbery modulus, even with more formation of flexible bonds in the networks when compared to the neat system.

Young's modulus behavior of the systems provides more evidence of the organoclay impact on the mechanical strength of ultimate nanocomposites. As shown in Figure 5.10 (B), Young's moduli of the TrPGDA/GDMP systems were compared upon changing the type of organoclays. Addition of acrylated organoclay increases Young's

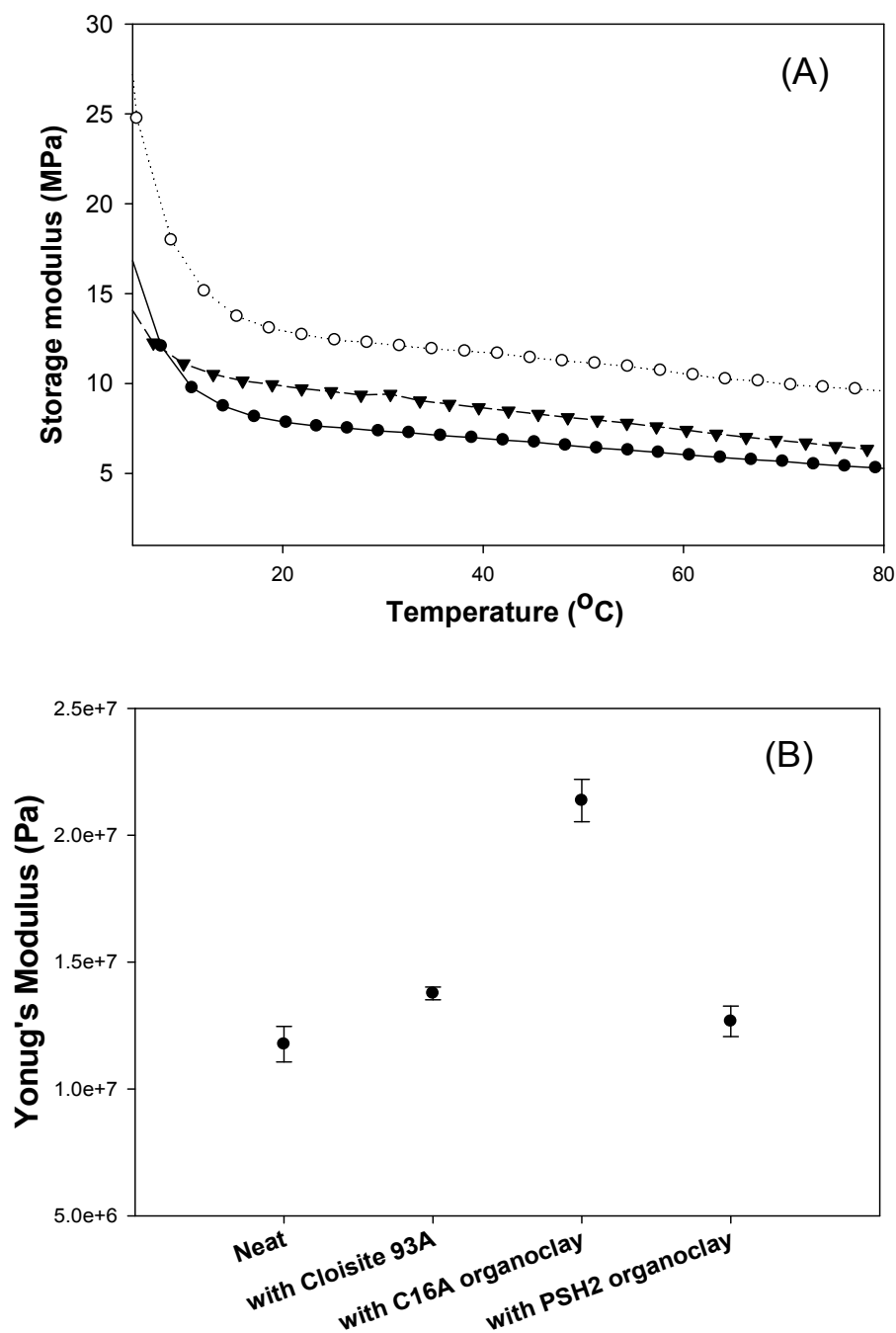


**Figure 5.10.** (A) Storage modulus profiles of 2:1 molar ratio TrPGDA/GDMP mixtures. Shown are profiles for neat TrPGDA/GDMP (●), TrPGDA/GDMP with 3 wt% C16A-acrylated organoclay (○), and 3 wt% PSH2 thiolated organoclay (▼). (B) Young's modulus of neat TrPGDA/GDMP system and TrPGDA/GDMP systems with addition of 3 wt% different type of organoclays. Samples were photopolymerized with 0.1 wt% DMPA using 365 nm light at  $3.6 \text{ mW/cm}^2$ .

modulus about 50% while C14AGT or PSH2 thiolated organoclay systems show similar values compared to those of unfilled neat or nonreactive CL93A organoclay systems. The small increase of Young's modulus by adding nonreactive CL93A organoclay is mainly due to the insufficient clay exfoliation as discussed for Figure 5.3 based on SAXS experiments, resulting in little formation of nano-scale clay morphology. Again, this behavior in Young's moduli of the systems confirms that increased acrylate homopolymerization by adding acrylated organoclay forms harder domains in the nanocomposites while thiolated organoclays make the networks more flexible.

Further evidence of this effect is provided by glass transition temperature behavior upon adding 3wt% of the different types of polymerizable organoclay in the same TrPGDA/GDMP system. As shown in Figure 5.11 (A), addition of C14AGT or PSH2 thiolated organoclays reduces the glass transition temperature, as indicated by the  $\tan \delta$  peak of the system, significantly due to enhanced thiol-ene reaction. The addition of C16A acrylated or non-reactive CL93A organoclays does not change the glass transition temperature from that of the neat system. In diacrylate/trithiol TrPGDA/TMPTMP, however, the glass transition temperature of the thiolated organoclay system shows almost the same value to that of the acrylated clay system and only a slight increase from the neat system as illustrated in Figure 5.11 (B). This behavior indicates that increased homogeneity in the cross-linked networks by incorporating trithiols restricts the chain mobility, thereby resulting in an increase in glass transition temperature in spite of the greater formation of flexible thioether linkages induced by incorporating thiolated organoclays. In addition, comparing the  $\tan \delta$  in Figure 5.11 (B), the width of  $\tan \delta$  peak for thiolated organoclay systems is slightly narrower than those of neat and acrylated organoclay systems. This decrease provides further evidence of increased thiol-ene reaction by the incorporation of thiolated organoclays because step-growth mechanism generates more homogeneous networks and thereby narrower peaks than acrylate homopolymerization.[24]

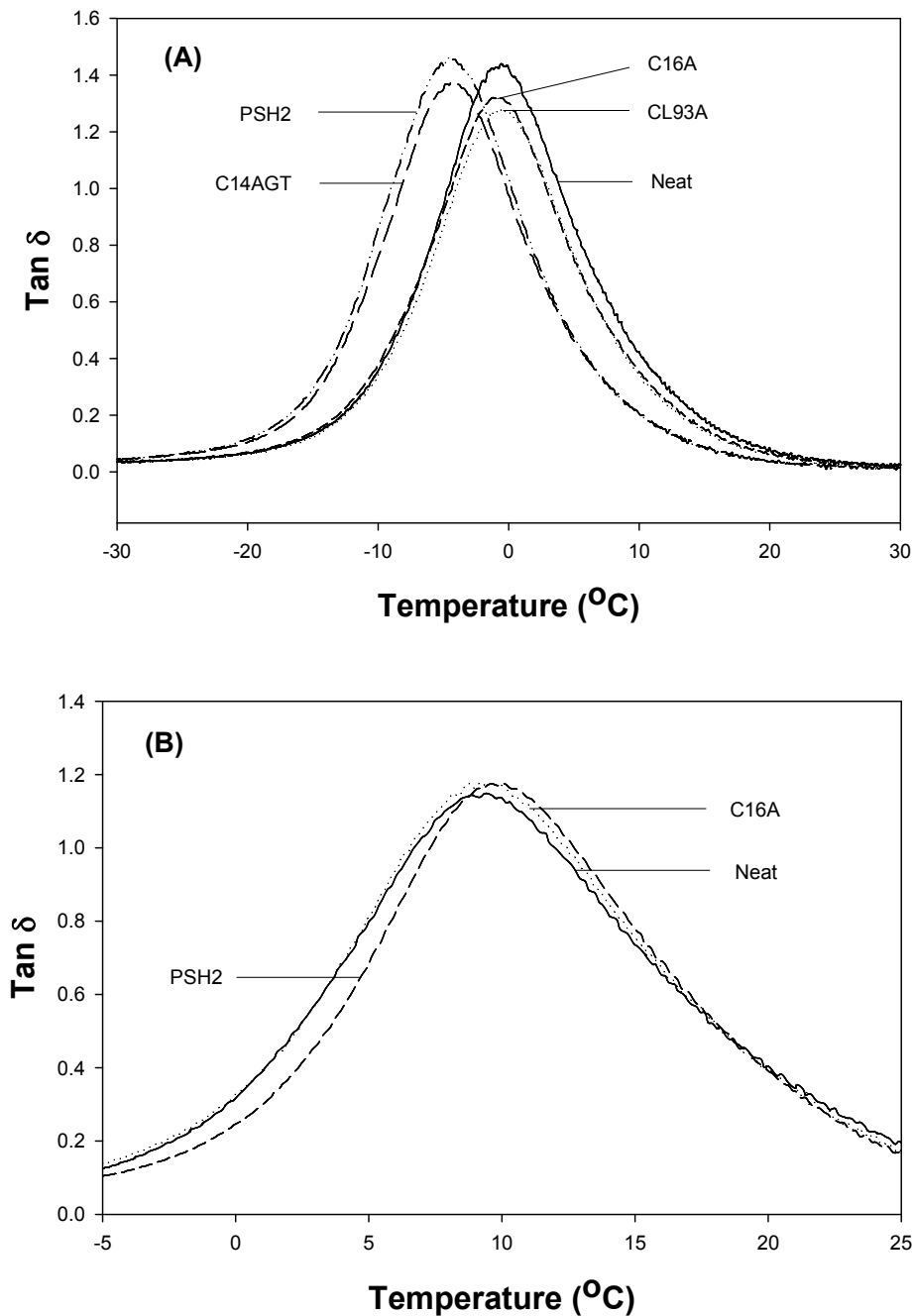


**Figure 5.11.**  $\tan \delta$  profiles as a function of temperature of 2:1 acrylate/thiol molar ratio mixtures. Shown are (A) profiles for neat TrPGDA/GDMP, TrPGDA/GDMP with 3 wt% CL93A nonreactive organoclay, 3wt% C16A acrylated organoclay, 3wt% C14AGT thiolated organoclay, and 3 wt% PSH2 thiolated organoclay, and (B) for neat TrPGDA/GDMP, TrPGDA/TMPTMP with 3 wt% C16A acrylated organoclay, 3wt% PSH2 thiolated organoclay. Samples were photopolymerized with 0.1 wt% DMPA using 365 nm light at  $3.6 \text{ mW/cm}^2$ .

These results indicate the importance of understanding the effects of polymerizable organoclays on reaction behavior. With different interaction between monomers and organoclays, the structure of photopolymerizable groups on the organoclay surface has substantial impact on polymerization behavior and ultimate nanocomposite properties. Upon achieving sufficient clay exfoliation, increased thiol functionality on organoclay surfaces induces much greater thiol-ene step growth reaction in thiol-acrylate systems while increase of monomer functionality does not enhance the step growth reaction. In addition, the difference in both the degree of thiol-ene reaction and final thiol conversion of monomers and in the ultimate network structure significantly affects the ultimate thermo-mechanical properties of nanocomposites. Understanding the important factors in designing the polymerizable organoclays in photopolymer systems will contribute to control of nanocomposites characteristics and applications in photopolymerization systems.

### Conclusions

To understand the important factors in designing polymer-clay nanocomposites based on *in situ* thiol-ene photopolymerization, the effects of polymerizable organoclays on the reaction behavior as well as ultimate composite properties have been investigated. To this end, polymerizable organoclays with different type and structure of reactive groups were incorporated into various thiol-acrylate systems. With well-exfoliated clay dispersion in the moderately cross-linked TrPGDA/GDMP system, the incorporation of thiol groups on the clay surface increases the photopolymerization rate and final thiol conversion, whereas acrylate groups on the surface do not change either significantly. In addition, while increasing monomer functionality decreases final thiol conversion, increasing thiol functionality in the organoclays enhances thiol-ene step growth reaction.

Different behavior between acrylated and thiolated organoclay systems in dark curing experiments suggests that the type of original functional groups on organoclay surfaces governs the structure of propagating radicals in the clay galleries, affecting overall degree of thiol-ene reaction in each system. These differences in reaction behavior induced by the type of organoclays significantly affect thermo-mechanical properties of ultimate nanocomposite. The incorporation of acrylated organoclays significantly increases the storage modulus of the nanocomposites with dominant acrylate homopolymerization. Addition of thiolated organoclays, on the other hand, makes polymer chains more flexible due to increased thio-ether linkages. Interestingly, while the glass transition temperature of the thiolated organoclay system decreases from that of the neat system, no decrease in the modulus of nanocomposites occurs.

Notes

1. Rodriguez, F.; Cohen, C., Ober, C. K.; Archer, L. A., *Principles of Polymer Systems*, Taylor & Francis, New York, **2003**, Ch.9, 405.
2. Vaia, R. A.; Giannelis, E. P. *Macromolecules* **1997**, 30, 7990.
3. Zanetti, M.; Lomakin, S.; Camino, G. *Macromol. Mater. Eng.* **2000**, 279, 1.
4. Reichert P.; Kressler J.; Mulhaupt R.; Stoppelmann G. *Acta Polym.* **1998**, 49, 116.
5. LeBaron, P. C.; Wang, Z.; Pinnavaia, T. J. *Appl. Clay Sci.* **1999**, 15, 11.
6. Ray, S. S.; Okamoto, M. *Prog. Polym. Sci.* **2003**, 28, 1539.
7. Uhl, F. M.; Davuluri, S. P.; Wong, S. C.; Webster, D.C. *Polymer* **2004**, 45, 6175.
8. Fu, X.; Qutubuddin, S. *Polymer* **2001**, 42, 807.
9. Gottler, L. A.; Lee, K.; Thakkar, Y. H. *Polymer Reviews* **2007**, 47, 291.
10. Ogawa, M.; Kuroda, K. *Bull. Chem. Soc. Jap.* **1997**, 70, 2593.
11. Wang, Z.; Pinnavaia, T. J. *Chem. Mater.* **1998**, 10, 1820.
12. Bongiovanni, R.; Ronchetti, M. S.; Turcato, E.A. *J. Colloid & Interf. Sci.* **2006**, 296, 515.
13. Decker, C.; Zahouily, K.; Keller, L.; Benfarhi, S.; Bendaikha. *J. Mater. Sci.* **2002**, 37, 4831.
14. Uhl, F. M.; Hinderliter, B. R.; Davuluri, S. P.; Croll, S. G. *Mater. Res. Soc.* **2004**, 16, 203.
15. Uhl, F. M.; Davuluri, S. P.; Wong, S. C.; Webster, D. C. *ANTEC Conf.* **2004**, 1892.
16. Tan, H.; Nie, J. *J. Appl. Polym. Sci.* **2007**, 106, 2656.
17. Decker, C.; Keller, L.; Zahouily, K.; Benfarhi, S. *Polymer* **2005**, 46, 6640.
18. Zahouily, K.; Benfarhi, S.; Bendaikha, T.; Baron, J. *Rad Tech Europe Conf.* **2001**, 583.
19. Decker, C. *Macromol. Rapid Commun.* **2002**, 23, 1067.
20. Owusu-Adom, K.; Guymon, C. A. *Polymer* **2008**, 49, 2636.
21. Owusu-Adom, K.; Guymon, C. A. *Macromolecules* **2009**, 42, 180.

22. Decker, C. *Polym. Int.* **1998**, 45, 133.
23. Decker, C. *Prog. Polym. Sci.* **1996**, 21, 593.
24. Hoyle, C. E.; Lee, T. Y.; Roper, T. *J. Polym. Sci. A: Polym. Chem.*, **2004**, 42, 5301.
25. Cramer, N. B.; Scott, J. P.; Bowman, C. N. *Macromolecules* **2002**, 35, 5361.
26. Morgan, C. R.; Magnota, F.; Ketley, A. D. *J. Polym. Sci.: Polym. Chem. Ed.*, **1977**, 15, 627.
27. Carioscia, J. A.; Lu, H.; Stanbury, J. W.; Bowman, C. N. *Dent. Mater.* **2005**, 21, 1137.
28. Senyurt, A. F.; Wei, H.; Hoyle, C. E.; Piland, S. G.; Gould, T. E. *Macromolecules* **2007**, 40, 4901.
29. Wei, H.; Li, Q.; Ojelade, M.; Madbouly, S.; Otaigbe, J. U.; Hoyle, C. E. *Macromolecules* **2007**, 40, 8788.
30. Cramer, N. B.; Reddy, S. K.; Lu, H.; Cross, T.; Raj, R.; Bowman, C. N. *J. Polym. Sci. A: Polym. Chem.*, **2004**, 42, 1752.
31. Lee, T. Y.; Smith, Z.; Reddy, S. K.; Cramer, N. B.; Bowman, C. N. *Macromolecules* **2007**, 40, 1466.
32. Owusu-Adom, K.; Guymon, C. A. *Macromolecules* **2009**, 42, 3275.
33. Kim S. K.; Guymon, C. A. *J. Polym. Sci. Part A Polym. Chem.* **2011**, 49, 465.
34. Lagaly, G.; Beneke, K. *Coll. Polym. Sci.* **1991**, 269, 1198.
35. Hamid S. M.; Sherrington D. C. *Polymer* **1987**, 28, 325.
36. McGrath, K. M.; Sherrington, D.C. *Polymer* **2006**, 37, 1453
37. Anseth, K. S.; Wang, C. M.; Bowman, C. N. *Macromolecules* **1994**, 27, 650
38. Tryson, G. R.; Shultz, A. R. *J. Polym. Sci.: Polym. Phys. Ed.* **1979**, 17, 2059
39. Katti, K. S.; Sikdar, D.; Katti, D. R.; Ghosh, P.; Verma, D. *Polymer* **2006**, 47, 403.
40. avidenko, N.; Garcí'a, O.; Sastre, R. *J. Appl. Polym. Sci.* **1995**, 97, 1016.
41. Cramer N. B, Davies T, O'Brien, A. K, Bowman, C. N. *Macromolecules* **2003**, 36, 4631.
42. Cramer, N. B.; Reddy, S. K.; O'Brien, A. K.; Bowman, C. N. *Macromolecules* **2003**, 36, 7964.



## CHAPTER 6

### EFFECTS OF POLYMERIZABLE ORGANOCCLAYS ON OXYGEN INHIBITION OF ACRYLATE AND THIOL-ACRYLATE PHOTOPOLYMERIZATION

Oxygen inhibition is of great concern in radical photopolymerization. This research investigates the effects of polymerizable organoclays on oxygen inhibition of acrylate and thiol-acrylate systems. Without use of thiol monomers, oxygen inhibition is difficult to overcome, although adding acrylated polymerizable organoclays slightly enhances polymerization in air. By incorporating thiols, on the other hand, polymerization rates and conversion continue to increase until thiol concentration reaches 30mol% reaching rates and conversions approximately 80% of those observed in nitrogen. Further improvements have been observed by adding suitable polymerizable organoclays. Addition of only 5wt% thiolated organoclays into the thiol-acrylate systems including 20mol% thiol enhances the conversion in air to almost identical levels of that achieved under nitrogen. Interestingly, addition of either non-reactive or acrylated organoclays usually decreases the polymerization. In addition, higher thiol conversions are achieved by adding thiolated organoclays due to increased thiol-ene reaction induced by the functional groups on the clay surfaces.

## Introduction

Increased environmental concerns have led many research groups to explore polymer processing technologies that do not use thermal energy or solvent during the process. One alternative platform is photopolymerization which uses light for initiation. Photopolymerization has many advantages including that it typically is performed at ambient temperature and the majority of photocurable monomer systems lead to 100% solid content, thereby eliminating the need for solvent.[1-4] The field of photopolymerization has thus rapidly grown with numerous products developed for many applications including films, dental materials, optical lenses, and coatings.[4-8] Most of these photopolymerized materials are produced using acrylate or methacrylate monomers due to the high reactivity of the acrylic double bonds over other double bond chemistries. Highly cross-linked networks formed by polymerization of multifunctional acrylate monomers produce materials with outstanding performance including exceptional thermal and mechanical properties.[4,9]

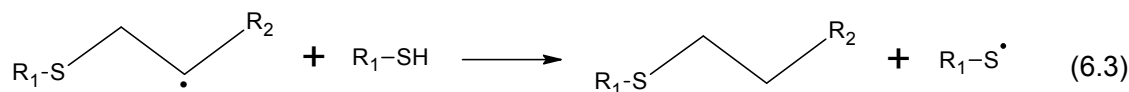
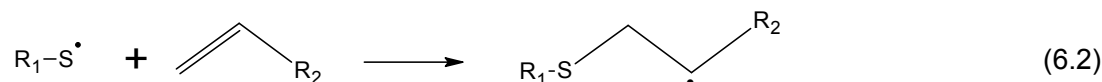
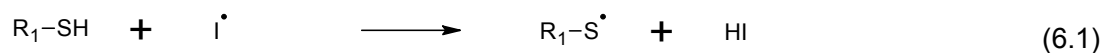
Despite the many advantages of acrylate-based photopolymerization, several disadvantages are still prevalent, which limit photopolymer applications.[10,11] In particular, severe oxygen inhibition in acrylate-based photopolymerization is of great concern. Oxygen molecules in air inhibit free radical (meth)acrylate-based photopolymerization by quenching the excited state of initiator upon irradiation and fast scavenging of the generated radicals in initiation stage very fast.[12] Peroxide radicals produced by reaction between oxygen and generated radicals are not effective radicals in initiating the polymerization due to low reactivity.[12-14] This inhibition lasts until all of oxygen molecules in the reacting system are consumed because the reaction rate of oxygen with radical species is usually several orders of magnitude faster than the propagation rate.[12,15] Particularly at the surface of the photopolymerized system, polymerization does not progress unless the rate of oxygen consumption is faster than the

diffusion rate of oxygen into the reacting media.[16-18] Photopolymerization is thus often performed under inert atmosphere such as nitrogen or with an impermeable film to prevent air from reaching the polymerization systems. The use of additives can be another alternative to suppress oxygen inhibition. Also due to the high cost and inconvenience of these processes, however, most of industrial photopolymer applications are polymerized at air atmosphere.[10-14] In many industrial applications, large amounts of photoinitiator with high light intensity are commonly used to induce fast consumption of oxygen molecules. While this method is an alternative strategy for using inert atmospheres, it often affects the ultimate performance of the photopolymer via residual initiator.[2,19,20]

Much research has been devoted to understanding and overcoming oxygen inhibition of acrylic photopolymerization systems. Studies have focused on fundamental kinetic study and modeling of the inhibition process.[21-23] dual initiation to consume oxygen molecules prior to reaction [24], and the addition of chemicals such as amines as a reducing agent or thiols as a chain transfer agent.[25-28] Among those methods, the addition of thiol monomers into the free radical photopolymerization systems has attracted significant interest because the inherent mechanism of thiol-ene systems significantly reduces oxygen inhibition. The properties of thiol-ene network systems can also be controlled based on the wide variety of commercially available monomers with ene functionality.[28,29]

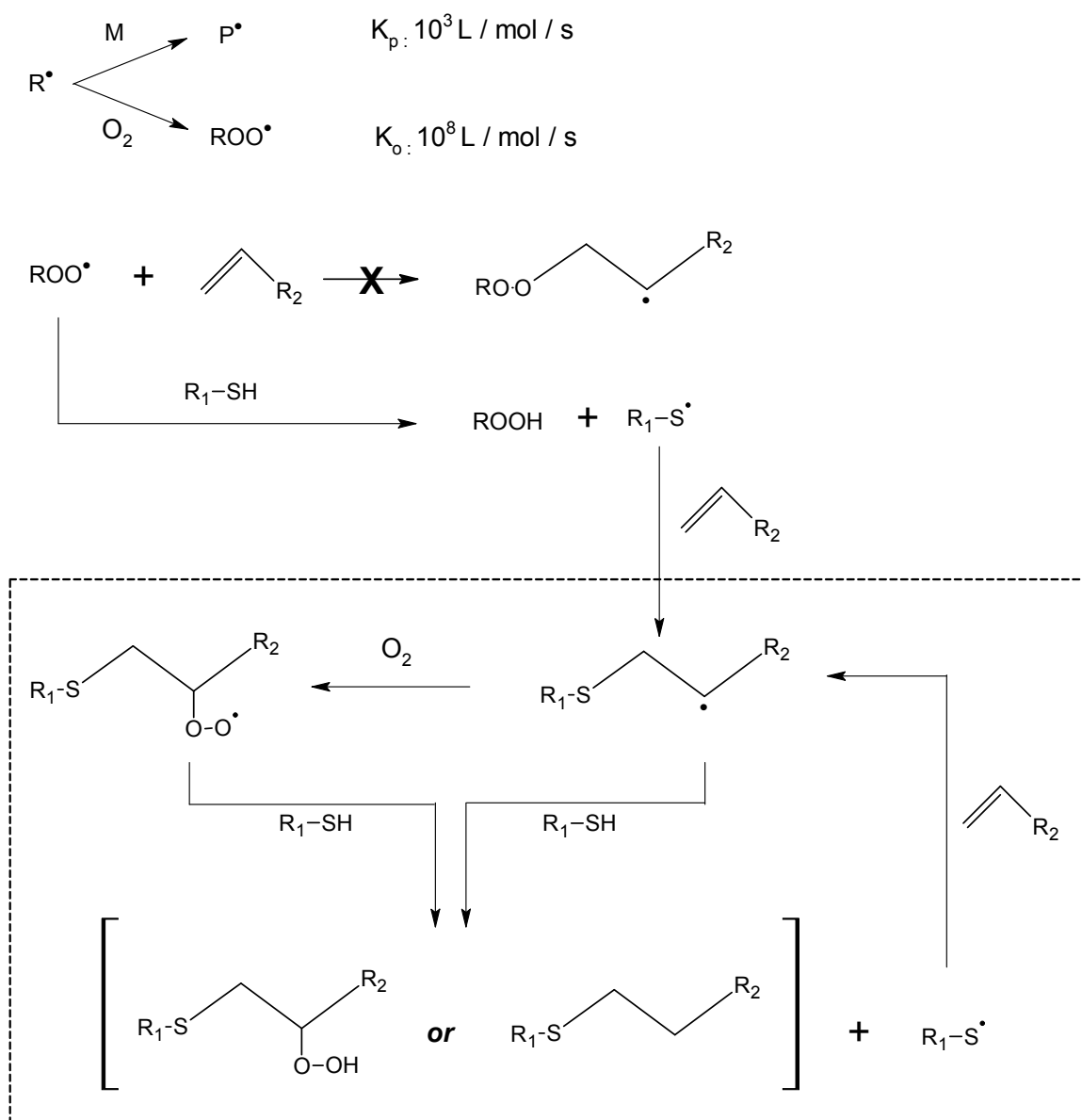
Recently, Hoyle and Bowman have extensively studied this copolymerization between double bonds and thiol groups to develop unique photopolymer systems overcoming many drawbacks of free-radical photopolymerization including oxygen inhibition.[29-33] The addition of thiol monomers into ene systems, including various vinyl and (meth)acrylate systems, significantly changes the reaction mechanism from a free-radical chain growth to a step-growth reaction. In a standard thiol-ene copolymerization, thiol monomers act as a chain transfer agent and polymerization

progresses via alternating reaction between the propagation of a thiyl radical with a double bond and the chain transfer reaction of a radical to a thiol to regenerate the thiyl radical as illustrated in scheme 6.1 by Equations 6.1 to 6.3.[22]



**Scheme 6.1.** Radical chain transfer mechanisms in thiol-ene reaction. Reactions represent (6.1) initiation of primary thiyl radicals, (6.2) formation of secondary radicals, and (6.3) secondary radical chain transfer to thiol groups.

These step-growth mechanisms based on this radical chain transfer to thiol monomers can reduce oxygen inhibition of the polymerization occurring in air. Scheme 6.2 outlines thiol-ene reactions when oxygen molecules are present.[19,22] Because the radical scavenging rate by oxygen is much higher than the propagation rate, most of the initiated radicals react with oxygen. While the resulting low reactivity peroxide radicals do not react with double bonds, the radicals may transfer to thiols thereby acting as chain transfer agents to generate thiyl radicals by hydrogen abstraction. These regenerated thiyl radicals then can either initiate the propagation reaction or consume oxygen molecules in the system rapidly via repeated reaction, resulting in successful propagation with rapid consumption of oxygen molecules in the system.[22,27]



**Scheme 6.2.** Schematic expression of the reaction mechanism of thiol-ene systems in the presence of oxygen.

While thiol-ene photopolymerizations show promise in overcoming oxygen inhibition, concerns still exist for expanded application. Particularly in thiol-ene systems using acrylate monomer, the ultimate conversion of thiol groups is usually much lower

than that of the acrylate double bonds because the step-growth reaction between thiols and double bonds competes with the faster acrylate homopolymerization.[32,33] In addition, the reaction between thiols and acrylic double bonds forms flexible thio-ether linkages in the polymer networks. This different network structure with low thiol conversion usually decreases the mechanical strength of the system, resulting in difficulty in obtaining a hard and tough material based on thiol-acrylate photopolymerization.[6,31] This shortcoming of thiol-acrylate systems may be significantly improved by incorporating well dispersed inorganic fillers, preferably with nanoscale dimension to form a polymer nanocomposite.

In recent years, our research group has developed unique polymerizable organoclays that can react with monomers during the polymerization. Upon incorporation of these reactive nanoparticles, the differences in the photopolymerization behavior of acrylate and thiol-acrylate systems have also been investigated. Previous research has demonstrated that the incorporation of appropriate polymerizable organoclays not only enhances clay exfoliation but also increases reaction rate in various (meth)acrylate and thiol-acrylate systems.[34,35] On the other hand, non-reactive organoclays usually decrease reaction rate by scattering and absorbing the light energy. In addition, particularly in thiol-acrylate systems, the type of reactive group in the polymerizable organoclay significantly affects the degree of thiol-ene reaction. It was observed that thiol functionalized organoclays enhance thiol-ene copolymerization while acrylate functionalized organoclays increase acrylate homopolymerization.[36-38] Based on the significantly different effects on thiol-ene reaction, it is reasonable to believe that the incorporation of polymerizable organoclays may influence the extent of oxygen inhibition during the photopolymerization process as well. In addition, the incorporation of clay particles in photopolymer systems may decrease the diffusion rate of oxygen molecules particularly near the surface where monomer mixtures are in contact to air, resulting in further decrease of oxygen inhibition.[39]

In this report, we discuss the effect of polymerizable organoclays on oxygen inhibition of acrylate and thiol-acrylate systems for which oxygen inhibits the polymerization to various extents. Various acrylate monomer systems were examined with different level of inherent oxygen inhibition. For thiol-acrylate systems, controlled amount of a trithiol was added to the acrylate mixtures. The photopolymerization behaviors of acrylate and thiol-acrylate systems were investigated utilizing photo-DSC and real-time FTIR in the presence and absence of oxygen. The synergetic effects of incorporating polymerizable organoclays on oxygen inhibition were examined at various thiol concentrations by comparing the results with neat systems. The polymerization rates in nitrogen atmosphere were used as the comparison criteria for the degree of oxygen inhibition of the systems polymerized under oxygen atmosphere. The difference in clay effects on oxygen inhibition based on the type of functional group on the clay surface is also discussed. With previous studies on photopolymerizable organoclay systems that show presenting many advantages regarding reaction behavior and composite properties, the results from this study may show promise for applications that must be processed in air.

## Experimental

### Materials

1,6-hexanediol diacrylate (HDDA), tripropyleneglycol diacrylate (TrPGDA), polyethyleneglycol (600) diacrylate (PEGDA, MW 742) and polyester based urethane acrylate oligomer (CN9009) were supplied by Sartomer. (Exton, PA). Trifunctional trimethylolpropane trimercaptopropionate (TMPTMP) was obtained from Aldrich. Cloisite Na (Southern Clay Products – Gonzalez, TX) was used for natural montmorillonite clay. Cloisite 93A (CL93A, Southern Clay Products), montmorillonite

clay modified with dihydrogenated tallow, was used as a typical nonreactive type organoclay. To produce polymerizable organoclays, sodium cations between silicate platelets of Cloisite Na were ion exchanged using acrylate or thiol functionalized quaternary ammonium surfactants as described elsewhere.[35] C16A acrylated organoclay bearing acrylate functional groups on the clay surfaces was produced utilizing hexadecyl-2-acryloyloxy(ethyl) dimethylammonium bromide (C16A surfactant) synthesized following the methodologies described previously.[34,35] PSH2 thiol functionalized organoclays were synthesized via Michael addition reaction between thiol groups of tri functional TMPTMP and acrylate groups of C16A acrylated organoclay based on the procedures reported elsewhere.[36] The chemical structures of monomers and surfactants used in this research are illustrated in Figure 6.1. Except where noted, 0.2 wt% 2,2-dimethoxyphenyl acetophenone (DMPA, Ciba Specialty Chemicals) was used as a free radical photoinitiator in all experiments. All chemicals including monomers and clays were used as received.

## Methods

Photopolymerization behavior in the presence of oxygen (air atmosphere) and absence of oxygen (nitrogen atmosphere) were monitored using a Perkin Elmer Diamond differential scanning calorimeter (DSC-7) modified with a medium pressure mercury arc lamp (photo-DSC). Rates of photopolymerization were measured at the irradiation intensity of  $3.0\text{mW}/\text{cm}^2$  using full spectra light. Before irradiation, liquid monomer samples were placed into DSC pans and kept for 6 minutes in the aerated DSC chamber for polymerization in the presence of oxygen or purged with dried nitrogen gas for 6 minutes to eliminate dissolved oxygen for polymerization under inert condition. Photopolymerization profiles were basically compared using the evolved polymerization



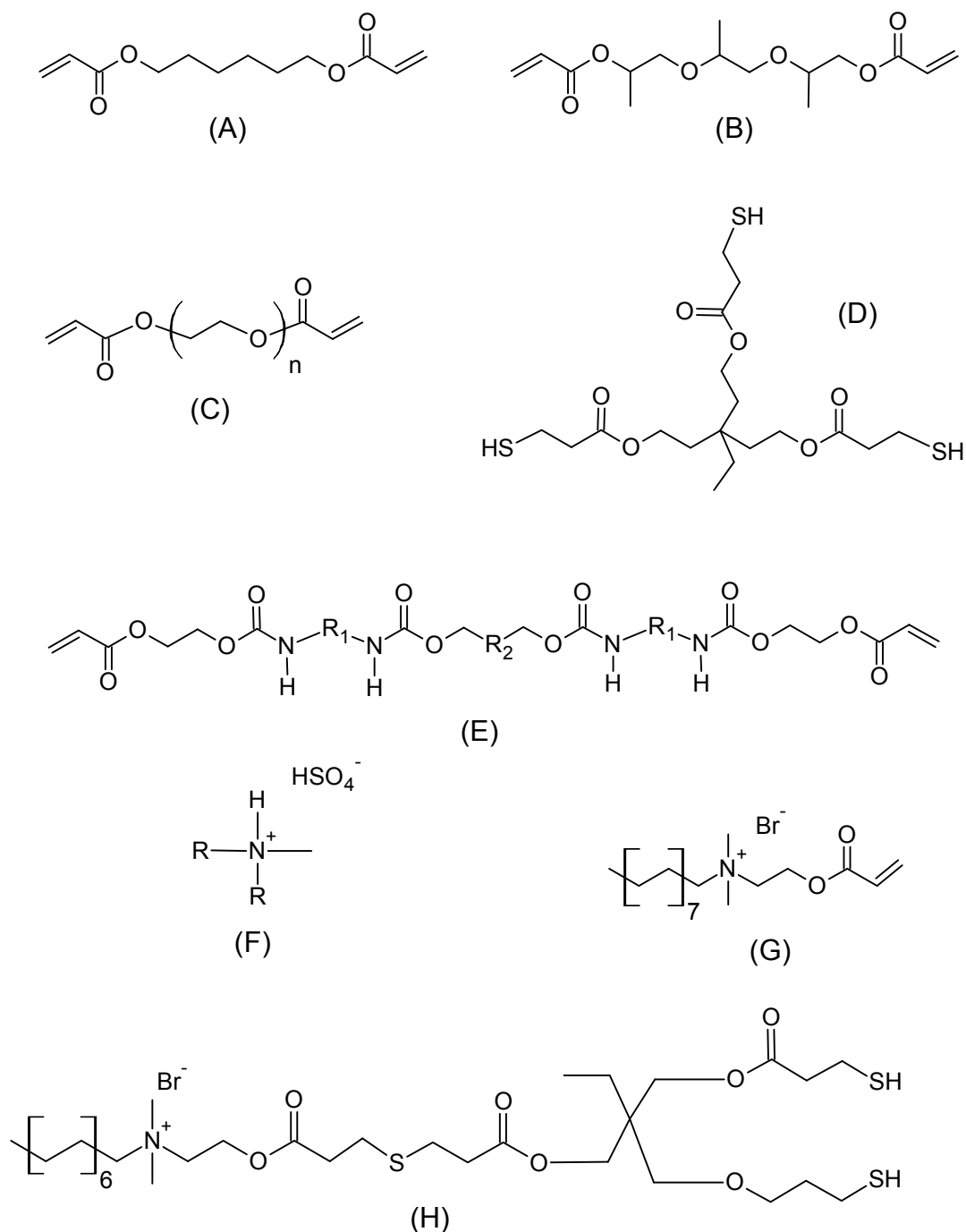


**Figure 6.1.** Chemical structures of (A) 1,6-hexanediol diacrylate (HDDA), (B) tripropylene glycol diacrylate (TrPGDA), (C) polyethyleneglycol diacrylate (PEGDA, MW=742), (D) trimethylolpropane tris(3-mercaptopropionate) (TMPTMP), (E) polyurethane diacrylate oligomer (CN9009), (F) methyl dihydrogenated tallow sulfonate, (CL93A) (G) hexadecyl-2-acryloyloxy(ethyl) dimethylammonium bromide (C16A) (H) tetradecyl 2-(bis(3-mercaptopropionate) mercaptopropionyl trimethylolpropyl) acetocyc(ethyl) dimethylammonium bromide (PSH2; Dithiol).

heat per unit mass during the polymerization as recorded by photo-DSC. Photopolymerization rates and ultimate conversion analysis were performed based on methodology described elsewhere using the polymerization enthalpies of 86,190 Joule/mol and 79,496 Joule/mol for acrylate homopolymerization and thiol-ene copolymerization, respectively.[40,41]

As a complementary method for studying polymerization kinetics for thiol-ene photopolymerization systems, real time infrared spectroscopy (RTIR, Thermo Nicolet Nexus 670) was utilized to obtain acrylate and thiol conversion profiles during the polymerization. Monomer samples were allowed to become saturated with oxygen, if appropriate, and were thereafter placed between two sodium chloride plates separated by 15 $\mu$ m glass bead spacers. Analysis was performed at ambient temperature under air atmosphere. Because the systems in RTIR experiments are essentially closed due to the sandwich arrangement of the salt plates, essentially no oxygen diffusion occurs during the polymerization, which is different from PDSC experiments. The UV initiating source was a medium pressure mercury lamp (EXPO Acticure) equipped with an optical fiber. During the polymerization, RTIR absorption spectra were continuously collected at 6 scans per second. Acrylate conversion was evaluated using the absorption band at 810  $\text{cm}^{-1}$  while thiol conversion was monitored at 2575  $\text{cm}^{-1}$ . [33] Conversion profiles as a function of time were obtained by monitoring the decrease in the height of the absorbance peak during polymerization. All polymerization reactions were performed with 365 nm light at the irradiation intensity of 2.9 ~ 3.2mW/cm<sup>2</sup> as measured at the sample surface.

### Results and Discussion

This report investigates the effects of various nonreactive and polymerizable organoclays on oxygen inhibition in acrylate and thiol-acrylate systems. According to

organic-inorganic composite theory, use of well dispersed inorganic fillers may improve many properties of polymer systems.[42-44] As the addition of thiol monomers into acrylic systems leads to significant decreases in thermo-mechanical properties, incorporation of organoclays might also compensate for property decreases induced by thiols. If polymerizable organoclays can allow less oxygen inhibition by enhancing the thiol-ene reaction and/or by repressing the diffusion of oxygen molecules, they could be effective materials for designing thiol-acrylate systems to overcome oxygen inhibition inherent in traditional acrylic photopolymerization systems.

In free radical polymerization, oxygen molecules strongly inhibit the polymerization by quenching radicals in the initiating and propagating processes. This inhibition lasts until most of the dissolved oxygen molecules are consumed because the oxygen quenching rates of the initiating or propagating radical species by oxygen, ranging from  $10^8$  to  $10^9$  mol/L/s, are of orders of magnitude faster than the typical rate of propagation in acrylate polymerization.[19,45] Due to dissolved oxygen or oxygen diffusion into the reaction media, effective propagation in air is only possible when the rate of oxygen consumption is faster than the oxygen diffusion rate. For this reason, overall inhibition time as well as the polymerization rate for open systems varies based on the rates of both oxygen consumption and diffusion. The overall oxygen inhibition of the system is thus influenced by a number of factors including viscosity, functionality, and the structure of a monomer system. For instance, high viscosity reduces the rate of oxygen diffusion [17,46], and high functionality monomers can increase the oxygen consumption rate and induce high viscosity at early stage of polymerization as well.[47] In addition, several chemical groups in monomer structure such as ethers [46], thio-ethers [48], and amides [49] containing highly abstractable hydrogens can also lead to rapid oxygen consumption by a hydrogen abstraction chain transfer reaction. Because the potential impact of organoclays on oxygen inhibition might be different based on the inherent extent of oxygen inhibition of the monomer system, monomer compositions

were chosen to exhibit a wide range of oxygen inhibition for better understanding the organoclay effect.

To this end, three monomer compositions were utilized in this study in considering both the chemical structure and viscosity of monomers. 1,6-hexanediol diacrylate (HDDA) was used as a monomer with low initial viscosity. Two mixed acrylate oligomer-monomer systems were formulated to reduce and vary the extent of inherent oxygen inhibition by increasing the monomer viscosity as well as by incorporating chemical groups such as ethers and/or urethane linkages containing abstractable hydrogens. Polyethyleneglycol diacrylate (PEGDA, Mw 742) / tripropyleneglycol diacrylate (TrPGDA) at a 1:1 weight ratio was used as an intermediate viscosity system with ether linkages in the monomer structures. To provide even higher viscosity and urethane chemical linkages in the monomer mixture, a polyester based urethane acrylate (CN9009) was added to PEGDA/TrPGDA system.

Figure 6.2 shows the photo-DSC polymerization profiles of these three systems polymerizes in air, namely neat HDDA, a mixture of PEGDA/TrPGDA, and a CN9009/PEGDA/TrPGDA mixture. The profile for PEGDA/TrPGDA under nitrogen is included for comparison. As expected, the extent of oxygen inhibition decreases with increases in viscosity. The lower viscosity HDDA with no abstractable hydrogens is completely inhibited by oxygen, and no apparent reaction is observed. Compared to HDDA system, it is expected that polymerization of TrPGDA may be less sensitive to oxygen because TrPGDA has ether linkage in the structure that facilitate hydrogen abstraction. However, polymerization in air (not shown) and previous reports [31] reveal that polymerization of neat TrPGDA is also completely inhibited by oxygen. This behavior indicates that branching at  $\alpha$  carbon position significantly decreases radical chain transfer by hydrogen abstraction and/or the low viscosity of TrPGDA still allows a high rate of oxygen diffusion. For this reason, an ether type oligomer (PEGDA) with a

linear structure is used to incorporate more abstractable hydrogens. TrPGDA is incorporated to allow control of viscosity.

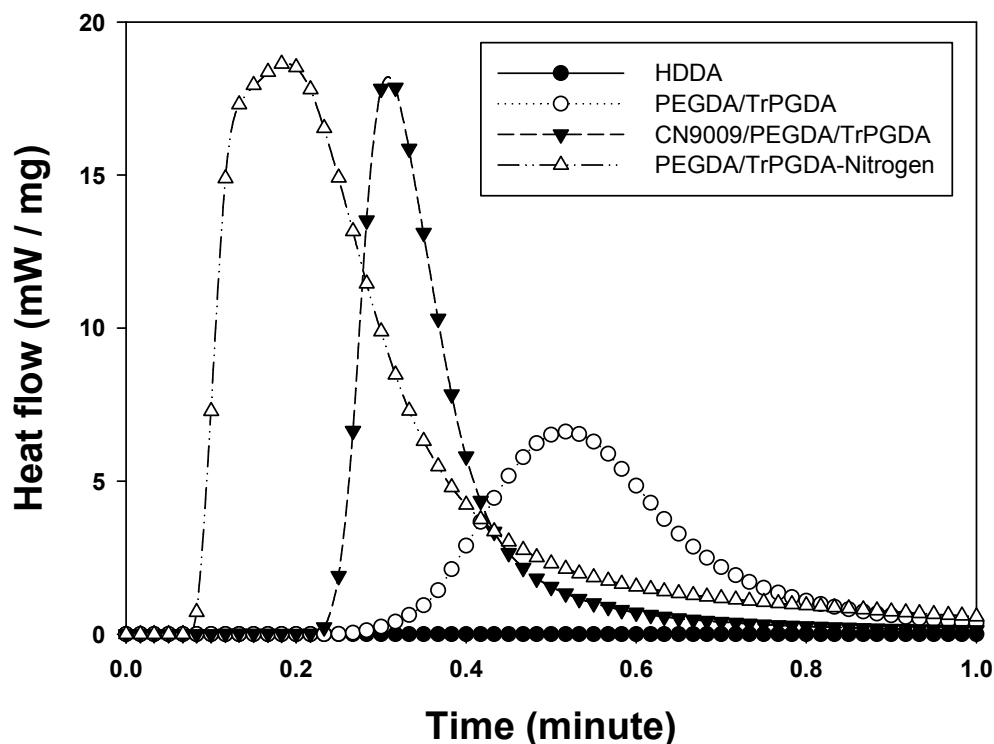


**Figure 6.2.** Photo-DSC polymerization profiles of HDDA (●), PEGDA/TrPGDA (50wt%/50wt%) (○), and CN9009/PEGDA/TrPGDA (30wt%/30wt%/40wt%) (▼) systems based on weight ratio. Samples were polymerized with approximately  $3.0\text{mW}/\text{cm}^2$  full spectra UV light using 0.2wt% DMPA in air, respectively. The profile for PEGDA/TrPGDA in nitrogen (Δ) is included for comparison.

As shown in Figure 6.2, polymerization progresses in oxygen to some degree when PEGDA is incorporated. Further reduction in the degree of oxygen inhibition is observed with a CN9009 urethane acrylate oligomer containing formulation, probably due to synergetic effects of increasing both system viscosity and the enhanced peroxide

radical chain transfer during the polymerization process. On the other hand, comparing two polymerization profiles of PEGDA/TrPGDA system under air and nitrogen atmosphere, the height of maximum heat flow as well as overall area of the profile in air are much smaller than those obtained under nitrogen atmosphere. While the maximum rate and final double bond conversion, determined based on the profiles in Figure 6.2 utilizing the methodology described elsewhere [40], of PEGDA/TrPGDA systems are approximately 0.046/sec and 0.75 under nitrogen respectively, the values decrease to 0.016/sec and 0.29 in air. Comparing the results between the two polymerization conditions, the maximum rate and final conversion of the polymerization in air indicate that over 60% of the produced radicals are inactivated by oxygen molecules. Due to this severe inhibition of most acrylate homopolymerization systems under air atmosphere, this report thus focuses on the use of thiol monomers to overcome the oxygen inhibition with polymerizable organoclays as a potentially synergetic additives that may further reduce oxygen inhibition, and may also potentially change aspects of the thiol-ene copolymerization.[36,37]

As previously discussed, thiol-ene photopolymerization is much less inhibited by oxygen than acrylate homopolymerization. This behavior is mainly due to the inherent step growth reaction mechanism of thiol-ene polymerization based on chain transfer of radicals to other thiol monomers by hydrogen abstraction. This radical chain transfer event to the thiol also occurs when the radicals are low reactivity peroxide radicals formed when initiating radicals react with oxygen molecules dissolved in the system. The peroxide radicals do not allow propagation in addition polymerization as illustrated in scheme 6.2 previously. The transfer of radical from peroxide to thiol thus results in significant reduction in oxygen inhibition. Figure 6.3 shows how the addition of thiol monomers into acrylate systems reduces the oxygen inhibition. Highly inhibited HDDA and less inhibited PEGDA/TrPGDA systems with different amounts of the tri-thiol TMPTMP were polymerized in air and monitored using photo-DSC. Polymerization heat

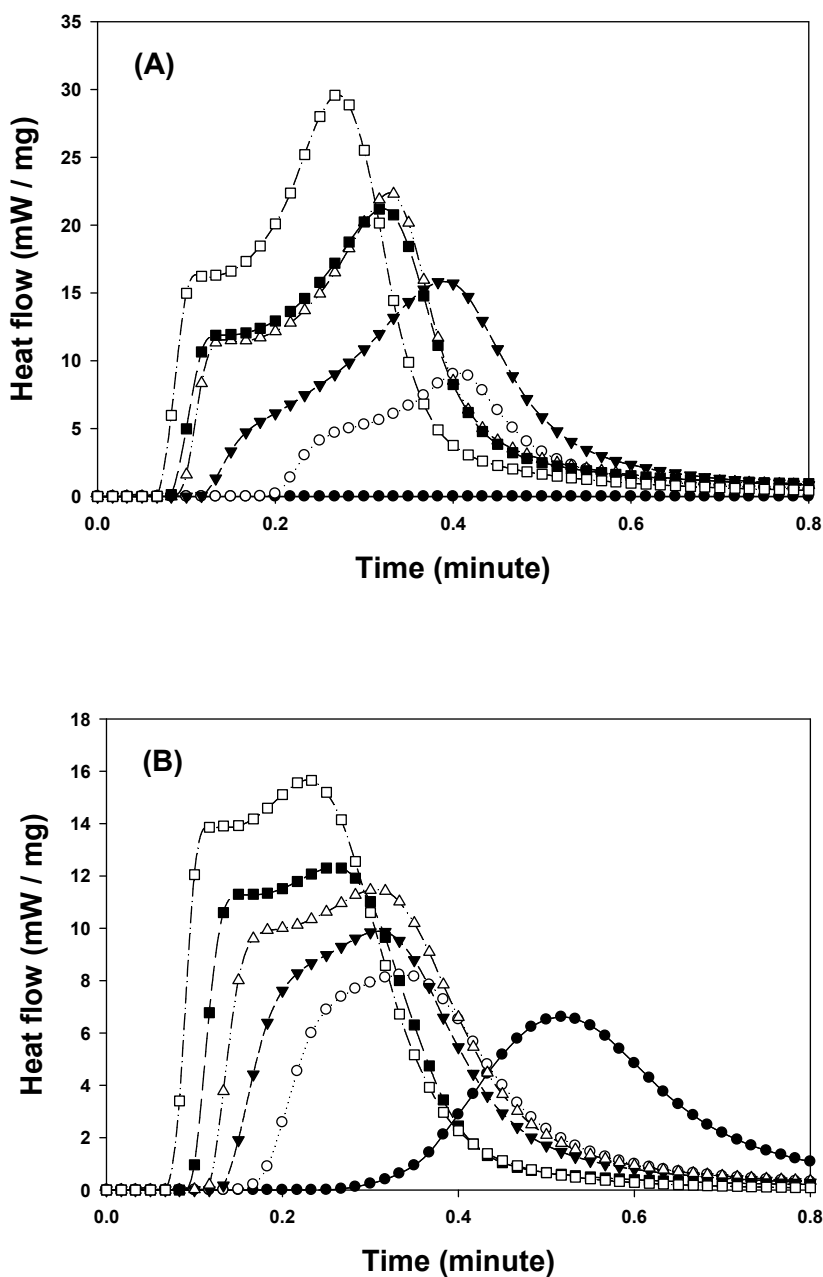


**Figure 6.3.** Photo-DSC polymerization profiles of two acrylate systems with increased concentration of TMPTMP thiol monomer. Photopolymerization was initiated with approximately  $3.0\text{mW/cm}^2$  full spectra UV light and each monomer system contained 0.2wt% DMPA. Shown are profiles in air for (A) neat HDDA (●), and HDDA with 5 mol% (○), 10 mol% (▼), 20 mol% (△), and 30 mol% (■) thiol groups and (B) neat PEGDA/TrPGDA (50wt%/50wt%) (●), and PEGDA/TrPGDA (50wt%/50wt%) with 5 mol% (○), 10 mol% (▼), 20 mol% (△), and 30 mol% (■) thiol based on functional group ratio. For comparison, heat release profile of the system with 30 mol% thiol polymerized in nitrogen is included in each figure (□).

profiles as a function of polymerization time are plotted in Figure 6.3 (A) for HDDA and Figure 6.3 (B) for PEGDA/TrPGDA systems with and without thiol (TMPTMP). Thiol contents for the thiol-acrylate mixtures were controlled based on the ratio of thiol functional groups to total functional groups in the system. The polymerization profiles containing 30mol% of thiol in nitrogen atmosphere are also included in each corresponding figure for comparison.

Addition of only 5 mol% thiol induces significantly faster polymerization in air. The polymerization rate continues to increase with the amount of TMPTMP as shown in Figure 6.3 (A). The profiles for the systems containing 20 and 30mol% thiol are almost the same indicating that further increases in thiol above 20mol% do not reduce oxygen inhibition significantly. In addition, comparing the profiles of the system containing 30mol% thiol, the polymerization profile in air nearly approaches that observed under nitrogen atmosphere demonstrating that oxygen inhibition has been considerably reduced with this amount of thiol. The behavior in Figure 6.3 (B) for PEGDA/TrPGDA systems appears very similar to that of the HDDA system. By incorporating 30mol% thiol, the polymerization rate in air has been significantly increased from the neat acrylate system and approaches that under nitrogen atmosphere although the rate is still significantly lower. Accurate conversion calculation of thiol-ene systems is difficult utilizing the polymerization heat profiles obtained by photo-DSC because thiol-ene copolymerization occurs in competition with acrylate homopolymerization and the degree of thiol-ene copolymerization varies depending upon the functional group ratio between thiol and double bond. Assuming, however, that there is no large difference in the degree of thiol-ene copolymerization between air and nitrogen atmosphere with the same thiol content, the area of the photo-DSC profile is related to the overall conversion allowing direct comparison of apparent conversion. The area of the profile polymerized in air using the monomer mixture with 30mol% thiol utilizing the PEGDA/TrPGDA mixture is about 90% of the area obtained from the profile of the same monomer system polymerized



under nitrogen. The degree of acrylate homopolymerization in nitrogen atmosphere could be slightly higher than in air resulting in some of this difference. Additionally, the heat released during acrylate homopolymerization is also slightly higher than that of thiol-ene copolymerization.[41] A 10% difference in overall area of the profiles between air and nitrogen atmosphere is too large, however, to conclude that a similar conversion has been achieved under both polymerization conditions. Therefore, while the thiol dramatically reduces oxygen inhibition, it does not eliminate it completely.

As previously demonstrated, when organoclays are incorporated into a thiol-ene system with good compatibility between clays and monomers, enhanced clay exfoliation is achieved and higher photopolymerization rate is induced. In addition, the addition of thiolated organoclays generally increases thiol-ene reaction while non-reactive or acrylated organoclays do not significantly change polymerization behavior of many thiol-acrylate compositions.[37,38] Adding organoclays may thus influence the extent of oxygen inhibition of a system by inducing a significant difference in the degree of thiol-ene reaction.

To investigate how the incorporation of organoclays affects oxygen inhibition, various organoclays with different functional groups on the surface were added into acrylate or thiol-acrylate systems. Figure 6.4 shows the polymerization profiles of PEGDA/TrPGDA systems in air with 5wt% of three different non-reactive and polymerizable organoclays via photo-DSC. The profile of neat PEGDA/TrPGDA is included for comparison. When 5wt% of non-reactive Cloisite 93A organoclay is incorporated, polymerization starts after 32 seconds while neat PEGDA/TrPGDA system begins reacting after 15 seconds of illumination. The polymerization rate, as determined by the maximum heat flow rate, also decreases 12% from that of the neat system. The addition of clay may reduce overall light energy via light absorption and/or light scattering by inorganic filler particles and thus may decrease the rate of radical formation during the polymerization. The reduced light energy would result in a longer time to

consume dissolved oxygen molecules. The total area of the profile is almost the same as that from the neat system, indicating that only polymerization rate is reduced without change in ultimate conversion.

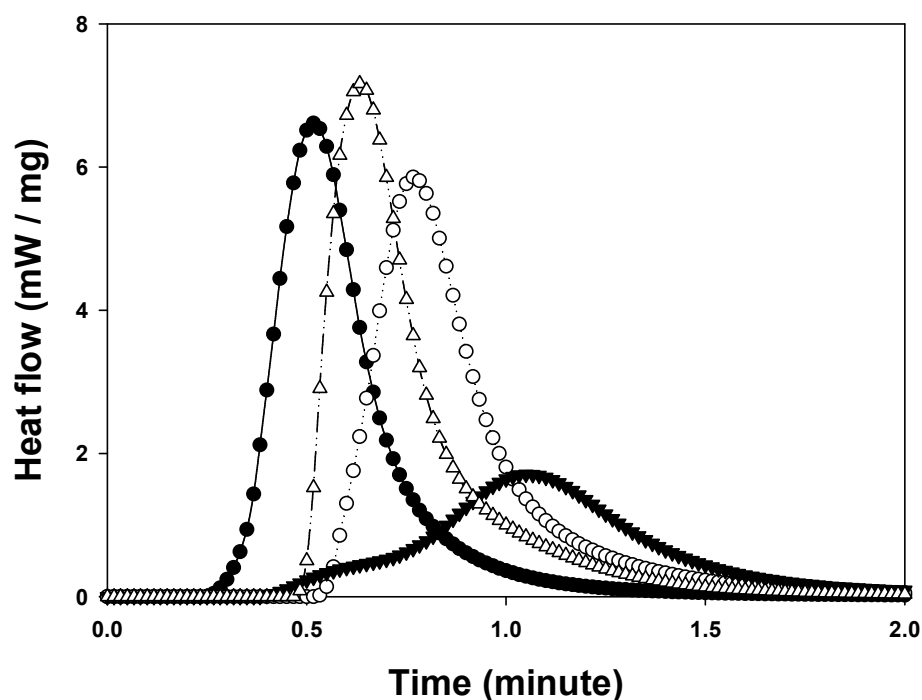


**Figure 6.4.** Photo-DSC polymerization profiles of PEGDA/TrPGDA (50wt%/50wt%) mixtures with incorporation of different types of organoclays. Shown are profiles of neat PEGDA/TrPGDA (●), and PEGDA/TrPGDA with 5wt% Cloisite 93A non-reactive organoclay (○), 5wt% of C16A acrylated polymerizable organoclay (△), 5wt% of PSH2 thiolated polymerizable organoclay (▼). Samples were polymerized with  $3.2\text{mW}/\text{cm}^2$  full spectra UV light using 0.2wt% DMPA in air.

On the other hand, addition of acrylated polymerizable organoclay increases both polymerization rate and ultimate conversion. Both maximum heat flow rate and total area of the profile for acrylated organoclay system increases more than 8% from those observed in the neat system even though the reaction induction time is 13 seconds longer.

This behavior implies that acrylated organoclays enhance polymerization rate once the initial oxygen concentration is sufficiently reduced to the point at which the rate of radical formation exceeds the diffusion rate of oxygen molecules from air. Supposing that the radical concentrations for neat and acrylated organoclay systems are approximately the same after the induction time, this behavior is in accordance with our previous results that the use of suitable polymerizable organoclays enhances photopolymerization rate as well as overall conversion of a system.[37] Interestingly, the addition of thiolated polymerizable organoclay significantly reduces the polymerization rate and overall conversion. The max heat flow rate and the area of profile decreases to 25% and 57% of the values obtained from the polymerization of neat system, respectively. These values are much lower than those from the system with non-reactive organoclays. According to the thiol-ene reaction mechanism, thiol groups on the organoclay surface can react with initiated radicals in the same manner thereby producing secondary radicals after reaction with one double bond in the system. These secondary radicals produced on the clay surfaces, however, have relatively low reactivity due to high steric hindrance of the thiolated surfactant structure. Especially when oxygen molecules are present, these hindered radicals will not readily react with other double bonds. Instead, mostly react with oxygen thereby generating peroxide radicals if there are no thiol monomers in the system. For this reason, without use of thiol monomers, thiolated organoclays scavenge initiated radical just similarly as oxygen molecules do. Therefore, adding acrylated organoclays in air is much more beneficial for reducing oxygen inhibition than non-reactive or thiolated organoclays for the polymerization of acrylate monomer systems.

Even though the use of acrylated organoclay is quite beneficial for acrylate polymerization systems in air, both polymerization rate and overall conversions of the PEGDA/TrPGDA systems in air are still below that achieved under inert conditions. Therefore, for further improvements in overcoming oxygen inhibition, other chemistries such as thiol comonomers may be incorporated. To investigate the potentially synergetic

effects of organoclay and thiol monomers on reducing oxygen inhibition, 5wt% of non-reactive or polymerizable organoclays bearing different functional groups were added into various thiol-acrylate systems. The photo-DSC polymerization profiles of systems with different amounts of TMPTMP trithiol and HDDA (di-acrylate monomer) are shown in Figure 6.5 (A) and Figure 6.5 (B) with 5wt% of C16A acrylated and PSH2 thiolated organoclays, respectively. Thiol concentration was increased from 0 mol% to 30 mol%. The polymerization profile under nitrogen atmosphere for the 30mol% thiol system with 5wt% PSH2 thiolated organoclay is also included.

As a whole, both reaction rate and polymerization degree of the clay-monomer systems in Figure 6.5 behave roughly in the same manner as was observed in Figure 6.3 (A) for neat systems of the same HDDA/TMPTMP mixtures. Increase of thiol functional groups induces significantly higher heat flow rates with larger areas under the reaction curve. The reduction in oxygen inhibition saturates at approximately 20~30mol% thiol. While the overall trends in Figure 6.5 (A) and (B) with different polymerizable organoclays are similar to each other, the systems with thiolated organoclays in Figure 6.5 (B) polymerize much faster with higher conversion in air than the systems in Figure 6.5 (A) with acrylated organoclays with the same thiol concentration. For instance, addition of 5mol% thiol in the thiolated organoclay system in Figure 6.5 (B) increases the polymerization rate considerably, whereas the same amount of thiol in the acrylated organoclay system in Figure 6.5 (A) induces a very small extent of reaction in air. In addition, upon comparing the two polymerization profiles of the systems containing 30mol% thiol in air and nitrogen in Figure 6.5 (B), the height of maximum heat flow and overall area of the profile in air are 69% and 96% of the values from the polymerization profile for the system containing the same 30mol% thiol under nitrogen atmosphere, respectively. In comparison, the maximum heat flow rate and area of the profile for the 30 mol% thiol system with acrylated organoclays in Figure 6.5 (A) are 47% and 54%, respectively using the same comparison criteria.

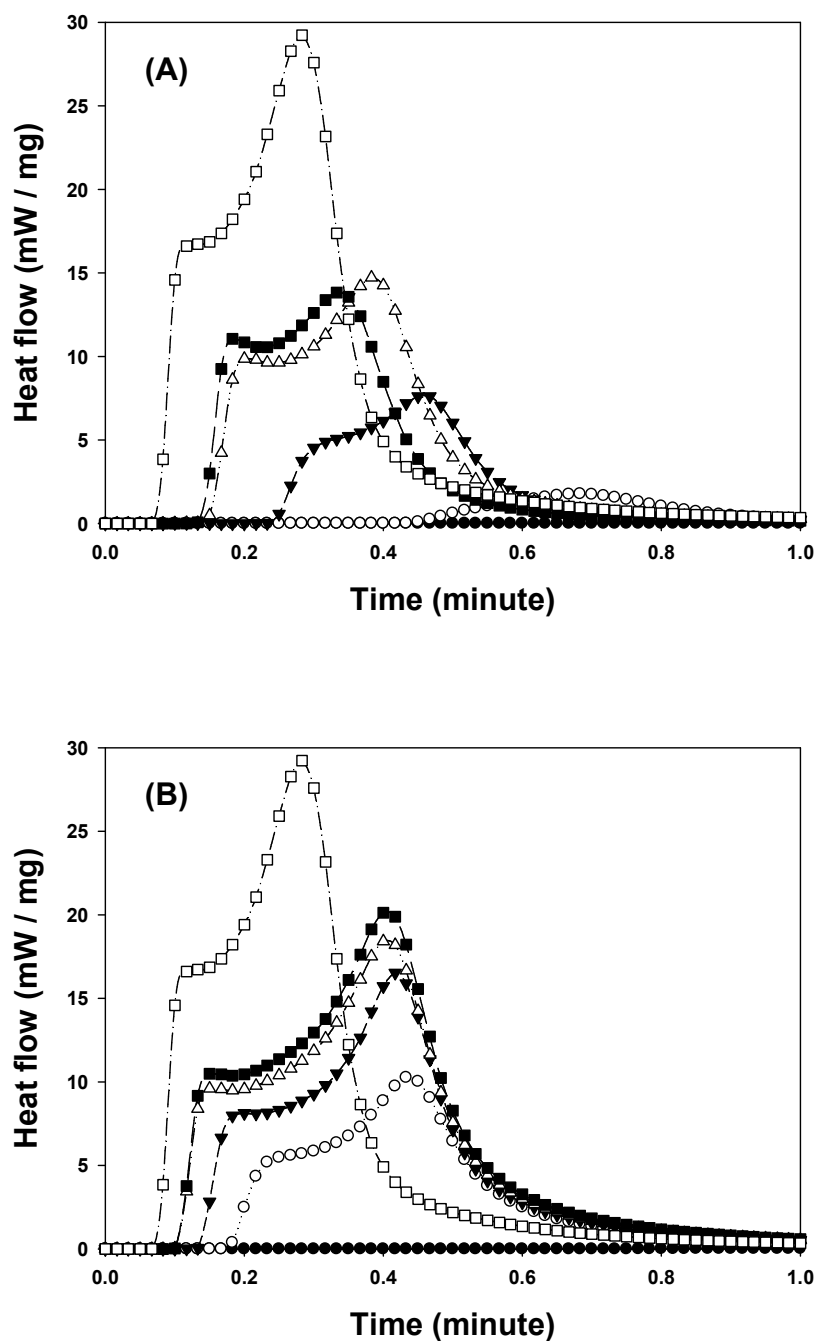


**Figure 6.5.** Photo-DSC polymerization profiles of HDDA systems with up to 30 mol% based on functional group TMPTMP trithiol with addition of (A) 5wt% C16A acrylated and (B) 5wt% PSH2 thiolated polymerizable organoclay. Samples were polymerized with  $3.0\text{mW}/\text{cm}^2$  full spectra UV light using 0.2wt% DMPA in air. Shown are profiles of neat HDDA ( $\bullet$ ), and HDDA with 5 mol% ( $\circ$ ), 10 mol% ( $\blacktriangledown$ ), 20 mol% ( $\Delta$ ), and 30 mol% ( $\blacksquare$ ) thiol. For comparison, the system with 30 mol% thiol including 5wt% PSH2 organoclay is also polymerized in nitrogen and included in each figure ( $\square$ ).

This result reveals that thiolated polymerizable organoclays mitigate oxygen inhibition to a much greater degree than acrylated organoclays when thiols and organoclays are used together. In addition, although the addition of thiolated organoclays in HDDA/TMPTMP systems does not bring the reaction rate in air to the same level of that in nitrogen, the conversion in air, indirectly determined by comparison of the areas of polymerization profiles in Figure 6.5 (B), is nearly same as that achieved under nitrogen atmosphere. This behavior indicates that the oxygen inhibition has been significantly reduced by the effect of thiolated organoclay.

As demonstrated in Figure 6.2, the use of ether type and more viscous urethane acrylate oligomers induces significant reduction in oxygen inhibition due to enhanced chain transfer by hydrogen abstraction mechanism and increased system viscosity. The synergetic effects of organoclay in reducing oxygen inhibition may be thus even more effective when the organoclays and thiols are incorporated into less inhibited acrylate systems including ether and/or urethane acrylate oligomers. To verify this hypothesis, 5wt% of different types of organoclay were added into a TrPGDA/PEGDA 50/50 wt% mixture containing 20mol% TMPTMP thiol. Figure 6.6 (A) shows the photo-DSC polymerization heat release profiles for the systems with and without 5wt% organoclay in air. A profile in nitrogen for the system with 5wt% thiolated organoclays is included again for discussion. As seen in the Figure 6.6 (A), the use of non-reactive Cloisite 93A organoclay significantly reduces the reaction rate in air while use of polymerizable organoclays either exhibits a similar reaction rate (C16A acrylated organoclay system) or even increases it (PSH2 thiolated organoclay system) compared to that observed in the neat TrPGDA/PEGDA/TMPTMP system. In addition, the polymerization profile of the formulation with 5wt% PSH2 thiolated organoclays in air is very close to the profile of the same system under nitrogen, indicating that polymerization progresses at almost the same rate.

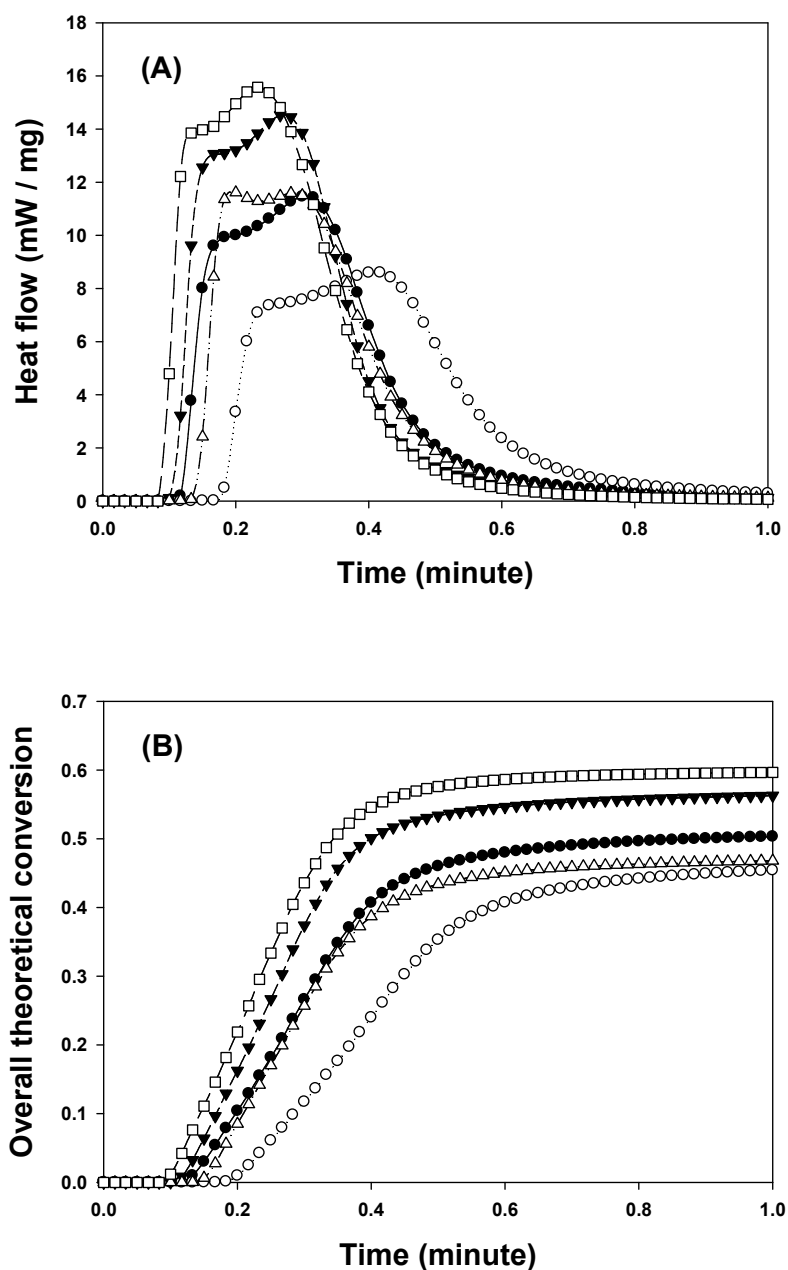


**Figure 6.6.** Photo-DSC polymerization profiles of PEGDA/TrPGDA (50wt%/50wt%) systems containing 20 mol% thiol from TMPTMP based on functional group ratio plotted by (A) heat flow rates and (B) overall theoretical conversions as a function of polymerization time. Samples were polymerized with  $3.2\text{mW}/\text{cm}^2$  UV light using 0.2wt% DMPA in air. Shown are profiles of neat PEGDA/TrPGDA (●), and PEGDA/TrPGDA with 5 wt% Cloisite 93A organoclay (○), 5wt% PSH2 thiolated organoclay (▼), and 5wt% C16A acrylated organoclay (Δ). For comparison, the system containing 20mol% thiol with 5wt% PSH2 organoclay is also polymerized in nitrogen and included in each figure (□).

To allow more direct comparison of these systems regarding conversion and polymerization rate, conversion analysis has been performed utilizing the heat flow rates of the systems in Figure 6.6 (A) using the methodology that is commonly used for analysis of (meth)acrylate systems. To calculate the conversion of thiol-ene copolymerization systems, the values of 86,190 Joule/mol and 79,496 Joule/mol were used for the polymerization enthalpies of acrylate homopolymerization and thiol-ene copolymerization, respectively.[40,41] The average polymerization enthalpy of the system containing 20mol% thiol is then determined to be 403.9 Joule/mg based on the assumption that all thiol and acrylate groups react. Assuming complete thiol conversion, 25% of the acrylate double bonds will copolymerize with the thiol while the remaining 75% of acrylate double bonds homopolymerize. Using this average polymerization enthalpy and exothermic heat profiles in Figure 6.6 (A), overall theoretical conversions for functional groups including acrylate and thiol groups in the systems are calculated and plotted in Figure 6.6 (B). Again, this comparison is not meant to provide absolute data but instead provide values for discussion because the exact degree of thiol-ene reaction will vary slightly based on the reaction condition as mentioned previously. The final conversion of the polymerized system with thiolated organoclays under nitrogen atmosphere is about 0.60 while the conversion of the neat system in air is approximately 0.50. The conversion profile of the neat system containing 20mol% thiol under nitrogen, (not included), overlaps significantly with the profile of the system with thiolated organoclays. Therefore, the conversion in air decreases by about 17% compared to that in nitrogen. Whereas the addition of either non-reactive Cloisite 93A or C16A acrylated organoclays decreases the conversion in air slightly, thiolated organoclays enhances the conversion in air to 0.57 which is more than 95% of the conversion achieved under nitrogen. The results in Figure 6.6 (A) and (B) thus reveal that the synergetic effect of thiol and organoclay on oxygen inhibition of TrPGDA/PEGDA system is more significant than for the HDDA system. Additionally, most of the oxygen inhibition can be



eliminated when suitable amounts of thiol and thiolated organoclay are incorporated together.

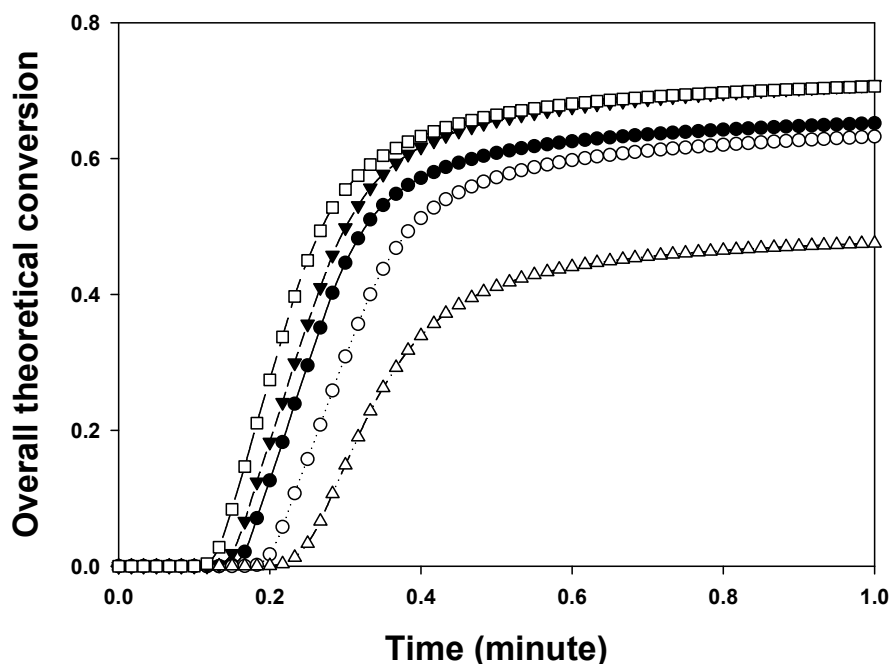


**Figure 6.7.** Photo-DSC polymerization profiles of CN9009/PEGDA/TrPGDA (30wt%/30wt%/40wt%) systems containing 20 mol% TMPTMP monomer based on functional group ratio, plotted by overall theoretical conversions as a function of polymerization time. Samples were polymerized at  $2.9\text{mW}/\text{cm}^2$  UV light using 0.2wt% DMPA in air. Shown are profiles of neat CN9009/PEGDA/TrPGDA (●), and CN9009/PEGDA/TrPGDA with 5 wt% Cloisite 93A organoclay (○), 5wt% PSH2 thiolated organoclay (▼), and 5wt% C16A acrylated organoclay (Δ). For comparison, the polymerization profile in nitrogen for the neat system containing 20mol% thiol is included (□).

Further improvement in reducing oxygen inhibition was observed in the more viscous CN9009/PEGDA/TrPGDA (30wt%/30wt%/40wt%) system containing 20mol% thiol based on the functional group ratio. Conversion analysis has been conducted in the same manner as described previously utilizing the photo-DSC polymerization heat

profiles of CN9009/PEGDA/TrPGDA mixtures with thiols. Considering the composition of acrylate and thiol functional groups, 321.6 Joule/mg was used as the polymerization enthalpy in calculating conversion for this monomer system with the results plotted in Figure 6.7. Both neat and organoclay containing systems polymerized in air are compared with the result obtained under nitrogen atmosphere for the acrylate/thiol mixture. By using highly viscous CN9009 acrylate oligomer with urethane groups in the structure, the gap in final conversion between the polymerization in air and nitrogen atmosphere is much less than the difference in the PEGDA/TrPGDA system.

The final conversions of the neat system in air and nitrogen are 0.68 and 0.72, respectively. The addition of non-reactive Cloisite 93A organoclay decreases reaction rate and final conversion, but to a much lower degree than in other acrylate systems. Different from the behavior in PEGDA/TrPGDA system, the addition of C16A acrylated organoclays significantly reduces polymerization rate and final conversion which only reaches 0.495 in air, only 70% of the conversion reached in the neat system. It is believed that the compatibility of acrylated organoclay with this monomer mixture is somewhat less than PEGDA/TrPGDA system. Thus, less exfoliated clay particles reduce light energy to a great extent, resulting in severe oxygen inhibition due to the low rate of radical formation. On the other hand, the profile of the system with PSH2 thiolated organoclay in air is almost identical to that of the neat system polymerized under nitrogen atmosphere. In addition, overall conversion reaches about 0.75, which is even higher than the value obtained under nitrogen, thereby indicating that the incorporation of thiolated organoclay in this thiol-ene copolymerization system not only completely eliminates the oxygen inhibition but also induces a higher conversion.

These results based on various base acrylate systems suggest that the use of thiolated organoclays induces higher synergetic effects on reducing or even eliminating oxygen inhibition when thiol monomers are included. To understand the effect of the type of functional group in the organoclay structure, HDDA systems that do not contain any

thiol groups in the formulations were polymerized without or with 5wt% C16A acrylated or PSH2 thiolated organoclays using photo-DSC in air. As discussed previously, no significant polymerization occurs when thiol monomers are not incorporated into the HDDA system with or without polymerizable organoclays.

Examining the profiles of the systems with no thiols carefully, however, distinctive differences can be seen. Figure 6.8 shows magnified PDSC polymerization profiles of HDDA systems with or without clay in air. No evolution of heat is observed in the neat HDDA system, indicating a complete inhibition of propagation. Low levels of heat generations can be seen when polymerizable organoclays are incorporated into the system. In addition, the pattern of heat evolution is different by organoclay type. While C16A acrylated organoclay generates low heat level after a short induction time, PSH2 thiolated organoclay induces a more distinctive heat flow profile which lasts for only a few seconds after a much longer induction time than that observed from the acrylated organoclay system. These phenomena suggest that oxygen diffusion into the organoclay galleries is relatively difficult. Thus, some propagation reaction may occur exclusively in the clay galleries as in a semi-closed system once initially dissolved oxygen molecules in the clay galleries are consumed. Because a small amount of acrylic radicals could successfully form on the surface of C16A acrylated organoclays, continuous but slow polymerization may be possible as shown in Figure 6.8. When PSH2 thiolated organoclays are used, on the other hand, a longer induction time is required for radicals to transfer to the thiol groups on the clay surface. Once thiyl radicals are formed, reaction between the thiyl radical and an acrylic double bond is possible and thereby generate a secondary radical as shown in Equation 6.2 in Scheme 6.1. The resultant secondary radicals, however, may not react further if there is no thiol group in the system due to its relatively low reactivity to acrylate double bonds as discussed previously. This sequence would allow just a short period of heat evolution in thiolated organoclay system. With enough thiol groups in the system, the higher peak intensity of thiolated organoclay in

Figure 6.8 may allow faster and greater conversion than that of the acrylated organoclay system. This explanation would account for the improved resistance to oxygen inhibition of thiolated organoclays when are combined with other thiols, compared to the effect of acrylated organoclay/thiol systems.

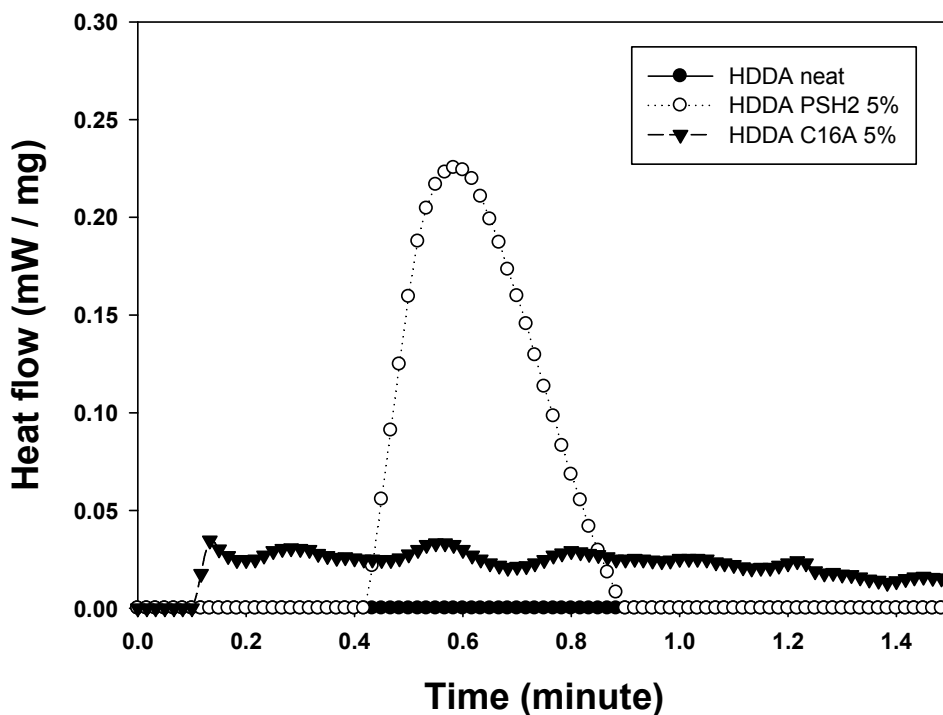


**Figure 6.8.** Photo-DSC polymerization profiles of the neat HDDA system (●), HDDA system with 5wt% C16A acrylated organoclay (▼), and with 5wt% of PSH2 thiolated organoclay (○). Samples were polymerized with 3.0mW/cm<sup>2</sup> UV light using 0.2wt% DMPA in air.

Due to the analytical limitation in photo-DSC methodology based on the heat evolution during a polymerization process, separate conversion results for acrylate and thiol functional groups of thiol-ene systems could not be compared. As mentioned, thiol-ene copolymerization progresses in competition with acrylate homopolymerization, and

thus the final conversion for each functional group can be varied not only by reaction atmosphere but also by the composition including thiol ratio, clay type, and concentration. Our previous research demonstrates that incorporation of thiolated organoclays significantly enhances thiol-ene copolymerization in nitrogen.[37,38] To investigate the effects of thiol and polymerizable organoclay on final conversion of thiol-ene systems in air, RTIR experiments were performed with different thiol ratios and types of polymerizable organoclay. To this end, C16A acrylate and PSH2 thiolated organoclays were added into PEGDA/TrPGDA mixtures containing increasing amounts of TMPTMP thiol monomer. In Figure 6.9, RTIR conversion profiles of the systems with addition of 5wt% acrylate organoclays are shown as a function of polymerization time. As mentioned in the experimental section, the samples were saturated with oxygen through extensive contact with air, and will be considered a semi-closed system once the upper sodium chloride plate is placed. Reaction induction times in Figure 6.9, therefore, are indication of the time necessary mainly for consumption of the initially dissolved oxygen molecules.

As shown in Figure 6.9 (A) profiles, final acrylate double bond conversion is approximately 0.95 for all thiol concentrations. Compared to the profiles obtained in photo-DSC experiments (see Figure 6.3 (B)), the reaction induction times are approximately half of those in PDSC experiments which is reasonable given that no significant oxygen diffusion occurs into the systems during polymerization time. In Figure 6.9 (B), however, the final thiol conversion decreases significantly from 0.93 to 0.62 with increasing thiol concentration due to lower collision probability between thiols and double bond with the higher concentration of thiols. Similar behavior was observed when PSH2 thiolated organoclays were added into the same monomer composition (not shown), albeit with slightly increased thiol conversion as a whole. Figure 6.10 summarizes the difference between acrylated and thiolated organoclay systems. Thiolated organoclay systems exhibit higher thiol conversion than acrylated organoclay systems

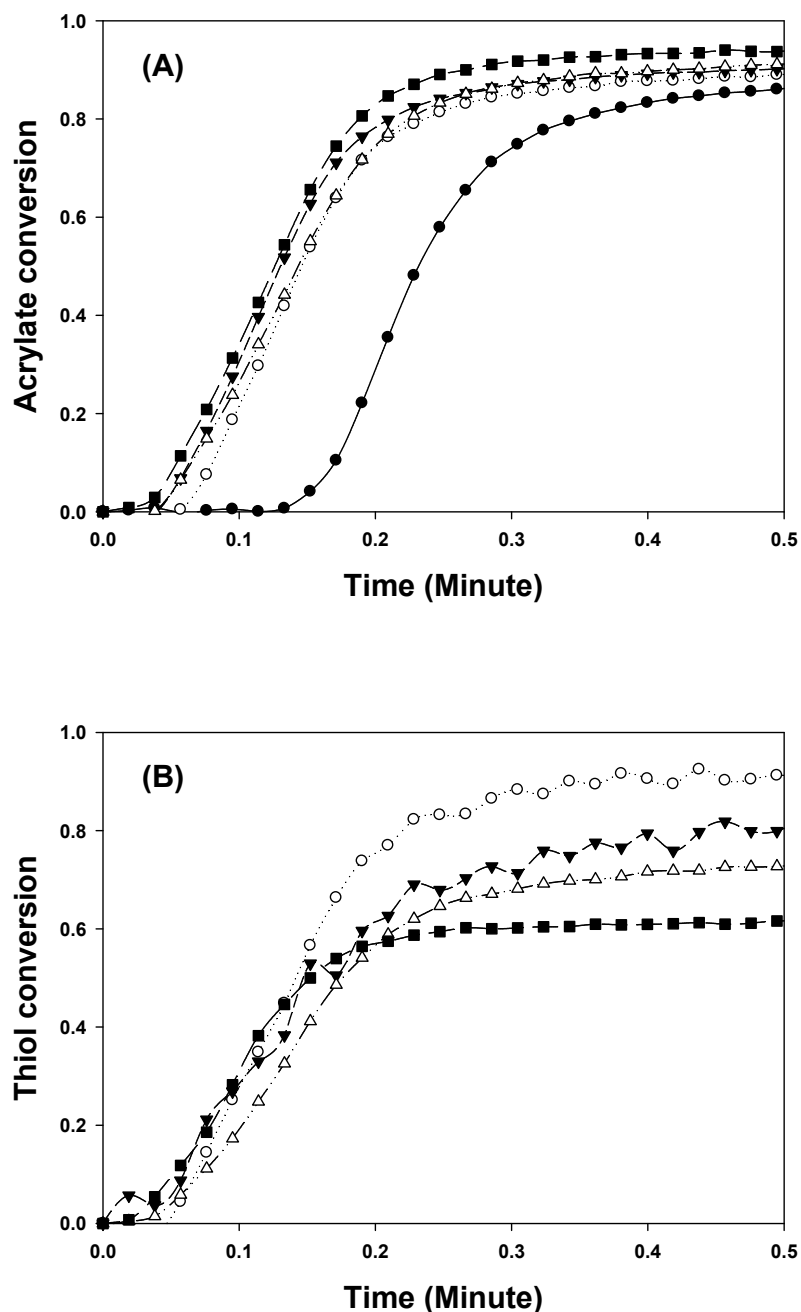


**Figure 6.9.** RTIR conversion profiles of PEGDA/TrPGDA (50wt%/50wt%) systems containing different amount of TMPTMP monomer with addition of 5wt% C16A acrylated organoclay. Photopolymerization was initiated with  $3.2\text{mW}/\text{cm}^2$  UV light and 0.2wt% DMPA in air. Shown are profiles of (A) acrylate double bond conversion of PEGDA/TrPGDA (●), and PEGDA/TrPGDA with 10 mol% (○), 15 mol% (▼), 20 mol% (▲), and 30 mol% (■) thiol, and (B) thiol conversion of PEGDA/TrPGDA with 10 mol% (○), 15 mol% (▼), 20 mol% (▲), and 30 mol% (■) of thiol based on functional group ratio.

and the difference increases with increasing thiol concentration. For systems with 30mol% thiol, thiol conversion with thiolated organoclay is almost 20% higher when compared with the acrylated organoclay system.

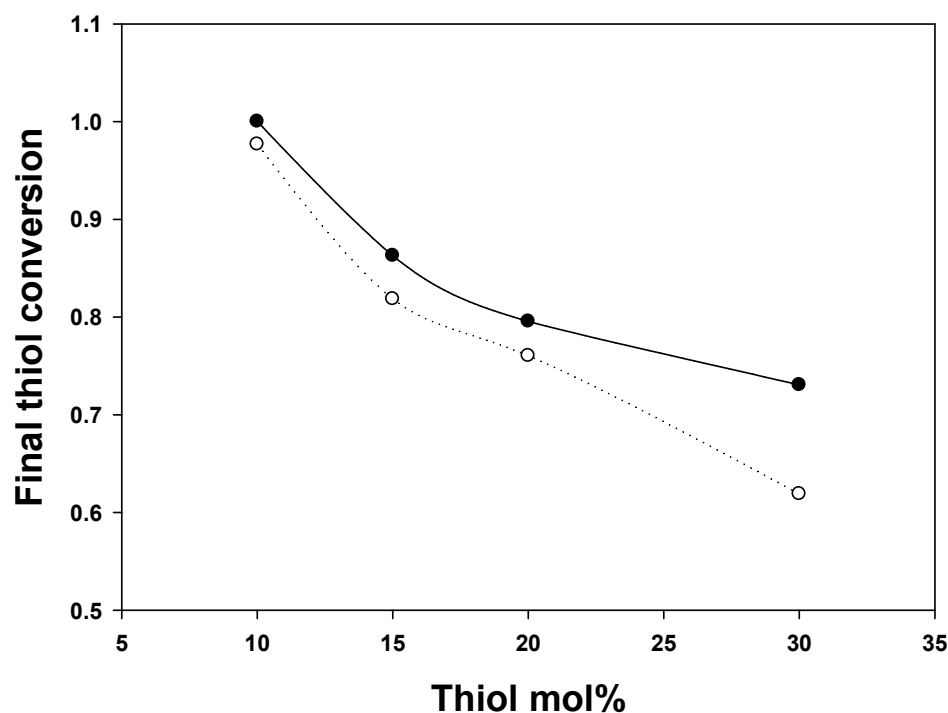


**Figure 6.10.** RTIR final thiol conversion profiles as a function of thiol mol% of PEGDA/TrPGDA (50wt%/50wt%) systems with addition of 5wt% polymerizable organoclays. Thiol mol% is controlled by increasing TMPTMP monomers up to 30mol% based on functional group ratio. Photopolymerization was initiated with  $3.2\text{mW}/\text{cm}^2$  UV light using 0.2wt% DMPA in air. Shown are profiles of final thiol conversions of the systems with 5wt% C16A acrylate organoclay ( $\circ$ ) and with 5wt% PSH2 thiolated organoclay ( $\bullet$ ).

In summary, the incorporation of thiol monomers induces significant reduction in oxygen inhibition of acrylate polymerization systems. The addition of thiolated organoclays allows further enhancements in polymerization rate and conversion in air.

Considering that use of compatible inorganic fillers often affords many advantages for polymer materials, this additional improvement in overcoming oxygen inhibition for acrylic polymerizations may be quite useful for many applications that must be processed in air.

### Conclusions

The effects of organoclays on oxygen inhibition in acrylate and thiol-acrylate systems have been investigated using three basic acrylate formulations with inherently different degrees of oxygen inhibition controlled by monomer structure and viscosity. HDDA monomer was used as a model highly inhibited system. Additionally, PEGDA/TrPGDA mixture and modified PEGDA/TrPGDA system including urethane type oligomer (CN9009) were used as intermediate and less inhibited acrylate systems, respectively. Without incorporation of thiol monomers, the HDDA system is completely inhibited by oxygen while the less inhibited formulations only reach 60% of the conversion in air at most as compared to nitrogen. While non-reactive or thiolated polymerizable organoclays significantly decrease the rate of polymerization for these acrylate homopolymerization systems, the addition of acrylated polymerizable organoclays slightly enhances polymerization in air, but the polymerization is still severely inhibited by oxygen. On the other hand, the addition of relatively small amount of thiol monomer reduces oxygen inhibition significantly. Incorporation of only 5 to 10 mol% thiol into acrylate systems considerably enhances polymerization reaction in air. The polymerization rate and conversion increase until thiol concentration reaches about 20 to 30mol%. Even with relatively high thiol contents, oxygen inhibition is still prevalent with overall polymerization rate still 20% lower compared than that observed under nitrogen. This gap can be overcome by adding a suitable type of polymerizable



organoclay. When thiols are incorporated over 20mol%, addition of 5wt% thiolated organoclays into these thiol-ene copolymerization systems enhances the conversion in air to over 95% of the value achieved under nitrogen, regardless of the type of basic acrylate composition in thiol-ene formulations. On the other hand, the addition of either non-reactive Cloisite 93A or C16A acrylated organoclay often decreases the conversion and polymerization rate in air. Higher thiol conversions are also achieved by adding thiolated organoclays due to increased thiol-ene reaction induced by the functional groups on clay surfaces. In summary, oxygen inhibition of acrylate radical photopolymerization systems can be effectively eliminated by adding suitable amounts of thiolated polymerizable organoclays and at least 20mol% thiol groups.

Notes

1. Wicks, Z. W. Jr.; Jones, F. N.; Pappas, P. *Organic Coatings. Science and Technology*; Wiley-Interscience: New York, **1998**, 630.
2. Fouassier, J. P.; Rabek, J.F. *Radiation curing in polymer science and technology*; Elsevier Applied Science: London, **1993**, Vol I: fundamentals and methods, 1.
3. Andrzejewska, E.; *Prog. Polym. Sci.* **2001**, 26, 605.
4. Decker, C. J. *Coat. Technol.* **1987**, 59, 97.
5. Fouassier, J. P. *Photoinitiation photopolymerization and photocuring: fundamentals and application*; Hanser Publishers: Munich, **1995**.
6. Carioscia, J. A.; Lu, H.; Stansbury, J. W.; Bowman, C. N. *Dent. Mater.* **2005**, 21, 1137.
7. Decker, C.; Moussa, K. *Macromol. Chem. Phys.* **1988**, 189, 2381.
8. Decker, C.; Moussa, K. *J. Coat. Technol.* **1993**, 65, 49.
9. Kloosterboer, J. G. *Adv. Polym. Sci.* **1988**, 84, 1.
10. Decker, C. *Macromolecules* **1989**, 22, 12.
11. Decker, C.; Moussa, K. *Makromol. Chem.* **1990**, 191, 963.
12. Turro N. J. *Modern molecular photochemistry*; University Science Books: Mill Valley, **1991**.
13. O'Brien, A. K.; Bowman, C. N. *Macromolecules* **2003**, 36, 7777.
14. Goodner, M. D.; Bowman, C. N. *Chem. Eng. Sci.* **2002**, 57, 887.
15. Andrzejewska, E.; Bogacki, M. B.; Andrzejewski, M.; Janaszcyk, M. *Phys. Chem. Chem. Phys.* **2003**, 5, 2635.
16. Dickey, M. D.; Burns, R. L.; Kim, E. K.; Johnson, S. C.; Stacey, N. A. Willson C. G. *AIChE J.* **2005**, 51, 2547.
17. Anseth, K. S.; Bowman, C. N. *Polym. React. Eng.* **1993**, 1, 499.
18. Lovestead, T. M.; Bowman, C. N. *Macromol. Theory Simul.* **2002**, 11, 729.
19. Decker, C.; Jenkins, A. D. *Macromolecules* **1985**, 18, 1241.
20. Pappav, P. *Radiation curing science and technology*; Plenum Press: New York, **1992**.

21. Krongauz, V. V.; Schmelzer, E. R. *Polymer* **1992**, 33, 1893.
22. O'Brien, A. K.; Cramer, N. B.; Bowman, C. N. *J. Polym. Sci. Part A: Polym. Chem.* **2006**, 44, 2007.
23. O'Brien, A. K.; Bowman, C. N. *Macromol. Theory Simul.* **2006**, 15, 176.
24. Decker, C.; Faure, J.; Fizet, M.; Rychla, L. *Photogr. Sci. Eng.* **1978**, 23, 137.
25. Hoyle, C.E.; Keel, M.; Kim, K. J. *Polymer* **1988**, 29, 18.
26. Lecamp, L.; Houllier, F.; Youssef, B.; Bunel, C. *Polymer* **2001**, 42, 2727.
27. Cramer, N. B.; Bowman, C. N. *J. Polym. Sci. Part A: Polym. Chem.* **2001**, 39, 3311.
28. Morgan, C.R.; Ketley, A.D. *J. Radiat Curing* **1980**, 7, 10.
29. Reddy, S. K.; Cramer, N. B.; Kalvaitas, M.; Lee, T. Y.; Bowman, C. N.; Aust. J. Chem. **2006**, 59, 586.
30. Li, Q.; Zhou, H.; Wicks, D. A.; Hoyle, C. E. *J. Polym. Sci. A: Polym. Chem.* **2007**, 45, 5103.
31. Roper, T. M.; Kwee, T.; Lee, T. Y.; Guymon, C. A.; Hoyle, C. E. *Polymer* **2004**, 45, 2921.
32. Cramer, N. B.; Reddy, S. K.; O'Brien, A. K.; Bowman, C. N. *Macromolecules* **2003**, 36, 7964.
33. Lee, T. Y.; Carioscia, J.; Smith, Z.; Bowman, C. N. *Macromolecules* **2007**, 40, 1473.
34. Owusu-Adom, K.; Guymon, C. A. *Polymer* **2008**, 49, 2636.
35. Owusu-Adom, K.; Guymon, C. A. *Macromolecules* **2009**, 42, 180.
36. Owusu-Adom, K.; Guymon, C. A. *Macromolecules* **2009**, 42, 3275.
37. Kim S. K.; Guymon, C. A. *J. Polym. Sci. Part A Polym. Chem.* **2011**, 49, 465.
38. Kim S. K.; Guymon, C. A. *Macromolecules* (submitted).
39. Sangermano, M.; Laka, N.; Malucelli, G.; Samakandeb, A.; Sanderson, R.D. *Progress in Organic Coatings* **2008**, 61, 89.
40. Anseth, K. S.; Wang, C. M.; Bowman, C. N. *Macromolecules* **1994**, 27, 650.
41. Hoyle, C. E.; Hensel, R. D.; Grubb, M. B. *J. Polym. Sci., Part A: Polym. Chem.* **1984**, 22, 1865.
42. Rodriguez, F.; Cohen, C.; Ober, C. K.; Archer, L. A. *Principles of Polymer Systems*, Taylor & Francis: New York, **2003**, Ch.9, 405.

43. Alexandre, M.; Dubois, P. *Mater. Sci. Eng.* **2000**, 28, 1.
44. Ray, S. S.; Okamoto, M. *Prog. Polym. Sci.* **2003**, 28, 1539.
45. Gou, L.; Coretsopoulos, C. N.; Scranton, A.B. *J. Polym. Sci. Part A: Polym. Chem.* **2004**, 42, 1285.
46. Lee, T. Y.; Guymon, C. A.; Jonsson, S. E.; Hoyle, C. E. *Polymer* **2004**, 45, 6155.
47. Lee, T. Y.; Kaung, W.; Jonsson, E. S.; Lowery, K.; Guymon, C. A.; Hoyle, C. E. *J. Polym. Sci. Part A: Polym. Chem.* **2004**, 42, 4424.
48. Andrzejewska, E.; Andrzejewski, M. *J. Polym. Sci. Part A: Polym. Chem.* **1998**, 36, 665.
49. Miller, C.W.; Hoyle, C. E.; Jonsson, S.; Nason, C.; Lee, T. Y.; Kuang, W. F.; Viswanathan, K. *ACS Symp. Ser.* **2003**, 847, 2.

**CHAPTER 7**

**DECREASED POLYMERIZATION SHRINKAGE THROUGH  
INCORPORATING POLYMERIZABLE ORGANOCCLAYS  
IN ACRYLATE AND THIOL-ACRYLATE PHOTOPOLYMERIZATIONS**

Two of the major drawbacks for acrylate photopolymers are high volume shrinkage and shrinkage stress during photopolymerization. This research focuses on incorporating polymerizable organoclays as inorganic fillers in thiol-acrylate systems to overcome the high polymerization shrinkage of acrylate homopolymerization. To this end, the effect of various polymerizable and non-polymerizable organoclays on polymerization shrinkage has been investigated utilizing acrylate as well as thiol-acrylate photopolymerization systems. The incorporation of only 3wt% thiolated organoclays induces an approximately 10% reduction in the volume shrinkage of both acrylate and thiol-acrylate systems while acrylated organoclays do not change shrinkage significantly. The impact of organoclays on polymerization induced shrinkage stresses are significant and vary depending upon the structure of organoclays. By incorporating only 5wt% polymerizable organoclays with appropriate functional groups, approximately 50% and 90% decreases in the shrinkage stress are observed for acrylate or thiol-acrylate monomer systems, respectively, whereas the same amount of non-reactive clays reduce shrinkage stress only 10 to 20%. RTIR and simultaneous near-IR conversion analysis suggest that enhanced interaction of the polymerizable organoclays with monomers as well as changes in reaction mechanism may induce the significant reduction in this shrinkage stress.

## Introduction

Photopolymers based on acrylate or methacrylate monomers have been widely used in industrial applications due to several process and performance advantages, such as high energy efficiency, low VOC emissions, facile control of the polymerization process, and desirable thermo-mechanical properties.[1-5] While (meth)acrylate photopolymers show great utility, improvement in volume shrinkage and shrinkage stress during photopolymerization would enhance potential photopolymer applications.[1, 6-8] Polymerization shrinkage occurs with reduction of free volume as van der Waals distances between liquid monomers are decreased in forming covalent bonds in solid polymer networks [8]. This volumetric change of the system is inevitably accompanied by stress development that induces many defects such as surface curling, cracking, or delaminating of cured materials during or after polymerization.[9,10] For instance, such low dimensional stability and subsequent evolution of high stress during the curing process often bring about significant problems in many adhesive and coating applications through decreasing peel-strength and/or by substrate deformation.[11-14]

Especially in polymerization systems based on chain polymerization of multi-functional acrylate or methacrylate monomers, high molecular weight polymer networks are formed immediately with initiation. This process induces early gelation or vitrification at low conversion, resulting in high volume shrinkage.[16-18] The shrinkage due to reaction of methacrylate double bonds is approximately 22.5 ml/mol, which is almost double of that for step-growth mechanisms such as thiol-ene polymerization.[19,20] Considerable research has focused on reducing polymerization shrinkage of (meth)acrylate systems, including use of bulky structured monomers [21,22] and oligomers [23,24] to reduce overall double bond concentration, and exploiting other polymerization techniques such as cationic ring opening or thiol-ene step-growth polymerizations that involve inherently lower polymerization shrinkage compared to

acrylate homopolymerization.[25-28] Another approach involves adding significant amounts of inorganic filler that reduces the volume ratio of monomers. Interactions between inorganic surfaces and polymer systems might further decrease the polymerization shrinkage by facilitating chain relaxation and rearrangement of the polymer network during polymerization.[12, 29-34]

This report focuses on combining thiol-acrylate systems with polymerizable organoclays as inorganic fillers to form photopolymer-clay nanocomposites exhibiting advanced properties including low polymerization shrinkage. The step-growth mechanism of thiol-ene systems delays gelation as high molecular weight polymer is formed only at higher conversions. This process is beneficial for reducing polymerization shrinkage due to facile rearrangement of polymer chains in the lower viscosity reactant mixture.[20,27,35] Adding organoclays to thiol-acrylate systems may provide further advantages in both network properties and shrinkage of the system. For example, the addition of thiols to acrylate photopolymerization systems significantly decreases the mechanical properties of the polymer through formation of more flexible thio-ether linkages in the network.[27,36] Incorporation of inorganic fillers into such a polymer system often increases mechanical properties such as modulus and toughness and thus would be helpful for overcoming this shortcoming of thiol-acrylate polymerization. Inorganic fillers such as organoclays could also decrease polymerization shrinkage by reducing the effective organic volume in the systems.[30,32]

Organoclays have recently attracted considerable research interest as an inorganic filler to form photopolymer nanocomposites due to their commercial availability and simple delamination chemistry. Additionally, the effects on photopolymerization kinetics and ultimate nanocomposites properties have also been studied for various (math)acrylate systems and epoxy cationic systems.[37-39] These studies, however, have utilized non-reactive organoclays that typically only allow intercalated clay dispersion at best. Our research group has developed unique polymerizable organoclays that react with

monomers during the polymerization. Incorporation of appropriate polymerizable organoclays increases reaction rate as well as clay exfoliation due to enhanced interaction between clay particles and the polymer matrix. The reaction mechanism is also changed by the type of functional groups in the organoclay. For example, when polymerizable organoclays are added to thiol-acrylate systems, thiol functionalized organoclay enhances thiol-ene copolymerization while acrylate functionalized organoclay increases acrylate homopolymerization, significantly affecting the ultimate network properties.[40-43]

With such changes in reaction behavior and thermo-mechanical properties of photopolymerization systems with clays, this report studies the effects of polymerizable organoclays on the polymerization shrinkage of both acrylate and thiol-acrylate systems. The fundamental hypothesis of this study is that increased interaction between clays and polymer networks as well as any change in reaction mechanism by incorporating polymerizable organoclays may induce improvements in polymerization shrinkage. To verify and generalize this assumption, polymerization shrinkage of various acrylate and thiol-acrylate systems were compared with different organoclays. The effect of incorporating thiol monomers into acrylate mixtures is also examined to clearly demonstrate the possible synergetic effects of organoclay and thiol on polymerization shrinkage. In addition to examining volume shrinkage and shrinkage stress, simultaneous conversion analysis utilizing near-IR and RTIR instrumental methods was performed to further understand the evolution of polymerization shrinkage in thiol-acrylate nanocomposites.

## Experimental

### Materials



1,6-hexanediol diacrylate (HDDA), tripropyleneglycol diacrylate (TrPGDA), Polyethyleneglycol (600) diacrylate (PEGDA, MW 742), and polyester based urethane acrylate oligomer (CN9009) acrylate monomers were obtained from Satomer Inc (Exton, PA). Trimethylolpropane triacrylate (TMPTA) and trimethylolpropane trimercaptpropionate (TMPTMP) were purchased from Aldrich.

Cloisite Na (CL Na, Southern Clay Products – Gonzalez, TX) was used as the source for montmorillonite clay source. Cloisite 93A (CL93A, Southern Clay Products), i.e. montmorillonite clay modified with dihydrogenated tallow, was used as a typical commercial nonreactive type organoclay. To produce polymerizable organoclays, sodium cations between silicate platelets of Cloisite Na natural clay were ion exchanged using acrylate or thiol functionalized quaternary ammonium surfactants as described elsewhere.[41] C16A acrylated organoclay bearing acrylate functional groups on the clay surfaces was produced utilizing hexadecyl-2-acryloyloxy(ethyl) dimethylammonium bromide (C16A surfactant) synthesized following the methodologies described previously.[44,45] PSH2 thiol functionalized organoclays were synthesized via Michael addition reaction between thiol groups of tri functional TMPTMP and acrylate groups of C14A acrylated organoclay modified by tetradecyl-2-acryloyloxy(ethyl) dimethylammonium bromide (C14A surfactant) based on procedures reported elsewhere [41,46]. The chemical structures of monomers and surfactants used in this research are illustrated in Figure 7.1. Except where noted, 0.5 wt% 2,2-dimethoxyphenyl acetophenone (DMPA, Ciba Specialty Chemicals) was used as the free radical photoinitiator in all experiments. All chemicals including monomers and clays were used as received.

## Methods

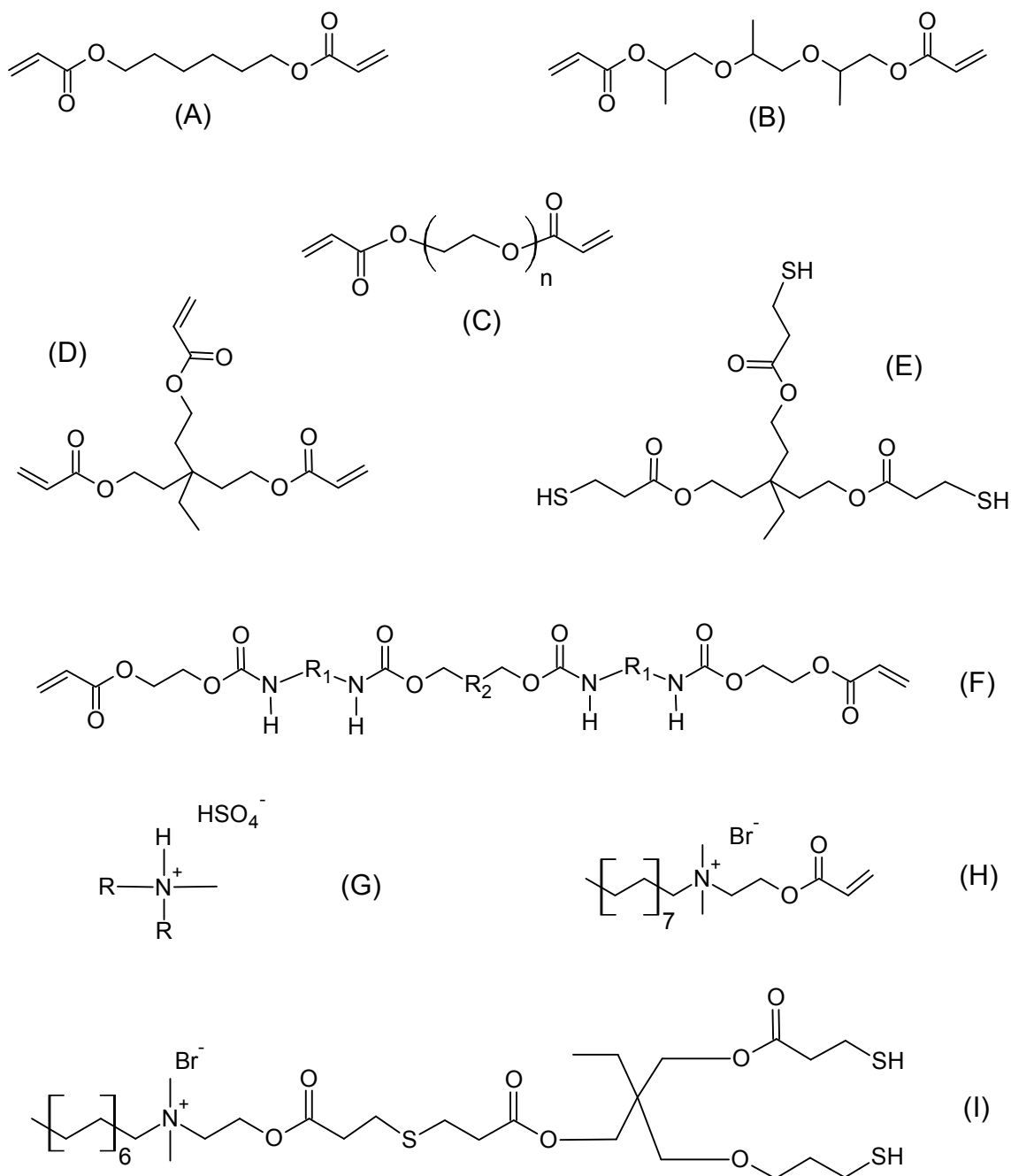


**Figure 7.1.** Chemical structures of monomers (A) 1,6-hexanediol diacrylate (HDDA), (B) tripropylene glycol diacrylate (TrPGDA), (C) polyethyleneglycol diacrylate (PEGDA, MW=742), (D) trimethylolpropane triacrylate (TMPTA), (E) trimethylolpropane tris(3-mercaptopropionate) (TMPTMP), and (F) polyurethane diacrylate oligomer (CN9009). Additionally, the chemical structure of organoclay modifiers (G) methyl dihydrogenated tallow sulfonate (CL93A), (H) hexadecyl-2-acryloyloxy(ethyl) dimethylammonium bromide (C16A), and (I) tetradecyl 2-(bis(3-mercaptopropionate) mercaptopropionyl trimethylolpropyl) acetoc(ethyl) dimethylammonium bromide (PSH2) are shown.

Volume shrinkage during photopolymerization was evaluated based on the density difference between the liquid monomer mixture and its photopolymerized solid sample. The density of liquid monomer mixtures ( $D_L$ ) were evaluated at 25°C by measuring the mass of a 100 ml sample. The liquid monomer mixture was then inserted into a sandwiched glass plate mold and polymerized using 3.3 mW/cm<sup>2</sup> light from a medium pressure mercury UV lamp for 20 minutes. To measure the volume of polymerized samples, cured sample bars were immersed into water and sonicated for 2 minutes to remove any bubbles on the sample surface. Solid density ( $D_S$ ) was calculated from the weight of cured polymer and increased water volume. Volume shrinkage was then determined from the density difference between liquid monomers and polymerized solid samples using Equation 7.1.

$$\text{Volume Shrinkage (\%)} = \left( \frac{\left( \frac{1}{D_L} \right) - \left( \frac{1}{D_S} \right)}{\left( \frac{1}{D_L} \right)} \right) \times 100(\%) \quad (7.1)$$

In order to evaluate the shrinkage stress of monomer mixtures during photopolymerization, a cantilever beam method modified from an ASTM standard [47] was utilized. Figure 7.2 shows the procedure for evaluating the photopolymerization induced shrinkage stress of a monomer system based on the deformation of a coated thin steel plate. Liquid monomer mixture with controlled coating thickness and length is placed on a 0.1 mm thick stainless steel plate (SUS-304). The coated plate is tightly clamped on one side and subsequently exposed to UV light. The metal plate deforms due to shrinkage stress through polymerization causing the unclamped side to rise. The shrinkage stress is then calculated from the height difference of the unclamped side between before and after polymerization based on Corcoran's relation as shown in in Equation 7.2.[48],

$$S = \frac{hE_s t^3}{3L^2 c (t + c)(1 - \gamma_s)} + \frac{hE_c (t + c)}{L^2 (1 - \gamma_c)} \quad (7.2)$$

where,  $S$  is shrinkage stress (MPa),  $h$  is the deflection of the cantilever (mm),  $E_s$  is the elastic modulus of the stainless steel substrate (193,000 MPa for SUS304 steel) [47],  $\gamma_s$  is the Poisson's ratio of the substrate (0.25 for SUS304 steel) [47],  $E_c$  is the elastic modulus of the coating materials (e.g. 14.5 MPa for thiol-acrylate compositions including 20mol% thiol functional groups, measured by DMA at 23°C),  $\gamma_c$  is the Poisson's ratio of the coating,  $L$  is the length of the coating,  $t$  is the thickness of the substrate, and  $c$  is the thickness of the coating.

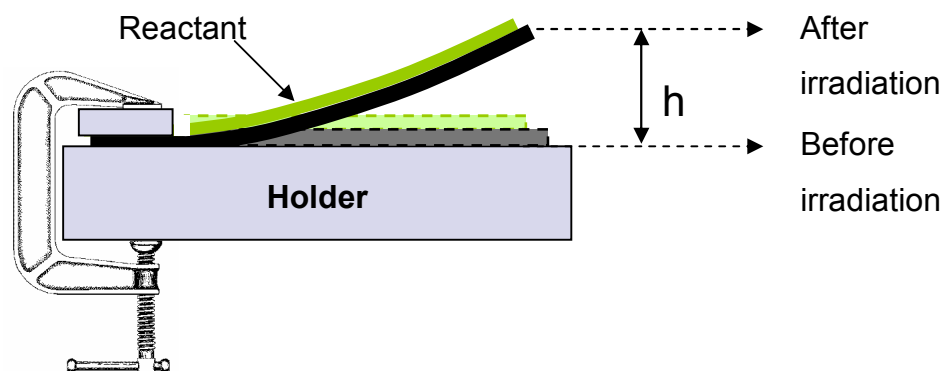


**Figure 7.2.** An illustration of the procedure (modified from ASTM D6991) for evaluating shrinkage stress during photopolymerization.

If the modulus of the coating is much smaller than the modulus of the substrate, as is the case for most polymers on rigid substrates, the second term of Equation 7.2 can be

neglected. For example, the modulus of cured acrylate and thiol-acrylate polymers in this report are measured between 10 to 30 MPa at room temperature, while the modulus of SUS-304 steel is about 193,000 MPa. In this case, the contribution of the second term in Equation 7.2 to the total shrinkage stress is much less than 1%.[47,48] Therefore, only the first term of Equation 7.2 was used for calculating the shrinkage stresses in this report. The thickness of a metal plate was chosen to allow optimal deflection range considering the modulus of the cured polymers.

To control the sample thickness, a specified amount of liquid monomer was placed on the designed area of a metal plate and spread out as evenly as possible. The actual coating thickness (typically 100  $\mu\text{m}$ ) was measured after curing using a digital caliper. Coated monomer mixtures were polymerized using 365 nm UV light at 15.0  $\text{mW}/\text{cm}^2$  from a medium pressure mercury lamp. After nitrogen purging for at least 3 minutes before irradiation to minimize oxygen inhibition, samples were polymerized for 20 minutes under nitrogen. At least 10 minutes was allowed before measurement of metal deflection to provide sufficient time for any post-cure effects.[49] Three samples were evaluated for each monomer system with the average value reported.

Kinetic studies of the UV-induced polymerizations for thiol-acrylate systems were performed based on real-time infrared spectroscopy (RTIR) utilizing a Nicolet Nexus 670 FTIR spectrometer with a KBr beam splitter and an MCT detector. Liquid monomer mixtures with about 15  $\mu\text{m}$  thicknesses were prepared between two sodium chloride plates and placed in the RTIR chamber. Polymerizations were initiated using a high pressure mercury lamp (EXFO Acticure) with a 365 nm filter. The series of infrared absorption spectra was obtained at a rate of 4scans/s under continuous UV irradiation. Thiol functional group and ene functional group conversion were monitored at 2575  $\text{cm}^{-1}$  (S-H stretching) and 810  $\text{cm}^{-1}$  (C-H stretching in double bond), respectively.[50] All reactions were performed using 15.5  $\text{mW}/\text{cm}^2$  under ambient temperature after purging the RTIR chamber for 2 minutes with dry nitrogen gas.

To study the evolution of shrinkage stress with increasing conversion, simultaneous double bond conversion analysis and shrinkage stress measurements were conducted using near-IR transmission through the monomer sample utilizing the same FTIR spectrometer used in the RTIR kinetic study. Liquid monomer about 110  $\mu\text{m}$  in thickness, approximately the same coating thickness used for shrinkage stress evaluation, was placed on a 1mm thick quartz glass plate. After obtaining the initial IR spectrum of the liquid monomer on the quartz plate prior to irradiation, the glass plate was moved into the curing chamber and placed near metal plates coated with the same monomer mixture. After both samples for conversion and stress measurement were irradiated for designated times under identical curing condition, IR spectra for cured samples on quartz plates were obtained simultaneously with the measurement of the metal deflection for shrinkage systems. Double bond conversion of the system was calculated from the change in peak height at  $6160\text{ cm}^{-1}$  for acrylate double bonds.[51]

### Results and Discussion

As discussed previously, high polymerization shrinkage during the photopolymerization is one of major disadvantages of (meth)acrylate systems and extensive studies have focused on its mitigation. One well established approach to reduce shrinkage is to add comonomers such as thiol or epoxy monomers with inherently low polymerization shrinkage. For example, thiol-acrylate photopolymers polymerize via two competing reaction mechanisms. The thiol-ene step growth mechanism produces a relatively homogeneous cross-linked network with lower shrinkage, while competing acrylate homopolymerization usually produces a more heterogeneous network with much higher shrinkage. Therefore, enhanced thiol-ene reaction can reduce polymerization shrinkage significantly compared to that of acrylate homopolymerization.[20,27,28]

Additionally, it has been demonstrated that adding polymerizable organoclays can either increase or decrease thiol-ene reaction according to the type of functional groups on the organoclay surface.[42,43] This behavior is induced primarily by the type of propagating radicals on the clay surface at early stages of polymerization, governing the subsequent reaction mechanism. While incorporation of thiols in the organoclay structure enhances the step growth reaction by providing thiyl radicals in the clay galleries, acrylic double bonds on the organoclay surface facilitates the chain growth acrylate homopolymerization reaction by forming primarily acrylic radicals in the galleries. If there is a significant difference in the degree of thiol-ene reaction with the type of polymerizable organoclay, the incorporation of polymerizable organoclays may also affect the extent of polymerization shrinkage in the system. In addition, adding thiol monomers into acrylate photopolymerization systems reduces polymerization shrinkage but also leads to significant decrease in thermo-mechanical properties such as modulus and glass transition temperature of cured products.[20,35,51] If incorporation of polymerizable organoclays can induce less polymerization shrinkage with increased thermo-mechanical properties, thiol-acrylate systems could be designed for expanded and new applications.

In order to investigate the effects of organoclays on polymerization shrinkage in thiol-ene photopolymer systems, volume shrinkage during photopolymerization were compared with and without use of organoclays. The volumetric change before and after polymerization was determined by measuring the density difference between the liquid monomer mixture and its photopolymerized solid sample for each formulation. For thiol-ene systems, a 1:1 weight mixture of PEGDA (MW=742) and TrPGDA was used as a model system for acrylate oligomer-monomer mixtures with moderate polymerization shrinkage. The tri-thiol TMPTMP was added to control the thiol content. To evaluate the effect of adding thiol monomers into this basic acrylate system on photopolymerization shrinkage, volume shrinkage of neat systems with different amounts of TMPTMP thiol

monomer were examined without incorporation of organoclays with results shown in Figure 7.3. The addition of small amounts of thiol into the acrylate mixture significantly decreases the polymerization shrinkage. With only 5 mol% thiol, a 20% decrease in volume shrinkage is induced compared to the neat acrylate mixture. With greater addition of thiol, the shrinkage decreases about 40% with 20mol% thiol. The polymerization shrinkage is not reduced further with thiol above 20mol%, indicating that 40% decrease in volume shrinkage is the maximum reduction for these thiol-acrylate systems with thiol addition.

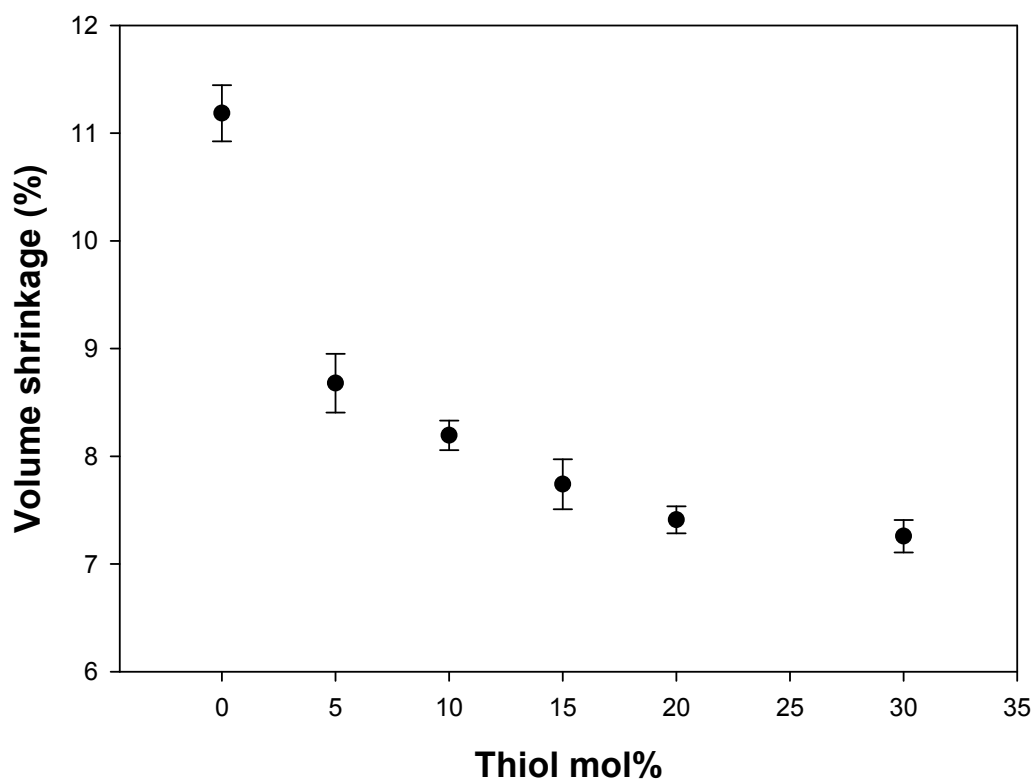


**Figure 7.3.** Polymerization induced volume shrinkage for PEGDA/TrPGDA/TMPTMP systems as a function of thiol mole ratio controlled by the amount of TMPTMP trithiol monomer into PEGDA/TrPGDA (50/50) mixture based on weight. Samples were photopolymerized with 0.5 wt% DMPA for 20 minutes at 3.3 mW/cm<sup>2</sup> using a medium pressure mercury UV lamp.



To demonstrate the potential of organoclay addition in further reducing polymerization volume shrinkage, 3wt% acrylate or thiolated organoclays were incorporated into the basic acrylate mixture and the thiol-acrylate system with 20mol% thiol. Figure 7.4 shows the effects of the polymerizable organoclays on polymerization volume shrinkage based on organoclay type. For both the basic acrylate mixture and the thiol-acrylate system, incorporation of only 3wt% thiolated organoclays induces another 10% reduction in volume shrinkage compared to neat systems. Adding acrylated organoclays, however, shows no significant impact on the polymerization. As the thiol-ene reaction is enhanced by adding thiolated organoclays [42], the clay addition reduces polymerization shrinkage of both systems.

Even this relatively small decrease in volume shrinkage by adding thiolated organoclays could be important for performance of nanocomposites because shrinkage stress is primarily induced at high conversion,[17,51] Above the gel point, only a few percent increase in conversion may induce significant increase in the strength of the polymer networks while the volume of the polymerization system decreases correspondingly to the ratio of conversion change. This results in a dramatic increase in shrinkage stress with a small increase in conversion at the end of the polymerization process. This build up in shrinkage stress often causes long term issues including substrate deformation, delamination, and mechanical failure A few percent improvements in the volume shrinkage may, therefore, induce a significant decrease in polymerization shrinkage stress that is crucial in many real applications such as coating and packaging especially on thin and/or weak substrates. To verify this potential, the effects of organoclays on the shrinkage stress during photopolymerization have been investigated with acrylate and thiol-acrylate systems.

The stress induced by polymerization shrinkage involves many factors such as the degree of volumetric change, conversion, modulus of the system, the substrate characteristics, and the adhesion to the substrates.[17,20,52] Various types of

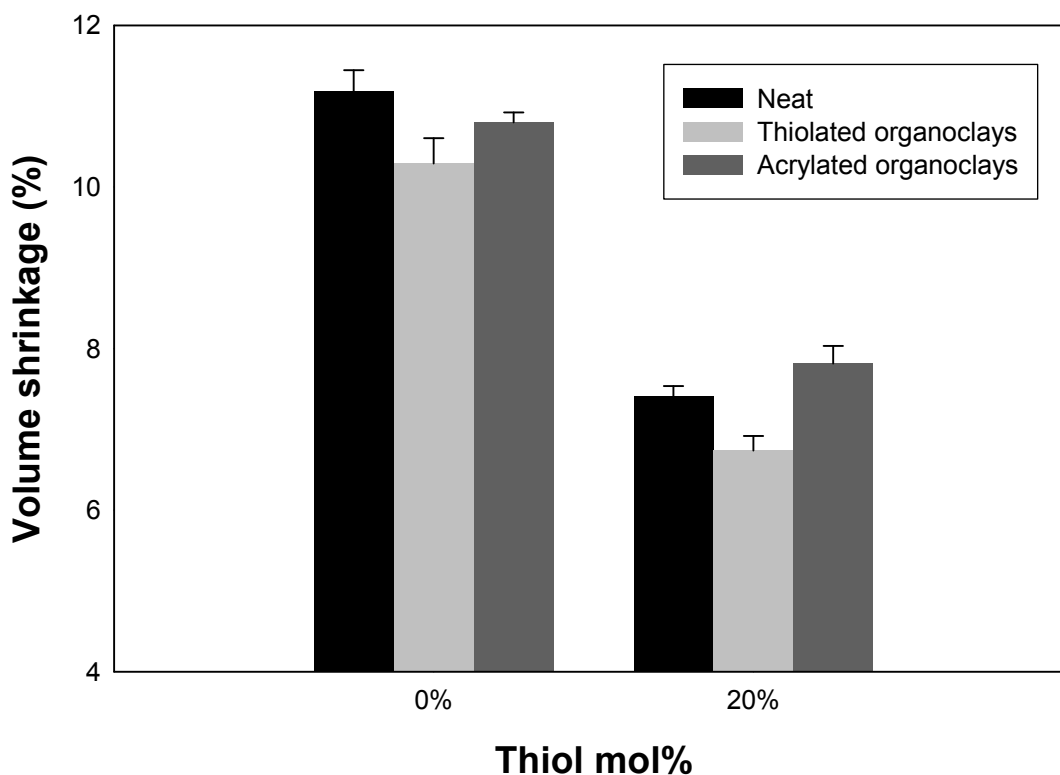


**Figure 7.4.** Polymerization induced volume shrinkage for PEGDA/TrPGDA (50/50) acrylate mixtures and PEGDA/TrPGDA /TMPTMP (50/50/15.6) thiol-acrylate mixtures including 20 mol% thiol without and with addition of 3wt% polymerizable organoclays. Ratios are based on mass. Samples were photopolymerized with 0.5 wt% DMPA for 20 minutes at 3.3 mW/cm<sup>2</sup> using a medium pressure mercury UV lamp.

experimental methods have been developed and employed to measure the shrinkage stress considering such factors. These methods include measurement of deflection curvature of coated elastic substrates,[53] the cantilever beam method,[54] the technique based on the bonded disk equipped with load cell,[55] and modified tensometer measurement [56] based on cantilever theory. In this research, a modified cantilever plate beam method based on the ASTM standard [47] was used to determine the shrinkage stress. The only deviations from the ASTM standard were slight changes in the thickness

and length of the cantilever steel plate. These modifications were necessary to allow sufficient deflection of the substrate plate during the photopolymerization of acrylate or thiol-acrylate systems that exhibit lower shrinkage stresses than the thick organic coatings that are the target applications of the ASTM standard. Experiments utilizing this modified method were performed and experimental reproducibility was examined by comparing the results with literature values obtained using a similar method.[54] The steel plates (50mm/5mm/0.1016mm in length/width/thickness) were used as in the reference while the wider plates with 10mm width were used for other measurements to improve the experimental accuracy. As calculated using Equation 7.2 and deflection during polymerization, the photopolymerization shrinkage stresses of TMPTA and TrPGDA that represent acrylate monomers with relatively high and low shrinkage stresses respectively are summarized in Table 7.1 and compared to literature values. In both high and low shrinkage stress systems, the experimental values are slightly higher than the literature values but the differences are not significant, indicating acceptable reproducibility for this method.

**Table 7.1.** Shrinkage stress of typical acrylate monomers.

Monomer	Deflection (h, mm)	Shrinkage stress* (MPa)	Literature value (MPa)
TMPTA	16.5 ± 1.0	21.8 ± 1.3	20.0
TrPGDA	1.7 ± 0.15	2.2 ± 0.2	1.5

\* Values were obtained by using steel plates with 5mm width as per literature experiments.[54] Samples were photopolymerized with 0.5 wt% DMPA for 20 minutes using 365 nm UV light at 15.0 mW/cm<sup>2</sup>.

Three formulations with inherently different degrees of polymerization shrinkage were utilized for evaluating effects of organoclay on shrinkage. Neat trimethylolpropane triacrylate (TMPTA) was used as a monomer with high shrinkage. A mixed acrylate oligomer-monomer formulation with CN9009/ PEGDA/TrPGDA (30/30/40 weight ratio)

was used as a system with intermediate shrinkage stress. A triacrylate/trithiol (TMPTA/TMPTMP mixture with 60/40 weight ratio) was used to represent a thiol-acrylate system with the lowest shrinkage stress. Figure 7.5 (A) shows the inherent shrinkage stress of these three systems without addition of organoclays. The shrinkage stress range of these three neat systems ranges from 8 MPa for the thiol-acrylate to 27 MPa for TMPTA. Figure 7.5 (B) shows the differences in beam deflection with different monomer systems. Three measurements were performed to determine an average deflection for each composition.

As mentioned previously, the evolution of stress by polymerization-induced shrinkage is closely related with the formation of the cross-linked network in a system. Correlation between the extent of shrinkage stress with irradiation time or with reactive group conversion of a system would be therefore helpful to understand polymerization shrinkage evolution. In order to study the shrinkage behavior as a function of the degree of polymerization, the double bond conversion was simultaneously examined utilizing near-IR spectroscopy during the polymerization process for evaluating the shrinkage stress. Because the coating thickness of the metal plate is significantly thicker than that of sandwiched monomer layer between the salt plates used in typical mid-range RTIR kinetic experiments, conversion profiles obtained by the RTIR experiments might be different from that for coated monomer mixtures on the metal plates during the shrinkage stress experiments. Therefore, near-IR spectra were utilized for measuring the conversions of coated monomer systems based on the longer path-length for adequate cross-section.[51] By placing sample for near-IR analysis adjacent to the cantilever plate, it is reasonable to assume that the conversions of the two monomer samples for near-IR conversion and stress analysis are nearly same during the polymerization if the same sample thickness is used in both measurements. By correlating the difference in peak height for double bonds with the metal deflection before and after irradiation for designated periods, the shrinkage stresses can be plotted as a function of the conversion.

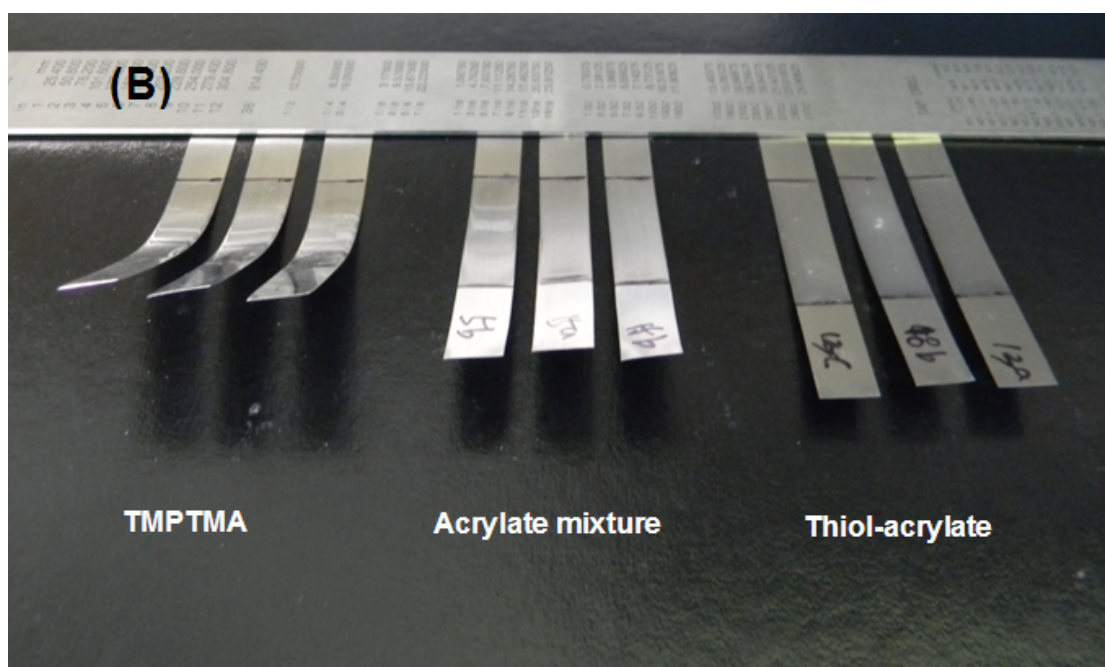
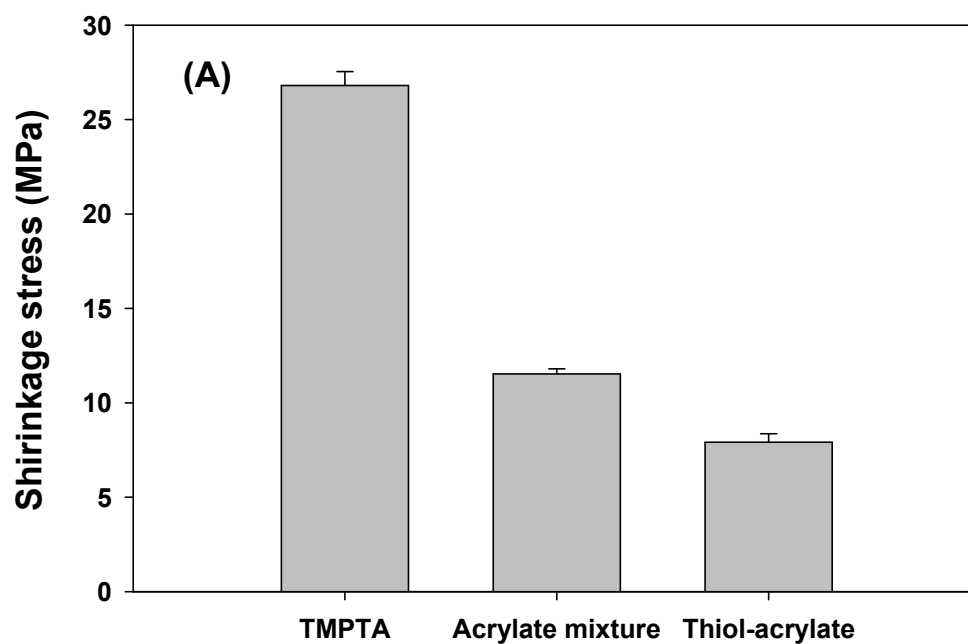


**Figure 7.5.** (A) Polymerization induced shrinkage stress and (B) deflection of the steel plates induced by shrinkage stress for neat TMPTMA, CN9009/PEGDA/TrPGDA (30/30/40) acrylate mixture, and TMPTA/TMPTMP (60/40) thiol-acrylate mixture. Ratios are based on mass. Samples were photopolymerized with 0.5 wt% DMPA for 20 minutes at 15.0 mW/cm<sup>2</sup> using 365 nm UV light.

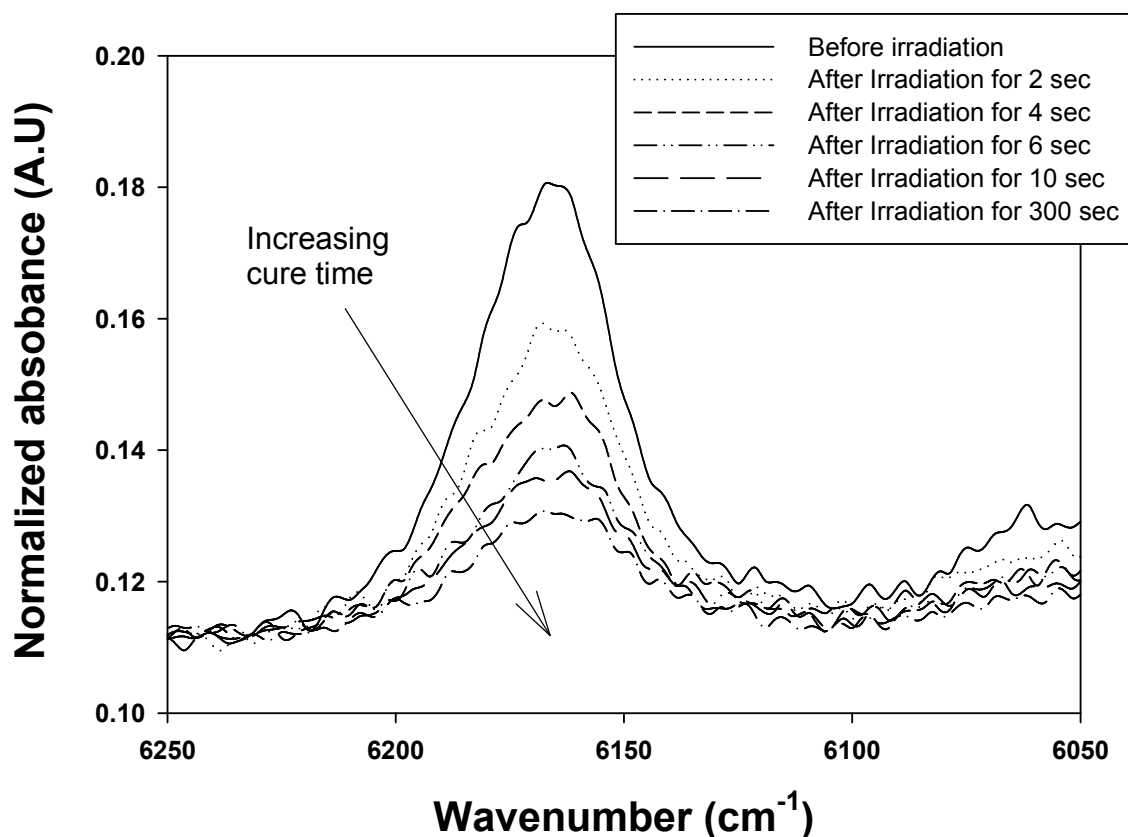


**Figure 7.6.** Near-IR spectra for neat TMPTA systems before (solid line) and after irradiation for specified time. Spectra were obtained using separate samples after irradiation for 2, 4, 6, 10, and 300 seconds, respectively. Samples were photopolymerized with 0.5 wt% DMPA at  $5.5 \text{ mW/cm}^2$  using 365 nm UV light.

Figure 7.6 shows the changes in the peak height at  $6160 \text{ cm}^{-1}$  for the double bonds of neat TMPTA upon exposure to UV light for different time periods. Each near-IR spectrum, obtained from separate sample sets, indicates the profile for before irradiation, and after irradiation for 2, 4, 6, 10, and 300 seconds, respectively. Because there can be slight differences in the coating thickness of each sample set, initial near-IR spectrum for all experimental sets were taken before irradiation. The peak heights for the samples after designated irradiation time were then compared after normalization of the peak height before polymerization. In addition, to obtain better correlation profiles between shrinkage

stresses and the conversion of the systems, the light intensity in these correlating experiments with simultaneous near-IR conversion analysis was decreased to  $5.5\text{mW/cm}^2$ . As shown in Figure 7.6 for triacrylate TMPTA, the double bond peak height rapidly decreases in the early stage of polymerization but does not reach 100% conversion with a peak remaining even with long irradiation times. This behavior is expected due to fast vitrification of the system and lack of species mobility at high conversions. In comparison, the peak completely disappears in the trithiol-triacrylate system after irradiation for 300 seconds (not shown), indicating late gelation of the system and much higher mobility allowed by the thiol-ene step polymerization.

To obtain correlation profiles between the conversion and the shrinkage stress of the systems, irradiation time was varied from 1 to 300 seconds. Figure 7.7 shows the shrinkage stress profiles for neat TMPTA and the TMPTA/TMPTMP (thiol-acrylate) system as a function of double bond conversion. Shrinkage stress for each conversion was calculated and averaged from the metal deflections. As shown in the figure, the evolution of polymerization-induced shrinkage stress in the triacrylate TMPTA occurs at the relatively low conversion of 90% after a short irradiation period of only 3 to 4 seconds. Once shrinkage stress begins to be significant, it rapidly builds up with small changes in conversion. This behavior in shrinkage stress evolution indicates fast vitrification by gelation at a very early stage of polymerization process. On the other hand, the evolution of the shrinkage stress in thiol-acrylate system occurs at much higher conversion and the stress buildup rate with conversion is much lower than in the acrylate system. This different behavior in shrinkage stress evolution is due to the unique characteristics of the thiol-acrylate polymerization.[20,51,56]

The step growth mechanism of the thiol-acrylate reaction delays the gelation of system and allows relaxation or rearrangement of propagating chains as unreacted liquid monomer and shorter chain polymers still are present until the late 'stage' of the polymerization process. Additionally, the conversion of thiol is usually lower than that

of acrylate groups because the thiol-ene reaction competes with acrylate homopolymerization. The ultimate thiol conversion for this TMPTA/TMPTMP thiol-acrylate system is about 0.65. Considering the remaining thiol groups, overall conversion including thiol and acrylate functional groups is about 0.83. If the profile for thiol-acrylate system in Figure 7.7 is plotted based on this overall conversion, the stress buildup rate would be slightly higher. Even considering the thiol conversion, the stress buildup rate in the thiol-acrylate system is much lower than for the acrylate system due to the dominant effect of the step-growth mechanism on the polymerization shrinkage.

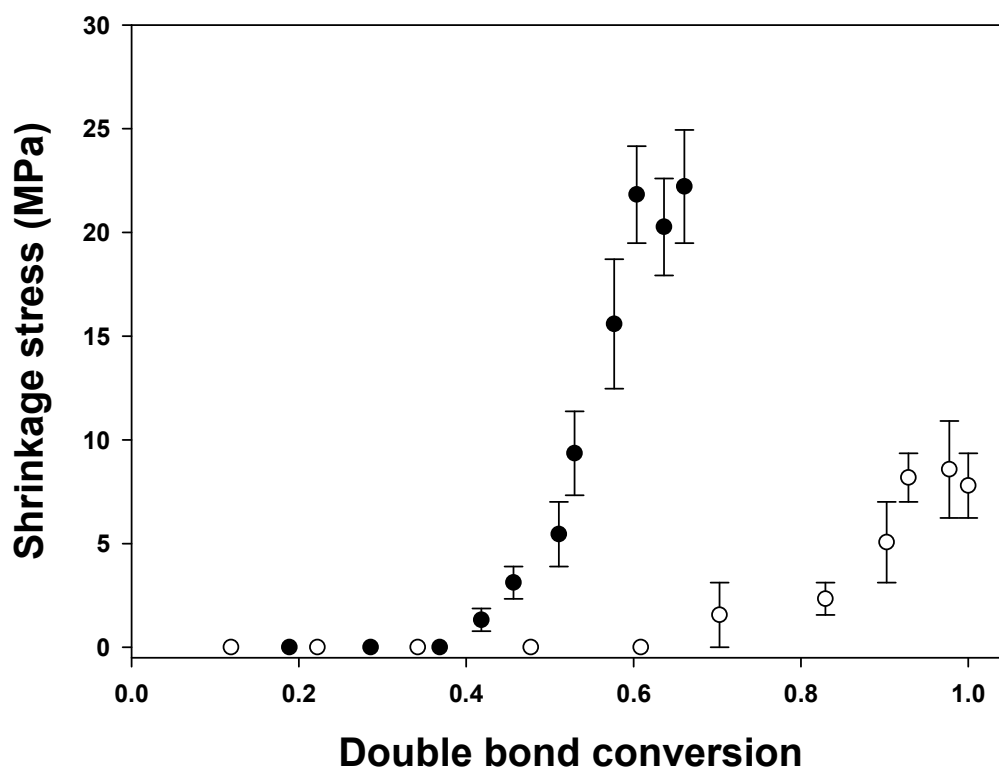


**Figure 7.7.** Polymerization induced shrinkage stress as a function of conversion for neat TMPTA (●) and TMPTA/TMPTMP (60/40) mixture (○). Samples were photopolymerized with 0.5 wt% DMPA using 365 nm UV light at 5.5 mW/cm<sup>2</sup>.



The results based on neat systems demonstrate that the incorporation of thiols in acrylate monomer system not only reduces the shrinkage stress but also decreases the buildup rate of the stress. The addition of polymerizable organoclays also affects the volume shrinkage of acrylate and thiol-acrylate systems and the impact varies with the type of functional group in the organoclay structure based on changes in polymerization mechanism. To determine if the organoclays show similar effects with shrinkage stress, the series of experiments were conducted with addition of 3wt% and 5wt% organoclays. The stress was measured for the three monomer compositions with different inherent shrinkage stress. Unmodified Cloisite Na clay is incorporated as well to evaluate the net inorganic filler effect of clay particles. As seen in Table 7.2 and 7.3, shrinkage stress typically decreases with incorporation of clays but the degree of decrease varies with the type of organoclay. In general, compared to the cases with unmodified clay, the addition of organically modified clays induces substantial reduction in shrinkage stresses for all monomer systems due to enhanced interaction with both monomers and the polymer network based on increased compatibility of organoclay. In addition, comparing the effects of two polymerizable organoclays on shrinkage stress, as observed in Figure 7.3 for volume shrinkage behavior, acrylated organoclays induces maximum reduction in the shrinkage stress of acrylate homopolymerization systems while thiolated organoclays performs better for the thiol-acrylate mixture.

For more facile comparison of the clay effects on the shrinkage stress, results from Table 7.3 with addition of 5wt% (organo)clays are graphically compared in Figure 7.8. The two acrylate systems in Figure 7.8 (A) exhibit the same basic behavior in shrinkage stress profile as a function of clay type. Incorporation of 5wt% Cloisite Na clay reduces the stress about 10% in both acrylate systems from that of the neat systems. The use of organically modified Cloisite 93A seems to be more effective in reducing shrinkage stress than natural clay. Maximum reduction in shrinkage stress is observed when acrylated polymerizable organoclays are incorporated while thiolated organoclays

**Table 7.2.** Shrinkage stress of different formulations with or without 3wt% organoclays.

Composition (wt ratio)	Organoclay	Deflection (h, mm)	Shrinkage stress (MPa)
TMPTA	Neat	17.1 ± 0.4	26.8 ± 0.7
	Cloisite Na (natural)	13.8 ± 1.3	21.7 ± 2.1
	Cloisite 93A	12.5 ± 0.5	19.5 ± 0.9
	C16A Acrylated	11.0 ± 0.9	17.0 ± 1.2
	PSH2 Thiolated	13.8 ± 0.3	21.6 ± 0.4
CN9009/TrPGDA /TMPTA (30/30/40)	Neat	7.7 ± 0.3	11.5 ± 0.3
	Cloisite Na (natural)	6.8 ± 0.3	10.1 ± 0.4
	Cloisite 93A	6.2 ± 0.5	9.2 ± 0.7
	C16A Acrylated	4.2 ± 0.3	6.2 ± 0.4
	PSH2 Thiolated	5.7 ± 0.3	8.5 ± 0.3
TMPTA/TMPTMP (60/40)	Neat	5.1 ± 0.3	7.9 ± 0.4
	Cloisite Na (natural)	3.7 ± 0.3	5.7 ± 0.4
	Cloisite 93A	2.5 ± 0.1	3.8 ± 0.1
	C16A Acrylated	1.7 ± 0.8	2.6 ± 1.2
	PSH2 Thiolated	1.2 ± 0.2	1.8 ± 0.2

**Table 7.3.** Shrinkage stress of three different formulations with 5wt% organoclays.

Composition (wt ratio)	Organoclay	Deflection (h, mm)	Shrinkage stress (MPa)
TMPTA	Cloisite Na (natural)	14.3 ± 0.8	22.1 ± 1.2
	Cloisite 93A	13.3 ± 1.5	20.8 ± 2.4
	C16A Acrylated	9.8 ± 0.3	15.3 ± 0.5
	PSH2 Thiolated	13.2 ± 1.0	20.7 ± 1.6
CN9009/TrPGDA /TMPTA (30/30/40)	Cloisite Na (natural)	6.5 ± 0.4	9.7 ± 0.5
	Cloisite 93A	5.5 ± 0.8	8.2 ± 1.1
	C16A Acrylated	3.5 ± 0.5	5.2 ± 0.8
	PSH2 Thiolated	5.5 ± 1.0	8.0 ± 1.5

In Table 7.2 and 7.3, samples were photopolymerized with 0.5 wt% DMPA for 20 minutes using 365 nm UV light at 15.0 mW/cm<sup>2</sup> irradiation intensity.

decreases shrinkage stress to about the same degree as the non-reactive Cloisite 93A organoclay. In general, the compatibility between clay and organic phase such as monomer mixture and polymers increases in this same order as examined by the degree of clay exfoliation utilizing small angle X-ray diffraction (SAXs).[42]

This shrinkage stress behavior indicates that shrinkage stresses in clay-polymer systems are closely related with the degree of interaction between clay and polymers. In addition, thiolated polymerizable organoclays acts much more like a non-reactive organoclay unless thiol monomers are in the monomer compositions. The shrinkage stresses of thiol-acrylate systems in Figure 7.8 (B) decrease more significantly by changing the clay type. In thiol-acrylate systems, thiolated organoclay induces much greater decrease in shrinkage stress than the other clays. As was demonstrated in previous studies,[42,43] thiolated organoclays can facilitate thiol-ene step reaction in a thiol-acrylate system and thus induce the largest decrease in the shrinkage stress of the thiol-acrylate system based on the slower build up of molecular weight and higher conversion at gelation and vitrification.

The shrinkage stress during polymerization is closely related with the overall polymerization behavior such as the reaction mechanisms and/or the polymerization kinetics of the systems. A small change in the degree of final conversion might also induce significant differences in ultimate shrinkage stress. In order to confirm that the reduction of shrinkage stress through clay addition is not based on decreases in final conversion, the final double bond conversions of the TMPTA-clay systems in Figure 7.8 (A) were examined utilizing simultaneous near-IR experiments and compared with that of neat TMPTA. Figure 7.9 shows the final acrylate conversion as a function of the clay type. Interestingly, no remarkable differences in final double bond conversions are observed. The final conversions fluctuate slightly but these fluctuations appear to be within experimental error without significant trend. These conversion results strongly support that reduction in shrinkage stress is primarily due to the degree of interaction

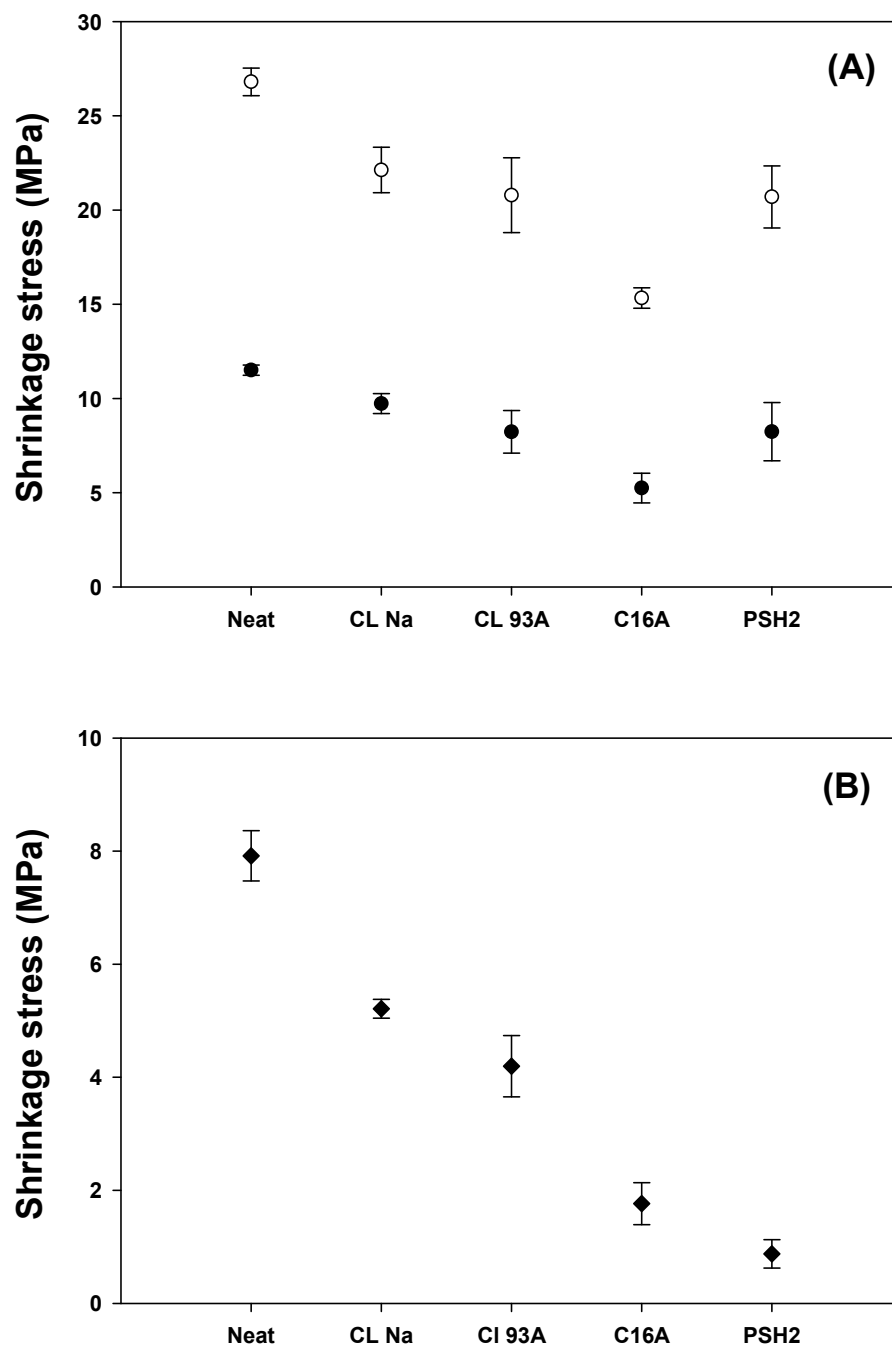


**Figure 7.8.** Polymerization induced shrinkage stress (A) for TMPTA (○) and CN9009/TrPGDA/TMPTMP (30/30/40) acrylate mixture (●), and (B) for TMPTMA/TMPTMP (60/40) thiol-acrylate formulations (◆) with 5wt% organoclay. Ratios are based on mass. Samples were photopolymerized with 0.5 wt% DMPA for 20 minutes at 15.0 mW/cm<sup>2</sup> using 365 nm UV light.

between the clay and the polymer network.

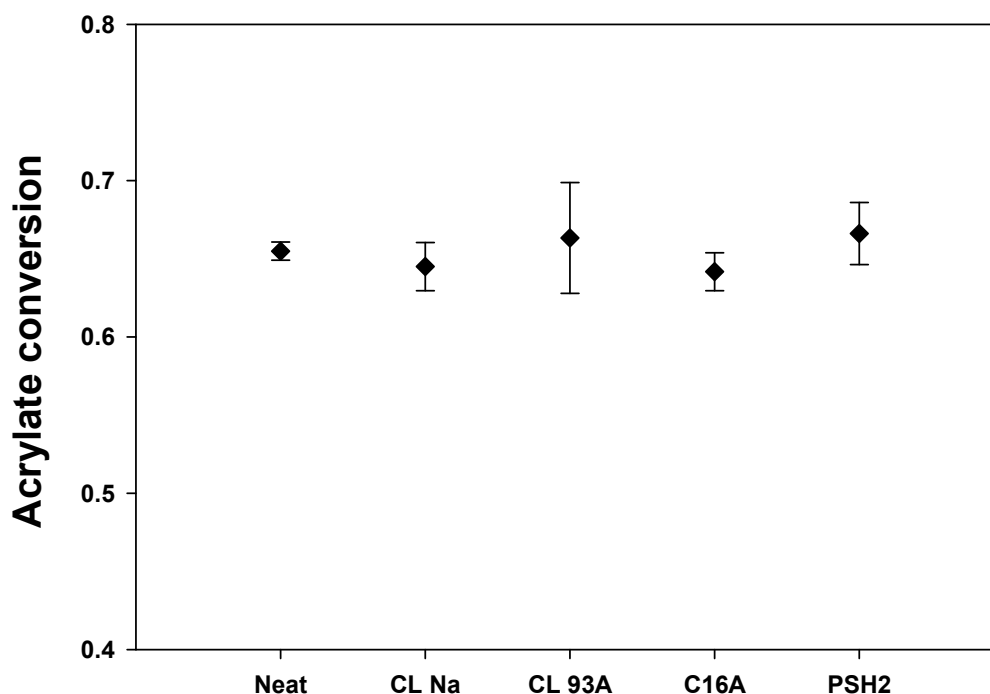


**Figure 7.9.** Final acrylate conversions obtained by simultaneous near-IR measurements during shrinkage tests for TMPTA systems or with without 5wt% organoclays. Samples were photopolymerized with 0.5 wt% DMPA for 20 minutes at 15.0 mW/cm<sup>2</sup> using 365 nm UV light.

On the other hand, for thiol-acrylate systems, the simultaneous near-IR experiments during the shrinkage stress measurements show that the final double bond conversions of all systems can reach unity regardless of the type of clay. As discussed previously, unreacted thiol groups still remain after finishing the curing process. Unfortunately, direct conversion analysis for thiol groups is not possible based on the simultaneous near-IR measurement because no thiol peak is found in the near-IR range. RTIR thiol

conversion profiles for TMPTA/TMPTMP thiol-acrylate systems with and without addition of clays were thus used for an indirect comparison of final thiol conversions. Due to the difference in sample thickness between near-IR and RTIR experiments, the reaction rate will be different between the two experiments but the final thiol conversions of the systems after a relatively long period of irradiation should be reasonably close and allow direct comparison. Figure 7.10 shows the RTIR thiol conversion profiles for thiol-acrylate systems with and without 5wt% clay. The neat and clay systems with natural (Cloisite Na) or non-reactive commercial organoclays (Cloisite 93A) show almost identical conversion profiles with a final thiol conversions of about 0.66. The conversion of thiolated organoclay (PSH2) system reaches about 0.70 for the thiol (5% higher than the neat system), whereas the acrylated organoclay (C16A) system shows final thiol conversion of about 0.61 which is 8% lower than the neat system.

While there are significant differences in shrinkage stress with the type of clays as shown in Figure 7.8 (B), the final thiol conversions do not match the trend in shrinkage stress behavior. Although the final thiol conversions for neat, Cloisite Na natural clay, and Cloisite 93A commercial organoclay systems are almost the same, the shrinkage stresses for these three systems are significantly different with the stress in the Cloisite 93A system about half that of the neat formulation. In addition, the final thiol conversion of the thiolated organoclay system is higher than that for all other systems while the shrinkage stress is significantly lower than the neat or other clay nanocomposite systems, indicating that differences in the final thiol conversion is not a critical factor in deciding final shrinkage stress of organoclay nanocomposite materials. One interesting phenomenon in this behavior is the different impact of thiolated organoclay on shrinkage stress. While thiolated organoclay acts much like a non-reactive organoclays in the acrylate system by decreasing shrinkage stress to the same degree as the non-reactive organoclay, this same clay induces the greatest decrease in the shrinkage stress of the thiol-acrylate of any organoclay. This behavior is induced because the addition of

thiolated organoclays enhances the thiol-ene step growth reaction in thiol-acrylate systems.[42]

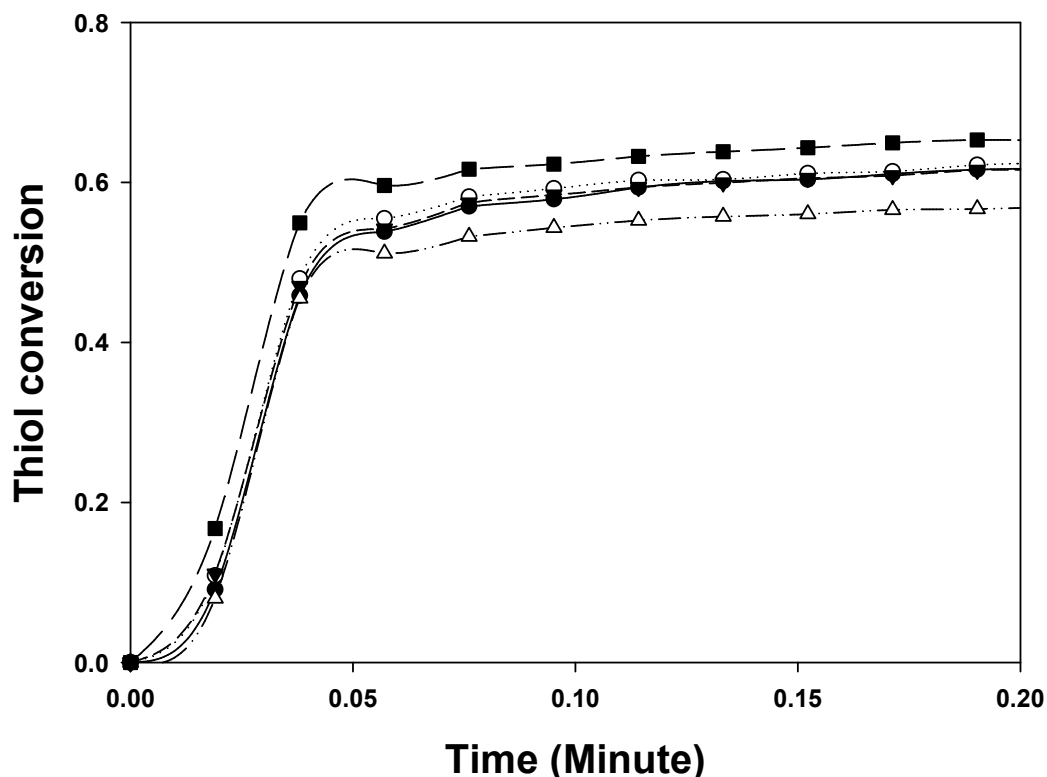


**Figure 7.10.** RTIR conversion profiles of thiol groups for TMPTA/TMPTMP (60/40) mixtures based on weight. Shown are thiol conversions for neat TMPTA/TMPTMP (●), TMPTA/TMPTMP with addition of 5wt% Cloisite Na natural clay (○), 5wt% Cloisite 93A organoclay (▼), 5 wt% C16A-acrylated organoclay (△), and 5 wt% PSH2 thiolated organoclay (■). Samples were photopolymerized with 0.5 wt% DMPA for 20 minutes at 15.0 mW/cm<sup>2</sup> using 365 nm UV light.

With good compatibility between organoclays and monomer, interaction between thiol monomers that diffused into the clay galleries and the functional groups on the clay surface facilitates either thiol-ene step copolymerization or acrylate homopolymerization based on the type of organoclays functional group added to the organoclay structure. This

effect of clay functional groups on reaction mechanism also can be seen in Figure 7.10 which shows the conversion profile of an acrylate/thiol mixture with different clays. The addition of thiolated organoclays induces higher thiol conversion than for the neat system while the conversion slightly decreases by incorporating acrylated organoclays due to enhanced acrylate homopolymerization. With increased interaction between polymerizable organoclays and monomer systems and incorporation of appropriate reactive groups, the shrinkage stress decreases substantially.

To compare the influence of clay structure on shrinkage stress more clearly, the shrinkage stress of clay-polymer systems for two different monomer compositions, as normalized by the stress in the neat system, are plotted in Figure 7.11 as a function of clay percentage. The normalized shrinkage stress profiles of the acrylate mixture with intermediate shrinkage stress (CN9009/TrPGDA/TMPTA) and of the trithiol/triacrylate mixture with relatively low shrinkage stress (TMPTA/TMPTMP) are shown in Figure 7.11 (A) and (B), respectively. Natural clay and nonreactive organoclay systems were compared with formulation including acrylated or thiolated polymerizable organoclays. For both monomer systems, the addition of only 3wt% clay significantly decreases the shrinkage stress regardless of the clay type. Further increases in clay continues to reduce shrinkage stress but not much more than the initial reduction by adding 3wt% clays, implying that the inorganic volumetric effect of clay addition is not a predominant factor for inducing significant stress reduction. Instead, considering the large decrease in shrinkage stress by addition of just 3wt% clay, other mechanisms such as relaxation and/or rearrangement of the networks by the interaction with clay particles would likely play more critical roles in reducing the stress. For instance, although there is no significant difference in unit volume of the three organoclays, each organoclay induces a different degree of improvement in shrinkage stress. Such behavior strongly suggests that organoclays exhibit differences in the degree of interaction with polymer network based on their inherent characteristics such as chemical compatibility to monomer, exfoliation



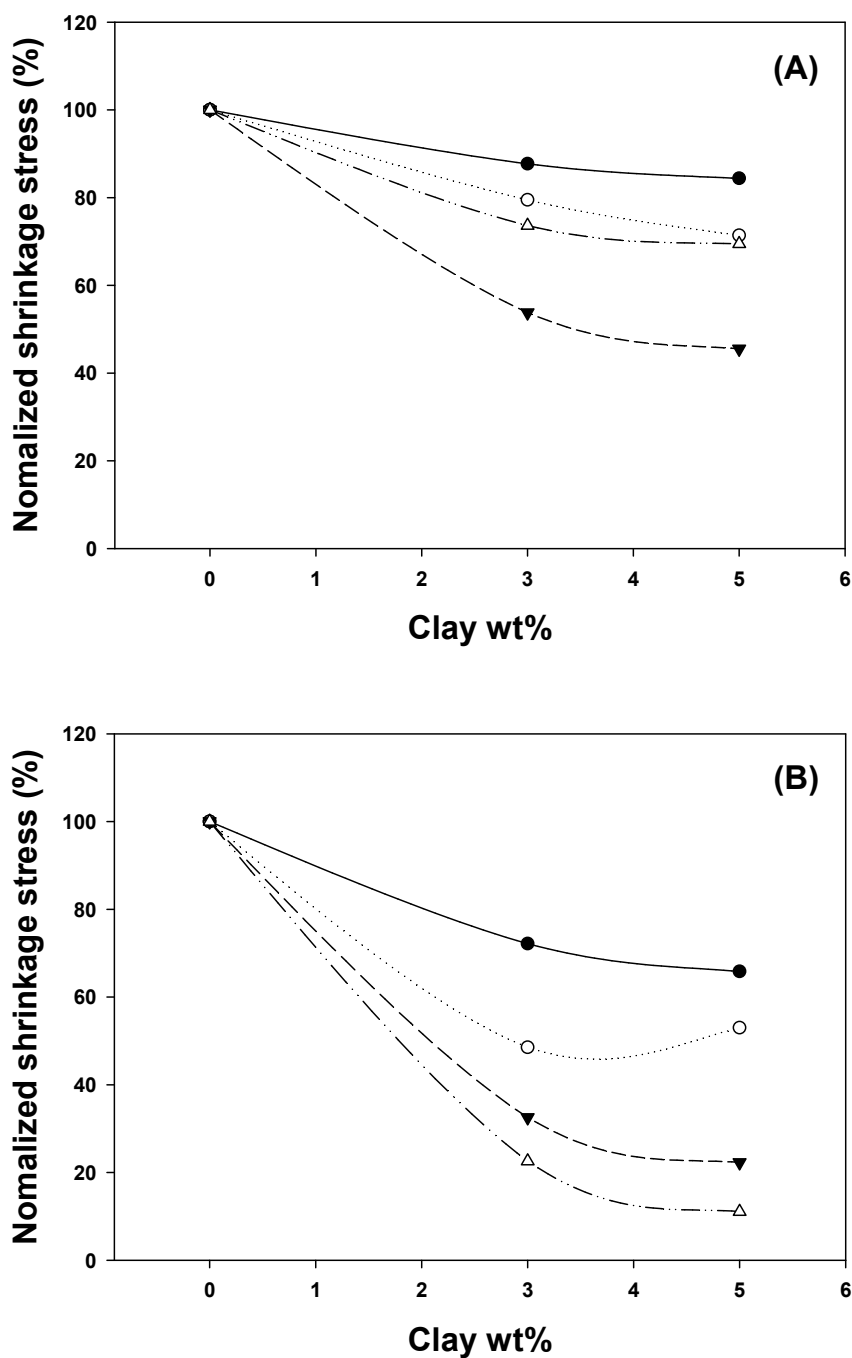


**Figure 7.11.** Shrinkage stress profiles as a function of clay wt% for (A) CN9009/TrPGDA/TMPTMA (30/30/40) acrylate mixture and (B) TMPTA/TMPTMP (60/40) thiol-acrylate mixture based on weight ratio with different types of clays. Shown are shrinkage stress profiles for the systems with Cloisite Na natural clay (◆), Cloisite 93A organoclay (○), C16A-acrylated organoclay (▼), and PSH2 thiolated organoclay. Samples were photopolymerized with 0.5 wt% DMPA for 20 minutes at 15.0 mW/cm<sup>2</sup> using 365 nm UV light.

morphology, ability to participate in the polymerization reaction, and ultimate affinity to the cross-linked networks being formed during polymerization.

From these results, acrylated functionalized organoclays are most effective in reducing the shrinkage stress of acrylate monomer systems. The incorporation of 5wt% acrylated organoclays into acrylate polymerization systems reduces shrinkage stress about 50% for both high shrinkage TMPTA and the moderate shrinkage CN9009 oligomer/TrPGDA/TMPTA system. The use of thiolated organoclays in acrylate monomer systems, however, seems to be less effective, only decreasing the stress about 30% to a level similar of that with a nonreactive organoclay. The addition of natural clays also decreases the stress to a much smaller degree. In thiol-acrylate mixtures, on the other hand, both thiolated and acrylated organoclays dramatically decrease the stress from that of the neat system. About 80% (with acrylated organoclays) or 90% (with thiolated organoclays) decrease in shrinkage stress is achieved by adding 5wt% organoclays while natural clay and nonreactive organoclays reduces the stress less than 40% with the same amounts of clay. This behavior implies that the improvement in the shrinkage stress is due not only to a rearrangement of clay particles but also to the impact of the polymerization mechanisms with different polymerizable organoclays. Interestingly, thiolated organoclays act similarly to nonreactive organoclays in acrylate mixture, indicating the clay interaction with polymerized networks is limited, at least in part, by the absence of thiol monomer in the formulation.

### Conclusions

To investigate the effects of adding organoclays on polymerization shrinkage, the volume shrinkage and shrinkage stress of acrylate and thiol-acrylate formulations have been examined during photopolymerization with and without addition of (organo)clays.

The addition of only 10 mol% thiol into acrylate mixtures can reduce the volume shrinkage up to 40% due to thiol-ene step growth reaction during the polymerization process. Another 10% reduction in volume shrinkage of both acrylate and thiol-acrylate systems is induced by the incorporation of only 3wt% thiolated organoclay, while acrylated organoclay does not change shrinkage significantly. Polymerization induced shrinkage stress is significantly reduced by the addition of clays. In general, polymerizable organoclays induce greater reduction in shrinkage stress than natural and nonreactive organoclays based on enhanced interaction with monomer and/or polymer networks during the polymerization process. The type of functional group in the clay structure also plays an important role for maximizing the reduction in shrinkage stress. Acrylated functionalized organoclays are more effective than thiolated organoclays for reducing the shrinkage stress of acrylate monomer systems in which no thiol monomers are included, whereas both thiolated and acrylated organoclays can greatly decrease the shrinkage stress of thiol-acrylate systems. By incorporating only 5wt% of an appropriate polymerizable organoclay, up to a 90% decrease in the shrinkage stress is observed for acrylate or thiol-acrylate monomer systems, whereas non-reactive clays reduce the stress by 20% at best.

Notes

1. Decker, C. *Prog. Polym. Science* **1996**, 21, 593.
2. Decker, C. *Acta. Polym.* **1994**, 45, 333.
3. Wicks, Z.W., Jr., Jones, F.N., Pappas, P. *Organic Coating. Science and Technology*, Wiley-Interscience, New York, **1998**, 630.
4. Tryson, G.R.; Shultz, A.R. *J. Polym. Sci.: Polym. Phys. Ed.*, **1979**, 17, 2059.
5. Zahouily, K.; Benfarhi, S.; Bendaikha, T.; Baron. *J. RadTech Europe Conf.* **2001**, 583.
6. Decker, C. *Polym. Int.* **1998**, 45, 133.
7. Beck, E.; Lokai, M.; Keil, E.; Nissler, H. *RadTech North America* **1996**, 160.
8. Natarajan, L. V.; Shepherd, C. K., Brandelik, D. M.; Sutherland, R. L.; Chandra, S.; Tondiglia, V. P.; Tomlin, D., Bunning, T.J. *Chem. Mater.* **2003**, 15, 2477.
9. Carvalho, R. M.; Pereira, J. C.; Yoshiyama, M.; Pashley, D. H. *Oper Dent.* **1996**, 21, 17.
10. Davidson, C. L.; Feilzer, A. J. *J. Dent.* **1997**, 25, 435.
11. Croll, S. G. *J. Coat. Technol.* **1980**, 52, 35.
12. Sato, K. *Prog. Org. Coat.* **1980**, 8, 143.
13. Oosterbroek, M.; Lammers, R.J.; van der Ven, J.J.; Perera, D.Y. *J. Coat. Technol.* **1991**, 66, 1267.
14. Magny, B.; Askienazy, A.; Pezron E. *Proc. RadTech Europe, Maastricht.* **1995**, 507, 400.
15. Bowman, C. N.; Anseth, K. S. *Macromol. Symp.* **1995**, 93, 269.
16. Lange, J. *Polym. Eng. Sci.* **1999**, 39, 1651.
17. Lu, H.; Stansbury, J. W.; Bowman, C. N. *J. Dent. Res.* **2005**, 84(9), 822.
18. Odian, G. *Principles of polymerization*. John Wiley & Sons, Inc. New York, **1991**, 3rd ed.
19. Patel, M. P.; Braden, M.; Davy, K. M. *Biomaterials* **1987**, 8, 53.
20. Lu, H.; Carioscia, J. A.; Stansbury, J. W.; Bowman, C. N. *Dent. Mater.* **2005**, 21, 1129.

21. Chung, C. M.; Lee, S. J.; Lim, J. G.; Jang, D. O. *J. Biomed. Mater. Res.* **2002**, 62, 622.
22. Pereira, S. G.; Osorio, R.; Toleano, M.; Nunes, T.G. *Dent. Mater.* **2005**, 21, 823.
23. Klee, J. E.; Schneider, C.; Holter, D.; Burgath, A.; Frey, H.; Mulhaupt, R. *Polym. Adv. Technol.* **2001**, 12, 346.
24. Grohn, F.; Kim, G.; Bauer, A.J.; Amis, E.J. *Macromolecules* **2001**, 34, 2179.
25. Chappelow, C. C.; Pinzino, C. S.; Power, M. D.; Holder, A. J.; Morrill, J. A.; Jeang, L. *J. Appl. Polym. Sci.* **2002**, 86, 314.
26. Tilbrook, D. A.; Clarke, R. L.; Howle, N. E.; Braden, M. *Biomaterials* **2000**, 21, 1743.
27. Hoyle, C. E.; Lee, T. Y.; Roper, T. *J. Polym. Sci. Part A Polym. Chem.* **2004**, 42, 5301.
28. Reddy, S. K.; Cramer, N. B.; Bowman, C. N. *Macromolecules* **2006**, 39, 3681.
29. Lu, H.; Lee, Y. K.; Oguri, M.; Powers, J. M. *Oper Dent.* **2006**, 31(6), 734.
30. Goldman, M. *Australian Dental J.* **1983**, 28(3), 156.
31. Kleverlaan, C. J. Ornelis.; Feilzer, A. J. *Dent. Mater.* **2005**, 21, 1150.
32. Lu, H.; Stansbury, J. W.; Bowman, C. N. *Dent. Mater.* **2004**, 20, 979.
33. Tomita, Y.; Chikama, K.; Nohara, Y.; Suzuki, N.; Furushima, K.; Endoh, Y. *Opt. Lett.* **2006**, 31, 1402.
34. Hata, E.; Tomita, Y.; *Opt. Lett.* **2010**, 35, 396.
35. Reddy, S. K.; Cramer, N. B.; Kalvaitas, M.; Lee, T. Y.; Bowman, C. N. *Aust. J. Chem.* **2006**, 59, 586.
36. Carioscia, J. A.; Lu, H.; Stanbury, J. W.; Bowman C. N. *Dent. Mater.* **2005**, 21, 1137.
37. Decker, C.; Keller, L.; Zahouily, K.; Benfarhi, S. *Polymer* **2005**, 46, 6640.
38. Uhl, F. M.; Davuluri, S. P.; Wong, S. C.; Webster, D. C. *Chem. Mater.* **2004**, 16, 1135.
39. Malucelli, G. ; Bongiovanni, R. ; Sangermano, M. ; Ronchetti, S. ; Priola, A. *Polymer* **2007**, 48, 7000.
40. Owusu-Adom, K.; Guymon, C. A. *Polymer* **2008**, 49, 2636.
41. Owusu-Adom, K.; Guymon, C. A. *Macromolecules* **2009**, 42, 180.
42. Kim, S. K.; Guymon, C. A. *J. Polym. Sci. Part A Polym. Chem.* **2011**, 49, 465.

43. Kim, S. K.; Guymon, C. A. *Europ. Polym. J.*
44. Lagaly, G.; Beneke, K. *Coll. Polym. Sci.* **1991**, 269, 1198.
45. Hamid, S. M.; Sherrington, D. C. *Polyme*, **1987**, 28, 325.
46. Owusu-Adom, K.; Guymon, C. A. *Macromolecules* **2009**, 42, 3275.
47. ASTM D 6991– 05, "Standard Test Method for Measurements of Internal Stresses in Organic Coatings by Cantilever (Beam) Method"
48. Corcoran E. M. *J. Paint Technology* **1969**, 41, 635.
49. Anseth, K. S.; Wang, C. M.; Bowman, C. N. *Macromolecules* **1994**, 27, 650.
50. Cramer, N. B.; Scott, J. P.; Bowman, C. N. *Macromolecules* **2002**, 35, 5361-5365.
51. Lee, T. Y.; Carioscia, J.; Smith, Z.; Bowman, C. N. *Macromolecules* **2007**, 40(5), 1473.
52. Stansbury, J. W. *Dent. Mater.* **2005**, 21, 56.
53. Feilzer, A. J.; Degee, A. J.; Davidson, C. L. *J. Dent. Res.* **1987**, 66, 1636.
54. Stolov, A. A.; Xie, T.; Penelle, J.; Hsu, S. L.; Stidham, H. D. *Polym. Eng. Sci.* **2001**, 41(2), 314.
55. Watts, D. C.; Cash, A. J. *Dent. Mater.* 1991, 7, 281.
56. Lu, H.; Stansbury, J. W.; Dickens, S. H.; Eichmiller, F. C.; Bowman, C. N. *J. Biomed. Mater. Res., Part B: Appl. Biomater.* **2004**, 70B, 206.

## CHAPTER 8

### PHOTOPOLYMER-CLAY NANOCOMPOSITE PERFORMANCE UTILIZING DIFFERENT POLYMERIZABLE ORGANOCCLAYS

The effects of polymerizable organoclays on thermo-mechanical characteristics, gas barrier properties, and thermal stability have been studied utilizing a thiol-acrylate mixture. Photopolymerization kinetic behavior shows that incorporation of thiolated organoclay into the thiol-acrylate composition induces a higher degree of step thiol-ene reaction than other organoclays. The addition of acrylated organoclay greatly increases tensile modulus with no significant change in either elongation or glass transition temperature of cured nanocomposites. On the other hand, the incorporation of thiolated organoclay decreases the glass transition temperature due to greater formation of flexible thio-ether linkages with higher thiol conversion. This enhanced flexibility results in significant increases in maximum elongation of the nanocomposite, but, interestingly, no reduction in Young's modulus is observed. Significant increases of 60% to 80% in toughness, as determined by the area of stress-strain curves in tensile experiments, have been observed by adding only 3wt% acrylated or thiolated organoclays while nonreactive organoclay actually decreases the toughness. Water vapor transmission rate (WVTR) of the photopolymer-clay nanocomposites has also been examined. While adding 3wt% natural clay reduces WVTR 16% compared to that of neat system, polymerizable and nonreactive organoclays induce about a 30% decrease, indicating similar efficiency in reducing gas permeability through addition of organoclays when clays are modified with organic surfactants.

## Introduction

The incorporation of clays into a polymer matrix with well-exfoliated morphologies can significantly enhance many performance characteristics of polymer composites such as mechanical and barrier properties, thermal stability, and chemical resistance with relatively small amounts of loading in comparison to systems based on micro-scale fillers.[1-3] *In situ* preparation of polymer-clay nanocomposites based on photopolymerization, on the other hand, provides a simple way to produce nano-scale dispersion of clay particles, avoiding several disadvantages of conventional processes involving thermal degradation or releasing volatile organic compounds (VOC) during the process.[3-6]

To obtain the clay exfoliation necessary for achieving advanced performance in clay nanocomposites, modification of clay surfaces by suitable surfactants is required to improve compatibility in polymer matrices.[3,4,7,8] However, most widely used non-reactive quaternary ammonium surfactants 9-11 may act as impurities affecting the final performance because they inherently do not participate in the polymerization reaction.[12] In this research, unique polymerizable surfactants have been developed to overcome this disadvantage of non-reactive surfactants. The incorporation of reactive groups on the clay surfaces using photopolymerizable surfactants may maximize the interaction between clay and organic phase during and after polymerization as well. Previous results have demonstrated that the addition of polymerizable organoclays into various acrylate photopolymer systems induce significant improvement in both nanocomposite properties with enhanced clay exfoliation and photopolymerization rate compared to the system with conventional nonreactive organoclays.[13-14] Increases of photopolymerization rate are also observed with incorporation of polymerizable organoclays, primarily due to greater immobilization of propagating radicals on the clay surface, subsequently resulting in decrease of bimolecular termination of propagating



radicals. Enhanced clay exfoliation facilitates this mechanism by increasing the effective surface area in the system.

Recent research has also focused on utilizing the potential of reactive clays in thiol-ene formulations. Due to its unique step polymerization mechanism and properties, thiol-ene photopolymerization has been widely studied in the past decade to help overcome major drawbacks of free radical polymerization such as oxygen inhibition and polymerization shrinkage during photopolymerization.[15-19] The effects of polymerizable organoclays on polymerization behavior as well as basic nanocomposite properties of the thiol-acrylate based photopolymers have been studied.[20-22] The incorporation of polymerizable organoclays increases both clay exfoliation and photopolymerization rates significantly as also observed in acrylate systems. Chemical compatibility between monomers and organoclay is of primary importance for achieving better clay exfoliation. Interestingly, the type of functional group on the clay surface significantly influences the polymerization behavior by affecting the stoichiometric balance between thiol and double bond in the clay gallery. Thiolated organoclays enhance thiol-ene reaction while acrylated organoclays encourage chain acrylate homopolymerization.[21,22]

Changes in polymerization behavior with different organoclays also induce significant differences in other aspects of the photopolymer system. For example, it was demonstrated that the addition of suitable polymerizable organoclays reduces oxygen inhibition and polymerization shrinkage of acrylate and thiol-acrylate systems significantly.[23,24] Addition of only 5wt% thiolated organoclays into thiol-acrylate copolymerization systems effectively eliminated oxygen inhibition during photopolymerization by reaching an almost identical conversion in air and nitrogen. This improvement is observed regardless of the basic acrylate composition in the thiol-acrylate formulations whereas the addition of either non-reactive or acrylated organoclay typically decreases the conversion and polymerization rate in air. Incorporation of only 5wt%

polymerizable organoclays modified with acrylate or thiol functional groups induces up to 90% decrease in the shrinkage stress while the reduction by the same amount of non-reactive clays is less than 20%. RTIR and simultaneous near-IR conversion analysis suggest that both changes in the reaction mechanism and enhanced interaction between the polymerizable organoclays and monomer systems facilitate this reduction in shrinkage stress.

Likewise, differences in polymerization behavior for organoclay-containing materials may affect final performance of the nanocomposites based on the close relation of polymer properties with both polymerization mechanism and resulting network structure. Particularly in thiol-acrylate systems, the reaction competition between the thiol-ene step-growth mechanism and faster acrylate homopolymerization often results in lower thiol conversion than that of acrylate double bonds.[25,26] This low thiol conversion further decreases the mechanical strength and barrier properties of thiol-acrylate photopolymers that already exhibit decreased glass transition temperatures from the more flexible thio-ether linkage.[27,28] This shortcoming of thiol-acrylate systems may be significantly improved by incorporating well dispersed organoclays that may not only increase the toughness of neat thiol-ene photopolymers, but also enhance gas barrier properties by generating longer path-length for gas molecules.[19,28-31]

The inherent control of reaction mechanism by incorporating polymerizable organoclays provides an intriguing means to control polymer properties. This research investigates the effects of polymerizable organoclays on the ultimate performance of photopolymer clay nanocomposites including gas barrier properties and various thermo-mechanical properties such as glass transition temperature, storage modulus, ultimate elongation, Young's modulus, and tensile strength in both acrylate and thiol-acrylate photopolymers. Additionally, reaction kinetics of systems with and without organoclays is investigated to provide context for the nanocomposite behavior. Toughness of the material, determined by the area of stress-strain curves, was also compared as a

parameter for discussing quantitative impact of organoclays on overall mechanical performance of nanocomposite materials. To study the effect of organoclays on improving gas barrier properties of photopolymer-clay systems, water vapor permeability was examined based on an industrial ASTM standard with different monomers as well as organoclay type. The results from this study provide an effective platform for design of advanced photopolymer-clay nanocomposites to overcome drawbacks in conventional acrylate photopolymer materials.

## Experimental

### Materials

Tripolypropylene glycol diacrylate (TrPGDA), polyethylene glycol (600) diacrylate (PEGDA, MW=742), trimethylolpropane triacrylate (TMPTA), and polyester based urethane acrylate oligomer (CN9009, MW ~2,000) were supplied by Sartomer Inc. (Exton, PA). Trifunctional trimethylolpropane trimercaptopropionate (TMPTMP) was obtained from Aldrich. Cloisite Na (Southern Clay Products – Gonzalez, TX) was used for natural montmorillonite clay. Cloisite 93A (CL93A, Southern Clay Products), montmorillonite clay modified with dihydrogenated tallow, was used as a typical nonreactive organoclay. To produce polymerizable organoclays, sodium cations between silicate platelets of Cloisite Na were ion exchanged using acrylate or thiol functionalized quaternary ammonium surfactants as described elsewhere.<sup>14</sup> C16A acrylated organoclay bearing acrylate functional groups on the clay surfaces was produced utilizing hexadecyl-2-acryloyloxy(ethyl) dimethylammonium bromide (C16A surfactant) synthesized following methodologies described previously.<sup>14,15</sup> PSH2 thiol functionalized organoclays were synthesized via Michael addition reaction between thiol groups of tri functional TMPTMP and the acrylate groups from C16A acrylated

organoclay based on prior procedures.[16] The chemical structures of monomers and surfactants used in this research are illustrated in Figure 8.1. Unless otherwise noted, 0.5 wt% 2,2-dimethoxyphenyl acetophenone (DMPA, Ciba Specialty Chemicals) was used as a free radical photoinitiator in all experiments. All chemicals including monomers and clays were used as received.

## Methods

Thiol-ene photopolymerization kinetics were studied using real time infrared spectroscopy (RTIR, Thermo Nicolet Nexus 670). RTIR samples were prepared by sandwiching monomer mixtures between two sodium chloride plates. Measurements were performed at ambient temperature after purging the RTIR chamber for 6 minutes with dry nitrogen gas. UV light was provided by an optical fiber from a medium pressure mercury lamp (EXFO Acticure). Functional group conversion was evaluated by monitoring the decrease in the height of the absorbance peak at  $810\text{ cm}^{-1}$  for acrylate and at  $2575\text{ cm}^{-1}$  for thiol.[32,33] Photopolymerization reactions were initiated with a 365 nm light at  $3.0\text{ mW/cm}^2$ .

Dynamic mechanic analysis (DMA- Q800 DMA TA Instruments) was conducted to investigate the effect of organoclays on ultimate thermo-mechanical properties. To fabricate samples (2mm x 13mm x 25mm) for testing, liquid monomer mixtures were injected between two microscope slides end-capped with 2 mm spacers. The sample was then irradiated for ten minutes on each side using 365 nm UV at  $3.6\text{ mW/cm}^2$  intensity under nitrogen atmosphere. To measure the modulus and glass transition temperature, samples were heated from  $-100^\circ\text{C}$  to  $100^\circ\text{C}$  at  $30^\circ\text{C/min}$ . Measurements were made using the two point bending mode at 1Hz frequency.

Tensile experiments were conducted based on DMA controlled force tensile mode



with 0.5N/min ramp rate at 30°C using rectangular samples (1mm x 5mm x 20mm), prepared using the same process described previously with 1mm spacing glass molds. The most important factor for achieving reproducibility of the tensile experiments was the force ramp rate. Whereas 2N/min ramp rate generated high experimental errors as high as 20%, the error was reduced to about 5% for all nanocomposite compositions by utilizing a relatively low ramp rate of 0.5N/min. Young's modulus was calculated utilizing the slope of the stress-strain curve.

Water vapor transmission rate (WVTR) of photopolymer-clay nanocomposites including 3wt% (organo)clay was examined based on an ASTM standard (ASTM E96 34) utilizing thin polymer films in comparison with neat systems. To fabricate the 100  $\mu$ m composite films, controlled amounts of liquid monomer mixtures were placed between thick glass plates (150mm x 150mm x 20 mm).

Glass plates were covered with 100 $\mu$ m thick polyvinylidene difluoride film to allow easy release of the cured polymer films. On one of the glass plates, thin tape spacers were attached to control the cured film thickness. After placing the monomer mixtures on the bottom glass plate, bubbles were removed by applying a vacuum to prevent pin-hole formation. Afterward, the upper plate was covered and the plates were clamped. The mold was then exposed to 250~450 nm UV light at 18 mW/cm<sup>2</sup> for 5 minutes on each side. Before covering the glass WVTR vessel (12cm diameter opening) with the prepared thin films, 100g of distilled water was charged into the vessel. The sealed vessels were placed in a convection hood controlled at 23°C and mass loss was measured. WVTR per unit area was calculated considering the thickness of composite films.

## Results and Discussion

Many results for organic-inorganic composites have shown that the use of well dispersed inorganic fillers improve properties of polymer systems.[1,4] If inorganic fillers can chemically react with the organic phase, interactions between the filler surface and polymer matrix may increase to a greater degree than in systems with nonreactive fillers.[26] Interestingly, the incorporation of polymerizable organoclays into photopolymerization systems typically enhances the polymerization rate, whereas the rate usually decreases when nonreactive clays are added due to reduction in incident light energy.[13,14] In addition, the type of functional group, e.g. (meth)acrylate or thiol, on the clay surface significantly affects the polymerization kinetics and mechanism of thiol-acrylate systems.[20-22]

The type of functional group on the organoclay surfaces directs polymerization behavior by affecting the stoichiometric balance between thiol and ene functional groups in the clay galleries and by affecting the primary type of radicals on the clay surfaces, resulting in different degree of thiol-ene reaction with different polymerizable organoclays. Such results indicate a great degree of interaction between the clay and polymers when reactive functional groups are incorporated on the clay surfaces. Therefore, it is reasonable to expect that more improvement in the ultimate composite performance could be achieved with polymerizable organoclays than with conventional nonreactive organoclays.

To verify this hypothesis, the effect of adding organoclays on thermo-mechanical property and polymerization behavior of thiol-ene photopolymer-clay systems was investigated with different reactive and nonreactive organoclays. In previous studies, low molecular weight monomers were used for thiol-acrylate compositions as the high functional group concentration in these systems allowed good contrast in polymerization kinetics.[21,22] For examination of the ultimate composite performance such as mechanical and barrier properties, however, polymerized materials need sufficient toughness to make and handle thin films. For instance, to conduct tensile tests using

acrylate or thiol-acrylate formulations, use of suitable amounts of oligomers that increase the toughness of cured polymers is needed because simple monomeric compositions based on low molecular weight multifunctional acrylate or thiol-acrylate mixtures are typically too brittle or weak for such experiments utilizing thin films. For this reason, mixtures of polyethyleneglycol diacrylate (PEGDA) and polyester based urethane acrylate (CN9009) were used for the oligomer system. Appropriate ratios were determined considering the flexibility and the strength of the cured films. Tripropyleneglycol diacrylate (TrPGDA) was also added to the oligomer mixture to adjust the viscosity of liquid reactant mixture. For the thiol-acrylate mixture, trithiol trimethylolpropane trimercaptopropionate (TMPTMP) was added to the basic acrylate mixture with CN9009/PEGDA/TrPGDA using a 3:3:4 mass ratio. The amount of TMPTMP was controlled based on the overall mole ratio between acrylate and thiol functional groups in the system.

Based on the potential impacts of polymerization behavior on network formation, understanding the relationship between polymerization kinetics and final properties may be crucial for improvement of basic thiol-acrylate materials. Therefore, the photopolymerization behavior was examined using RTIR kinetic experiments. The acrylate conversion and thiol conversion as a function of time for CN9009/PEGDA/TrPGDA systems including 20mol% thiol from TMPTMP are shown in Figure 8.2 with and without 5wt% organoclays. As shown in the reaction conversion profiles (Figure 8.2(A)), the incorporation of the different organoclays does not change the acrylate conversion profiles significantly. Ultimate acrylate conversion varies only from 0.90 for the system with nonreactive organoclay to 0.96 by adding acrylated polymerizable organoclay with the neat system showing a conversion of 0.93. The addition of nonreactive organoclay slightly decreases polymerization rate but not nearly to the degree observed in previous research [21,22] when a nonreactive organoclay was added to low molecular weight monomeric thiol-acrylate polymerization systems. This difference



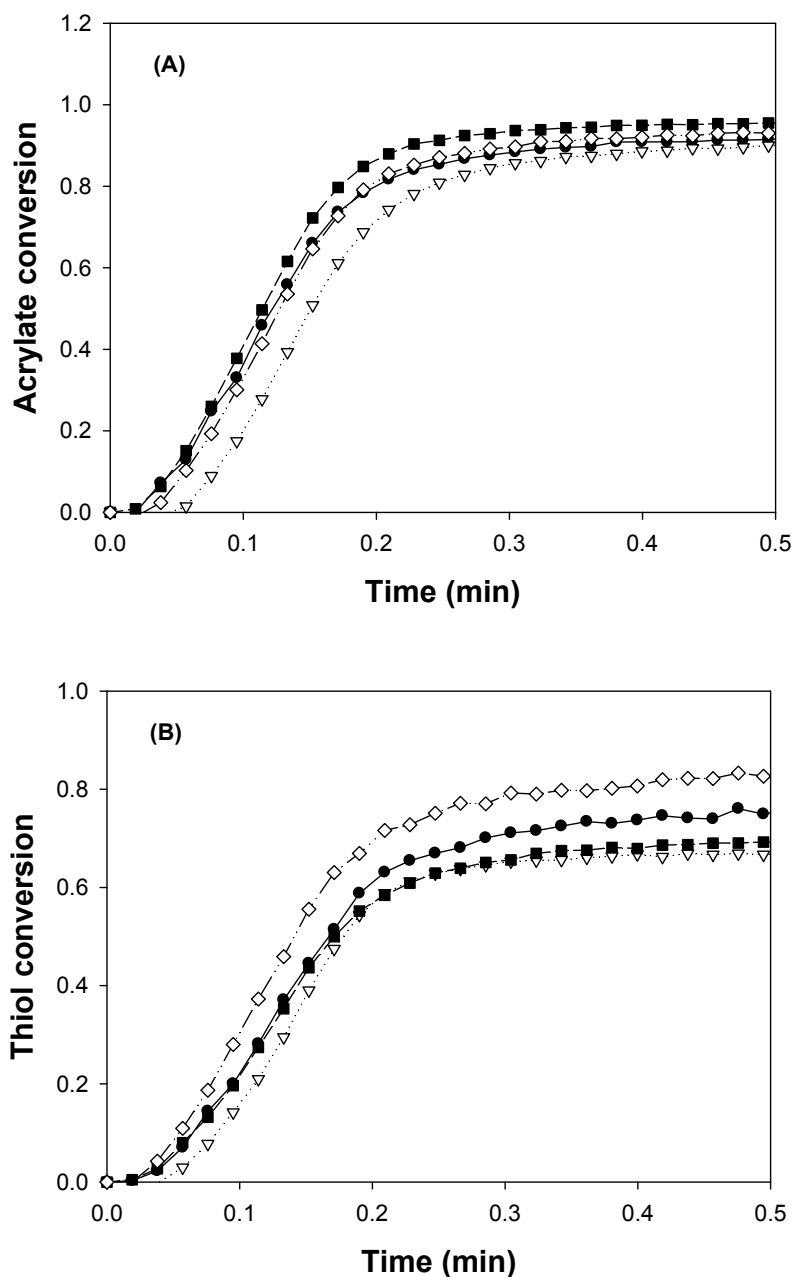


**Figure 8.2.** RTIR conversion profiles of CN9009/PEGDA/TRPGDA (3:3:4 by mass) mixtures including 20mol% thiol from TMPTMP with and without addition of 3wt% organoclays. Shown are profiles of (A) acrylate conversion for neat CN9009/PEGDA/TRPGDA (●), CN9009/PEGDA/TRPGDA/TMPTMP with 3 wt% CL93A (▽), 3 wt% C16A (■), and 3 wt% PSH2 (◇) organoclay and (B) thiol conversion for neat CN9009/PEGDA/TRPGDA/TMPTMP (●), CN9009/PEGDA/TRPGDA/TMPTMP with 3 wt% CL93A (▽), 3 wt% C16A (■), and 3 wt% PSH2 (◇) organoclay. Polymerizations were initiated with 0.2 wt% DMPA using 365nm light at 3.0 mW/cm<sup>2</sup>.

indicates that the increased system viscosity from incorporating oligomers reduces bimolecular termination which is more dominant in low viscosity monomer systems.

Thiol conversion profiles in Figure 8.2(B), however, show much different behavior based on the type of organoclay. Incorporation of a thiolated organoclay induces significant increases in photopolymerization rate and final thiol conversion. The incorporation of either non-reactive CL93A or acrylated C16A organoclay decreases ultimate thiol conversion to about 70% from 79% in the neat system, while the same amount of PSH2 thiolated organoclays increases thiol conversion to 87%, corresponding to a 10% enhancement. Even in this oligomer-monomer mixture that is similar to many practical formulations in industrial applications, it appears that ultimate thiol conversion can be varied over a 20% range simply with changing the organoclay type.

To determine whether these kinetic effects influence thermo-mechanical properties of thiol-ene photopolymer-clay systems, dynamic mechanical analysis (DMA) experiments were conducted for the same CN9009/PEGDA/TrPGDA/TMPTMP system including 20mol% thiol. The storage modulus profiles as a function of temperature with addition of 5 wt% organoclays are shown in Figure 8.3. The incorporation of either nonreactive CL93A or C16A acrylated organoclay increases the rubbery storage modulus, whereas the modulus of the thiolated organoclay system is slightly less than that of the neat system. Based on similar or enhanced degree of acrylate homopolymerization in CL93A and acrylated organoclay system, the inorganic filler generates a higher modulus than in the neat system. For the thiolated organoclay systems where the thiol conversion is much higher than that of the neat system, on the other hand, the storage modulus decreases due to formation of more flexible thio-ether linkages in the polymer network, which mitigates the strengthening effect from the inorganic filler. This modulus behavior of photopolymer clay systems confirms that increased acrylate homopolymerization through addition of acrylated organoclay forms harder domains in the nanocomposites

while thiolated organoclays induces a more flexible network due to enhanced thiol-ene step growth reaction.

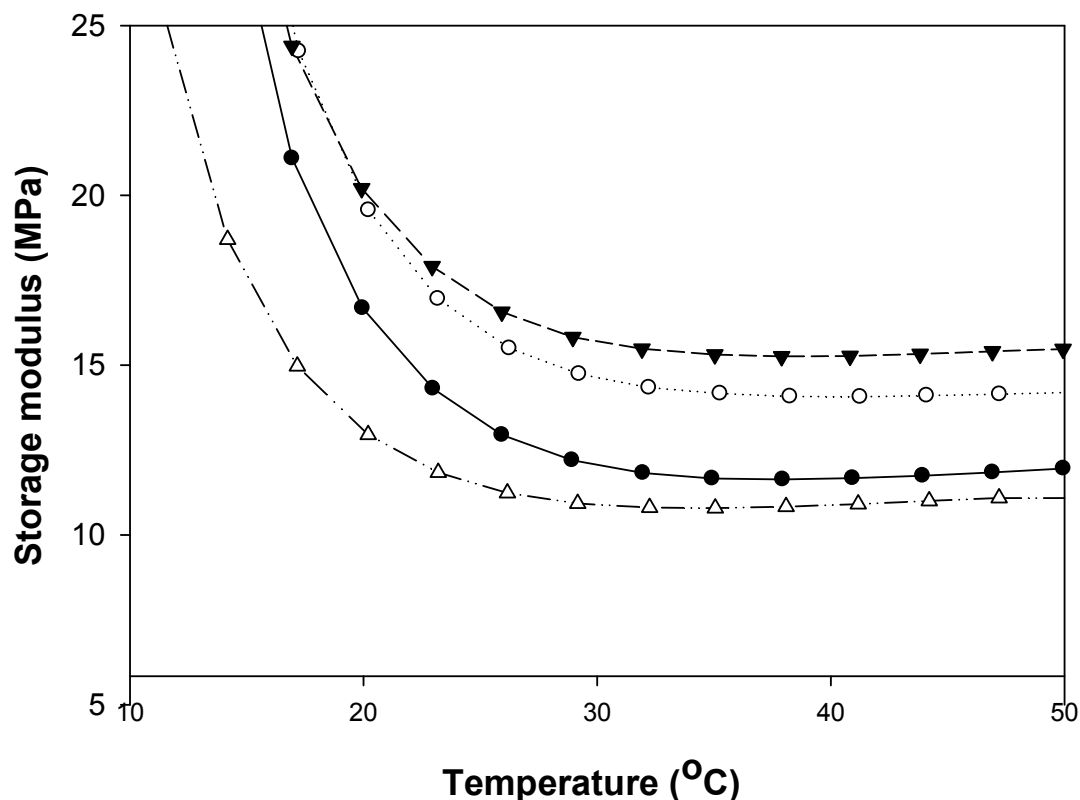


**Figure 8.3.** Storage modulus profiles of CN9009/PEGDA/TRPGDA (3:3:4 by mass) mixtures including 20mol% thiol from TMPTMP with and without addition of 5wt% organoclays. Shown are profiles for neat CN9009/PEGDA/TRPGDA/TMPTMP (●), CN9009/PEGDA/TRPGDA/ TMPTMP with 5 wt% CL93A (○), with 5 wt% C16A-acrylated organoclay (▼), and 5 wt% PSH2 thiolated organoclay (Δ). Samples were photopolymerized with 0.5 wt% DMPA using 365 nm light at 3.6 mW/cm<sup>2</sup>.

Further evidence of this effect is provided by the glass transition temperature behavior of these thiol-acrylate systems with addition of polymerizable organoclays into the CN9009/PEGDA/TrPGDA/TMPTMP formulation. As shown in Figure 8.4 (A), no significant change in the glass transition temperature, as indicated by the tan  $\delta$  peak of the

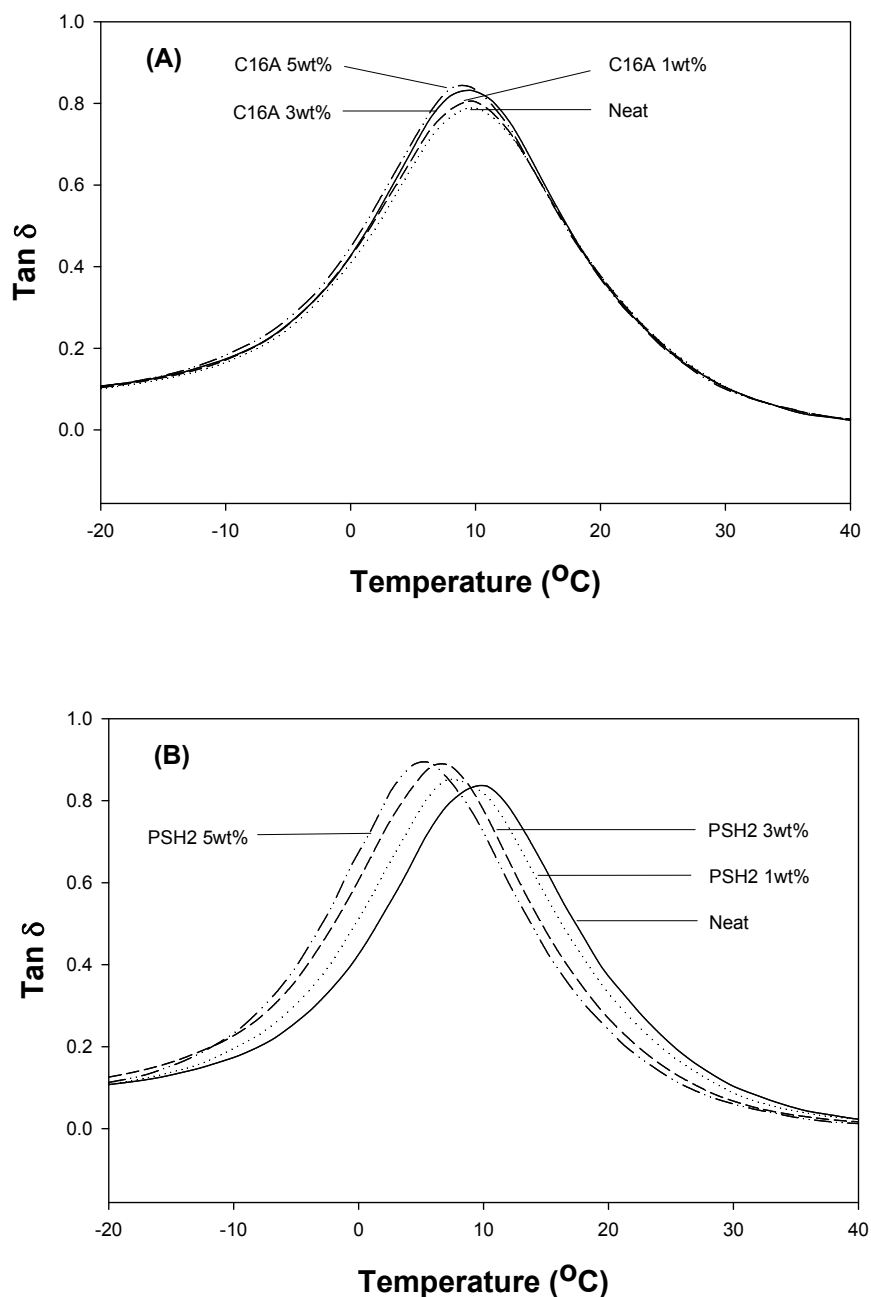


**Figure 8.4.**  $\text{Tan } \delta$  profiles as a function of temperature of CN9009/PEGDA/TRPGDA (3:3:4 by mass) mixtures including 20mol% thiol from TMPTMP with increase of organoclay amount. Shown are profiles of the systems (A) with 1wt%, 3wt%, and 5wt% C16A acrylated organoclays and (B) with 1wt%, 3wt%, and 5wt% PSH2 thiolated organoclays. The profile for the neat CN9009/PEGDA/TRPGDA/TMPTMP system is included in each figure for comparison. Samples were photopolymerized with 0.5 wt% DMPA using 365 nm light at  $3.6 \text{ mW/cm}^2$ .

system, is observed when increasing the amount of C16A acrylated organoclay up to 5wt%. The addition of PSH2 thiolated organoclays, however, decreases the glass transition temperature as shown in Figure 8.4 (A), due to the enhancement of thiol-ene reaction and greater flexibility in the network. The glass transition temperature decreases about 3°C from that of the neat system by the addition of only 1wt% thiolated organoclay and continues to decrease by increasing the clay amount up to 5wt% with a 6°C substantial decrease.

In many applications, tensile properties such as toughness, overall elongation, and Young's modulus are practical indicators regarding material performance. To investigate the organoclay effects on these mechanical properties of photopolymer clay composites, tensile elongation experiments were performed utilizing DMA for the 20 mol% thiol CN9009/PEGDA/TrPGDA/TMPTMP composition. Figure 8.5 shows the tensile stress profiles as a function of strain until break of the cured films produced with increased amounts of thiolated or acrylated organoclays. The stress-strain profile for the neat system is also included in each figure for comparison. By adding thiolated organoclays as shown in Figure 8.5(A), ultimate elongation to break for the photopolymer clay composites are enhanced while the slope of the profiles, corresponding to the stiffness, (or Young's modulus), of the materials, does not change significantly. The addition of only 3wt% thiolated organoclay induces an enhancement of over 70% in ultimate elongation. Interestingly, the addition of acrylated organoclays increases the stiffness of the materials while the overall elongation to break does not change significantly as shown in Figure 8.5(B). By adding 1, 3, and 5wt% acrylated organoclay, the Young's moduli of photopolymer-clay composites increase 20% as with 1wt% organoclay to as much as 80% with 5wt% organoclay as compared to the neat system. These different results in tensile behavior are primarily due to the difference in polymerization mechanisms based on the type of reactive groups in polymerizable organoclays. Again, based on facilitated acrylate homopolymerization by incorporation of acrylated organoclays, cross-linking

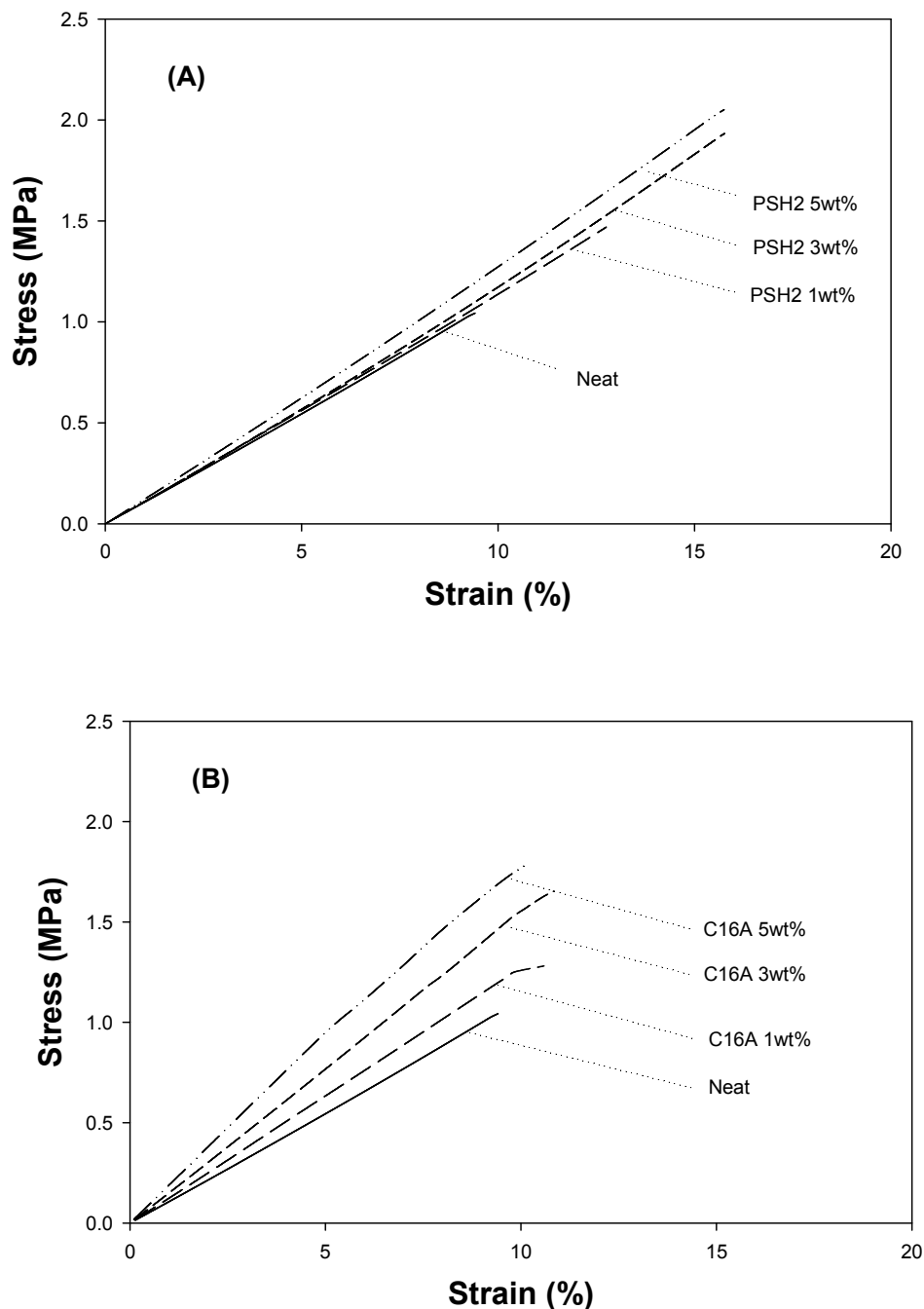


**Figure 8.5.** DMA tensile profiles of CN9009/PEGDA/TRPGDA (3:3:4 by mass) mixtures including 20mol% thiol from TMPTMP with increase of organoclay amount. Shown are profiles of the systems (A) with 1wt%, 3wt%, and 5wt% PSH2 thiolated organoclays and (B) with 1wt%, 3wt%, and 5wt% C16A acrylated organoclays. The profile for the neat CN9009/PEGDA/TRPGDA/TMPTMP system is included in each Figure for comparison. Samples were photopolymerized with 0.5 wt% DMPA using 365 nm light at 3.6 mW/cm<sup>2</sup>.

density is increased which induces greater stiffness in the composites. Thiolated organoclays, on the other hand, produce more flexible polymer networks that are able to withstand greater deformation by enhancing the thiol-ene reaction that allows more homogeneous polymerization with reduced cross-linking density based on the step-growth reaction. While one acrylate double bond acts as a difunctional group in chain acrylate homopolymerization, which induce the polymer network, the same double bond in a thiol-ene step mechanism reacts with thiol only once thus becoming monofunctional, resulting in lower cross-linking density.

Figure 8.6 shows the overall comparison of organoclay effects in elongation properties by adding 3wt% of nonreactive, acrylated, and thiolated organoclays into the thiol-acrylate mixture. This comparison clearly demonstrates how the organoclays structure induces different tensile properties in thiol-acrylate photopolymer clay composites. While adding nonreactive organoclay (Cloisite 93A) slightly increases the stiffness with some decrease in ultimate elongation, addition of polymerizable organoclays improves either ultimate elongation (thiolated organoclay) or Young's modulus (acrylated organoclay). This behavior also indicates that the interaction between clay surfaces and polymer matrices are significantly improved by incorporating reactive groups on the clay surfaces,[14,21] not only by inducing enhanced clay exfoliation but also by reacting with monomers and oligomers during the photopolymerization, forming strong covalent bonds between the filler surface and organic polymer networks.

In addition to tensile strength and elongation, the overall toughness of a material is an important parameter indicating energy absorptive capacity and durability of materials in many engineering applications. The toughness of a material is typically defined as the overall energy needed to deform the materials to failure and is commonly found from the area under stress-strain curves in tensile experiments.[35] Figure 8.7 (A) shows the toughness as calculated by the area under the stress-strain curve and normalized to the toughness of the neat system. Toughness of composites with 3wt% of

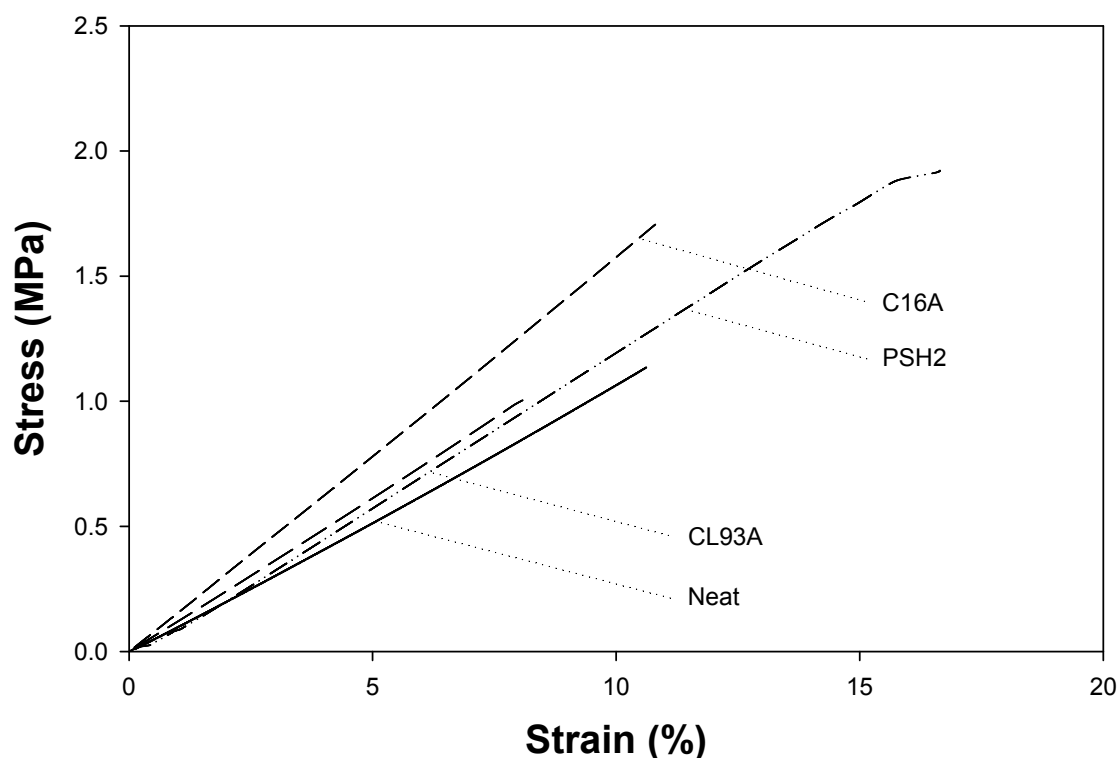


**Figure 8.6.** Comparison of DMA tensile profiles by adding 3wt% different type of organoclays into CN9009/PEGDA/TRPGDA (3:3:4 by mass) mixtures including 20mol% thiol from TMPTMP. The profile for the neat CN9009/PEGDA/TRPGDA/TMPTMP system is included for comparison. Samples were photopolymerized with 0.5 wt% DMPA using 365 nm light at 3.6 mW/cm<sup>2</sup>.

organoclays into thiol-acrylate mixture including 20mol% thiol are compared. The average toughness for each composition was obtained based on three independent tensile experiments. The addition of either C16A acrylated or PSH2 thiolated polymerizable organoclays induces 60 and 80% increases in toughness of the thiol-acrylate mixture compared to that of neat system, respectively while nonreactive Cloisite 93A decreases the toughness about 10%.



To determine the impact of the polymerizable organoclay in the acrylate photopolymerization system without thiol, tensile experiments were performed to evaluate the formulation utilizing the basic acrylate mixture as summarized in Figure 8.7 (B). Incorporation of nonreactive CL93A organoclay slightly reduces the toughness again. The addition of the two polymerizable organoclays induces a 30 to 40% increase in toughness of the acrylate mixture with thiolated organoclay producing the greatest toughness increase. This trend is similar to that observed in the thiol-acrylate mixtures but the degree of enhancement is significantly smaller in each organoclay system. It is also important to note that the use of thiolated organoclay also increases the elongation of composite films significantly whereas adding acrylated organoclay basically induces the highest Young's modulus. These results provide opportunity to control the mechanical properties of nanocomposites simply by choosing the organoclay type to control. For instance, with significant enhancement in overall toughness of both polymerizable organoclay systems, the use of acrylated organoclay can make materials stiffer while the addition of thiolated organoclay produces more flexible nanocomposites than the neat system.

Gas barrier properties for many gases such as oxygen and water vapor are often important characteristics in many photopolymer applications such as coating and film packaging. It is well known that the addition of plate shape inorganic fillers such as silicates and micas can often improve the gas barrier properties by generating a longer diffusion path for gaseous materials.[19] To demonstrate the impact of organoclay on barrier properties, the water vapor transmission rate (WVTR) through photopolymer clay nanocomposite films including organoclays was compared. In studying the gas transfer rate, homogeneity in the thickness of the thin film and the absence of defects are critical to achieve good experimental results. The ultimate cured film thickness was thus controlled to 100 microns with at most 5% error. In addition, to make thin films that are not easily damaged during removal from the mold, the toughness of the cured film

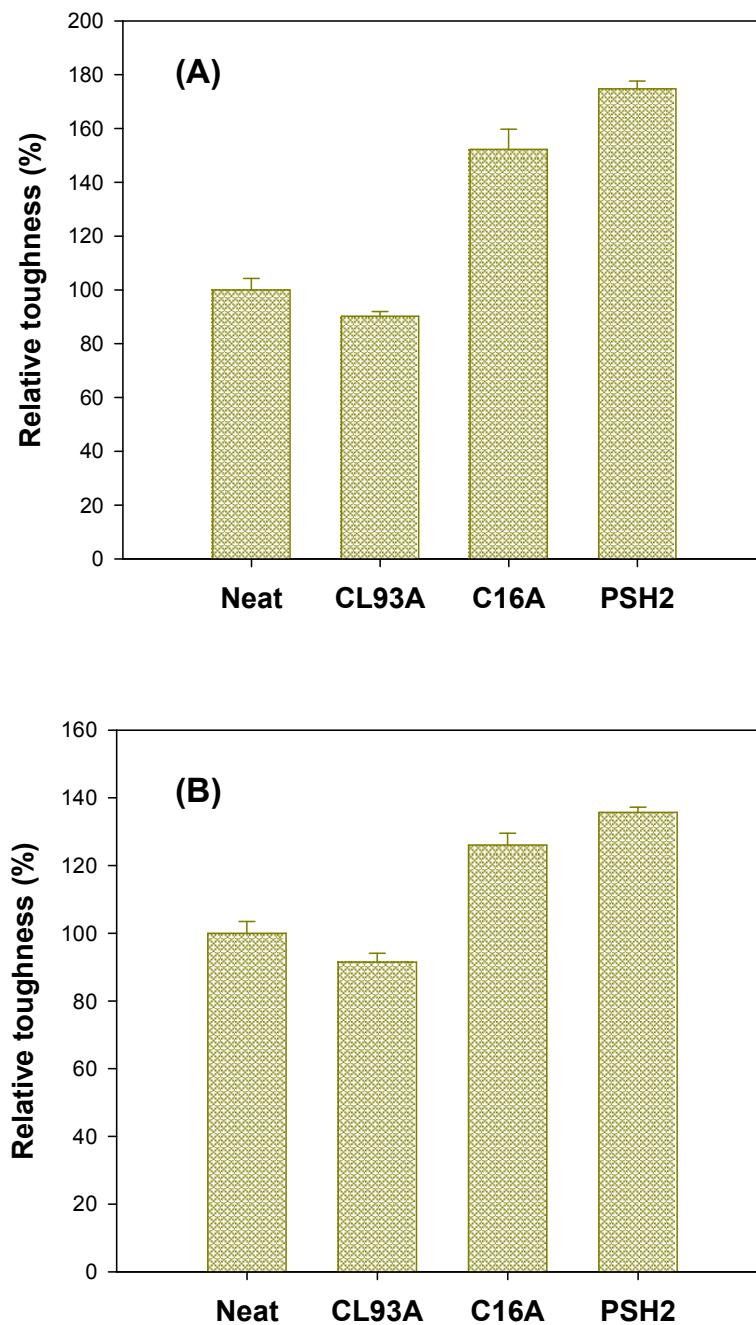


**Figure 8.7.** Comparison of relative toughness of the systems without or with addition of 3wt% different type of organoclays into (A) CN9009/PEGDA/TRPGDA (3:3:4 by mass) acrylate mixtures and (B) CN9009/PEGDA/TRPGDA (3:3:4 by mass) thiol-acrylate mixtures including 20mol% thiol from TMPTMP. Toughness is calculated from the area of stress-strain curves in Figure 8.5 and 8.6.

needed to be increased from that observed in the mechanical testing. To this end, the thiol concentration of the basic thiol-acrylate formulation was decreased to 8mol%. The ratio of acrylic monomer-composition was not changed. To compare the experimental reproducibility with an ASTM standard, 100  $\mu\text{m}$  PET film (Mylar) was used as the control system. The measured WVTR value of the PET film was compared with the literature value obtained based on a similar methodology.[36]

To investigate the organoclay effect on WVTR of photopolymer clay systems, 3wt% of various organoclays were incorporated and compared with neat and natural clay systems. Figure 8.8 shows the water loss through the composite films as a function of time for the CN9009/PEGDA/TrPGDA mixture including 8mol% thiol from TMPTMP. The neat system is also evaluated for comparison with the result for Mylar PET film included to confirm experimental reproducibility. Measurements were performed for 28 days by recording the weight change from the initial weight of each experimental set. As shown in Figure 8.8, adding 3wt% organoclays more significantly decreases the rate of water loss through the composite film than adding CL Na natural clay, but there appears to be no significant difference between organoclay systems. Even the system with nonreactive CL93A organoclay exhibits a similar trend in weight change as compared to those of systems with polymerizable organoclays.

Water vapor transmission ratio (WVTR) for each system is calculated from the overall water loss after 28 days. This data is summarized in Figure 8.9 after normalization for the film thickness. Each WVTR value is thus based on a 100 micron thickness. As shown in Figure 8.9, WVTR of a 100 micron Mylar film is 4.3  $\text{g}/\text{m}^2/\text{day}$  with literature value using similar experimental condition at 3.5  $\text{g}/\text{m}^2/\text{day}$ .[36,37] The experimental value is slightly higher than the reference values but experimental accuracy appears reasonable. Addition of 3wt% natural clay (CL Na) reduces WVTR about 16% from the value of the neat system. Further decrease in WVTR is observed when organoclays are incorporated into the thiol-acrylate mixture. Approximately 30% reduction in WVTR is

achieved by adding 3wt% CL93A or polymerizable organoclays, suggesting that the clay effect on water permeability is within the experimental error when clay is organically modified and thereby dispersed with at least an intercalated morphology. The

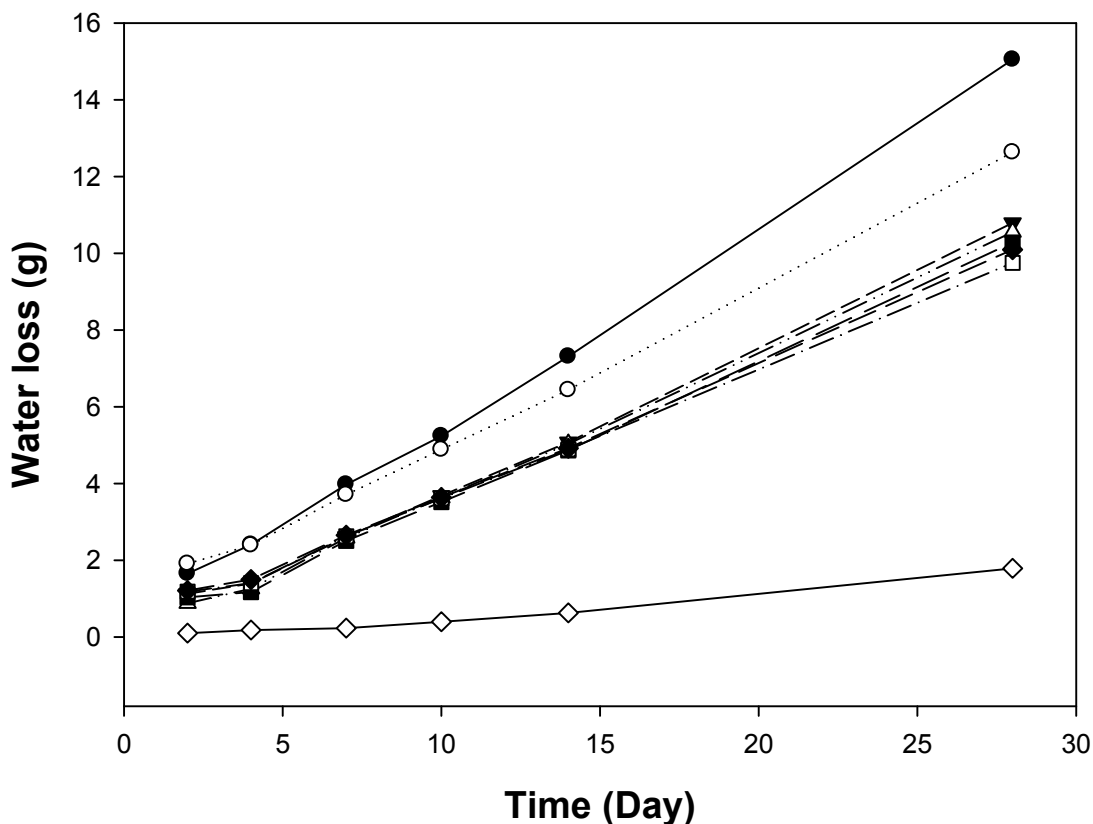


**Figure 8.8.** Water weight loss profiles as a function of time from water vapor permeation tests based on the ASTM E96 standard with and without addition of 3wt% organoclay into CN9009/PEGDA/TRPGDA (3:3:4 by mass) mixtures including 8mol% thiol from TMPTMP. Shown are profiles normalized by film thickness of the systems with 100 $\mu$ m thick films for neat CN9009/PEGDA/TRPGDA/TMPTMP (●), CN9009/PEGDA/TRPGDA/TMPTMP with 3 wt% CL Na natural clay (○), with 3 wt% CL93A organoclay (▼), with 3 wt% C16A-acrylated organoclay (Δ, ■), and with 3wt% PSH2 thiolated organoclays (□, ◆). Samples were photopolymerized with 0.5 wt% DMPA using 250~450 nm light at 18 mW/cm<sup>2</sup>. The result using Mylar PET (100 $\mu$ m) film (◇) is included for evaluation of experimental accuracy.

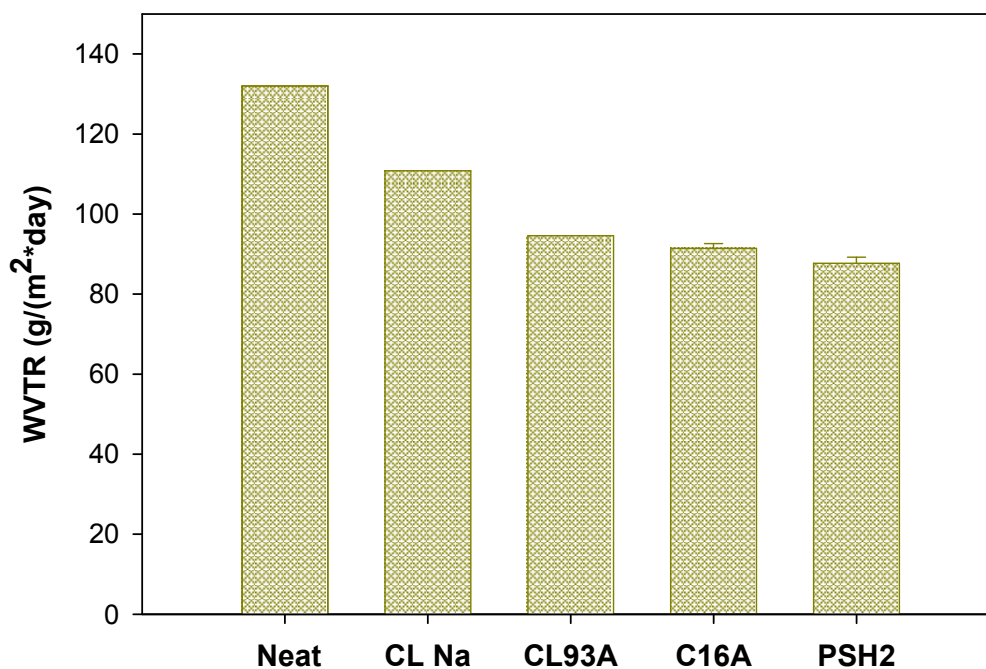


**Figure 8.9.** Water Vapor Transmission Rate (WVTR) as a function of (organo)clay type in the thiol-acrylate systems based on CN9009/PEGDA/TRPGDA (3:3:4 by mass) mixtures including 8mol% thiol from TMPTMP without or with addition of 3wt% different type of organoclay. WVTR is calculated utilizing the results from Figure 8.8.

incorporation of thiolated organoclay induces decreases in glass transition temperature of the composites due to increased thiol-ene reaction as discussed previously, which may increase gas molecule passage through the composite layer. This WVTR behavior clearly shows that barrier properties are not detrimentally affected by incorporating thiolated organoclays into thiol-acrylate systems. The results are particularly interesting because a 30% decrease in WVTR is possible by adding only 3wt% organoclay.

The copolymerization of acrylate and thiol monomers produces more homogeneous networks with higher refractive index than acrylate polymers due to higher

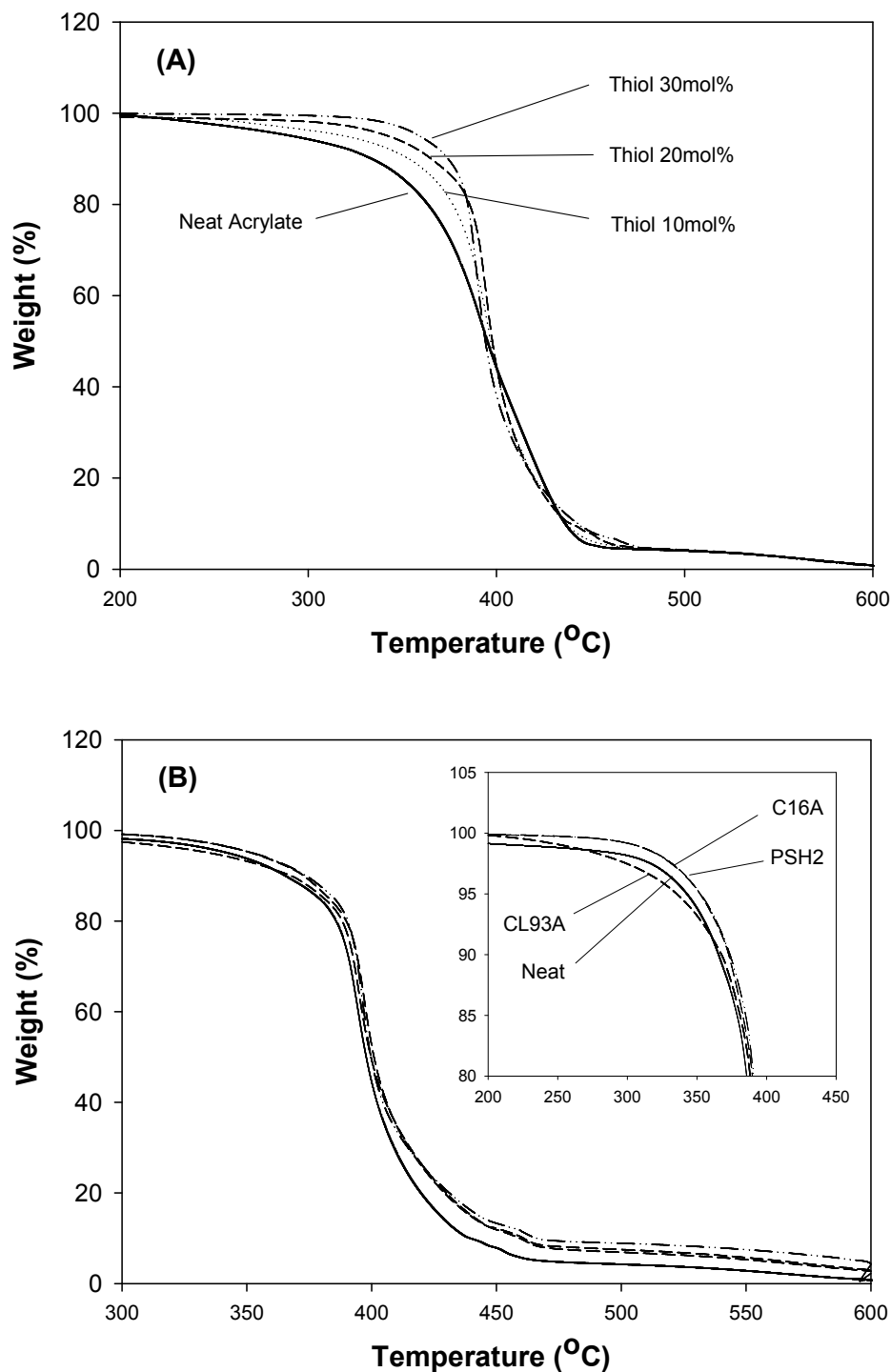


**Figure 8.10.** TGA thermal degradation profiles in air of (A) PEGDA/TrPGDA (50/50 by mass) systems with gradual increase of TMPTMP thiol monomers up to 30 mol% and (B) PEGDA/TrPGDA (50/50 by mass) systems including 20mol% thiol from TMPTMP without or with addition of 5wt% organoclays. Samples were polymerized at  $3.0\text{mW}/\text{cm}^2$  using 0.2wt% DMPA.

atomic mass of sulfur in the thiol.[38] Similarly, the inclusion of heavier atoms in polymer networks often increases the thermal stability of polymeric materials but little is known about this effect in thiol-ene systems. In addition, it has been reported that incorporating clays enhances the thermal stability of acrylate polymers significantly.[6, 39] To investigate how the addition of thiol monomers as well as the inclusion of organoclays affects the thermal stability of ultimate thiol-acrylate photopolymer-clay nanocomposites, TGA experiments have been performed for the thiol-acrylate systems with and without addition of organoclays.

Figure 8.10 shows TGA profiles of thiol-acrylate systems without organoclays by increasing TMPTMP thiol monomers into PEGDA/TrPGDA mixture (Figure 8.10 (A)) and with addition of 5wt% organoclays (Figure 8.10 (B)). Comparing the profiles in Figure 8.10 (A), significant enhancement in thermal stability is observed by increasing thiol mol%. The neat acrylate system shows an initial degradation temperature of about 250°C. The degradation temperature is elevated to over 350°C by adding 30mol% of thiol functional groups. As seen in Figure 8.10 (B), however, the addition of organoclays into thiol-ene polymer including 20mol% thiol does not change the degradation temperature significantly. Again, no significant decrease in thermal stability is observed by adding thiolated organoclay though it induces a lower glass transition temperature than other organoclays. Cautiously comparing the profiles in Figure 8.10 (B), thiolated organoclay system show even slightly enhanced thermal stability at below degradation temperature than other systems.

### Conclusions

Incorporation of organoclay affects polymerization behavior and ultimate nanocomposite performance including thermo-mechanical and gas barrier properties in

photocurable thiol-acrylate systems. Incorporation of thiolated organoclay induces higher thiol-ene reaction than other organoclays which has a significant effect on nanocomposite characteristics. The addition of only 5wt% acrylate organoclay, which enhances acrylate homopolymerization, increases the tensile modulus 80% with no significant changes in elongation and glass transition temperature. Thiolated organoclay, on the other hand, with greater thiol-ene polymerization induces greater flexibility in the nanocomposites with decreased glass transition temperature. Adding 3wt% thiolated organoclays induces a 70% increase in elongation without changing Young's modulus significantly. The toughness of nanocomposites, as measured by the area under stress-strain curves, is substantially improved by adding polymerizable organoclays. The addition 3wt% acrylated or thiolated polymerizable organoclays induces 60% and 80% increases in toughness respectively, while nonreactive organoclay actually decreases toughness. Additionally, gas barrier properties of clay nanocomposites are also influenced by addition of organoclays. Both polymerizable and nonreactive organoclays improve WVTR of the nanocomposites. While adding 3wt% natural clay reduces WVTR 16% compared to that of neat system, polymerizable and nonreactive organoclays decrease it about 30%.



Notes

1. Rodriguez, F.; Cohen, C.; Ober, C. K.; Archer, L. A. *Principles of Polymer Systems*, Taylor & Francis, New York, 2003, Ch.9, 405.
2. Vaia, R. A.; Giannelis, E. P. *Macromolecules* **1997**, 30, 7990.
3. Alexandre, M.; Dubois, P. *Mater. Sci. Eng.* **2000**, 28, 1.
4. Ray, S. S.; Okamoto, M. *Prog. Polym. Sci.* **2003**, 28, 1539.
5. Uhl F. M.; Davuluri S. P.; Wong S. C.; Webster D. C. *Chem. Mater.* **2004**, 16, 1135.
6. Beck, E.; Lokai, E.; Nissler, H. *RadTech Int. North America, Nashville*, **1996**, 160.
7. LeBaron, P. C.; Wang, Z.; Pinnavaia, T. J. *Appl. Clay Sci.* **1999**, 15, 11.
8. Ogawa, M.; Kuroda, K.; Bull. *Chem. Soc. Jap.* **1997**, 70, 2593.
9. Wang, Z.; Pinnavaia, T. J. *Chem. Mater.* **1998**, 10, 1820.
10. Decker, C.; Zahouily, K.; Keller, L.; Benfarhi, S.; Bendaikha, T.; Baron, J. *J. of Mater. Sci.* **2002**, 23, 4831.
11. Uhl, F. M.; Hinderliter, B. R.; Davuluri, S. P. *Mater. Res. Soc.* **2004**, 16, 203.
12. Tan, H.; Nie, J. *J. of Appl. Polym. Sci.* **2007**, 106, 2656.
13. Owusu-Adom, K.; Guymon, C. A. *Polymer* **2008**, 49, 2636.
14. Owusu-Adom, K.; Guymon, C. A. *Macromolecules* **2009**, 42, 180.
15. Decker, C. *Polym. Int.* **1998**, 45, 133.
16. Decker, C. *Prog. Polym. Sci.* **1996**, 21, 593.
17. Cramer N. B.; Scott J. P.; Bowman C. N. *Macromolecules* **2002**, 35, 5361.
18. Hoyle, C. E.; Lee, T. Y.; Roper, T. J. *Polym. Sci. A: Poly. Chem.* **2004**, 42, 5301.
19. Morgan, C. R.; Magnota, F.; Ketley, A. D. J. *Polym. Sci.: Polym. Chem. Ed.*, **1977**, 15, 627.
20. Owusu-Adom, K.; Guymon, C. A. *Macromolecules* **2009**, 42, 3275.
21. Kim S. K.; Guymon C. A. *J. Polym. Sci. Part A Polym. Chem.* **2011**, 49, 465.
22. Kim S. K.; Guymon C. A. submitted to *Europ. Pol. J*

23. Kim S. K.; Guymon C. A. submitted to *Polymer*
24. Kim S. K.; Guymon C. A. *In preparation*
25. Cramer, N. B.; Reddy, S. K.; O'Brien, A. K.; Bowman, C. N. *Macromolecules* **2003**, 36, 7964.
26. Lee, T. Y.; Carioscia, J.; Smith, Z.; Bowman, C. N. *Macromolecules* **2007**, 40, 1473.
27. Roper, T. M.; Kwee, T.; Lee, T. Y.; Guymon, C. A.; Hoyle C. E. *Polymer* **2004**, 45 2921.
28. Carioscia, J. A.; Lu, H.; Stansbury, J. W.; Bowman, C. N. *Dent. Mater.* **2005**, 21, 1137.
29. Zanetti, M.; Lomakin, S.; Camino, G. *Macromol. Mater. Eng.* **2000**, 279, 1.
30. Reichert P.; Kressler J.; Mulhaupt R.; Stoppelmann G. *Acta Polym.* **1998**, 49, 116.
31. Senyurt, A. F.; Wei, H.; Hoyle, C. E.; Piland, S. G.; Gould, T. E. *Macromolecules* **2007**, 40, 4901.
32. Cramer, N. B.; Scott, J. P.; Bowman, C. N. *Macromolecules* **2002**, 35, 5361.
33. Lee, T. Y.; Carioscia, J.; Smith, Z.; Bowman, C. N. *Macromolecules* **2007**, 40, 1473.
34. ASTM E96M-05, "Standard Test Methods for Water Vapor Transmission of Materials"
35. Rodriguez, F., Cohen, C., Ober, C. K., Archer, L. A., *Principles of Polymer Systems*, Taylor & Francis, New York, 2003, Ch.9, 263.
36. Auras, A. R.; Singh S. P.; Singh J. J. *Packaging Technology and Science* **2005**, 18:4, 207.
37. Wang C.; Lai P.C.; Syu S. H, Leu J. *Surface & Coatings Technology* **2011**, 206, 318.
38. Chan, W. J.; Zhou, H.; Hoyle, E. C.; Lowe, B. A. *Chem. Mater.* **2009**, 21, 1579.
39. Uhl, F. M.; Davuluri, S. P.; Wong, S. C.; Webster, D. C. *Polymer* **2004**, 45, 6175.

## CHAPTER 9

### CONCLUSIONS AND RECOMMENDATIONS

Nanocomposite materials based on various polymer matrices including inorganic particles with nanometer scale dimension have been intensively studied due to their unique characteristics that are not observed in conventional materials. This nanocomposite technology has had a significant impact on material design in various high-end applications including such as aerospace parts and biomaterials and will continue to attract research interest. One of the important challenges in nanocomposite production is the development of easy, cost-effective, and environmentally friendly processes. This motivation has guided research in producing nanocomposite materials based on *in situ* photopolymerization that combines the unique advantages of UV curing technology with potentially enhanced performance upon addition of nanometer scale inorganic fillers such as organoclays. Natural clay particles are relatively inexpensive and easily delaminated to nanometer scale through simple organic modification. With the recent and rapid expansion of photopolymer applications due to many advantages in processing and performance, therefore, research groups have studied *in situ* clay photopolymerization in pursuing new and advanced photopolymer materials.

The goal of this research has been the development of photopolymer clay nanocomposites having enhanced physical, thermal and barrier properties utilizing unique thiol-ene photopolymerization technique. Through extensive studies on dispersing organoclays modified by various quaternary ammonium surfactants, the factors governing the degree of clay exfoliation in diverse acrylate and thiol-acrylate monomer compositions have been demonstrated. Accompanying kinetic studies have revealed that the polymerization behavior of the systems including organoclays is closely related with clay morphology and the incorporated reactive groups in the organoclay structure.

Subsequent examination of various performance characteristics of photopolymer clay nanocomposites have shown the great influence of clay particles on properties of cured polymer networks and the possibility to modulate ultimate nanocomposite performance simply by controlling the organoclay structure. One major portion of this research has focused on detailed understanding of the correlations among the factors in nanocomposite formation such as monomer composition, clay dispersion, and photopolymerization behavior and their effect on evolution of ultimate nanocomposite properties. Another important thrust for this research have been centered around overcoming two major drawbacks in conventional free radical photopolymerization; i.e. severe polymerization shrinkage and oxygen inhibition. By introducing some degree of thiol-ene step reaction mechanism and by incorporating appropriate types of polymerizable organoclays, remarkable improvements in both hurdles has been achieved. Based on this research, fundamental understanding regarding the overall influence of incorporating systematically modified clay particles has been gained and this knowledge provides useful information in control of nanocomposite process and performance. The important achievements from this work are briefly summarized below with supporting results and the suggestion for future work.

Generally, while inorganic fillers may improve many thermal and mechanical properties of polymer materials, the addition of fillers into photopolymerizable systems decreases the reaction rate by both scattering and absorbing the incident light that initiates photopolymerization. Preliminary kinetic studies with only 1 wt% of natural montmorillonite clay significantly lowered the photopolymerization rate of tripropyleneglycol diacrylate (TrPGDA) and further decreases were observed by increasing clay concentration up to 10 wt%. Interestingly, the addition of well exfoliated clay particles modified with polymerizable surfactants bearing reactive groups induces a higher rate of photopolymerization, whereas the use of nonreactive organoclay still decreases the rate. It is believed that both increased surface area of polymerizable

organoclays based on enhanced clay exfoliation and incorporated reactive groups in the clay structure induce more interaction with monomers and thus immobilization of propagating chains on the clay surface might be facilitated, which decreases termination rate significantly. These synergetic clay effects may compensate for the light interference of clays resulting in increased overall polymerization rate, suggesting that the characteristics of organoclays and subsequent exfoliation behavior might be very important in photopolymerization behavior.

On the basis of this hypothesis, the relationship between clay exfoliation and photopolymerization kinetics was investigated utilizing various thiol-acrylate compositions by examining both reactive and nonreactive organoclays. Because monomer-clay interaction can be altered by the compatibility between the components, it is important that the polarity of monomers be close to that of the organoclays that may exhibit a wide range of polarities depending upon the organic modifiers. In addition, the difference in monomer diffusivity into clay galleries between thiol and acrylate monomers could potentially affect the stoichiometric balance especially near the functionalized clay surfaces, which may also significantly affect the photopolymerization behavior. For this reason, the effects of both monomer structure and the type of polymerizable organoclay on the thiol-ene photopolymerization behavior have been examined. Considering polarity, functionality, and viscosity of monomers, 1,6-hexanediol diacrylate (HDDA) was compared with less hydrophobic tripropyleneglycol diacrylate (TrPGDA). For thiol monomers, 1,6-hexanedithiol (HDT), which has a similar structure to HDDA, was selected as the dithiol monomer and trimethylolpropane trimercaptpropionate (TMPTMP) was used as a trithiol monomer to increase cross link density as well as the viscosity of monomer systems.

To investigate the impact of polymerizable organoclays on reaction behavior, 3 wt% C16A acrylated organoclay or PSH2 thiolated organoclay was mixed into HDDA/HDT and TrPGDA/HDT mixtures based on a 2:1 molar ratio. The polymerization

rate, examined by photo-DSC and RTIR, of HDDA/HDT system with thiolated organoclay is much faster than the system with acrylated organoclay. By changing the monomer system to TrPGDA/HDT, on the other hand, both polymerizable organoclays increase the polymerization rate significantly with increased clay concentration. Interestingly, further study correlating the acrylate conversion with the thiol conversion during polymerization revealed that adding thiolated organoclay facilitates thiol-ene step reaction whereas acrylated organoclay increases the acrylate homopolymerization. In addition, final thiol conversion significantly increases through incorporation of thiolated organoclays. The addition of 5 wt% thiolated organoclay into TrPGDA/TMPTMP increases final thiol conversion 50% from that of the unfilled system and further increases the conversion with increased clay concentration. These results strongly suggest that chemical compatibility between acrylate monomers and organoclays as well as the type of reactive group on the clay surface are important for polymerization kinetics and mechanisms by affecting the type of dominant reactions in the clay galleries.

Because the degree of clay exfoliation is an indicator for overall monomer-clay compatibility and also important for understanding the impacts of the clay surface functionality during the photopolymerization, exfoliation behavior of these thiol-acrylate compositions with 3 wt% organoclay was studied utilizing small angle X-ray scattering (SAXS). When incorporated into the HDDA/HDT mixture, C16A acrylated organoclay showed a noticeable primary and secondary peak corresponding to d-spacing of 3.7 nm and 1.8 nm, respectively. After polymerization, a significant decrease in intensity for the peaks was observed, indicating further exfoliation through polymerization. Thiolated organoclay systems, however, showed no obvious peaks before and after polymerization indicating better clay exfoliation. On the other hand, the exfoliation behavior in the TrPGDA/HDT mixture is quite different. C16A acrylated organoclay was almost completely exfoliated before polymerization, whereas thiolated organoclay showed intermediate exfoliation and was completely exfoliated after polymerization. This implies

acrylated organoclay has greater compatibility with polar monomer systems while the compatibility of thiolated organoclay, which is less polar due to further organic modification, decreases by increasing the polarity of the monomer system.

This behavior is consistent with the polymerization behavior of each system. The addition of polymerizable organoclays increases polymerization rate in sufficiently exfoliated clay systems while the rate decreases with lower degrees of clay exfoliation. To further understand the difference in photopolymerization mechanism, dark curing experiments were performed by monitoring the post reaction after shuttering light and thus eliminating initiation. To this end, moderately cross-linked TrPGDA/GDMP and more highly cross-linked TrPGDA/TMPTMP systems with a 2:1 functional group ratio was utilized with 3wt% C16A acrylated or PSH2 thiolated organoclays. Addition of acrylated organoclays induces much higher dark acrylate conversion than the neat systems while incorporating thiolated organoclays increases the dark thiol conversion in both monomer systems. Based on this behavior, it is reasonable to conclude that chemical compatibility is the primary factor influencing clay exfoliation. Additionally, the type of functional group on the clay surface significantly directs polymerization behavior not only by affecting the stoichiometric balance between thiol and acrylate in the clay galleries but also by determining the type of predominant species of propagating radicals on the clay surfaces. Thiolated organoclays enhance thiol-ene reaction with increased thiol conversion while acrylated organoclays facilitates acrylate homopolymerization in thiol-acrylate photopolymerization.

These differences in clay exfoliation and polymerization behavior upon incorporation of organoclays may affect final performances of nanocomposites. To demonstrate how these differences affect the ultimate thermo-mechanical properties of nanocomposites, dynamic mechanical analysis (DMA) experiments were conducted for TrPGDA/GDMP systems that were utilized for kinetic studies. The incorporation of 3wt% acrylated organoclays enhances the rubbery storage modulus, whereas the modulus

of thiolated organoclay systems increases just slightly from that of neat system. It is apparent that dominant acrylate homopolymerization in acrylated organoclay system generates higher modulus than in thiolated organoclay system where the polymerization occurs via an enhanced thiol-ene step growth mechanism, resulting in softening of polymer chains by greater formation of flexible thio-ether linkages. In addition, about 50% increases in Young's modulus were observed by adding C16A acrylated organoclay while C14AGT or PSH2 thiolated organoclay systems show similar values compared to those of neat and nonreactive CL93A organoclay systems. The small increase of Young's modulus by adding nonreactive organoclay is mainly due to the insufficient clay exfoliation, resulting in less formation of nano-scale clay morphology. Further evidence is provided by glass transition temperature behavior upon adding 3wt% different polymerizable organoclays in this system. Addition of C14AGT or PSH2 thiolated organoclays reduces  $T_g$  significantly due to enhanced thiol-ene reaction, whereas the addition of C16A acrylated or non-reactive CL93A organoclays does not change  $T_g$  from that of the neat system. Again, this  $T_g$  behavior of the systems confirms that increased acrylate homopolymerization by adding acrylated organoclay forms harder domains in the nanocomposites while thiolated organoclays make the networks more flexible.

Even with the many advantages of acrylate-based photopolymerization, several disadvantages limit photopolymer applications. In particular, severe oxygen inhibition in acrylate-based photopolymerization is of great concern. The addition of thiol monomers into ene systems significantly changes the reaction mechanism from a free-radical chain growth to a step-growth reaction in which thiol monomers act as a chain transfer agent. This reaction mechanism can significantly reduce oxygen inhibition by chain transferring a peroxide radical produced by oxygen molecule to a thiol to regenerate the thiyl radical. This step-growth mechanism is also beneficial for reducing polymerization shrinkage due to facile rearrangement of polymer chains in the liquid reactant mixture upon delayed gelation until the system reaches high conversion. In addition, based upon significant



effects of polymerizable organoclays on the degree of thiol-ene reaction, the use of appropriate polymerizable organoclays may further decrease the extent of oxygen inhibition and polymerization shrinkage with inherent filler effects decreasing the diffusion rate of oxygen molecules system as well as inducing relaxation or rearrangement of polymer networks.

To investigate the synergetic effects of organoclay and thiol monomers on reducing oxygen inhibition, 5wt% nonreactive and polymerizable organoclays were added into three acrylate systems exhibiting inherently different degrees of oxygen inhibition based on differences in hydrogen abstraction and viscosity. Without incorporation of thiol monomers, the lowest viscosity HDDA system with no abstractable hydrogen was completely inhibited by oxygen. The less inhibited and more viscous formulations such as PEGDA/TrPGDA and CN9009/PEGDA/TrPGDA systems can reach at most 60% of the degree of polymerization in air as compared to that in nitrogen. While adding nonreactive and thiolated organoclays significantly decreases the rates in these acrylated systems, the addition of acrylated polymerizable organoclays slightly enhances polymerization in air, but the polymerization is still severely inhibited by oxygen. On the other hand, regardless of the type of basic acrylate composition, addition of 5wt% thiolated organoclays into thiol-acrylate systems including 20mol% thiols enhances the rates in air significantly to virtually identical rates achieved under nitrogen, whereas incorporating either non-reactive or acrylated organoclay often decreases the conversions and polymerization rates in air.

Volume shrinkage and subsequent induced stress are important to control and understand not only for dimensional stability of materials and but also for preventing substrate deformation in coating and packaging applications. Similar to the organoclay impact on oxygen inhibition, adding polymerizable organoclays significantly affects the polymerization shrinkage with the impact varying by organoclay type. For PEGDA/TrPGDA system by incorporating up to 10mol% thiol, a maximum of 40%

reduction in volume shrinkage, as examined by density difference between liquid monomers and cured solid samples is observed. An additional 10% reduction for both acrylate and thiol-acrylate systems is induced by adding only 3wt% thiolated organoclays, while acrylated organoclay does not change shrinkage significantly. Polymerization induced shrinkage stress evaluated by utilizing an ASTM standard is substantially reduced by adding clays into various acrylate and thiol-acrylate systems that show different extents of inherent shrinkage stress. A much greater reduction in shrinkage stress with polymerizable organoclays with enhanced interaction with monomer and/or polymer networks is observed than that in systems with natural and nonreactive organoclays. Therefore, the functional group type in the clay structure also plays an important role for maximizing the reduction in shrinkage stress. Acrylated organoclays are more effective than thiolated organoclays for reducing the shrinkage stress of various acrylate systems such as high shrinkage TMPTA and moderate shrinkage CN9009/PEGDA/TrPGDA systems, whereas both thiolated and acrylated organoclays greatly decreased the shrinkage stress of TMPTA/TMPTMP thiol-acrylate systems. The addition of only 5wt% of appropriate polymerizable organoclay induces up to a 90% decrease in the shrinkage stress, whereas the same amount of nonreactive clays reduces the stress to less than 20%. These results regarding oxygen inhibition and shrinkage behavior with organoclays demonstrate that these two major drawbacks of acrylate radical photopolymerization systems can be effectively overcome by synergetic effects of the suitable type of polymerizable organoclays with minimal use of thiol monomers.

Because the ultimate goal of this research is the development of advanced photopolymer clay nanocomposites with improved performance utilizing polymerizable organoclays, understanding the overall impact of polymerizable organoclays on ultimate nanocomposite performance is also important for providing practical information in material design. On the basis of evidences that the type of organoclay induces significantly different photopolymerization behavior as well as thermo-mechanical

properties, characterization of some important material properties have been performed. Tensile properties such as elongation and toughness are good indicators for mechanical performance of a material. To study the organoclay effects in tensile properties, DMA tensile experiments have been conducted by adding 3wt% various non-reactive and polymerizable organoclays into CN9009/PEGDA/TrPGDA thiol-acrylate mixture including 20mol% thiol from TMPTMP. Interesting differences in tensile property behavior was observed by organoclay type. While the addition of only 3wt% of acrylate organoclay increases the tensile modulus 60% with no significant changes in elongation of cured nanocomposites, adding 3wt% thiolated organoclays induces a 70% increase in elongation while Young's modulus does not change significantly. With this unique behavior by organoclay type, it is remarkable that both polymerizable organoclays induce up to an 80% increases in toughness, compared by the area of stress-strain curves, while nonreactive organoclay actually decreases the toughness.

Gas barrier properties for many gases such as oxygen and water vapor are important characteristics in many photopolymer applications such as coating and film packaging. The addition of plate shape inorganic fillers may inherently improve the gas barrier properties by generating a longer diffusion path for gaseous materials. To evaluate the impact of organoclays on barrier properties, the water vapor transmission rate (WVTR) based on ASTM standard was compared utilizing 110 $\mu$ m films of CN9009/PEGDA/TrPGDA compositions including both 8 mol% thiol from TMPTMP and 3wt% various organoclays. With at least intercalated clay morphology, no significant difference between polymerizable and nonreactive organoclays was observed. Approximately 30% reduction in WVTR is achieved by adding 3wt% organoclays while 3wt% natural clay (CL Na) reduces WVTR about 16% from the value of the neat system. Further decrease in WVTR is observed when organoclays are incorporated into the thiol-acrylate mixture. Considering the significant improvements in other performance aspects

by adding polymerizable organoclays, 30% improvement in barrier properties with only 3wt% organoclays may also increase the usefulness of polymerizable organoclays.

Through this work, the importance of a fundamental understanding of the crucial factors in processing photopolymer clay nanocomposites including clay dispersion, photopolymerization, and evolution of nanocomposite properties and performance has been verified based on various acrylate and thiol-acrylate systems. Use of appropriate type of polymerizable organoclay for a monomer system promises enhanced clay exfoliation and thereby polymerization behavior as well as ultimate nanocomposite properties can be controlled. In particular, control of the compatibility between components and the choice in the types of reactive moieties of polymerizable organoclays are important challenges for designing specific characteristics of photopolymer clay nanocomposites. Understanding how these key factors determine the structure and properties of the nanocomposites in various photopolymerization systems can potentially contribute to increase of photopolymer applications. While the knowledge from this research provides important tools for designing advanced and new photopolymers, additional research is recommended based on novel polymerizable organoclays and expansion to other polymerization systems.

This research has mainly focused on acrylate and thiol-acrylate for the base polymer material considering their wide variety of current use in industrial production. Recently, another type of photo-curing technique, namely epoxy cationic photopolymerization, has been attracting renewed research interest because of its unique characteristics. As with thiol-ene photopolymerization, it involves low shrinkage and no oxygen inhibition during the polymerization process. In addition, the ultimate polymer usually exhibits excellent adhesion properties to many substrates such as metals, plastics and paper. In addition, radical and cationic photopolymerization can occur at the same time by use of suitable photoinitiator systems with hybrid monomer mixtures, e.g. epoxy with acrylate monomers. This hybrid radical-cationic photopolymerization system can

impart diversity in properties via interpenetrating polymer networks. Polymerizable organoclays bearing corresponding epoxy moieties in the clay structure would be applied for modulating and enhancing hybrid photopolymerization systems. To this end, preliminary studies were performed utilizing polymerizable organoclays possessing epoxy functional groups. These organoclay analogues were prepared by further Michael addition reaction to thiolated organoclays using a hybrid monomer with both acrylate and glycidyl group in the structure. One example of an epoxy terminated organoclay was produced from acryloyloxy-ethyl-trimethyl-ammonium chloride (AETAC). In contrast to the results for acrylic or thiol-ene system, however, a large decrease in polymerization rate by adding organoclays was observed in epoxy cationic photopolymerization systems and varied by surfactant structures, which implies that the efficacy of cationic initiation was limited by impurities in the surfactants or ammonium surfactants themselves by scavenging protonic acid. To overcome the large decrease in reaction rate induced by the addition of organoclays, more properly designed surfactants such as phosphonium bromide, chloride, and iodide types should be developed for this cationic system. Overall, the use of organoclays in epoxy cationic systems presents many challenges for future studies but may be highly useful for expanding the range of properties for these materials.

Through this research, well exfoliated clay morphology can be achieved in various photopolymer compositions. Further control of clay dispersion morphology based upon potential needs, especially the orientation of delaminated clay layer in a particular direction may be highly beneficial for improving several aspects of clay based polymer nanocomposites. For instance, the orientation of these plate-like clay layers could induce significant enhancement in barrier properties by effectively blocking the transport of gaseous molecules in polymer networks with continuous formation of wall-like dispersion morphology. In addition, this oriented morphology could change the aspect ratio of each clay layer to an approximately unlimited value in two lateral directions, which may result in enormous increase of biaxial tensile strength of cured polymer films

or sheets. One possible route to reach this goal is use of the plentiful hydroxyl groups on the edge surfaces of montmorillonite natural clay. Prior to clay exfoliation, appropriate polymerizable groups could be introduced on the surface of aggregated natural clay particle via suitable reaction with the surface hydroxyl groups, followed by organic modification of each clay layer through the ion exchange methodology provided in this research but using a nonreactive surfactant. Through these modification procedures, polymerizable groups can exist only at the edges of each delaminated clay plate. After mixing into monomer mixtures with exfoliated morphology, subsequent polymerization would then generate oriented clay morphology by reaction between monomer functional groups and polymerizable groups on the edge of clay layers. Achieving this oriented clay morphology, it is expected that the required amount of clay would be greatly reduced without sacrificing the significant improvements in various properties, which could be another beneficial impact of the technique.

Though many advances have been demonstrated in processing photopolymer clay nanocomposites in this research, some practical aspects in using this technology based on utilizing polymerizable organoclays remain for further study. One is the difficulty in increasing a clay amount over 10% due to substantial increases of system viscosity beyond this concentration. Some industrial applications still need highly filled photopolymer nanocomposites for various reasons such as cost reduction and density control. Development of nanocomposites including greater than 10 wt% concentration of organoclay may thus be useful for allowing wide variety of application windows. To increase filler concentration, it is recommended to use mixed clay formulations comprised of organoclays and other fillers such as natural clay or mica. Critical performance will be achieved by inclusion of organoclay while other minor properties could be controlled by choice of the other filler and its ratio in the filler mixture.

The other important challenge is dispersion stability of clay particles in the monomer mixture. Many polymerizable organoclays developed in this research exhibit

reasonable dispersion stability for at least three days. Some industrial production, however, requires long-term formulation stability for many end uses. This challenge may appear simple to solve, but will, in fact, involve significant research including fundamental chemical and physical studies. Interestingly, the decrease of clay concentration significantly prolongs the dispersion stability. For example, while the TrPGDA/C16A acrylated organoclay mixture with 5 wt% clay concentrations exhibits about a week of dispersion stability, the same organoclay-monomer mixture with 1 wt% clay concentration shows over a month of stability. If the aforementioned clay orientation is achieved and thereby the amount of clay can be decreased with sufficient properties, this concern in formulation stability may be overcome in most applications.

One other minor recommendation for practical use of polymerizable organoclays is stabilization of the clay-monomer mixture preventing any unexpected reaction prior to photopolymerization. Particularly for thiolated organoclays, thiol-ene reaction can occur without irradiation and addition of stabilizer such as an inhibitor may be necessary. Simple trials show the addition of 200 to 500ppm of radical scavenger successfully suppresses the thiol-ene reaction during storage. By adding the inhibitor, no meaningful difference in photopolymerization rate was observed for various thiol-acrylate formulations except for lengthening the reaction induction time by about 3 seconds when  $3\text{mW/cm}^2$  is used. This delay of reaction was even eliminated by increasing the light intensity to  $6\text{mW/cm}^2$ .

In summary, this work has established a fundamental understanding in design and use of polymerizable organoclays for fabricating advanced photopolymer clay nanocomposites with contemporary acrylate and thiol-ene photopolymerization systems. In the preparation of clay nanocomposites, the extent of clay exfoliation is critical for control of nanocomposite processes and properties. It has been clearly demonstrated that monomer polarity, functionality, and viscosity play important roles in achieving an enhanced clay exfoliation by determining the compatibility between monomers and

organoclays, which subsequently affects the polymerization kinetics. With enhanced clay exfoliation, increased rates of photopolymerization are observed. In addition, the type of polymerizable groups in the organoclay governs the polymerization behavior and is closely related with the characteristics of the nanocomposite formation process and ultimate performance. In particular, incorporating thiol functionalized organoclays enhances the thiol-ene step-growth reaction while acrylated organoclays facilitate acrylate homopolymerization in various thiol-acrylate formulations. This critical influence of polymerizable organoclays on reaction mechanisms has substantial impact on many nanocomposite properties and thereby can be used as a simple but powerful tool for controlling properties of photopolymer systems. This work has also shown that oxygen inhibition and polymerization induced shrinkage during photopolymerization can be successfully overcome by using suitable type of polymerizable organoclays, which may be highly useful in many industrial productions. Upon deep understanding morphology-polymerization behavior-performance relationship, significant improvement and/or optimization of nanocomposite properties has been achieved such as tensile, gas barrier, and thermo-mechanical properties. The knowledge obtained from the series of this research will present useful means for control of the nanocomposite process and performance and should devote to development of other nano-structured polymerizable filler materials.



## BIBLIOGRAPHY

- Aguzzi, C.; Cerezo, P.; Viseras, C.; Caramella, C. *Appl. Clay Sci.* **2007**, 36, 22.
- Alexandre, M.; Dubois, P. *Mater. Sci. Eng.* **2000**, 28, 1.
- Anderson, H. A. *CARBON BLACK INDUSTRY*; Handbook of Texas Online (<http://www.tshaonline.org/handbook/online/articles/doc01>): Texas State Historical Association, accessed December 27, **2011**.
- Andrzejewska, E.; Andrzejewski, M. *J. Polym. Sci. Part A: Polym. Chem.* **1998**, 36, 665.
- Andrzejewska, E.; Bogacki, M. B.; Andrzejewski, M.; Janaszczyk, M. *Phys. Chem. Chem. Phys.* **2003**, 5, 2635.
- Andrzejewska, E.; *Prog. Polym. Sci.* **2001**, 26, 605.
- Anseth, K. S.; Bowman, C. N. *Polym. React. Eng.* **1993**, 1, 499.
- Anseth, K. S.; Wang, C. M.; Bowman, C. N. *Macromolecules* **1994**, 27, 650.
- Aranda, P.; Ruiz-Hitzky, E. *Chem Mater* **1992**, 4, 1395.
- ASTM D 6991– 05, "Standard Test Method for Measurements of Internal Stresses in Organic Coatings by Cantilever (Beam) Method".
- ASTM E96M-05, "Standard Test Methods for Water Vapor Transmission of Materials"
- Auras, A. R.; Singh S. P.; Singh J. J. *Packaging Technology and Science* **2005**, 18(4), 207.
- Avidenko, N.; Garcí'a, O.; Sastre, R. *J. Appl. Polym. Sci.* **1995**, 97, 1016.
- Balazs, A.C.; Singh, C.; Zhulina, E. *Macromolecules* **1998**, 31, 8370.
- Baughman, R. H.; Zahkidov, A. A.; De Heer, W. A. *Science* **2002**, 297, 787.
- Beck, E.; Lokai, E.; Nissler, H. *RadTech Int. North America, Nashville* **1996**, 160.
- Blumstein, A. *J. Polym. Sci. Part A.* **1965**, 3, 2665
- Bongiovanni, R.; Ronchetti, M. S.; Turcato, E.A. *J. Colloid & Interf. Sci.* **2006**, 296, 515.
- Bottino, F. A.; Fabbri, E.; Fragala, I. L.; Malandrino, G.; Orestano, A.; Pilatti, F.; Pollicino, A. *Macromolecular Rapid Communications* **2003**, 24, 1079.
- Bowman, C. N.; Anseth, K. S. *Macromol. Symp.* **1995**, 93, 269.
- Brindly, S. W.; Brown, G. *Crystal structure of clay minerals and their X-ray diffraction*; Mineralogical Society: London, **1980**.

- Brule, B.; Flat, J. J. *Macromol. Symp.* **2006**, 233, 210.
- Carioscia, J. A.; Lu, H.; Stanbury, J. W.; Bowman C. N. *Dent. Mater.* **2005**, 21, 1137.
- Carrado, K. A. *J. Appl. Clay Sci.* **2000**, 17, 1
- Carvalho, R. M.; Pereira, J. C.; Yoshiyama, M.; Pashley, D. H. *Oper Dent.* **1996**, 21, 17.
- Chakrabarti, A.; Lu, J.; Skrabutenas, J. C.; Xu, T.; Xiao, Z.; Maguire, J. A.; Hosmane, N. S. *Journal of Materials Chemistry* **2011**, 21, 9491.
- Chan, W. J.; Zhou, H.; Hoyle, E. C.; Lowe, B. A. *Chem. Mater.* **2009**, 21, 1579.
- Chappelow, C. C.; Pinzino, C. S.; Power, M. D.; Holder, A. J.; Morrill, J. A.; Jeang, L. *J. Appl. Polym. Sci.* **2002**, 86, 314.
- Chung, C. M.; Kim, M. S.; Roh, Y. S. *J. Mater. Sci. Lett.* **2002**, 21, 1093.
- Chung, C. M.; Lee, S. J.; Lim, J. G.; Jang, D. O. *J. Biomed. Mater. Res.* **2002**, 62, 622.
- Clapper, J. D.; Guymon, C. A. *Macromolecules* **2007**, 40, 1101.
- Corcoran E. M. *J. Paint Technology* **1969**, 41, 635.
- Cramer N. B, Davies T, O'Brien, A. K, Bowman, C. N. *Macromolecules* **2003**, 36, 4631.
- Cramer N. B.; Scott J. P.; Bowman C. N. *Macromolecules* **2002**, 35, 5361.
- Cramer, N. B.; Bowman, C. N. *J. Polym. Sci. Part A: Polym. Chem* **2001**, 39, 3311.
- Cramer, N. B.; Reddy, S. K. ; O'Brien, A. K. ; Bowman, C. N. *Macromolecules* **2003**, 36, 7964.
- Cramer, N. B.; Reddy, S. K.; Lu, H.; Cross, T.; Raj, R.; Bowman, C. N. *J. Polym. Sci. A: Polym. Chem.*, **2004**, 42, 1752.
- Cramer, N. B.; Reddy, S. K.; O'Brien, A. K.; Bowman, C. N. *Macromolecules* **2003**, 36, 7964.
- Cramer, N. B.; Scott, J. P.; Bowman, C. N. *Macromolecules* **2002**, 35, 5361.
- Croll, S. G. *J. Coat. Technol.* **1980**, 52, 35.
- Davidenko N.; Garcí'a O.; Sastre, R. *J. Appl. Polym. Sci.* **1995**, 97, 1016.
- Davidson, C. L.; Feilzer, A. J. *J. Dent.* **1997**, 25, 435.
- Decker, C. *Acta. Polym.* **1994**, 45, 333.
- Decker, C. J. *Coat. Technol.* **1987**, 59, 97.
- Decker, C. *Macromol. Rapid Commun.* **2002**, 23, 1067.
- Decker, C. *Macromolecules* **1989**, 22, 12.

- Decker, C. *Polym. Int.* **1998**, 45, 133.
- Decker, C. *Prog. Polym. Sci.* **1996**, 21, 593.
- Decker, C.; Faure, J.; Fizet, M.; Rychla, L. *Photogr. Sci. Eng.* **1978**, 23, 137.
- Decker, C.; Jenkins, A. D. *Macromolecules*, **1985**, 18, 1241.
- Decker, C.; Keller, L.; Zahouily, K.; Benfarhi, S. *Polymer* **2005**, 46, 6640.
- Decker, C.; Moussa, K. *J. Coat. Technol.* **1993**, 65, 49.
- Decker, C.; Moussa, K. *Macromol. Chem. Phys.* **1988**, 189, 2381.
- Decker, C.; Moussa, K. *Makromol. Chem.* **1990**, 191, 963.
- Decker, C.; Zahouily, K.; Keller, L.; Benfarhi, S.; Bendaikha, T.; Baron, J. *J. Mater. Sci.* **2002**, 37, 4831.
- Decker, C.; Zahouily, K.; Keller, L.; Benfarhi, S.; Bendaikha, T.; Baron, J. *Proc. RadTech North America*, **2002**, 309.
- Dickey, M. D.; Burns, R. L.; Kim, E. K.; Johnson, S. C.; Stacey, N. A. Willson C. G. *AIChE J.* **2005**, 51, 2547.
- Eastoe, J.; Summers, M.; Heenan, R. K. *Chem. Mater.* **2000**, 12, 3533.
- Fan, X.; Xia, C.; Advincula, R. C. *Langmuir*, **2003**, 19, 4381.
- Feilzer, A. J.; Degee, A. J.; Davidson, C. L. *J. Dent. Res.* **1987**, 66, 1636.
- Filippi, S.; Mameli, E.; Marazzato, C.; Magagnini, P. *Euro. Polym. J.* **2007**, 43, 1645.
- Fouassier, J. P. *Photoinitiation photopolymerization and photocuring: fundamentals and application*; Hanser Publishers: Munich, **1995**.
- Fouassier, J. P.; Rabek, J.F. *Radiation curing in polymer science and technology*; Elsevier Applied Science: London, **1993**, Vol I: fundamentals and methods, 1.
- Fu, X.; Qutubuddin, S. *Polymer* **2001**, 42, 807.
- Gao, D.; Heimann, R. B.; Williams, M. C.; Wardhaugh, L. T.; Muhammad, M. *J Mater Sci* **1999**, 34, 1543.
- Gelfer, M. Y.; Burger, C.; Nawani, P.; Hsiao, B. S.; Chu, B.; Si, M.; Rafailovich, M.; Panek, G.; Jeschke, G.; Gunnar, F. A. Y.; Gilman, J. W. *Clays Clay Miner.* **2007**, 55, 140.
- Giannelis, E. P.; Krishnamoorti, R.; Manias, E. *Adv. Polym. Sci.* **1999**, 118, 108
- Gilman, J. W.; Awad, W. H.; Davis, R. D.; Shields, J.; Harris, Jr. R. H.; Davis, C.; Morgan, A. B.; Sutto, T. E.; Callahan, J.; Trulove, P. C.; DeLong, H. C. *Chem Mater* **2002**, 14, 3776.
- Gilman, J.W. *Appl. Clay Sci.* **1999**, 15, 31.

- Goldman, M. *Australian Dental J.* **1983**, 28(3), 156.
- Goodner, M. D.; Bowman, C. N. *Chem. Eng. Sci.* **2002**, 57, 887.
- Gottler, L. A.; Lee, K.; Thakkar, Y. H. *Polymer Reviews* **2007**, 47, 291.
- Gou, L.; Coretsopoulos, C. N.; Scranton, A.B. *J. Polym. Sci. Part A: Polym. Chem.* **2004**, 42, 1285.
- Greenland, D. J. *J. Colloid Sci* **1963**, 18, 647.
- Grohn, F.; Kim, G.; Bauer, A.J.; Amis, E.J. *Macromolecules* **2001**, 34, 2179.
- Grubbs, R. R. *Polymer Rev.* **2007**, 47, 197.
- Hamid S. M.; Sherrington D. C. *Polymer* **1987**, 28, 325.
- Hasegawa, N.; Okamoto, H.; Kawasumi, M.; Usuki, A. *J Appl Polym Sci* **1999**, 74, 3359.
- Hata, E.; Tomita, Y.; *Opt. Lett.* **2010**, 35, 396.
- Hatton, R. A.; Miller, A. J.; Silva, R. R. P. *J. Mater. Chem.* **2008**, 18, 1183.
- Hill, L. W. *Prog. Org. Coat.* **1997**, 31, 235.
- Hoyle, C. E.; Hensel, R. D.; Grubb, M. B. *J. Polym. Sci., Part A: Polym. Chem.* **1984**, 22, 1865.
- Hoyle, C. E.; Lee, T. Y.; Roper, T. *J. Polym. Sci. Part A Polym. Chem.* **2004**, 42, 5301.
- Hoyle, C.E.; Keel, M.; Kim, K. J. *Polymer* **1988**, 29, 18.
- Jana, S. C.; Prieto, A. J. *Appl. Polym. Sci.* **2002**, 86, 2159.
- Jayasuriya, N.; Bosak, S.; Regen, S. L. *J. Amer. Chem. Soc.* **1990**, 112, 5851.
- Jeon, H. S.; Rameshwaram, J. K.; Kim, G.; Weinkauff, D. H. *Polymer*, **2003**, 44, 5749.
- Jiang, C.Y.; Mark, J. E. *Makromol. Chem.* **1984**, 185, 2609.
- Joynes, D.; Sherrington, D. C. *Polymer* **2006**, 37, 1453.
- Karásek, L.; Sumita. M. *J. Mat Sci* **1996**, 31(2), 281.
- Karesoja, M.; Jokinen, H.; Karjalainen, E.; Pulkkinen, P.; Torkkeli, M.; Soininen, A.; Ruokolainen, J.; Tenhu, H. *J. Polym. Sci. A: Poly. Chem.* **2009**, 47, 3086.
- Karian, H. G. *Handbook of Polypropylene and Polypropylene Composites*; Marcel Dekker: New York, **1999**, p.1.
- Katti, K. S.; Sikdar, D.; Katti, D. R.; Ghosh, P.; Verma, D. *Polymer* **2006**, 47, 403.
- Kawasumi, M. *J. of Polym. Sci. Part A* **2004**, 42, 819

- Keller, S. L.; Decker, C.; Zahouily, K.; Benfarhi, S.; Le Meins, J. M.; Mische-Brendle, J. *Polymer* **2004**, 45, 7437
- Kim S. K.; Guymon C. A. *In preparation*
- Kim S. K.; Guymon C. A. submitted to *Europ. Pol. J*
- Kim S. K.; Guymon C. A. submitted to *Polymer*
- Kim S. K.; Guymon, C. A. *J. Polym. Sci. Part A Polym. Chem.* **2011**, 49, 465.
- Kim, H. S.; Yang, S. H.; Kim, J.; Park, H. J. *J. Thermal Analysis and Calorimetry* **2004**, 76, 395.
- Klee, J. E.; Schneider, C.; Holter, D.; Burgath, A.; Frey, H.; Mulhaupt, R. *Polym. Adv. Technol.* **2001**, 12, 346.
- Kleverlaan, C. J. Ornelis.; Feilzer, A. J. *Dent. Mater.* **2005**, 21, 1150.
- Kloosterboer, J. G. *Adv. Polym. Sci.* **1988**, 84, 1.
- Krishnamoorti, r.; Vaia, R. A.; Giannelis, E. P. *Chem Mater* **1996**, 8, 1728.
- Krongauz, V. V.; Schmelzer, E. R. *Polymer* **1992**, 33, 1893.
- Lagaly, G.; Beneke, K. *Coll. Polym. Sci.* **1991**, 269, 1198.
- Lange, J. *Polym. Eng. Sci.* **1999**, 39, 1651.
- LeBaron, P. C.; Pinnavaia, T. J. *Chem. Mater.* **2001**, 13, 3760.
- LeBaron, P. C.; Wang, Z.; Pinnavaia, T. J. *Appl. Clay Sci.* **1999**, 15, 11. v2.
- Lecamp, L.; Houllier, F.; Youssef, B.; Bunel, C. *Polymer* **2001**, 42, 2727.
- Lee, C. H.; Kim, H. B.; Lim, S. T.; Choi, H. J.; Jhon, M. S. *J. Mater. Sci.* **2005**, 40, 3981.
- Lee, T. Y.; Bowman, C. N. *Polymer* **2006**, 47, 6057.
- Lee, T. Y.; Carioscia, J.; Smith, Z.; Bowman, C. N. *Macromolecules* **2007**, 40(5), 1473.
- Lee, T. Y.; Guymon, C. A.; Jonsson, S. E.; Hoyle, C. E. *Polymer* **2004**, 45, 6155.
- Lee, T. Y.; Kaung, W.; Jonsson, E. S.; Lowery, K.; Guymon, C. A.; Hoyle, C. E. *J. Polym. Sci. Part A: Polym. Chem.* **2004**, 42, 4424.
- Lee, T. Y.; Smith, Z.; Reddy, S. K.; Cramer, N. B.; Bowman, C. N. *Macromolecules* **2007**, 40, 1466.
- Leone, G.; Boglia, A.; Bertini, F.; Canetti, M.; Giovanni, R. *J. Polym. Sci. A: Polym. Chem.* **2010**, 48, 4473.
- Li, Q.; Zhou, H.; Wicks, D. A.; Hoyle, C. E. *J. Polym. Sci. A: Polym. Chem.*, **2007**, 45, 5103.

- Li, Y.; Ishida, H. *Langmuir* **2003**, 19, 2479.
- Li, Y.; Ishida, H. *Polymer* **2003**, 44, 6571.
- Lomborg, B. *The Skeptical Environmentalist: Measuring the Real State of the World.*; Cambridge University Press: Ney York, **2001**, p.138.
- Lovestead, T. M.; Bowman, C. N. *Macromol. Theory Simul.* **2002**, 11, 729.
- Lu, H.; Carioscia, J. A.; Stansbury, J. W.; Bowman, C. N. *Dent. Mater.* **2005**, 21, 1129.
- Lu, H.; Lee, Y. K.; Oguri, M.; Powers, J. M. *Oper Dent.* **2006**, 31(6), 734.
- Lu, H.; Stansbury, J. W.; Bowman, C. N. *Dent. Mater.* **2004**, 20, 979.
- Lu, H.; Stansbury, J. W.; Bowman, C. N. *J. Dent. Res.* **2005**, 84(9), 822.
- Lu, H.; Stansbury, J. W.; Dickens, S. H.; Eichmiller, F. C.; Bowman, C. N. *J. Biomed. Mater. Res., Part B: Appl. Biomater.* **2004**, 70B, 206.
- Lyatskaya, Y.; Balazs, A. C. *Macromolecules* **1998**, 31, 6676.
- Magny, B.; Askienazy, A.; Pezron E. *Proc. RadTech Europe, Maastricht.* **1995**, 507, 400.
- Malucelli, G. ; Bongiovanni, R. ; Sangermano, M. ; Ronchetti, S. ; Priola, A. *Polymer* **2007**, 48, 7000.
- Mark, J. E.; Pan, S. J. *Makromol. Chem., Rapid Commun.* **1982**, 3, 681
- Matteucci, S.; Kusuma, V. A.; Sanders, D.; Swinnea, S.; Freeman, B. D. *J. Membr. Sci.* **2008**, 307, 196.
- McGrath, K. M.; Drummond, C. J. *Colloid Polym. Sci.* **1996**, 274, 612.
- McGrath, K. M.; Sherrington, D.C. *Polymer* **2006**, 37, 1453
- Medalia A. I. *Rubber Chem. Technol.* **1986**, 59, 432.
- Michas, J.; Paleos, C. M.; Dais, P. *Liquid Crystals* **1989**, 5, 1737.
- Miller, C.W.; Hoyle, C. E.; Jonsson, S.; Nason, C.; Lee, T. Y.; Kuang, W. F.; Viswanathan, K. *ACS Symp. Ser.* **2003**, 847, 2.
- Moniruzzaman, M.; Winey, K. I. *Macromolecules* **2006**, 39, 5194.
- Morgan, C. R.; Magnota, F.; Ketley, A. D. *J. Polym. Sci.: Polym. Chem. Ed*, **1977**, 15, 627.
- Morgan, C.R.; Ketley, A.D. *J. Radiat Curing* **1980**, 7, 10.
- Morlat, S.; Mailhot, B.; Gonzalez, D.; Gardette, J. *Chem. of Mater.* **2004**, **16**, 377
- Nagai K.; Ohishi, Y. *J. Polym. Sci., Part A*, **1987**, 25, 1.

Natarajan, L. V.; Shepherd, C. K.; Brandelik, D. M.; Sutherland, R. L.; Chandra, S.; Tondiglia, V. P.; Tomlin, D., Bunning, T.J. *Chem. Mater.* **2003**, 15, 2477.

Noh, M. W.; Lee, D. C. *Polym Bull* **1999**, 42, 619.

North, A.M. *Reactivity, Mechanism, and Structure in Polymer Chemistry*; Wiley-Interscience, **1974**.

O'Brien, A. K.; Bowman, C. N. *Macromol. Theory Simul.* **2006**, 15, 176.

O'Brien, A. K.; Bowman, C. N. *Macromolecules* **2003**, 36, 7777.

O'Brien, A. K.; Cramer, N. B.; Bowman, C. N. *J. Polym. Sci. Part A: Polym. Chem.* **2006**, 44, 2007.

Odian, G. *Principles of Polymerization*, 4<sup>th</sup> ed.; John Wiley & Sons: Hoboken, NJ, **2004**.

Odian, G. *Principles of polymerization*. John Wiley & Sons, Inc. New York, **1991**, 3rd ed.

Ogawa, M.; Kuroda, K. *Bull. Chem. Soc. Jap.* **1997**, 70, 2593.

Okada, A.; Fukumori, K.; Usuki, A.; Kojima, Y.; Sato, N.; Kurauchi, T.; Kamigaito, O. *Polym. Prepr.* **1991**, 32, 540.

Okada, A.; Kawasumi, M.; Kurauchi, T.; Kamigaito, O. *Polym. Prepr.* **1987**, 28, 447.

Okamoto, M.; Morita, S.; Taguchi, H.; Kim, Y. H.; Kotaka, T.; Tateyama, H. *Polymer* **2000**, 41, 3887.

Oosterbroek, M.; Lammers, R.J.; van der Ven, J.J.; Perera, D.Y. *J. Coat. Technol.* **1991**, 66, 1267.

Oral, A.; Tasdelen, M.A.; Demirel, A.L.; Yagci, Y. *J. Polym. Sci. A: Poly. Chem.* **2009**, 47, 5328.

Owusu-Adom, K.; Guymon, C. A. *Macromolecules* **2009**, 42, 180.

Owusu-Adom, K.; Guymon, C. A. *Macromolecules* **2009**, 42, 3275.

Owusu-Adom, K.; Guymon, C. A. *Polymer* **2008**, 49, 2636.

Pappas, S. P. *Encyclopedia of Polymer Science and Engineering*; Pappas, S.P., Ed.; Wiley-Interscience: New York **1988**, Vol. 11, p.186.

Pappav, P. *Radiation curing science and technology*; Plenum Press: New York, **1992**.

Patel, M. P.; Braden, M.; Davy, K. M. *Biomaterials* **1987**, 8, 53.

Pereira, S. G.; Osorio, R.; Toleano, M.; Nunes, T.G. *Dent. Mater.* **2005**, 21, 823.

Polowinski, S. *Prog. Polym. Sci.* **2002**, 27, 537.

Porter, T. L.; Hagerman, M.E.; Reynolds, B. P.; Eastman, M. E. *J Polym Sci, Part B: Polym Phys* **1998**, 36, 673.

- Pramoda, K. P.; Hussain, H.; Koh, H.M.; Tan, H.R.; He, C. B. *J. Polym. Sci. A: Polym. Chem.* **2010**, 48, 4262.
- Ray, S. S.; Okamoto, M. *Prog. Polym. Sci.* **2003**, 28, 1539.
- Reddy, S. K.; Cramer, N. B.; Kalvaitas, M.; Lee, T. Y.; Bowman, C. N. *Aust. J. Chem.* **2006**, 59, 586.
- Reddy, S. K.; Cramer, N. B.; Bowman, C. N. *Macromolecules* **2006**, 39, 3681.
- Reichert P.; Kressler J.; Mulhaupt R.; Stoppelmann G. *Acta Polym.* **1998**, 49, 116.
- Rigbi, Z. *Adv. Polym. Sci.* **1980**, 36, 21.
- Rodriguez, F., Cohen, C., Ober, C. K., Archer, L. A. *Principles of Polymer Systems*, Taylor & Francis: New York, 2003; Ch.9, 405.
- Roffey, C.G. *Photopolymerisation of Surface Coatings*; Wiley: New York **1982**.
- Roper, T. M.; Kwee, T.; Lee, T. Y.; Guymon, C. A.; Hoyle, C. E. *Polymer* **2004**, 45, 2921.
- Rust, F. F.; Vaughan, W. E. *U.S. Pat. 2,392,294*, **1946**.
- Sangermano, M.; Laka, N.; Malucelli, G.; Samakandeb, A.; Sanderson, R.D. *Progress in Organic Coatings* **2008**, 61, 89.
- Sato, K. *Prog. Org. Coat.* **1980**, 8, 143.
- Schaffer, A.; Saxena, S. D.; Antolovich, T. H.; Sanders, Jr.; and Warner. S.B. *The Science and Design of Engineering Materials*; IRWIN [now McGraw-Hill]: Chicago, **1999**.
- Senyurt, A. F.; Wei, H.; Hoyle, C. E.; Piland, S. G.; Gould, T. E. *Macromolecules* **2007**, 40, 4901.
- Seymour, R. B. *Polymer Composites VSP*, **1990**, p. 48.
- Shaffer, G. D. *J. Field Archaeology* **1993**, 20(1), 59.
- Shah, R. K.; Paul, D. R. *Polymer*, **2006**, 47, 4075.
- Shen, T.; Gu, J. J.; Xu, M.; Wu, Y. Q.; Bolen, M.L.; Capano, M.A.; Engel, L.W.; Ye, P. D. *Appl. Phys. Lett.* **2009**, 95, 172105.
- Small, D. M. *J. Coll. Int. Sci.* **1977**, 58, 581.
- Sposito, N.; Skipper, N. T.; Sutton, R.; Park, S. H.; Soper, A. K.; Greathouse, J. A. *Proc. Natl. Acad. Sci.* **1999**, 96, 3358.
- Stansbury, J. W. *Dent. Mater.* **2005**, 21, 56.
- Stolov, A. A.; Xie, T.; Penelle, J.; Hsu, S. L.; Stidham, H. D. *Polym. Eng. Sci.* **2001**, 41(2), 314.



- Takahashi, K.; Kido, J.; Kuramoto, N.; Nagai, K. *J. Coll. Int. Sci.* **1995**, 172, 63.
- Tan, H.; Nie, J. *J. Polym. Sci. A: Poly. Chem.* **2007**, 106, 2656.
- Theng, B. K. G. *The Chemistry of Clay-Organic Reactions*; Wiley: New York, **1974**.
- Thwe, M. M.; Liao, K. *Composite. Part A*, **2002**, 33, 43.
- Tilbrook, D. A.; Clarke, R. L.; Howle, N. E.; Braden, M. *Biomaterials* **2000**, 21, 1743.
- Tomita, Y.; Chikama, K.; Nohara, Y.; Suzuki, N.; Furushima, K.; Endoh, Y. *Opt. Lett.* **2006**, 31, 1402.
- Tryson, G. R.; Shultz, A. R. *J. Polym. Sci.: Polym. Phys. Ed.* **1979**, 17, 2059.
- Turro N. J. *Modern molecular photochemistry*; University Science Books: Mill Valley, **1991**.
- Uhl, F. M.; Davuluri, S. P.; Wong, S. C.; Webster, D. C. *ANTEC Conf.* **2004**, 1892.
- Uhl, F. M.; Davuluri, S. P.; Wong, S. C.; Webster, D. C. *Chem. Mater.* **2004**, 16, 1135.
- Uhl, F. M.; Davuluri, S. P.; Wong, S. C.; Webster, D. C. *Polymer* **2004**, 45, 6175.
- Uhl, F. M.; Hinderliter, B. R.; Davuluri, S. P.; Croll, S. G. *Mater. Res. Soc.* **2004**, 16, 203.
- Uhl, F. M.; Webster, D. C.; Davuluri, S. P.; Wong, S. C. *Euro. Polymer J.* **2006**, 42, 2596.
- Usuku, A.; Kojima, Y.; Kawasumi, M.; Okada, A.; Fukushima, Y.; Kurauchi, T.; Kamigaito, O. *J. Mater. Res.* **1993**, 8, 1185.
- Vaccari, A. *Appl. Clay Sci.* **1999**, 14, 161.
- Vaia, R. A.; Giannelis, E. P. *Macromolecules* **1997**, 30, 7990.
- Wang C.; Lai P.C.; Syu S. H, Leu J. *Surface & Coatings Technology* **2011**, 206, 318.
- Wang, J. H.; Young, T. H.; Lin, D. J.; Sun, M. K.; Huag, H. S.; Cheng, L. P. *Macromol. Mater. Eng.* **2006**, 291, 661.
- Wang, W. N.; Lenggoro, I. W.; Okuyama, K. *J. Coll. Int. Sci.* **2005**, 288, 423.
- Wang, Z.; Pinnavaia, T. J. *Chem. Mater.* **1998**, 10, 1820.
- Wang, Z.; Pinnavaia, T. J. *Chem. Mater.* **1998**, 10, 3769.
- Watts, D. C.; Cash, A. J. *Dent. Mater.* 1991, 7, 281.
- Wei, H.; Li, Q.; Ojelade, M.; Madbouly, S.; Otaigbe, J. U.; Hoyle, C. E. *Macromolecules* **2007**, 40, 8788.
- Weimer, M. W.; Chen, H.; Giannelis, E.P.; Sogah, D.Y. *J Am Chem Soc* **1999**, 121, 1615.

Wicks, Z. W. Jr.; Jones, F. N.; Pappas, P. *Organic Coatings. Science and Technology*; Wiley-Interscience: New York, **1998**, 630.

Xia, X.; Yih, J.; D'Souza, N. A.; Hu, Z. *Polymer* **2003**, 44, 3389.

Zahouily, K.; Benfarhi, S.; Bendaikha, T.; Baron, J. *Rad Tech Europe Conf.* **2001**, 583.

Zahouily, K.; Decker, C.; Benfarhi, S. *J. Proc. RadTech North America* **2002**

Zahouily, K.; Decker, C.; Benfarhi, S.; Baron. **2002**, *RadTech North America*

Zanetti, M.; Lomakin, S.; Camino, G. *Macromol. Mater. Eng.* **2000**, 279, 1.

Zeng, C.; Lee, L. J. *Macromolecules*, **2001**, 34, 3098.

Zhang, G. ; Jiang, C. ; Su, C. ; Zhang, H. *J. Polym. Sci.: Polym.* **2003**, 89, 3155.

Zhang, Q.; Fu, Q.; Jiang, L.; Lei, Y. *Polym. Int.* **2000**, 48, 1561